

**BENZOBISOXAZOLE CRUCIFORMS AND GUANOSINE DERIVATIVES:  
SYNTHESES, STRUCTURAL ANALYSES, AND OPTICAL PROPERTIES**

---

A Dissertation Presented to  
the Faculty of the Department of Chemistry  
University of Houston

---

In Partial Fulfillment  
of the Requirements for the Degree  
Doctor of Philosophy

---

By  
Jaebum Lim  
December 2012

**BENZOBISOXAZOLE CRUCIFORMS AND GUANOSINE DERIVATIVES:  
SYNTHESES, STRUCTURAL ANALYSES, AND OPTICAL PROPERTIES**

---

Jaebum Lim

APPROVED:

---

Dr. Ognjen Š. Miljanić, Chairman

---

Dr. T. Randall Lee

---

Dr. Scott R. Gilbertson

---

Dr. Allan J. Jacobson

---

Dr. Stanko R. Brankovic

---

Dean, College of Natural Sciences and  
Mathematics

*Dedicated to my parents*

*Younghae Lim and Bunjo Park*

*for their encouragement and support*

*in all of my life's endeavor*

## ACKNOWLEDGMENTS

The completion of a Ph.D. would not have been achieved without the encouragement and support of my group mates in the Miljanić Research Group. It is too obvious to deny that the most influential person during my graduate career is my advisor, Ognjen Ščepan Miljanić. Ognjen, Your advice, discipline, and guidance have been absolutely necessary to my growth as a chemist over past four and a half years. Apparently I am the luckiest graduate student in the Department of Chemistry at University of Houston purely because I am your first graduate student given all your dedication from the beginning of my Ph.D. course. Now, I can tell you that I have perhaps enjoyed suffering for the study we did.

I also wish to show my appreciation to the faculty of the Department of Chemistry at UH. Dr. Lee, I will remember your advice that you gave me the other day. Besides, you always allowed me to join your Christmas group party as well as summer group trip that made me completely relax and feel like a huge family. Dr. May, you showed me new area of organic synthesis; for example, chiral auxiliary. Dr. Albright, if you had retired before I had come to Houston, I could not have known that there was "Bonding" class. Dr. Daugulis, you taught me oxidative addition and reductive elimination. For two years in the beginning, I had priceless lessons from all great professors, and I think that it is impossible to have the same opportunity to take such classes of high quality.



In this page, I want to call my friend's names to show my heart. First of all, I thank my batch who started this graduate program with me. Ed Foster: If some people ask me "Had you ever experienced the ultimate BBQ?" I can immediately answer "Yes". Your pork rib and beef brisket are the best, and make those of Goode BBQ just pieces of meat. You were not just my friend, but also my English teacher. Thank you so much. Brian Lundy: You made me feel old, but you always welcomed me and gave me your refrigerator with full of beers. Oussama Zenasni: You helped me a lot to become Americanized although you are not an American. Karolina Osowska! I wouldn't forget that you were there when I had really really hard time. I also want to thank Teng-Hao, Qing, Rio, Ha, Chia-Wei, and Maxim. I will say "thank you" in Korean to my Korean friends: MJ, Seungsoo, DK, Dahye, Chulsoon, Hana, Soojung, Sangho, Joonhyung , and Jeongho.

There is no word and no sentence in any language which enables me to express my gratitude to my parents, Younghae Lim and Bunjo Park. If there is, it may be "I LOVE YOU."

**BENZOBISOXAZOLE CRUCIFORMS AND GUANOSINE DERIVATIVES:  
SYNTHESES, STRUCTURAL ANALYSES, AND OPTICAL PROPERTIES**

---

A Dissertation Presented to  
the Faculty of the Department of Chemistry  
University of Houston

---

In Partial Fulfillment  
of the Requirements for the Degree  
Doctor of Philosophy

---

By

Jaebum Lim

December 2012

## ABSTRACT

This dissertation presents two studies in supramolecular chemistry; one is the chemistry of *benzobisoxazole cruciforms* in which two linearly conjugated  $\pi$  systems meet at the unsaturated center, and the other is that of *guanosine derivatives*.

**Chapter One.** This chapter summarizes the previous work on molecular cruciforms: tetrakis(arylethynyl)benzenes, distyrylbis(arylethynyl)benzenes, tetrakis(aryl-vinyl)benzenes, and tetraethynylethenes.

**Chapter Two.** The synthesis, optical properties, and computational calculation of benzobisoxazole-based molecular cruciforms are presented. The potential use of donor/acceptor substituted cruciforms as sensors is also discussed, and optical response of cruciform compounds to different concentration of trifluoroacetic acid in the liquid state is presented.

**Chapter Three.** A method for the identification method of carboxylic acids, organoboronic acids, phenols, amines, ureas, and tetrabutylammonium salts is described using one of donor/acceptor substituted benzobisoxazole-cruciforms as the sensor.

**Chapter Four.** Structural study of benzobisoxazole cruciforms is presented: their solid state structures, obtained by X-ray crystallography, are presented.

**Chapter Five.** The synthesis and structural analysis of 8-arylethynyl substituted guanosine derivatives is presented. The structural effects of this substitution, in comparison to the previous work in guanosine chemistry, is also discussed.

## TABLE OF CONTENTS

### **Chapter One            Cruciforms: Cross-Conjugated Molecules**

1.1	Introduction.....	1
1.2	Tetrakis(arylethynyl)benzenes.....	4
1.3	Distyrylbis(arylethynyl)benzenes.....	10
1.4	Tetrakis(arylvinyl)benzenes.....	15
1.5	Tetraethynylethenes.....	22
1.6	Conclusion.....	27

### **Chapter Two            Synthesis, Computational Studies, and Optical Properties of Benzobisoxazole Cruciforms**

2.1	Introduction.....	29
2.2	Results and Discussion.....	32
2.2.1	Synthesis.....	32
2.2.2	Computational Studies.....	34
2.2.3	Optical Properties.....	41

2.2.4	Optical Response to Protonation.....	44
2.3	Conclusions and Outlook.....	49
2.4	Experimental Section.....	51
2.4.1	General Experimental Methods.....	51
2.4.2	Synthesis of 2,6-Diphenyl-4,8-dibromobenzo[1,2- <i>d</i> ;4,5- <i>d'</i> ]bisoxazole( <b>14</b> ) .....	52
2.4.3	Synthesis of 2,6-Di( <i>p</i> -( <i>N,N</i> -dimethyl)amino)phenyl-4,8-dibromobenzo[1, 2- <i>d</i> ;4,5- <i>d'</i> ]bisoxazole ( <b>15</b> ).....	52
2.4.4	Synthesis of 2,6-Dipyridin-4-yl-4,8-dibromobenzo[1,2- <i>d</i> ;4,5- <i>d'</i> ]bisoxazole ( <b>16</b> ).....	53
2.4.5	Synthesis of Cruciform <b>1</b> .....	54
2.4.6	Synthesis of Cruciform <b>2</b> .....	55
2.4.7	Synthesis of Cruciform <b>3</b> .....	57
2.4.8	Synthesis of Cruciform <b>4</b> .....	58
2.4.9	Synthesis of Cruciform <b>5</b> .....	59
2.4.10	Synthesis of Cruciform <b>6</b> .....	61
2.4.11	Synthesis of Cruciform <b>7</b> .....	62

2.4.12	Synthesis of Cruciorm <b>8</b> .....	63
2.4.13	Synthesis of Cruciform <b>9</b> .....	64

### **Chapter Three Identification of Carboxylic Acids, Organoboronic Acids, Phenols, Amines, Ureas, and Tetrabutylammonium Salts with Cruciform **6****

3.1	Introduction.....	66
3.2	Results and Discussion.....	69
3.2.1	Optimization of the Ratio between Fluorescent Sensor and Analytes....	69
3.2.2	Qualitative Discrimination of Carboxylic Acids with Fluorescent Sensor <b>6</b> .....	71
3.2.3	Qualitative Discrimination of Organoboronic Acids with Fluorescent Sens or <b>6</b> .....	75
3.2.4	Qualitative Discrimination of Substituted Phenols with a Hybrid Sensing System.....	77
3.2.5	Qualitative Discrimination of Amines and Ureas with a Hybrid Sensing System.....	80
3.2.6	Qualitative Discrimination of Anions with a Hybrid Sensing System.....	83

3.3	Conclusions and Outlook.....	86
3.4	Experimental Section.....	87
3.4.1	General Methods.....	87
3.4.2	Discrimination of <b>C1–C16</b> , <b>B1–B9</b> , and <b>P11–P14</b> Using Solutions of Cruciform <b>6</b> .....	88
3.4.3	Calculation of RGB Changes.....	89
3.4.4	Discrimination of <b>P1–P12</b> with Solution of Cruciform <b>6</b> Combined with <b>B1</b> or <b>B5</b> .....	92
3.4.5	Discrimination of Amines and Ureas Using Cruciform <b>6</b> and Boronic Acid Additives: Boronic Acid Variation.....	93
3.4.6	Discrimination of Amines and Ureas Using Cruciform <b>6</b> and Boronic Acid Additives: Solvent Variation.....	94
3.4.7	Discrimination of Anions Using Cruciform <b>6</b> and Boronic Acid Additives: Boronic Acid Variation.....	95
3.4.8	Discrimination of Anions Using Cruciform <b>6</b> and Boronic Acid Additives: Solvent Variation.....	96
3.4.9	Fluorescence Titration of a Mixture of <b>6</b> and <b>B5</b> with TBACl.....	98

**Chapter Four      Structural      Studies      of      Benzobisoxazole      Cruciforms’  
Organization in the Solid State**

4.1	Introduction.....	100
4.2	Results and Discussion.....	103
4.2.1	Synthesis of Materials.....	103
4.2.2	X-Ray Crystal Structure Analysis.....	105
4.2.2.1	Cruciform <b>1</b> .....	105
4.2.2.2	Cruciform <b>2</b> .....	108
4.2.2.3	Cruciform <b>8</b> .....	111
4.2.2.4	Cruciform <b>20</b> .....	112
4.2.2.5	Cruciform <b>21</b> .....	114
4.2.2.6	Cruciform <b>22</b> .....	116
4.2.2.7	Cruciform <b>23</b> .....	118
4.2.2.8	Cruciform <b>24</b> .....	121
4.2.3	Discussion.....	123
4.3	Conclusion and Outlook.....	127
4.4	Experimental Section.....	128



4.4.1	General Procedures.....	128
4.4.2	Synthesis of Cruciform <b>20</b> .....	129
<b>Chapter Five</b>	<b>Synthesis and Structural Analysis of 8-Arylethynyl Substituted Guanosine Derivatives</b>	
5.1	Introduction.....	131
5.2	Results and Discussion.....	137
5.2.1	Synthesis of Compounds <b>28</b> and <b>45</b> .....	137
5.2.2	X-Ray Crystal Structure Analysis.....	138
5.3	Conclusion and Outlook.....	143
5.4	Experimental Section.....	144
5.4.1	General Methods.....	144
5.4.2	Synthesis of Compound <b>28</b> .....	145
5.4.3	Synthesis of Compound <b>29</b> .....	147
5.4.4	Synthesis of Compound <b>30</b> .....	148
5.4.5	Synthesis of Compound <b>31</b> .....	149
5.4.6	Synthesis of Compound <b>32</b> .....	150

5.4.7	Synthesis of Compound <b>33</b> .....	151
5.4.8	Synthesis of 1,4-Bis[2-[4-[2-(trimethylsilyl)ethynyl]phenyl]ethynyl] -benzene.....	152
5.4.9	Synthesis of 1,4-Diiodo-2,5-dipentoxybenzene.....	153
5.4.10	Synthesis of 1,4-Dipentoxy-2,5-bis[2-(trimethylsilyl)ethynyl]benzene.	153
5.4.11	Synthesis of Compound <b>34</b> .....	154
5.4.12	Synthesis of Compound <b>35</b> .....	155
5.4.13	Synthesis of Compound <b>36</b> .....	156
5.4.14	Synthesis of Compound <b>37</b> .....	157
5.4.15	Synthesis of Compound <b>38</b> .....	158
5.4.16	Synthesis of Compound <b>39</b> .....	159
5.4.17	Synthesis of Compound <b>40</b> .....	160
5.4.18	Synthesis of Compound <b>41</b> .....	161
5.4.19	Synthesis of Compound <b>42</b> .....	162
5.4.20	Synthesis of Compound <b>43</b> .....	163
5.4.21	Synthesis of Compound <b>44</b> .....	163
5.4.22	Synthesis of Compound <b>45</b> .....	164

5.4.23	Crystal Data for Compound <b>28</b> .....	164
5.4.24	Crystal Data for Compound <b>29</b> .....	166
<b>References</b> .....		168

*Note: Chapter 1 contains compounds labeled **1** through **212**. A separate numbering system is used for Chapters 2–5. The compounds are numbered **1** through **53**.*

## ABBREVIATIONS AND ACRONYMS

AcO	acetate
AN	acetonitrile
BBO	benzo[1,2- <i>d</i> :4,5- <i>d'</i> ]bisoxazole
BODIPY	boron-dipyrromethene: 4,4-difluoro-4-bora-3 <i>a</i> ,4 <i>a</i> -diazas-indacene
Bu	<i>n</i> -butyl
CB	chlorobenzene
CF	chloroform
CH	cyclohexane
COF	covalent organic framework
Cy	cyclohexyl
DCM	dichloromethane
DFT	density functional theory
DHA	dihydroazulene
DIPA	diisopropylamine
DMA	<i>N,N</i> -dimethylanilino

DMF	<i>N,N</i> -dimethylformamide
DMSO	<i>N,N</i> -dimethyl sulfoxide
DNA	deoxyribonucleic acid
ESI	electrospray ionization
Et	ethyl
Et <sub>3</sub> N	triethylamine
Et <sub>2</sub> O	ether
EtOH	ethanol
FMO	frontier molecular orbital
Hex	<i>n</i> -hexane
H <sub>2</sub> O	water
HOMO	highest occupied molecular orbital
HRMS	high resolution mass spectrometry
IR	infrared
LED	light-emitting diode
LRMS	low resolution mass spectrometry
LUMO	lowest unoccupied molecular orbital

Me	methyl
MeOH	methanol
MOF	metal-organic framework
NMP	<i>N</i> -methyl-2-pyrrolidone
NMR	nuclear magnetic resonance
OLED	organic light-emitting diode
PCBM	1-(3-(methoxy-carbonyl)propyl)-1-phenyl[6.6]C <sub>61</sub>
PCC	pyridinium chlorochromate
Ph	phenyl
Pyr	pyridinyl
RNA	ribonucleic acid
TBA	tetra- <i>n</i> -butylammonium
<i>t</i> Bu	<i>tert</i> -butyl
TCB	1,2,4-trichlorobenzene
TDDFT	time-dependent density functional theory
TES	triethylsilyl
TFA	trifluoroacetic acid

THF	tetrahydrofuran
TIPS	triisopropylsilyl
TMS	trimethylsilyl
TMSA	(trimethylsilyl)acetylene
TPA	two-photon absorption
UV	ultraviolet
VHF	vinylheptafulvene

## Chapter One

### Cruciforms: Cross-Conjugated Molecules

#### 1.1 Introduction

Conjugated organic compounds are molecular entities whose structure have a carbon backbone with alternating single and multiple bonds.<sup>1</sup> The conjugation in a molecular system is the interaction of one *p*-orbital with another across an intervening  $\sigma$ -bond in such structures. The term is also extended to the analogous interaction involving a *p*-orbital containing an unshared electron pair. Overlapping *p*-orbitals allow a delocalization of  $\pi$ -electrons across the whole conjugated system, which means that  $\pi$ -electrons belong to a group of atoms rather a single bond or atom. Thanks to the delocalization of  $\pi$ -electrons, conjugated systems have unique properties that give rise to strong colors, and are widely used for synthetic dyes and pigments.<sup>2</sup> Conjugated systems can also exhibit the electronic properties of metals and semiconductors, as exemplified by graphene and pentacene.<sup>3</sup> The mechanism of generating colors and exhibiting metallic properties is often explained with an electronic transition between the highest occupied molecular orbital (HOMO) and the lowest unoccupied molecular orbital (LUMO).<sup>4</sup> The nature of conjugated molecules, especially their reactivity, electronic and optoelectronic properties, is dependent on the energy gap between frontier molecular orbitals (FMOs) of conjugated system. For this reason, the study of conjugated systems has often been focused on what affects HOMO and LUMO, how to regulate the energy gap between FMOs,<sup>5</sup> as well as on the applications of conjugated systems.<sup>6-9</sup> The diverse properties of



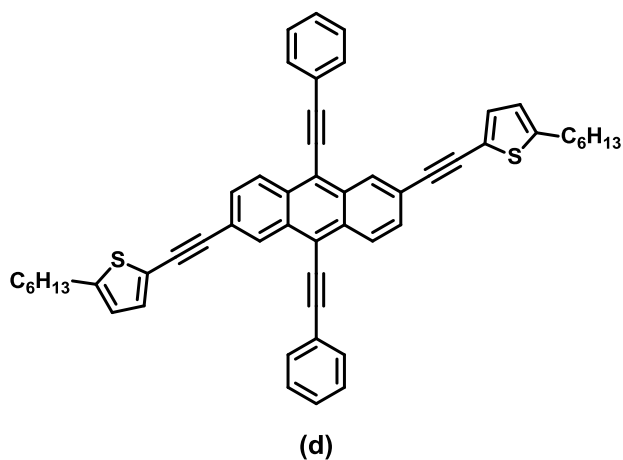
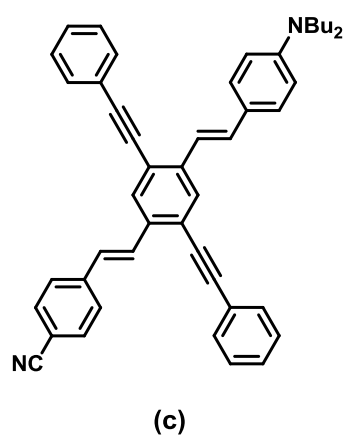
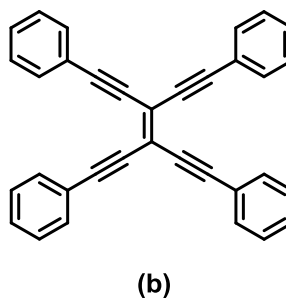
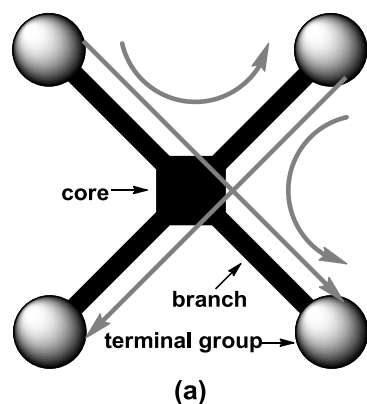


**Chart 1.1** (a) Schematic view of a molecular cruciform and its four possible conjugated pathways (gray arrows), and three examples: (b) 1,2,4,5-tetrakis(phenylethynyl)ethene, (c) 1,4-distyryl-2,5-bisphenylethynylbenzene, and (d) 2,2'-[[9,10-bis(2-phenylethynyl)-2,6-anthracenediyl]di-1,2-ethynediyl]bis[5-hexylthiophene].

conjugated molecules are possible for the use in a variety of applications including light-emitting diodes,<sup>6</sup> field-effect transistors,<sup>7</sup> chemical sensors,<sup>8</sup> and solar cells.<sup>9</sup>

Moreover, full conjugation on the cross-shaped backbone can give promising properties to the cruciform compound for electronic and optical applications with four

conjugated pathways which are possibly tuned by the decoration of four end-groups (Chart 1.1).<sup>10</sup> In order to achieve a fully conjugated cruciform compound, the cross section in the system generally consists of either an aromatic ring or an ethene, and four directional branches are either unsaturated vinyl or ethynyl groups or a combination of these two functional groups. The core is one of the important parts of the cruciform compound because it connects four branches and determines the angle of the cross

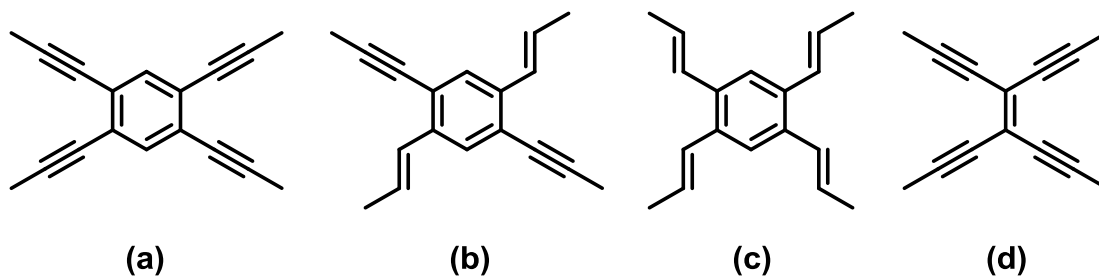


**Chart 1.2** Selected core-branch combinations explored in conjugated cruciform.

section. The most commonly used central core in cruciform compounds is the benzene moiety, but quadruply substituted ethene, heterocycles, and small acenes have also been studied. Both disubstituted *trans*-vinyl and ethynyl moieties are usually selected as connectors to attach various functional groups to the center of target cruciform compound; the latter is preferred because it is more rigid than the former, which allows rotational mode through the bond between the core and the vinyl branch. In many examples of cruciform compounds, the core and four arms provide only the rigid platform,<sup>11</sup> rather than the interaction sites. Four terminal groups at the ends of branches are mostly used as interaction sites and decorated with diverse components in purpose of various applications (Chart 1.1). Therefore, the study of molecular cruciforms can be divided into several areas according to both the anatomical point of view and the

applications of these cross-conjugated molecules. In this chapter, four broadest families of cruciform compounds will be introduced, grouped by their structures, i.e. the combinations of a core with four arms (Chart 1.2). Synthetic strategies for the preparation of these systems will be shown alongside typical characterization methods, and their possible applications.

## 1.2 Tetrakis(arylethynyl)benzenes

The biggest family of cruciform compounds are tetrakis(arylethynyl)benzene derivatives. A SciFinder search on August 12, 2012 revealed approximately 120 cruciform compounds having the core-branch combination **A** shown in Chart 1.2. Haley's group has exhaustively studied tetra(arylethynyl)benzene derivatives **1–33** (Chart 1.3).<sup>12</sup> Their studies have been focused on the effects of four terminal groups that are varied between donor and acceptor substituents, as well as electron-neutral phenyl group. Upon addition of these substituents to the end groups of cruciform scaffold, they had shown the interesting electronic and optical properties of molecular cruciforms. The synthesis of molecular cruciforms **1–8**<sup>12j</sup> was introduced, and their structure-property relationship was also studied in comparison with bis(dehydrobenzoannuleno)benzenes, in which there are two diacetylene bridges between end-groups:  $R_1-R_2$ ,  $R_3-R_4$  or  $R_1-R_4$ ,  $R_2-R_3$ .<sup>12i</sup> Molecular orbital plots of simplified structures of **1–5** showed that the HOMO and the LUMO of donor/acceptor substituted cruciforms **3–5** were localized on the conjugated pathway of donor-donor and that of acceptor-acceptor respectively, but those of **1** and **2** were not. This result was also observed from the bis(dehydrobenzoannuleno)benzenes

No.	R <sub>1</sub>	R <sub>2</sub>	R <sub>3</sub>	R <sub>4</sub>	No.	R <sub>1</sub>	R <sub>2</sub>	R <sub>3</sub>	R <sub>4</sub>
1	a	a	a	a	21	c	c	j	j
2	c	c	c	c	22	c	j	c	j
3	c	c	d	d	23	c	j	j	c
4	c	d	c	d	24	c	c	k	k
5	c	d	d	c	25	c	k	c	k
6	c	c	e	e	26	c	k	k	c
7	c	e	c	e	27	c	c	l	l
8	c	e	e	c	28	c	l	c	l
9	c	c	f	f	29	c	l	l	c
10	c	f	c	f	30	c	c	m	m
11	c	f	f	c	31	c	m	c	m
12	c	c	g	g	32	c	m	m	c
13	c	g	c	g	33	m	m	m	m
14	c	g	g	c	34	b	b	b	b
15	c	c	h	h	35	d	d	d	d
16	c	h	c	h	36	i	i	i	i
17	c	h	h	c	37	b	b	d	d
18	c	c	i	i	38	b	d	b	d
19	c	i	c	i	39	b	d	d	b
20	c	i	i	c					

a

b

c

d

e

f

g

h

i

j

k

l

m

**Chart 1.3** Survey of structures of donor/acceptor-functionalized tetrakis(arylethynyl)-benzenes and BODIPY-incorporated cruciform compounds.

having comparative donor/acceptor arrangement of **1–5**. The enhancement of the optical activity transitioning from neutral to tetra-donor to donor/acceptor systems was demonstrated through large bathochromic shifts of the UV/Vis  $\lambda_{\text{max}}$  and the development of strong charge-transfer bands. Instead of nitrophenyl groups, pyridyl groups as electron acceptors were introduced to the terminals of molecules **9–17**.<sup>12g</sup> Molecular orbital plots of these nine molecules showed the similar propensity with those of cruciforms decorated with nitrophenyl group, but the stronger solvatochromism was observed and the higher quantum yields were achieved from pyridyl-decorated cruciforms. These nine molecules can also bind to  $\text{Zn}^{2+}$  cations stoichiometrically in solution, but only very weakly, compared to **59**.<sup>16s</sup> Molecules **18–26**<sup>12e</sup> have been synthesized and compared with previously reported **3–17**. The results showed that the weaker acceptor groups exhibited visibly fluorescent intramolecular charge transfer behavior, moderately narrow optical band gaps, moderately high quantum yields, and strong fluorescence solvatochromism. Haley's group recently reported BODIPY-incorporated cruciforms **27–33**,<sup>12a</sup> and examined the electronic absorption and emission spectra of each molecule. Computational studies were also employed to corroborate the relative energy levels and gaps for each cruciform. Cruciform **27** and **30** showed the localized HOMO and LUMO on the conjugated pathway of donor-substituted branches and BODIPY-terminals respectively. In some instances the BODIPY unit was able to enhance the quantum yields to levels not seen with the other tetrakis(arylethynyl)benzene cruciforms, despite the tendency to fluoresce quench in polar solvents.

Another group of donor/acceptor-functionalized tetrakis(phenylethynyl)benzenes (**34–39**, Chart 1.3) was theoretically studied by Sun's group to investigate two-photon

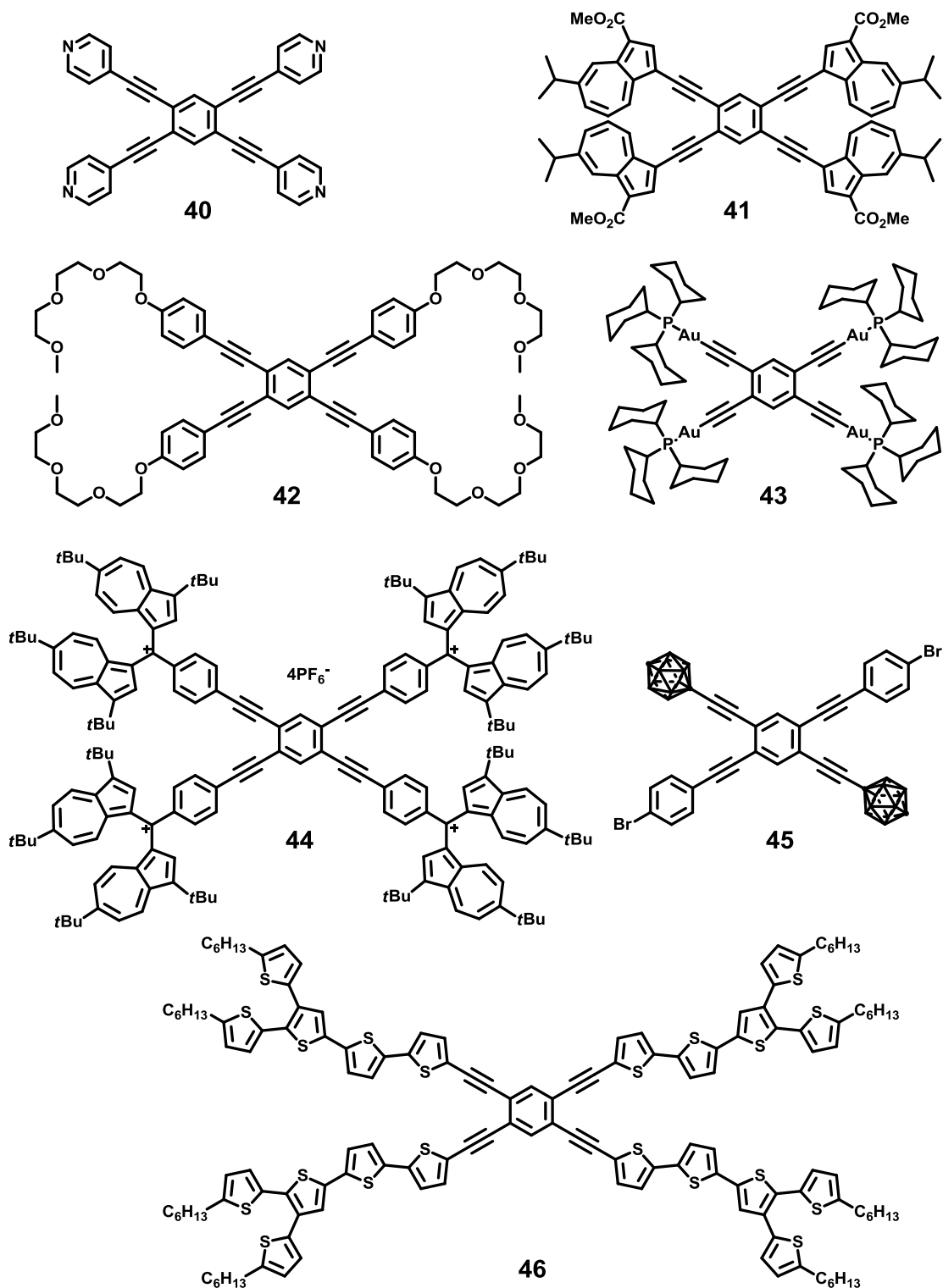
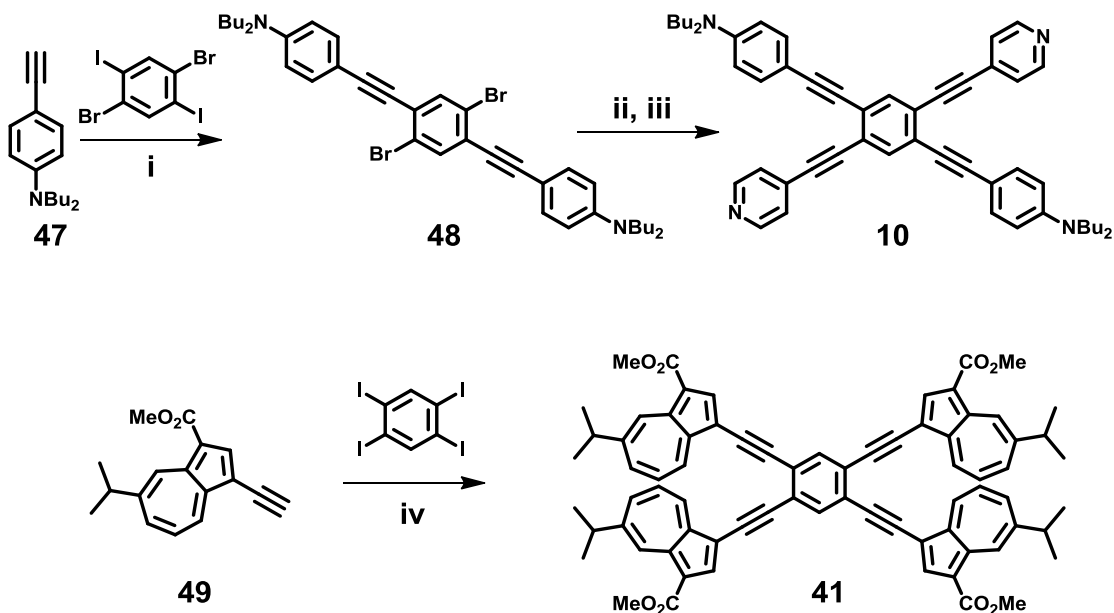


**Chart 1.4** Examples of structural variations among tetrakisethynylbenzene cruciforms. cruciforms.



**Scheme 1.1** Synthesis of cruciforms **10** and **41**: (i) Pd(PPh<sub>3</sub>)<sub>4</sub>, CuI, DIPA, THF, 89%; (ii) TMSA, Pd(PPh<sub>3</sub>)<sub>4</sub>, CuI, DIPA, THF; (iii) aq KOH, 4-bromopyridine, Pd(PPh<sub>3</sub>)<sub>4</sub>, CuI, DIPA, THF, 65 °C, 60% (two steps); (iv) Pd(PPh<sub>3</sub>)<sub>4</sub>, CuI, Et<sub>3</sub>N, THF, 77%.

absorption properties using computational methods.<sup>13</sup> Sun's group also compared six cruciforms with corresponding benzoannulenes in the similar way of Haley's group research. Unlike Haley's and Sun's groups, other researchers had mostly taken the advantages of cruciform backbone as one of star-shaped cores playing a bridge to connect multiple components,<sup>10h,14</sup> and as a part of molecular machine (Chart 1.4).<sup>15</sup>

Considering the size of molecular cruciform, the synthetic method is relatively simple due to the symmetric components in the molecule such as a mirror plane, a rotation axis, and an inversion center. The key C–C bond formations to assemble tetraethynylbenzene cruciforms occur between  $sp^2$  carbon of central benzene ring and  $sp$  carbon of terminal alkynes via Sonogashira coupling in most cases. Another Sonogashira

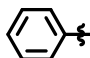
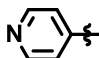
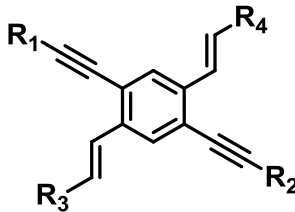
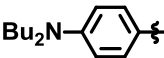
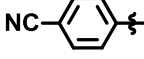
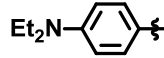
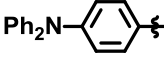
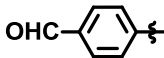
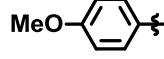
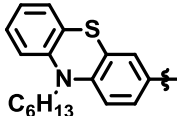
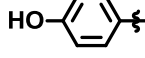
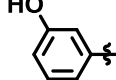
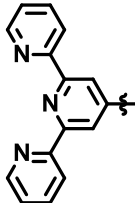
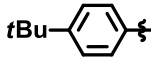
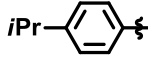
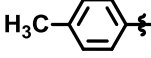
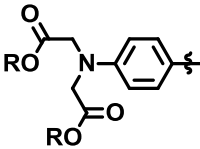
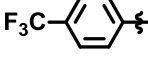
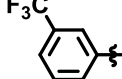
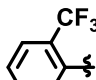
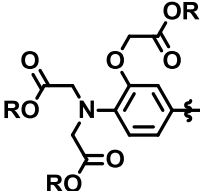
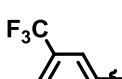
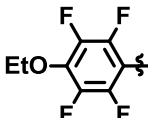
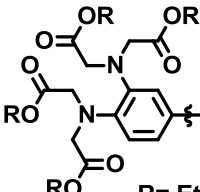
coupling between the end group and the terminal alkyne already attached to the central benzene ring completes the synthesis of a molecular cruciform. The syntheses of tetraethynylbenzene cruciforms **10**<sup>12g</sup> and **41**<sup>14d</sup> are shown as representative, in Scheme 1.1. Donor and acceptor parts are attached to a central tetrahalobenzene ring in a stepwise manner that takes advantage of the different reactivity between aryl bromides and aryl iodides toward cross-coupling. Two-fold cross-coupling of the donor alkyne **47** to 1,4-dibromo-2,5-diiodobenzene gives the linearly conjugated compound **48** as one of three key intermediates of **2–32**. Compound **48** was obtained under mild reaction conditions that allow selective coupling to the more reactive iodides. TMSA is consecutively coupled to the bromine positions on the central ring under increased temperature to overcome the lower reactivity of aryl bromides and the unfavorable match with electron-rich arenes in the Sonogashira reaction. Two-fold coupling of 4-bromopyridine with the product of an electron-rich alkyne gives the final product **10** in good yield. To synthesize tetra(arylethynyl)benzenes having four identical branches, such as **41**, **44**, and **46**, 1,2,4,5-tetraiodobenzene is employed instead of 1,4-dibromo-2,5-diiodobenzene in the previous scheme. Four-fold Sonogashira coupling of **49** with 1,2,4,5-tetraiodobenzene under mild reaction conditions produces **41** in 77% yield.

### 1.3 Distyrylbis(arylethynyl)benzenes

The second large group of molecular cruciforms is based on 1,4-distyryl-2,5-bis(arylethynyl)benzene derivatives. Instead of having four ethynyl branches, two vinyl branches were introduced to the same axis as shown in Chart 1.2B. Bunz' group<sup>16</sup> had



exhaustively investigated this cruciform family, with a dazzling variety of electronic and functional properties at their terminal parts. They also demonstrated that some cruciforms in their gallery were possibly used as sensor molecules for various analytes such as metal cations,<sup>16h,n</sup> aromatic carboxylic acids,<sup>16c</sup> and amines.<sup>16b,i</sup> Bunz' group had started their research about cruciforms as model compounds for functionalized poly(*para*-phenyleneethynylene)s.<sup>16s</sup> They first synthesized compounds **50–56** as model building blocks, and demonstrated that those cruciform blocks were versatile and tunable chromophores where the position of HOMO and LUMO can be changed by the introduction of donor/acceptor substituents. UV/Vis and fluorescence spectroscopy as well as computational calculation with Spartan were used to demonstrate their conclusion. Bunz' group had also investigated the complete spatial separation of HOMO and LUMO through metal ion sensing experiments with compounds **50, 54, 58, and 59**.<sup>16r</sup> These preliminary results were perhaps the inspiration for them to further study 1,4-distyryl-2,5-bis(arylethynyl)benzenes as functional fluorophores. Extensive inspection of compounds **51, 54, 56, and 58–63** was performed by observing their fluorescence response to metal triflates, NMR experiments, TFA titration, and *ab initio* calculations with Spartan.<sup>16n</sup> Pyridine-containing cruciforms **51** and **58** were employed in supramolecular polymers that are assembled with either a ditopic bis-Pd or bis-Pt pincer complexes.<sup>16l,o</sup> Hydroxycruciforms **64–65**<sup>16m</sup> and **73–75**<sup>16i</sup> were synthesized for the purpose of amine-sensing. Employing multiple ester groups to two vinyl branches which enable the cruciform molecules to be dissolved in water after hydrolysis reactions, water soluble cruciforms **76–78**<sup>16f,h</sup> were synthesized and their optical properties were studied at different pH values, in the presence of metal cations, as well as in different solvents.

	a		p										
	b		q										
	c												
	d		r	No.	R <sub>1</sub>	R <sub>2</sub>	R <sub>3</sub>	R <sub>4</sub>	No.	R <sub>1</sub>	R <sub>2</sub>	R <sub>3</sub>	R <sub>4</sub>
	e		s	50	h	h	a	a	72	n	n	s	s
	f			51	h	h	p	p	73	e	e	f	f
	g		t	52	e	e	e	e	74	f	f	e	e
	h			53	m	m	k	k	75	f	f	f	f
	i			54	a	a	b	b	76	a	a	u	u
	j		u	55	m	m	b	b	77	a	a	v	v
	k			56	n	n	b	b	78	a	a	w	w
	l			57	k	k	b	b	79	n	n	f	f
	m		v	58	p	p	i	i	80	a	a	b	h
	n			59	p	p	b	b	81	a	a	p	h
	o		w	60	a	a	a	a	82	a	a	b	q
				61	a	a	i	i	83	a	a	b	p
				62	o	o	b	b	84	a	a	d	p
				63	q	q	b	b	85	i	i	p	p
				64	h	h	f	f	86	r	r	h	h
				65	h	h	g	g	87	r	r	b	b
				66	l	l	f	f	88	r	r	b	h
				67	t	t	i	i	89	r	r	p	h
				68	b	b	s	s	90	b	b	f	f
				69	h	h	s	s	91	f	f	b	b
				70	p	p	s	s	92	a	a	p	p
				71	l	l	s	s					

**Chart 1.5** Survey of distyrylbis(arylethynyl)benzene cruciforms studied by the Bunz group since 2003.

To explore the construction of self-assembled probes capable of discriminating simple inorganic anions, compound **67** was prepared and equipped with  $\text{Zn}^{2+}$  ions to the bays of terpyridine moieties.<sup>16k</sup> This complex sensor could clearly differentiate fluoride from the other halides. Cruciforms **68–72**<sup>16j</sup> were equipped with two sulfur-containing phenothiazine terminals, and their metalochromic properties were investigated due to strong oxidizing ability of sulfur atom for most metals. Unsymmetrical cruciforms **80–84** were studied to give answers to questions that could not be addressed with the symmetrical cruciforms **54**, **59**, and **85**.<sup>16e</sup> One of the questions is about the presence of excited-state decomplexation or enhanced complexation upon binding of metal cations to **80–84**. In other word, will excited-state photoacidity be enhanced? Bunz investigated the photoacidity and metalochromicity of unsymmetrical cruciforms through observing optical response of acid titration, metal binding at different solvent polarity. Their answer was that unsymmetrical cruciforms neither display excited-state decomplexation nor enhanced photoacidity. Aldehyde-substituted donor-acceptor cruciforms **86–89**<sup>16b</sup> were synthesized, and the fact that they are useful dosimeters for primary amines, primary diamines, and secondary amines was demonstrated through NMR study. Especially, these aldehyde cruciforms could detect 1,*n*-diamines in concentrations lower than 100 ppm. Single molecular sensor is not the only way of identification of various analytes such as metal cations and amines. The combination of three reactive cruciform fluorophores **54**, **63**, and **92** was also used as a sensor to discern ten different aromatic carboxylic acids by protonation-induced fluorescence shifts, even though those ten acids have closely spaced  $\text{pK}_a$  values. Recently, Bunz' group reported two amphoteric cruciforms **90** and **91** having 4-(dibutylamino)phenyl groups and 4-hydroxyphenyl groups.<sup>16b</sup> These cruciforms

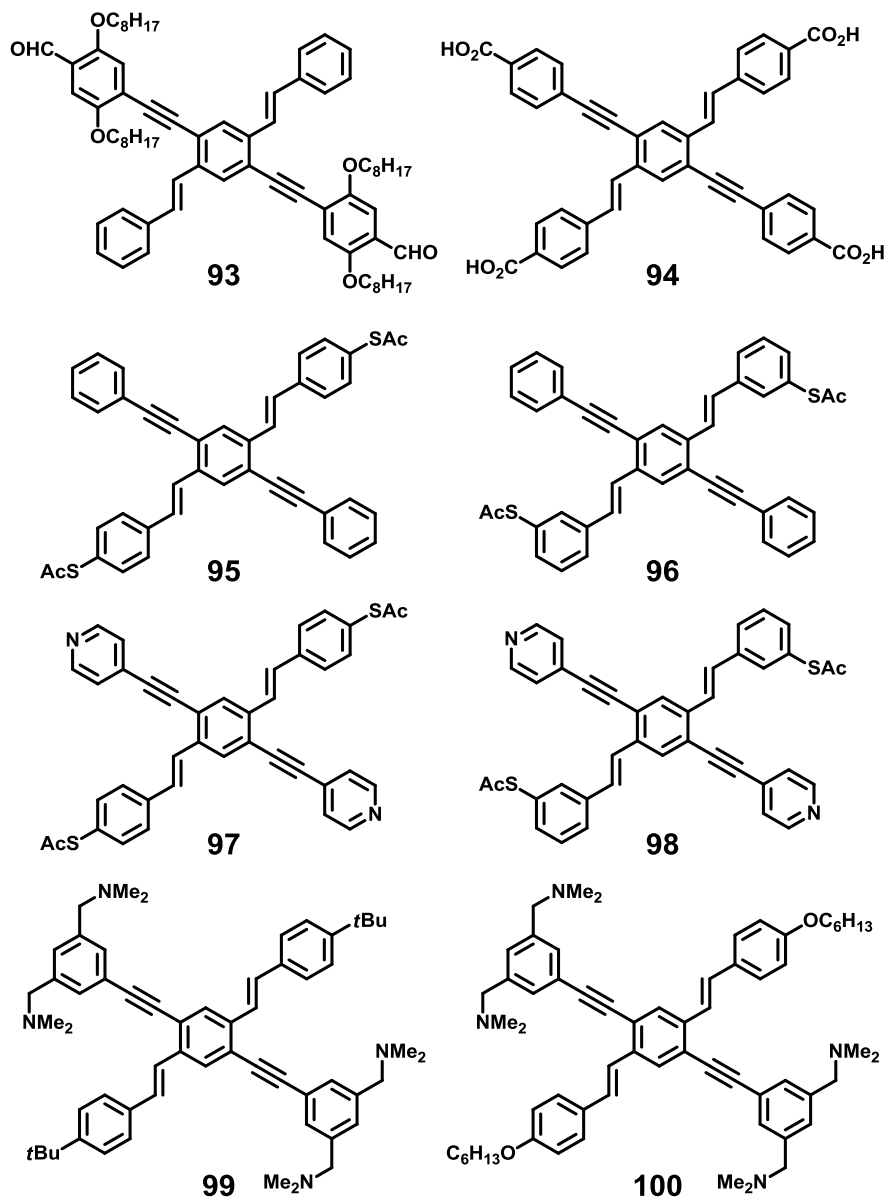
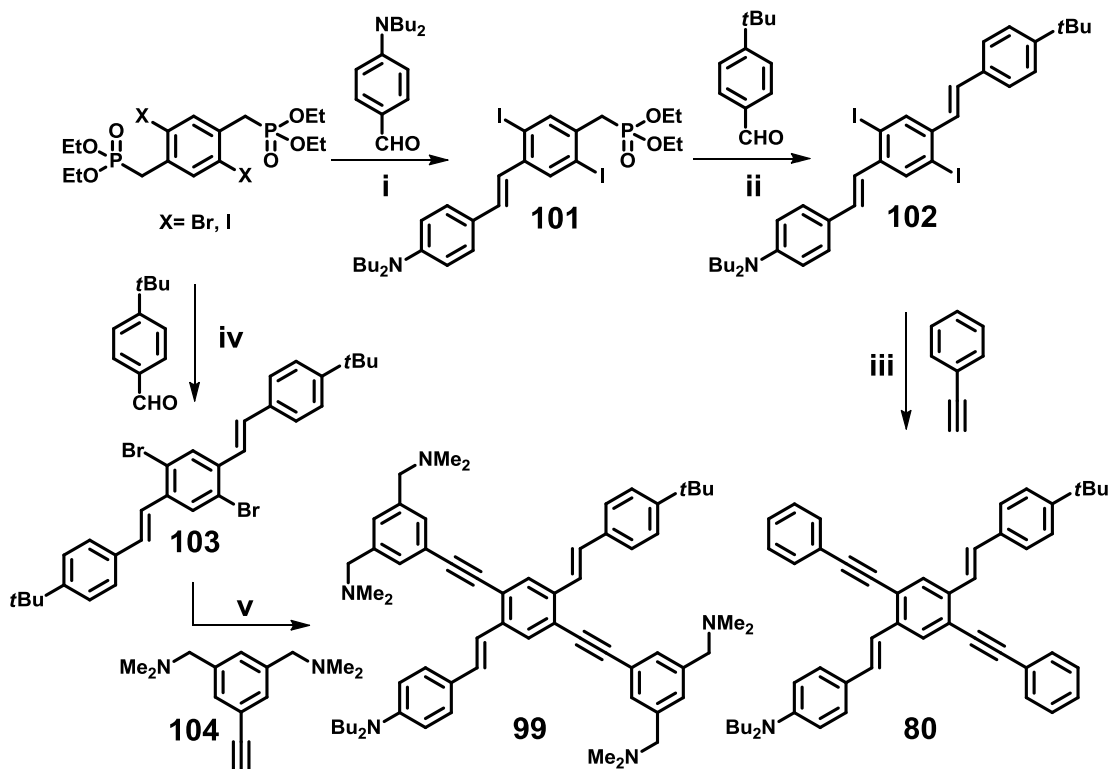


**Chart 1.6** Distyrylbis(arylethynyl)benzenes studied by the groups of Schubert (**93**),<sup>17e</sup> Yaghi. (**94**),<sup>17a</sup> Mayor (**95–98**),<sup>17c,d</sup> and Smith(**99**, **100**).<sup>17b</sup>

displayed significant changes in absorption and emission when exposed to diverse analytes: TFA, tetrabutylammonium hydroxide, and metal triflates.

Distyrylbis(arylethynyl)benzenes were also studied by four other groups (Chart 1.6).<sup>17</sup> The cruciform **93** with an aldehyde group and two long alkoxide groups was synthesized as a monomer for poly(phenyleneethylene)-poly(phenylenevinylene) systems by Schubert's group.<sup>17e</sup> Yaghi's group employed cruciform **94** as a linker between  $\text{Zr}_6\text{O}_4(\text{OH})_4$  cuboctahedral units to build MOF-535.<sup>17a</sup> Cruciforms **97** and **98** having pyridine moieties at the end of ethynyl branches were synthesized as single-molecule switches positioned between Au electrodes.<sup>17c,d</sup> Two cruciforms **95** and **96** having phenyl group instead of pyridine group were also synthesized for the control experiment in the same study. Smith's group had synthesized two cruciforms **99** and **100** and used them for metal ion detection.<sup>17b</sup> Both compounds showed a photoluminescence response to  $\text{Zn}^{2+}$  and  $\text{Cu}^{2+}$  over other common metal ions that they screened.

The synthetic strategy generally used to prepare distyrylbis(arylethynyl)benzenes relies on the Horner-Wadsworth-Emmons reaction to install stiryl substituents and Sonogashira cross-coupling to put into place alkynyl groups. To describe the synthetic methods, compounds **80** and **99** were chosen as representative of unsymmetrical and symmetrical cruciforms. The synthesis of both cruciforms started from diphosphate derivatives that gave compounds **101** and **103** after the modified Wittig reaction with 1 equivalent of 4-(*N,N*-dibutylamino)benzaldehyde and 2 equivalents of 4-*tert*-butylbenzaldehyde, respectively. Another Horner-Wadsworth-Emmons reaction of **101** with 1 equivalent of 4-*tert*-butylbenzaldehyde yields unsymmetrical *para*-distyrylbenzene **102**. The introduction of the secondary axis is achieved by coupling of **102** to phenylacetylene, to give the cruciform **80**. Cruciform **99** is synthesized through



**Scheme 1.2** Syntheses of cruciform **80** and **99**: (i) KO $t$ Bu, THF, 0 °C, 49%; (ii) KO $t$ Bu, THF, 0 °C, 83%; (iii) PdCl<sub>2</sub>(PPh<sub>3</sub>)<sub>2</sub>, CuI, piperidine, THF, 87%; (iv) KO $t$ Bu, THF, 60%; (v) Pd(PPh<sub>3</sub>)<sub>4</sub>, CuI, Et<sub>3</sub>N, DMF, 10%.

Sonogashira cross-coupling reaction of the arylhalide **103** with **104**, which is synthesized in 4 steps starting from 1-bromo-3,5-dimethylbenzene.

#### 1.4 Tetrakis(arylvinyl)benzenes

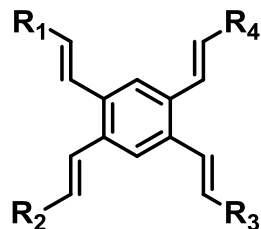
Unlike tetrakis(arylethynyl)benzenes and distyrylbis(arylethynyl)benzenes, the third family of cruciform compounds that consist of four vinyl branches have been studied by many research groups. They have focused their research interests on the use of

the geometrical properties of tetrakis(arylvinyl)benzenes rather than the electronic structure of cruciform compounds with donor/acceptor decoration. Terminal groups introduced to the tetraethenylbenzene-core are summarized in Chart 1.7, and the list of all tetrakis(arylvinyl)benzenes is shown in Chart 1.8.

Cruciforms with donor/acceptor decoration are **114–117**, **123**, **124**, **132**, and **138–142**.<sup>18</sup> The first computational study of donor/acceptor decorated cruciforms was performed by Jiang's group.<sup>18a,b</sup> They focused on the prediction of one-photon and two-photon absorption (TPA) behavior of four molecular cruciforms comparing with corresponding compounds having linear- and trigonal-symmetric centers. Cruciform compounds **114–117** had shown larger TPA cross-sections than the linear and the trigonal compounds. Especially, compound **116** with four acceptor substituents displayed the largest TPA activity in the visible region among three of them. Compounds **107**<sup>19g,h</sup> and **128**<sup>18e</sup> were also studied by Jiang group for the purpose of enhancing TPA property. Cross-conjugated tetradentate ligand **107** was not used only for TPA experiment, but was also employed as the linkage between Au nanoparticles,<sup>19a,e</sup> a part of photoswitching rhenium complexes,<sup>19b</sup> component of sphere-shaped coordination polymer with Pd complex<sup>19c</sup> and metal-organic two-dimensional networks,<sup>19d</sup> and, finally, as a component of trigonal prism assembly with *cis*-(Me<sub>3</sub>P)<sub>2</sub>(OTf)<sub>2</sub>.<sup>19f</sup> Perry group synthesized **123** and **132** as well as their linear model compounds, and they reported the one- and two-photon absorption properties of both cruciform- and linear-compounds.<sup>18c</sup> Compound **123** having







No.	R <sub>1</sub>	R <sub>2</sub>	R <sub>3</sub>	R <sub>4</sub>	No.	R <sub>1</sub>	R <sub>2</sub>	R <sub>3</sub>	R <sub>4</sub>	No.	R <sub>1</sub>	R <sub>2</sub>	R <sub>3</sub>	R <sub>4</sub>
105	i	i	i	i	119	v	v	v	v	133	z	z	z	z
106	r	r	r	r	120	w	w	w	w	134	c'D	c'D	c'D	c'D
107	j	j	j	j	121	x	v	x	v	135	c'A	c'D	c'A	c'D
108	u	u	u	u	122	x	x	v	v	136	n	n	n	n
109	e	g	e	g	123	b	b	b	b	137	o	o	o	o
110	s	g	s	g	124	a	a	a	a	138	p	p	q	q
111	y	y	y	y	125	c'A	c'A	c'A	c'A	139	p	q	q	p
112	m	m	m	m	126	a'	a'	a'	a'	140	p	q	p	q
113	k	k	k	k	127	v	x	x	v	141	d	l	l	d
114	d	d	d	d	128	f	f	f	f	142	d	l	d	l
115	d	d	l	l	129	c'C	c'C	c'C	c'C	143	c'B	c'B	c'B	c'B
116	l	l	l	l	130	t	t	t	t	144	c'E	c'A	c'A	c'A
117	c	c	c	c	131	b'	b'	b'	b'	145	c'E	c'A	c'E	c'A
118	j	j	h	h	132	b	l	b	l	146	c'E	c'E	c'E	c'E

**Chart 1.8** Survey of tetrakis(arylvinyl)benzenes decorated with the ornaments in by employing the quadratic response theory with B3LYP and CAM-B3LYP functionals.<sup>18d</sup> They selected nine model molecules that have different length of branches between core benzene and terminal nitro/amino group as well as different arrangement of branches: 1,5-diamino-2,4-dinitrobenzene, 1,4-diamino-2,5-dinitrobenzene, 1,2-diamino-4,5-dinitrobenzene, **115**, and **138–142**. After performing exhaustive calculation, they concluded that both the length and the arrangement of branches are important to increase

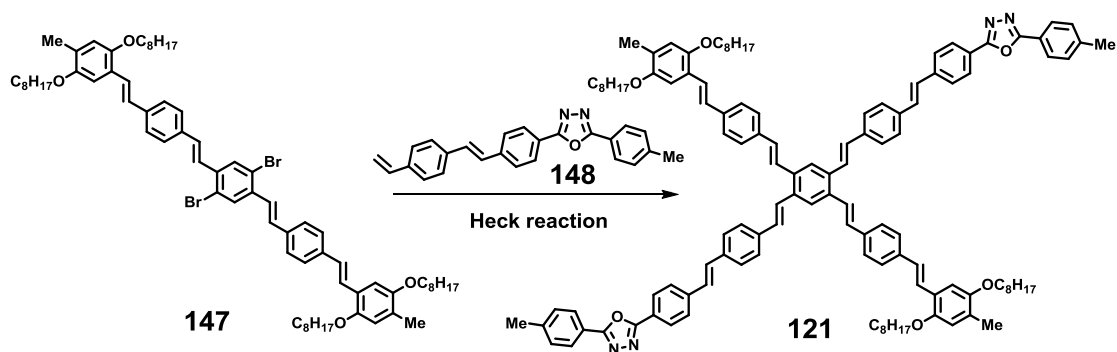
TPA cross-section. The longer branches the cruciform has, the larger TPA cross-section is observed. Cruciform **115** with *ortho* substitution of both donor and acceptor groups showed the largest TPA cross section among the three tetrakis(arylvinyl)benzenes.

Joo's and Choi's groups had reported the synthesis and the semiconducting properties of ten cruciform compounds containing bithiophenes, terthiophenes, thienothiophenes, and dithienothiophenes as the substituents.<sup>20</sup> In the structures of thiophene-decorated cruciforms, tetravinylbenzene-center was adopted as dendrimeric core rather than the junction used for HOMO/LUMO localization as Haley's and Bunz' group did. Bithiophene-derivatives were used to ornament seven compounds **125**, **134**, **135**, and **143–146**. Cruciform **129** has four identical terthiophene arms, and cruciforms **126** and **131** have thienothiophene- and dithienothiophene-based arms, respectively.<sup>20i</sup> The first generation of cruciform dendrimers **125** and **126** display a *p*-type semiconducting behavior, and their solubility was better than the linear conjugated oligothiophene simply because of more aliphatic chains. Later, Joo's and Choi's groups synthesized dithienothiophene-based compound **131** and compared its semiconducting property with previously reported **125** and **126** in charge terms of carrier mobility.<sup>20j</sup> Compound **131** exhibited the highest carrier mobility than any other star-shaped molecules and conjugated dendrimers reported before. These compounds had been extensively studied for the application to organic thin film transistor.<sup>20g,h,i</sup> The terthiophene-based molecule **129** also showed good solubility in common organic solvents as well as semiconducting properties in organic field-effect transistors with its good self-film forming property.<sup>20k</sup> For convenient wet-chemistry processing, cruciform dendrimers **134** and **135** decorated with pentadienyl end groups were synthesized. The

pentadienyl end groups allow photon-induced polymerization reaction of the soluble monomers **134** and **135**, and an insoluble network can be created after the polymerization reaction.<sup>20f</sup> Donor- $\sigma$ -acceptor molecules **144–146** were introduced by Choi's group for studying the self-organization of each perylene diimide moieties and bithiophene-based cruciform central part as well as their applications in photovoltaic devices.<sup>20d</sup> *Ab initio* optimized structure of **144** shows localized HOMO on bithiophene-based cruciform and localized LUMO on perylene diimide appendix.<sup>20c</sup>

Galvin's group also employed tetrakis(arylvinyl)benzene as a dendrimeric core for optoelectronic applications.<sup>21</sup> They reported the synthesis of dendrimeric core **112** having four aldehyde terminals as connectors for the extension of conjugated branches.<sup>21e</sup> Starting with **112**, point-symmetric cruciform dendrimer **120** was synthesized through Knoevenagel condensation with corresponding phenylacetonitrile. Other point-symmetric cruciform dendrimers **119** and **121** were obtained through Horner-Wadsworth-Emmons and Heck reactions from 2,5-bis(diethylphosphonomethyl)-1,4-dibromobenzene. Compounds **122** and **127** were also constructed in the same reaction pathway starting from 4,5-dibromo-2-[(diethoxyphosphoryl)methyl]benzylphosphonate.<sup>21b,c,d</sup> To study a structure-property relationship, the three isomers, **121**, **122**, and **127**, were examined in terms of photophysical characterization, electrochemistry, X-ray diffraction analysis, atomic force microscopy, and device fabrication and testing. They showed almost identical photophysical properties and HOMO-LUMO energy levels, but the best LED device efficiencies were seen in **122**. Cruciform dendrimer **121** was employed for the use as oligo photosensitizer combined with 1-(3-(methoxy-carbonyl)propyl)-1-phenyl-[6,6]C<sub>61</sub>(PCBM) for organic solar cells.<sup>21a</sup> Some of cruciform tetravinylbenzenes were

synthesized as a part of specific reaction library such as **105** for reaction of alkenyl Grignard reagents with polyhalobenzenes, **106** as one of target compound for Pd-catalyzed alkenylation reaction, **108** as an intermediate for benzoannulene synthesis.<sup>22</sup> The synthesis of compounds **109** and **110** was reported presumably because of their potential to be used as OLED materials,<sup>23a</sup> but no results have been published since. Squaraine dyes were synthesized in various geometries including linear, trigonal, and



**Scheme 1.3** Syntheses of cruciform **121**: tri-*o*-tolylphosphine, tributylamine, Pd(OAc)<sub>2</sub>, DMF, 95 °C, 86%

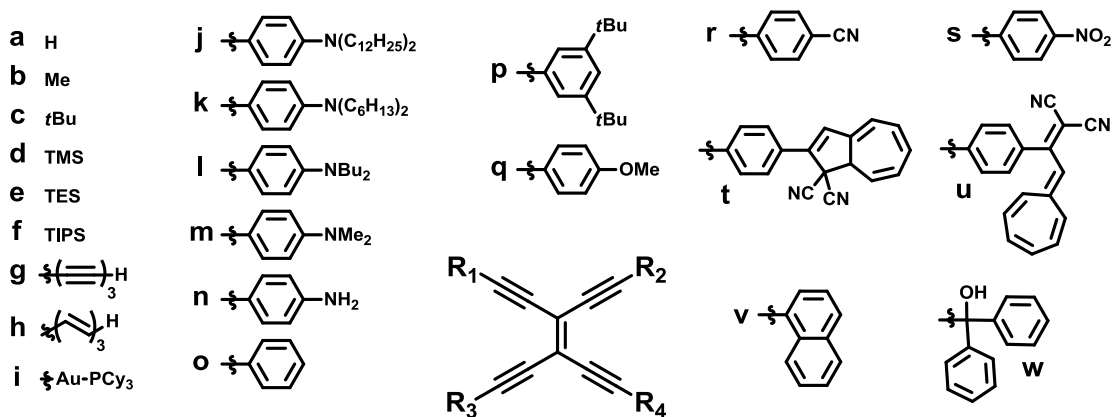
square planar, as well as tetrahedral structures. Among them, the only example in which intramolecular steric interaction between squaraine moieties is possible was the cruciform-possessing dye **111**.<sup>23b</sup> The crystal structure of **113**, which is one of constitutional isomer of **107** was reported by Brian et al.,<sup>23c</sup> but the further investigation wasn't reported despite the multiple binding sites like **107**. Cruciform **118** was designed for the use of self-assembled electrooptic thin films which was induced by the

substitution reactions benzyliodide-functionalized surface with pyridine moieties of two branches of **118**.<sup>23d,e</sup> Dendrimeric cruciforms **130**<sup>23f</sup> and **133**<sup>23h</sup> decorated with oligo(ethylene oxide)s and terpyridines were synthesized respectively. The former was utilized to prepare gold clusters and hollow microfibers with citrate-stabilized Au nanoparticles,<sup>23g</sup> and the latter participated in the study of the ultrafast photoinduced dynamics<sup>23i</sup> and used as a monomer for metallo-supramolecular block copolymer.<sup>23j</sup> One of fluorescent DNA intercalator precursors **137**, the hydrolysis product of **136**, was also designed by Nigel et al.<sup>23k</sup>

The synthetic methods of tetra(arylviny)benzenes are similar with those of distyrylbis(arylethynyl)benzenes. Instead of Sonogashira cross-coupling reaction, Pd-catalyzed Heck reaction is employed to make bonds between arylhalide core and vinyl branches. The selected example is the synthesis of cruciform **121** that shows semiconducting property. The compound **147** was prepared with the same synthetic procedure used to obtain **103** (Scheme 1.2), then coupled with **148** through Heck cross-coupling reaction to yield **121** in 86% (Scheme 1.3).

## 1.5 Tetraethynylethenes

Tetraethynylethene-cruciforms mentioned in this chapter are summarized in Chart 1.9. The first tetraethynylethene cruciform is tetrakis(phenylethynyl)ethene **149** reported by Hori et al. in 1969 through the dimerization reaction of 1,5-diphenyl-3-bromo-1,4-pentadiyne with potassium *t*-butoxide in the mixture of THF and *N*-methyl-2-pyrrolidone (NMP).<sup>24</sup> Six years later, Hauptmann reported the synthesis of **149–152** by



No.	R <sub>1</sub>	R <sub>2</sub>	R <sub>3</sub>	R <sub>4</sub>	No.	R <sub>1</sub>	R <sub>2</sub>	R <sub>3</sub>	R <sub>4</sub>	No.	R <sub>1</sub>	R <sub>2</sub>	R <sub>3</sub>	R <sub>4</sub>
149	o	o	o	o	171	q	q	d	f	192	o	o	o	s
150	b	b	b	b	172	s	s	d	f	193	d	e	f	s
151	c	c	c	c	173	m	m	s	f	194	e	d	f	s
152	d	d	d	d	174	q	q	s	f	195	f	f	q	q
153	a	a	a	a	175	m	m	m	f	196	w	w	w	w
154	f	f	e	d	176	s	s	s	f	197	m	f	t	f
155	p	p	p	p	177	f	m	m	f	198	f	m	t	f
156	g	g	g	g	178	f	j	j	f	199	f	m	u	f
157	h	h	h	h	179	f	s	s	f	200	r	r	r	r
158	m	m	s	s	180	d	o	o	d	201	f	l	l	f
159	m	s	m	s	181	m	s	s	m	202	f	k	k	f
160	o	o	d	d	182	j	s	s	j	203	f	v	v	f
161	n	n	f	f	183	o	s	s	o	204	f	s	f	s
162	m	m	f	f	184	f	m	d	f	205	f	m	f	m
163	j	j	f	f	185	f	j	d	f	206	f	l	f	l
164	s	s	f	f	186	f	s	d	f	207	f	k	f	k
165	m	s	f	f	187	f	m	f	s	208	f	j	f	j
166	o	o	s	s	188	f	m	s	f	209	f	v	f	v
167	n	n	s	s	189	f	j	s	f	210	k	k	d	f
168	j	j	s	s	190	f	f	f	d	211	o	o	d	f
169	m	m	d	f	191	f	f	f	s	212	i	i	i	i
170	j	j	d	f										

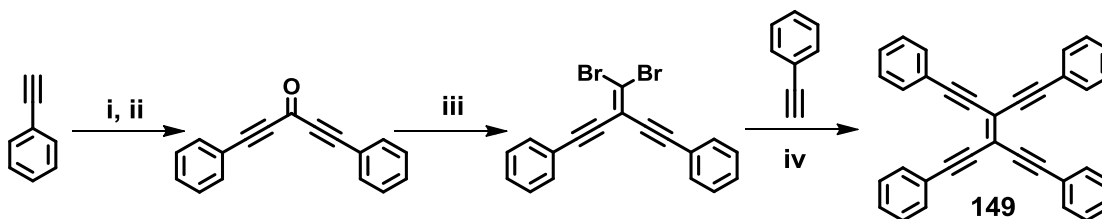
**Chart 1.9** Survey of tetraethynylethene cruciforms **149–212**, decorated with terminal groups a–w.

dehydrogenation reactions of corresponding 1,1,2,2-tetraethynylethanes with *n*-BuLi and *t*-BuOCl.<sup>25</sup> In the early 1990s, Diederich's group used another synthetic strategy for tetraethynylethenes **152** and **162**,<sup>26</sup> that is, Wittig dihalomethylenation reaction followed by the use of dialkynylcopperlithium reagents introduced by Posner et al.<sup>27</sup> For fifteen years since the introduction of new approach to tetraethynylethenes, Diederich's group have studied most of tetraethynylethene-cruciforms<sup>28</sup> in Chart 1.9 except **156**, **157**, **196**, **200**, and **212**. Using the high crystallinity and  $\pi$ -electron donating ability of tetrakis(phenylethynyl)ethene **149**, they tried to make cocrystals with fluorene derivatives as  $\pi$ -electron acceptors.<sup>28a,d</sup> The crystal structure showed donor-acceptor stacks in 1:2 ratio of cruciform/fluorene molecules. The fact that ethene-based cruciforms can be used as building blocks for two-dimensional carbon-rich network was also demonstrated by Diederich's group using compounds **152** and **153**.<sup>28b</sup> His research group actually reported large number of ethene-cruciform compounds having at least one hydrogen-terminal that were not counted because of countless examples of their employments as intermediates of chemical reactions; **153** was selected as one of pioneering examples. The table in Chart 1.9 shows that 45 compounds contain at least one of silane groups as the end group, that is, important protecting groups for terminal alkynes. Electrochemical properties of monomeric tetraethynylethenes **149**, **152**, **154**, and **155** were performed in 0.1M solution of Bu<sub>4</sub>NPF<sub>6</sub> in THF using a Hg working electrode, and compared with those of oligomeric derivatives.<sup>28c</sup> Through electrochemical studies the authors concluded that the monomers and oligomers based on tetraethynylethene underwent successive reductive electron transfers and their reduction products were chemically stable on the time-scale of the electrochemical experiments. Donor/acceptor-substituted tetraethynylethenes **159**–

**194**, more than a half of cruciforms in Chart 1.9, were prepared *via* Pd-catalyzed Sonogashira cross-coupling reactions,<sup>28f</sup> and their electronic and photonic properties were investigated with a special emphasis on the effects caused by degree and pattern of donor/acceptor substitution around the central tetraethynylethene core. To show the structure-property relationships, they measured the macroscopic third-order nonlinear optical susceptibility for compounds **158**, **162**, **165**, **173**, **174**, **177**, **179**, **181**, **184**, **186–188**, and **195**.<sup>28e</sup> One of important properties of tetraethynylethene core is reversible photoisomerization between *cis* and *trans* forms.<sup>28g</sup> This property was summed with the reversible electrocyclization property of dihydroazulene (DHA) unit, which can be transformed into a vinylheptafulvene (VHF) moiety upon irradiation, and a proton sensitive *N,N*-dimethylanilino (DMA) group. Compound **198** consists of all three pieces, and it can be isomerized into compound **197** under irradiation step with 366 nm of UV light.<sup>28h</sup> Electrocyclization of **198** with 411 nm of UV light under acidic condition can cause the transformation of a DHA unit into a VHF moiety, and give **199**. **198** can be regenerated by thermal electrocyclization of **199**. As mentioned above, many of substituted tetraethynylethenes with trialkylsilyl groups, **172**, **177–179**, **201–211**, were employed to synthesize perethynylated dehydroannulenes, expanded radialenes, and radiaannulenes.<sup>28i</sup> Compounds **204–209** could be obtained through *cis-trans* isomerization reactions of compounds **177–179** and **201–203**. Compounds **156**, **157**, **196**, **200**, and **212**, which were not studied by Diederich's group, were introduced by four research groups. Ethylene-centered cruciform **156** and **157** were used as model molecules for computational calculation to study the polarizability and the second hyperpolarizability of **149** and its several lithiated derivatives.<sup>29</sup> Ethylene tetrasubstituted



with 3-hydroxy-3,3-diphenyl-2-propynyl branches, **196**, was synthesized as one of dimethyl acetamide inclusion compounds.<sup>30</sup> Koentjoro et al. had introduced different pathway to synthesize symmetric ethene-based cruciforms decorated with four identical branches.<sup>31</sup> Instead of using Wittig-type reaction and organocopper-lithium reagents, they



**Scheme 1.3** Syntheses of cruciform **149**: (i) *n*-BuLi, HCO<sub>2</sub>Et, -78 °C; (ii) PCC, DCM, 63% (two steps); (iii) CBr<sub>4</sub>, PPh<sub>3</sub>, DCM; (iv) PdCl<sub>2</sub>(PPh<sub>3</sub>)<sub>2</sub>, CuI, BuNH<sub>2</sub>, benzene, 41% (two steps).<sup>28a</sup>

had chosen Sonogashira cross-coupling to introduce terminal alkyne into 1,1,2,2-tetrachloroethene, and synthesized **149**, **152**, and **200**. Che's group recently reported the importance of core part of cross-conjugated compound by comparing molecule **212** with **43** in Chart 1.4.<sup>14a</sup> Using density functional theory (DFT) and time-dependent DFT (TDDFT), they provided a theoretical rationale to show where the heavy-atom effect is. Their results show that neither the high symmetry nor the number of Au<sup>I</sup> ions govern the photophysics of tetragold(I)ethynyl complexes of **212** and **43**; rather, their central ethene and benzene cores play a decisive role: the T<sub>1</sub> excited state is very low-lying with ethene as the central ligand, whereas it is moderately low when benzene is the central bridge.

The synthetic strategy to access the tetraethynylethene cruciforms is shown in Scheme 1.3, using the synthesis of tetrakis(phenylethynyl)ethene as a representative.

Deprotonation of phenylacetylene with *n*-butyllithium is followed by the reduction of ethyl formate gives bis(phenylethynyl)-substituted secondary alcohol. Sequential oxidation of the alcohol species with pyridinium chlorochromate yields the symmetric ketone in 63%. Wittig dihalomethylenation reaction of ketone gives 1,1-dibromo-2,2-bis(phenylethynyl)ethene which is not purified. The final product **149** is obtained through Sonogashira cross-coupling of dibromoethene with two equivalents of phenylacetylene in 41% yield.

## 1.6 Conclusion

Four cruciform families—tetrakis(arylethynyl)benzenes, distyrylbis(arylethynyl)benzenes, tetrakis(arylvinyl)benzenes, and tetraethynylethenes—were introduced in chronological order for each family. Four big research groups, Haley, Bunz, Choi, and Diederich groups, have significantly contributed to the study of each cruciform family to show the effect of terminal donor/acceptor groups on HOMO/LUMO of fully conjugated scaffolds through the measurement of photonic and electronic properties as well as computational calculations. For tetrakis(arylethynyl)benzene and tetraethynylethene families, Haley's and Diederich's groups have mainly focused on the investigations of structure-property relationships of each cruciform family introducing various aryl and silyl groups. Large portion of the study of distyrylbis(arylethynyl)benzene cruciforms was performed by Bunz et al. whose research was very kaleidoscopic from the investigation of donor/acceptor effects on HOMO/LUMO of molecular cruciform to the use of cruciform compounds as sensor materials to detect or to discriminate various

analytes such as metal cations, carboxylic acids, and inorganic anions. Unlike these three research groups, Choi's and others who studied tetra(arylvinyl)benzene cruciforms had focused their research interests on the application of structural and electronic properties of cross-conjugated scaffold to electronic devices such as thin-film transistor and organic light-emitting diode using its semiconducting properties.

The symmetric elements of four cruciform families perhaps make the synthetic strategy to access them straightforward. Four coupling reactions were enough to describe the synthetic pathway to show how to synthesize the huge number of cruciform compounds: a total of 203 cruciform molecules introduced in this chapter. Sonogashira cross-coupling reaction was the most powerful tool to attach ethynyl branches to both benzene and ethene cores. The Horner-Wadsworth-Emmons reaction and Heck reaction were employed to introduce vinyl branches to the benzene core. The ethene core could be obtained through Wittig reaction between the ketone which is the half of cruciform structure with two branches and the ylide of tetrabromomethane.

Considering the number of substituents that were used for the decoration of end-groups of cruciforms, the variation of core structure has not been achieved because of several critical requirements for the core part. To give fully conjugated cross-shaped molecules, the core should also have unsaturated cyclic or conjugated chain structure. Once the core candidate meets this requirement, it has to have at least four positions which can be connected with four branches. The next three chapters of this thesis will introduce heterocycle-based cruciforms constructed around the central benzobisoxazole core.

## Chapter Two

### Synthesis, Computational Studies, and Optical Properties of Benzobisoxazole

#### Cruciforms<sup>32</sup>

##### 2.1 Introduction

Optical and electronic properties of conjugated  $\pi$ -systems, as well as their reactivity, are strongly influenced by their FMOs.<sup>33</sup> In principle, these important characteristics could be predictably engineered through modulations of HOMO and LUMO of a conjugated  $\pi$ -system. Unfortunately, the situation is not quite as simple in reality: FMOs are delocalized and extensively overlap with each other in most conjugated molecules, and thus their independent modification is prevented. In the past two decades, several classes of molecular structures have been designed to spatially isolate (i.e. localize) the two FMOs. Geometrically predominant motif among these platforms is that of a *cruciform*,<sup>34</sup> that is, an X-shaped molecule in which two fully conjugated  $\pi$ -circuits intersect at a central core. Examples of cruciform structures include tetrakis(arylethynyl)benzenes,<sup>12</sup> distyrylbis(arylethynyl)benzenes,<sup>16</sup> tetrastyrylbenzenes,<sup>23</sup> tetrakisalkynylethenes,<sup>28</sup> and biphenyl-based swivel-cruciforms.<sup>35</sup> Not surprisingly, the resulting tunability of cruciforms' optical and electronic properties led to proposed applications of these cruciforms as fluorescent sensors for a variety of analytes,<sup>12,16,17b</sup> organic light-emitters,<sup>36</sup> components of dye-sensitized solar cells,<sup>37</sup> elements for molecular electronics,<sup>17c-d,35,38,39</sup> and nonlinear optics materials.<sup>12,23</sup>

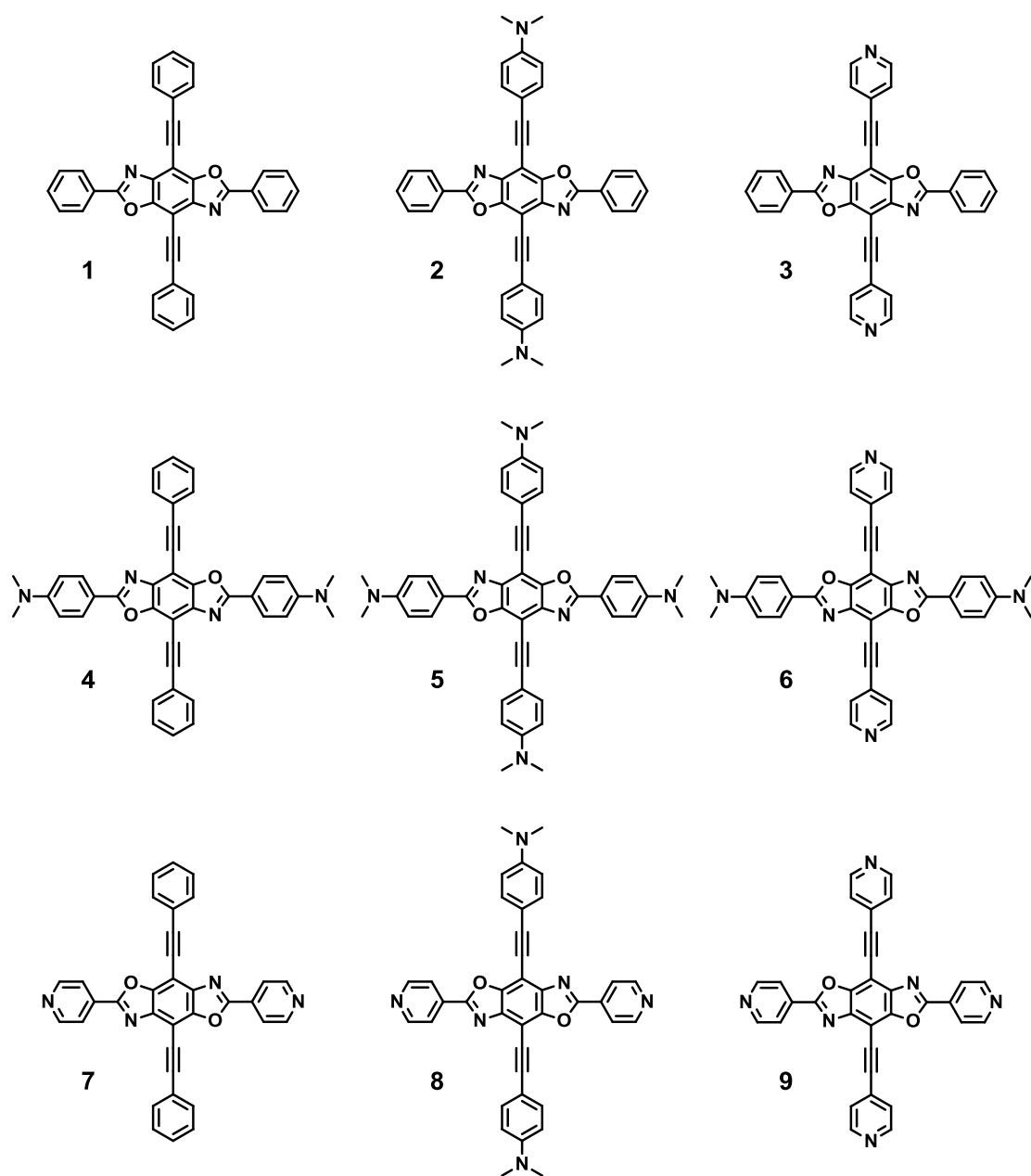
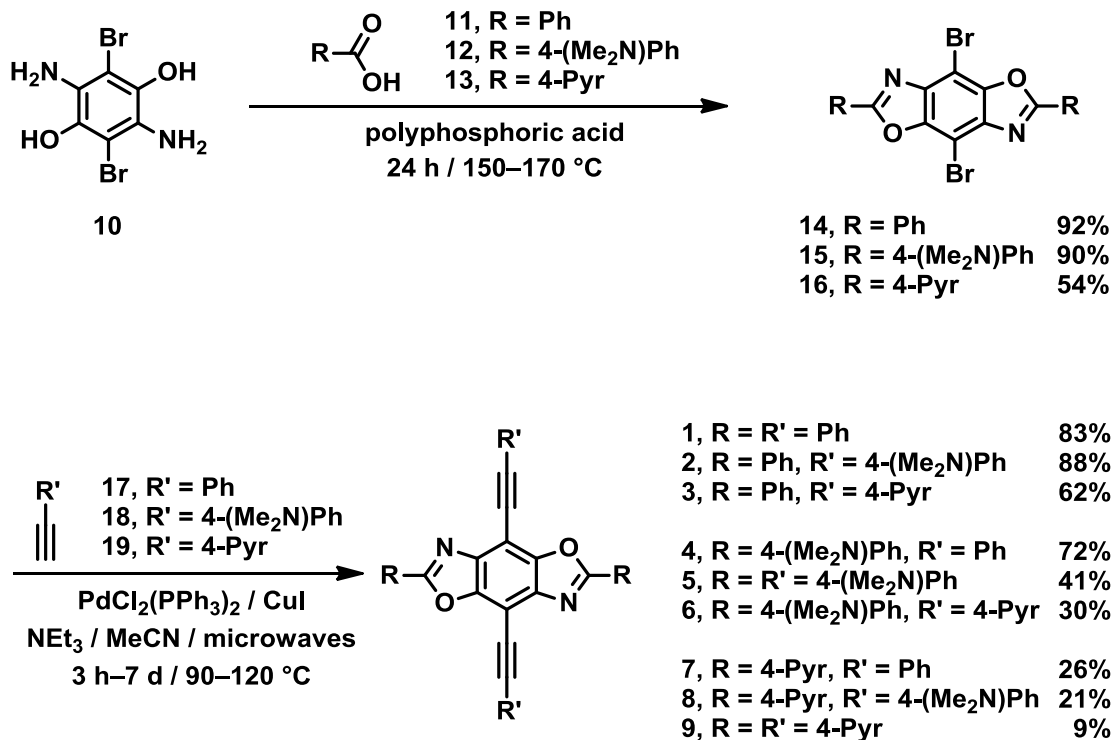


**Chart 2.1** Benzobisoxazole-based cruciform-shaped compounds **1–9** that will be discussed in this chapter.

In previous studies of cruciform systems, summarized in Chapter 1, the central core of the molecule served as a neutral conjugated connector for the four linearly conjugated "arms". Diversification of substituents along these arms was the main strategy for changing both cruciforms' electronic and molecular recognition properties, and mostly depended on the introduction of substituents with resonance and/or inductive donor or acceptor properties. Relatively less attention had been paid to the influence of the central core on the properties of the cruciform. This omission is unusual, as chemical modification of the cruciform's core could dramatically affect its geometry, as well as its orbital, electronic, and optical properties. Furthermore, additional molecular recognition motifs could be designed and introduced into the cruciform's core.

In this chapter, synthesis and detailed computational and spectroscopic characterization of heterocyclic cruciforms with spatially separated FMOs are presented. Fully conjugated cruciform-shaped compounds **1–9** (Chart 2.1) are characterized by the central heterocyclic benzobisoxazole<sup>40,41</sup> nucleus; stemming from this core are the horizontal benzobisoxazole *x*-axis and a vertical bis(arylethynyl)benzene *y*-axis. The terminal aryl substituents along each axis were varied pairwise from electron-neutral phenyl group, through electron-rich 4-(*N,N*-dimethylamino)phenyl substituent, to the electron-poor pyridyl group to explore how substituents' electronic effects influence the separation of FMOs and the associated optical characteristics. This study was motivated by the pioneering reports of modular synthesis of benzobisoxazole cruciform by Nuckolls and coworkers,<sup>42</sup> who used these systems as components of a molecular electronics toolkit.<sup>43</sup> This chapter presents the synthesis of **1–9**, computational investigation of their



**Scheme 2.1** Synthesis of cruciforms **1–9**.

FMOs, their UV/Vis absorption and emission properties, as well as the response of these properties to protonation.

## 2.2 Results and Discussion

### 2.2.1 Synthesis

Cruciform compounds **1–9** were synthesized using two-step protocol described in Scheme 2.1. Dehydrative condensation of 2,5-diamino-3,6-dibromobenzene-1,4-diol (**10**)<sup>44</sup> with carboxylic acids<sup>45</sup> **11–13** produced sparingly soluble intermediates **14–16**, in which the electronic nature of the substituents along the horizontal axis was either neutral (**14**, phenyl), electron-poor (**15**, pyridyl), or electron-rich (**16**, 4-(dimethylamino)phenyl). Each of these intermediates underwent microwave-assisted<sup>46</sup> Sonogashira coupling<sup>47</sup> with

three different terminal alkynes—phenylacetylene (**17**), 4-ethynyl-*N,N*-dimethylaniline (**18**), and 4-ethynylpyridine (**19**)—to afford nine final cruciforms **1–9**. The yields of the final coupling step varied from 9 % to 88 %, and were presumably compromised by (a) the low solubilities of starting materials **14–16**, (b) the possibility of complex formation between pyridine-containing cruciforms and palladium/copper catalysts,<sup>12g</sup> and (c) electronically unfavorable match between some alkyne and aryl bromide coupling partners. Pure cruciform compounds were obtained as yellow to dark red powders after column chromatography and/or recrystallization, and seem to be indefinitely stable in both solid state and solution. All nine cruciforms are soluble in preparatively useful concentrations in chlorinated solvents at 25 °C, and sparingly, but sufficiently for absorption and emission studies (vide infra), in majority of other common organic solvents.

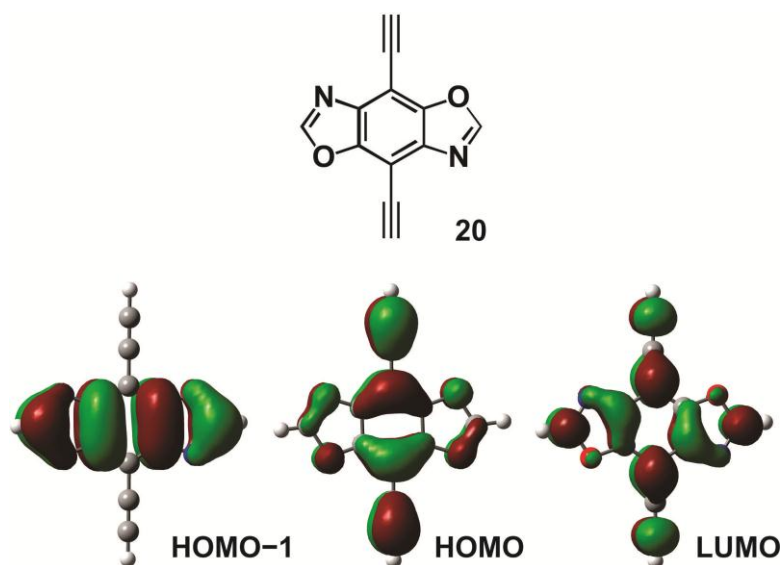


**Figure 2.1** Selected molecular orbitals of the parent bis(ethynyl)benzobisoxazole **20**.



### 2.2.2 Computational Studies

In order to evaluate the spatial separation of FMOs in cruciforms **1–9** and attempt to predict their optical response to acidic analytes, molecular orbital calculations on these systems were performed. Calculations were done using the Gaussian 09W<sup>48</sup> software package and its accompanying graphical interface program GaussView 5.0. The B3LYP hybrid density functional<sup>49</sup> and a standard 3-21G basis set were used for the geometry optimizations. Compounds **6** and **8** were initially optimized within a  $C_s$  symmetry constraint and both converged to structures with  $C_{2h}$  symmetry. Accordingly, the other cruciform structures were optimized within a  $C_{2h}$  symmetry constraint.

An orbital analysis of the parent bis(ethynyl)benzobisoxazole **20** (Figure 2.1) revealed that its HOMO is symmetric ( $b_g$  symmetry in  $C_{2h}$ ) and LUMO antisymmetric ( $a_u$  symmetry in  $C_{2h}$ ) with respect to the molecule's inversion center. Both orbitals have significant density in the central benzene ring, on the oxazole heteroatoms, and along the C≡C bond. The key difference between the two is the orbital density along the oxazole C–H bonds: the HOMO has very little density in that area, but the LUMO does. This means that while both the HOMO and the LUMO can delocalize across the vertical axis of the cruciform, only the LUMO can effectively "spill over" onto the horizontal axis.

This qualitative feature of the parent system translates onto all cruciforms (Figure 2.2–2.4): HOMOs of **1–3**, **5**, and **7–9** have virtually no density in the peripheral rings of the horizontal axis. Significant density in the HOMO along the horizontal axis is found only in cruciforms **4** and **6**, which are both substituted with electron-donating 4-(*N,N*-dimethylamino)phenyl groups. Energetically just below the  $b_g$  HOMO in **20** (0.84 eV lower in energy) is another orbital of  $b_g$  symmetry (denoted as HOMO–1 in Figure 2.1).

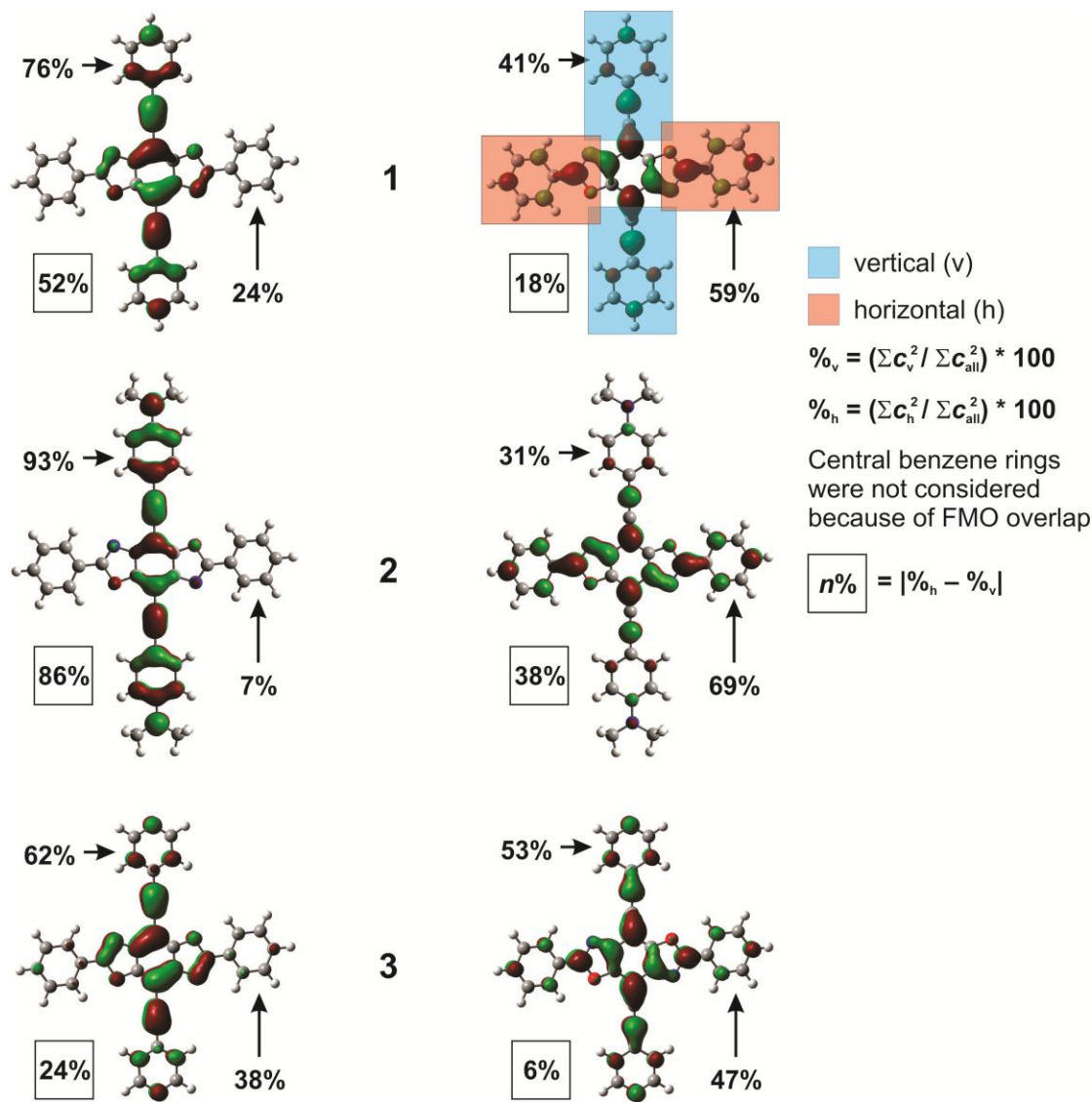


**Figure 2.2** FMOs for cruciforms 1–3. HOMOs are shown on the left of the corresponding cruciform's number, LUMOs on the right of it. The two percentages next to each orbital's representation denote their relative densities along the vertical (%<sub>v</sub>) and horizontal (%<sub>h</sub>) axis of the corresponding molecule (for axes definition, see molecule 1). Number in the square next to each orbital's representation indicates that orbital's relative localization (0% = completely delocalized, 100% = completely localized).

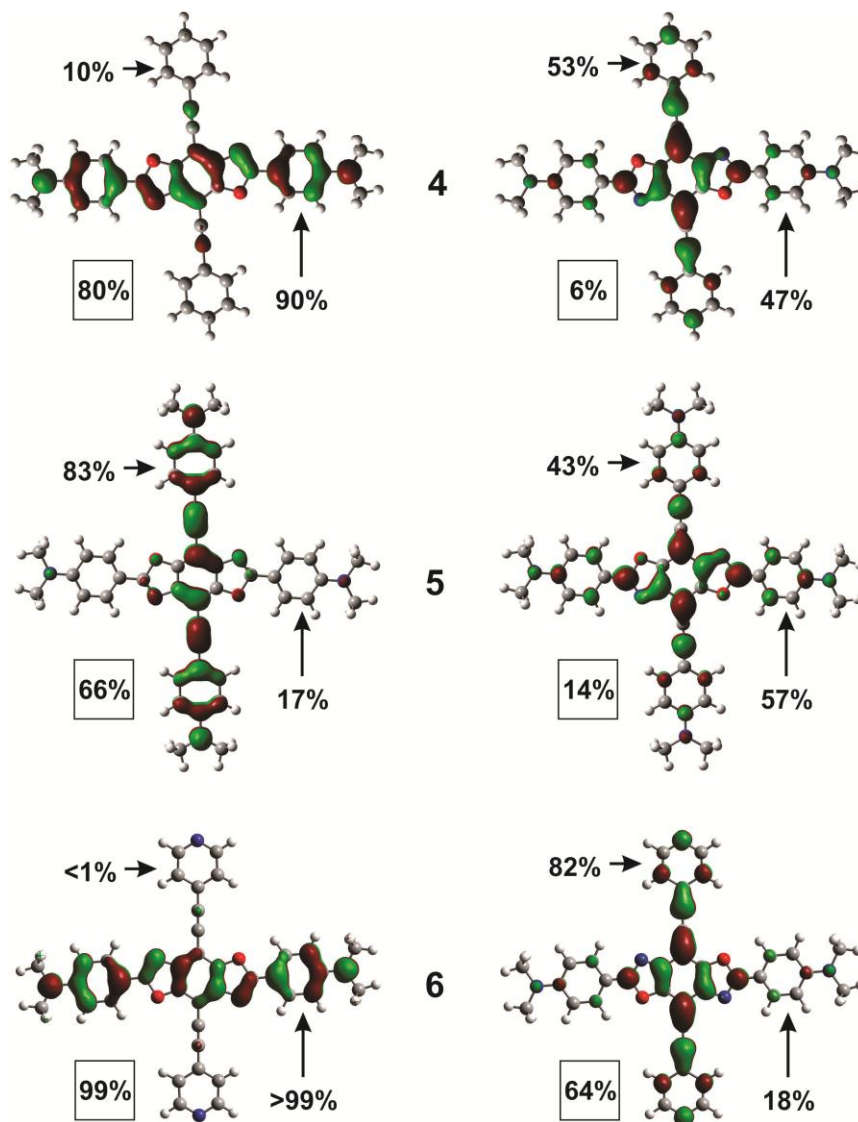


**Figure 2.3** FMOs for cruciforms **4–6**. HOMOs are shown on the left of the corresponding cruciform's number, LUMOs on the right of it.

It has very large amplitudes at the oxazole carbons where the horizontal groups are substituted. Therefore, strong electron donating groups destabilize this orbital so that it becomes the HOMO. In contrast to **4** and **6**, cruciform **5** has four 4-(*N,N*-dimethylamino)phenyl substituents—along both the horizontal and vertical axes—but

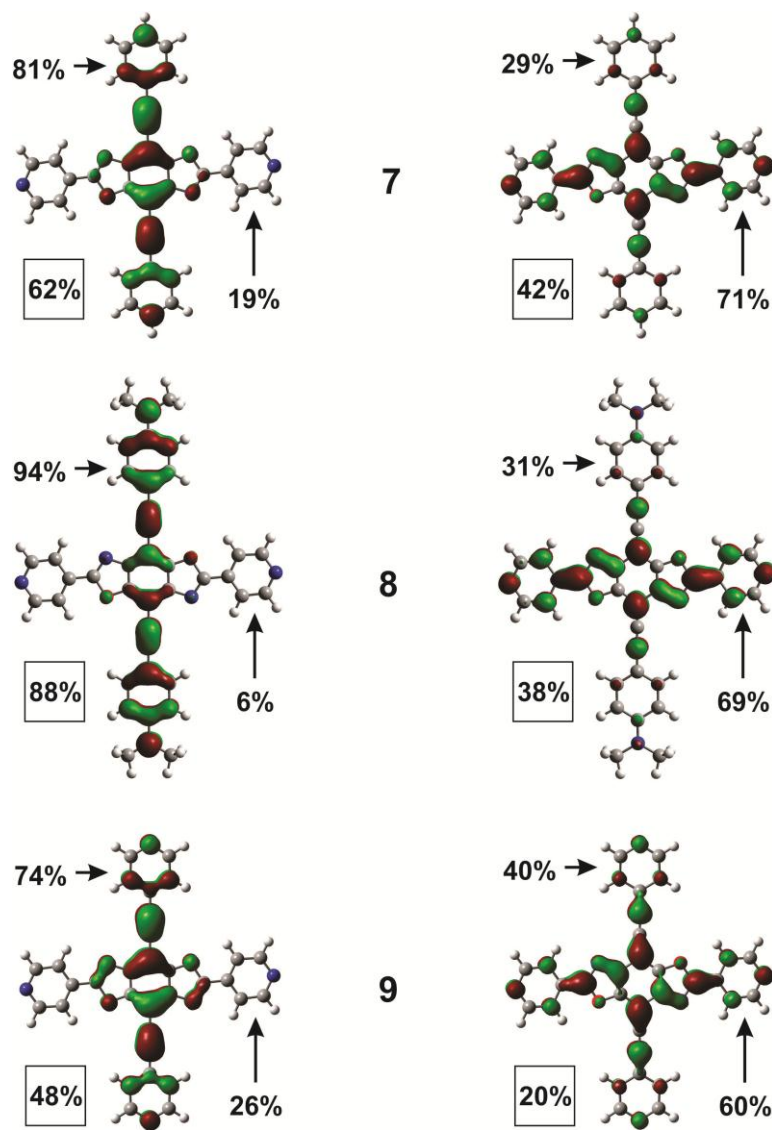


**Figure 2.4** FMOs for cruciforms 7–9. HOMOs are shown on the left of the corresponding cruciform's number, LUMOs on the right of it.

still localizes its HOMO along the vertical axis since the electron donating substituents destabilize both the HOMO and HOMO–1 by approximately the same amount. Analysis of the LUMO distributions is somewhat more complex, as this orbital communicates freely with both the horizontal and vertical axes of the molecule. The substitution is thus

critical in determining whether the LUMO will be localized, and, if so, on which portion of the molecule. To put this analysis of orbital localization onto a quantitative footing, a simple numeric analysis of corresponding orbital coefficients was performed. Each cruciform was divided into its horizontal (shaded in light red, illustrated on compound **1** in Figure 2.2) and vertical (shaded in light blue, illustrated on compound **1** in Figure 2.2) axis. The atoms of the central benzene ring were ignored because they belong to both axes, and all cruciforms show significant FMO overlap in that region. Then, for both the HOMO and the LUMO, squared orbital coefficients for "vertical" atoms were summed, divided by the sum of squared orbital coefficients for all atoms in the cruciform (excluding the central benzene ring), and multiplied by 100. The resulting number represents the percentage of HOMO/LUMO density along the vertical axis of the molecule (%<sub>v</sub>, Figure 2.2). The analogous process was repeated for the horizontal axis (%<sub>h</sub>, Figure 2.2); for each individual orbital, the percentage distributions on the vertical and horizontal axes added up to 100%. The corresponding axis localization percentages are shown next to the individual orbital representations in Figure 2.2–2.4. Finally, each orbitals' localization is described by a single number (Figure 2.2–2.4, numbers in squares) which is defined as localization percentage and is equal to  $|\%_h - \%_v|$ .<sup>50</sup>

Several general trends can be observed. In all cruciforms, the HOMO is more localized than the LUMO, and—regardless of the extent of localization—the HOMO and the LUMO are mostly positioned along different axes of the molecule, except in cruciform **3**. Cruciform **6** has both the most localized HOMO (99%) and the most localized LUMO (64%), and thus has the highest spatial separation of FMOs. Also strongly separated are the FMOs of **2**, **8**, and **7** (to a somewhat attenuated degree).

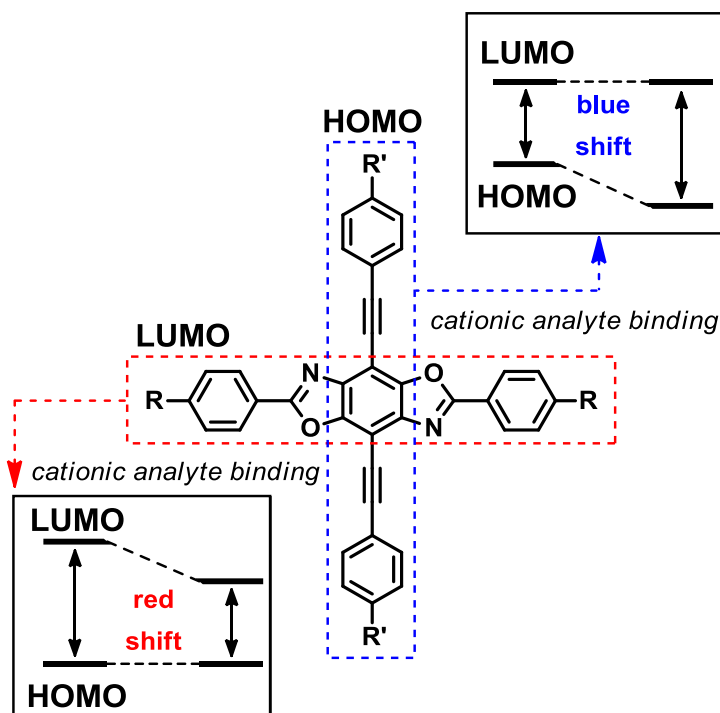


**Figure 2.5** Anticipated optical shifts accompanying cationic analyte binding to different portions of cruciforms with spatially separated FMOs.

Cruciforms **4** and **5** have strongly localized HOMOs (80% and 66%, respectively), but rather delocalized LUMOs (6% and 14%, respectively). Finally, FMOs of cruciforms **1**, **3**, and **9** are relatively delocalized (6–52% localization). These trends are caused by the combination of (a) predisposition of the bis(ethynyl)benzobisoxazole skeleton to localize its HOMO orbital along the vertical axis, and (b) the donor/acceptor substitution pattern, which tends to localize the HOMO along the electron-rich and the LUMO along the electron-poorer axis of the molecule. The latter factor is general and has precedence in Bunz's<sup>16d,j,n,q,s</sup> and Haley's<sup>12b,g,i</sup> systems, but the former effect of the benzobisoxazole core is unique, and it introduces an additional level of control over the orbital separation in cruciform systems.

These computational results suggest what the sensing response of individual cruciforms should be. Cruciforms **2**, **6**, **7**, and **8** would bode well as sensors for protons (and possibly metals), since analyte binding to their basic sites should dominantly affect one of the FMOs and, thus, alter the HOMO–LUMO gap. Protonation of cruciform **2**

**Table 2.1** Optical properties and calculated HOMO–LUMO gaps for cruciforms **1–9**.

Compound	Absorption $\lambda_{\text{max}}$ (nm)	Emission $\lambda_{\text{max}}$ (nm)	Stokes shift ( $\text{cm}^{-1}$ )	Calculated HOMO–LUMO gap (eV, nm)
<b>1</b>	367	407	2678	3.16, 392
<b>2</b>	443	529	3670	2.47, 502
<b>3</b>	368	419	3308	3.24, 383
<b>4</b>	437	497	2763	2.98, 416
<b>5</b>	421	486	3177	2.87, 432
<b>6</b>	458	544	3452	2.79, 444
<b>7</b>	367	439	4469	3.01, 412
<b>8</b>	468	597	4617	2.44, 508
<b>9</b>	367	409	2798	3.17, 391

should occur at its basic dimethylaniline sites; thus the HOMO should be stabilized, leading to a blue (hypsochromic) shift in absorption (Figure 2.5). In contrast, cruciform **7** should be protonated along the horizontal pyridine-bearing axis, leading to a stabilized LUMO and a corresponding red (bathochromic) shift. Donor-acceptor substituted compounds **6** and **8** present interesting cases because of their two possible non-equivalent protonation sites. Protonation at their pyridine-based LUMOs would cause a red shift, while protonation along the dimethylaniline-centered HOMO would cause a blue shift. With a sufficient amount of acid, both shifts could occur in a sequence—but it is hard to

predict which one would be first: tabulated  $pK_a$  values for parent dimethylaniline and pyridine are virtually identical (5.15 and 5.25, respectively) and can vary by as many as four  $pK_a$  units depending on the substituent in the 4-position.<sup>51</sup> In the next two sections, the way to establish the order of protonation using optical responses of cruciforms **1–9** will be explained.

Cruciforms **4** and **5** have only one of their frontier orbitals localized. In **4**, protonation along the horizontal axis should affect both FMOs, but would exhibit significantly larger stabilizing effect on HOMO—thus presumably leading to a blue shift analogous to that in **2**. In **5**, basic groups are positioned along both the horizontal and the vertical axes. Protonation of "vertical" nitrogens would lead to a blue shift (stabilized HOMO), while protonation of "horizontal" basic groups should lead to a (smaller) red shift. Again, order of protonation is difficult to predict *a priori*, and had to be elucidated experimentally.

Finally, cruciforms **1**, **3**, and **9** are expected to show uneventful optical response to protonation, as any change would likely affect both the HOMO and the LUMO to a comparable extent.

Computations also produced HOMO–LUMO energy gap values (Table 2.1), which roughly correlate with  $\lambda_{\text{max}}$  values obtained from UV/Vis spectra (vide infra).

### 2.2.3 Optical Properties

Dilute solutions of cruciforms **2**, **4–6**, and **8** are strongly colored (Figure 2.6A). Under a hand-held UV lamp ( $\lambda_{\text{exc}} = 365$  nm), all of the prepared cruciforms also exhibit bright emission (Figure 2.6B). Emission wavelengths of donor–acceptor systems (e.g. **8**,



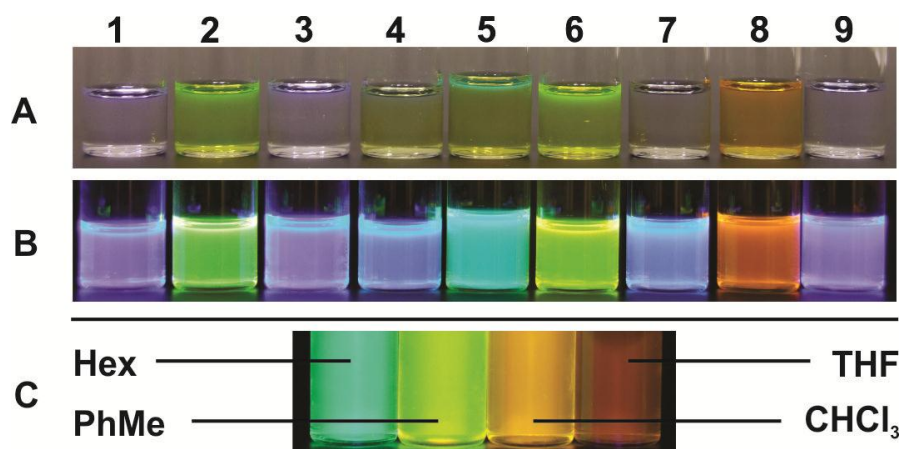


**Figure 2.6** (A) Colors of CH<sub>2</sub>Cl<sub>2</sub> solutions of cruciforms **1–9** under visible light. (B) Fluorescence colors of CH<sub>2</sub>Cl<sub>2</sub> solutions of **1–9** under light from a handheld UV lamp ( $\lambda_{\text{exc}} = 365$  nm). (C) Strong fluorescence solvatochromic behavior of **8** ( $\lambda_{\text{exc}} = 365$  nm).

Figure 2.6C) show a strong solvent dependence, suggesting a charge-separated excited state.<sup>12e,12g,16q</sup>

All prepared cruciforms were analyzed by UV/Vis absorption and emission spectroscopies in dilute CH<sub>2</sub>Cl<sub>2</sub> solutions. Their normalized absorption and emission spectra are shown in Figure 2.7, grouped into three sets of three spectra each that correspond to cruciforms with an identical horizontal axis. In general, electronic absorption spectra of cruciforms **1–9** are characterized by two broad bands: the lower energy band appearing between approx. 350 and 500 nm, and the higher energy absorption between approx. 300 and 400 nm. UV/Vis spectra of **1** and **3** are almost superimposable; in contrast, the lowest energy absorption of **2** is bathochromically shifted by 75 nm, indicating possible intramolecular charge transfer (Figure 2.7, top left).<sup>12e,12g,16q</sup> The orbital pictures are consistent with this explanation. The FMOs of **2** are

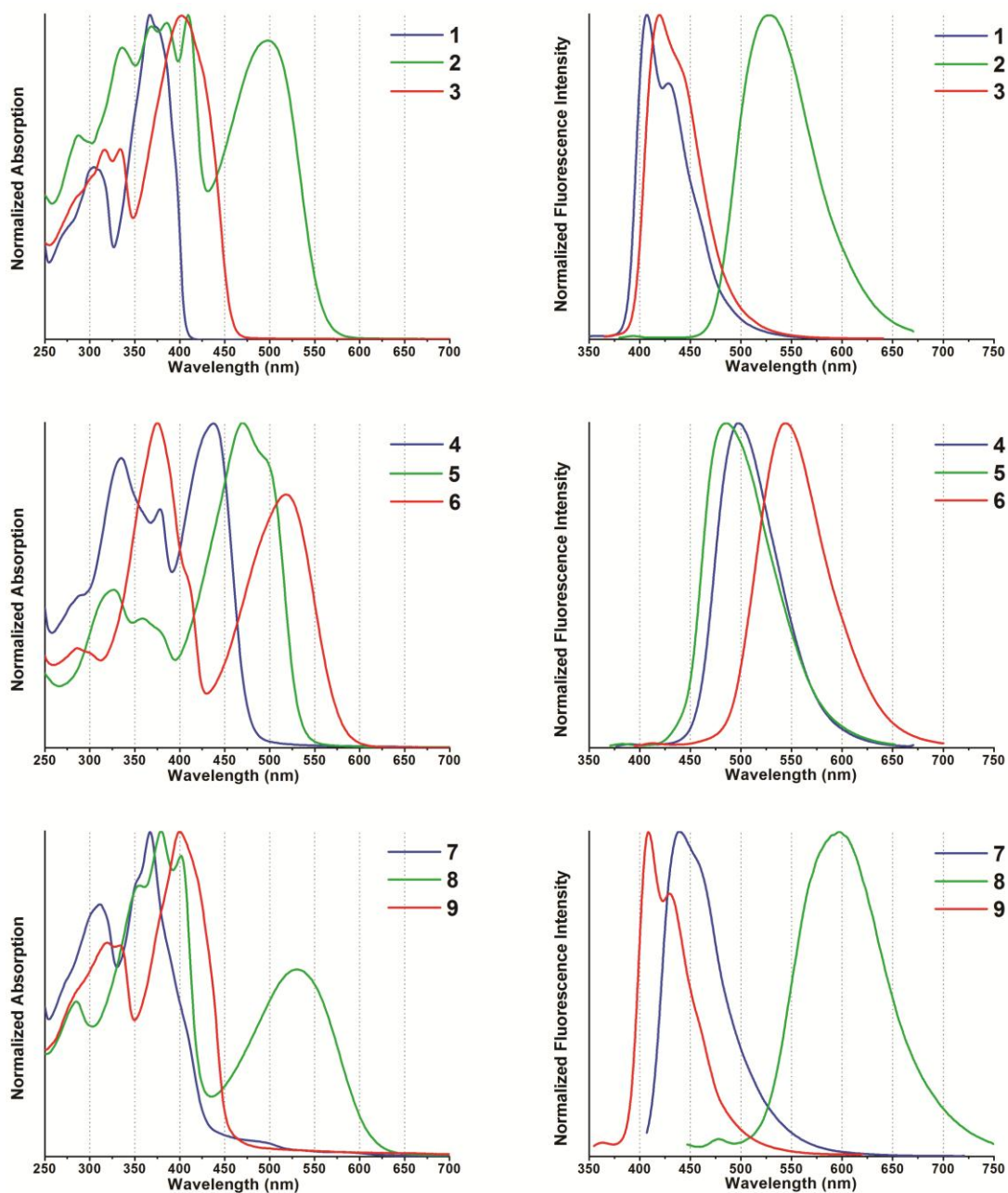


**Figure 2.7** Normalized UV/Vis absorption (left) and emission (right) spectra of cruciforms 1–9 in  $\text{CH}_2\text{Cl}_2$ . Excitation wavelengths used were 320 (1), 350 (2 and 4), 335 (3), 341 (5), 356 (6), 377 (7), 417 (8), and 325 (9) nm.

spatially significantly more separated than the delocalized FMOs of **1** and **3**. This situation also occurs in the spectra of **7–9** (Figure 2.7, bottom left). The absorption spectra of **7** and **9** are almost superimposable, but in their emission spectra,  $\lambda_{\text{max}}$  for **7** is slightly bathochromically shifted, consistent with a greater degree of donor–acceptor character (relative to **9**). A 100-nm shift to lower energies in the spectrum of **8** (with spatially separated orbitals) is indicative of charge transfer in the excited state. In compounds **4–6**, qualitative differences in UV/Vis spectra are the largest, but their  $\lambda_{\text{max}}$  values are quite similar, in the 430–457 nm range. As expected, compound **6** has the highest  $\lambda_{\text{max}}$  among the three, owing to its significantly localized FMOs and presumably the strongest charge transfer in the excited state. The normalized emission spectra (Figure 2.7) parallel these observations very closely.

#### 2.2.4 Optical Response to Protonation

Since cruciforms **1–9** carry basic pyridyl, 4-(*N,N*-dimethylamino)phenyl, and oxazole groups, the next series of experiments examined their optical (UV/Vis absorption and emission) response to protonation with trifluoroacetic acid (TFA). All of these experiments were performed in dilute CH<sub>2</sub>Cl<sub>2</sub> solutions and their results have been summarized in Figure 2.8–2.10 for both absorption and emission spectra. As predicted by the orbital analysis, the absorption spectra of cruciforms with poorly localized FMOs—that is, compounds **1**, **3**, and **9**—showed negligible response to protonation. However, the changes in their emission spectra were more dramatic. Compound **1** showed the quenching of fluorescence at high TFA concentrations, which we tentatively attribute to the protonation of oxazole nitrogen atoms ( $\text{p}K_{\text{a}} = 0.8$ ) which is possibly protonated by

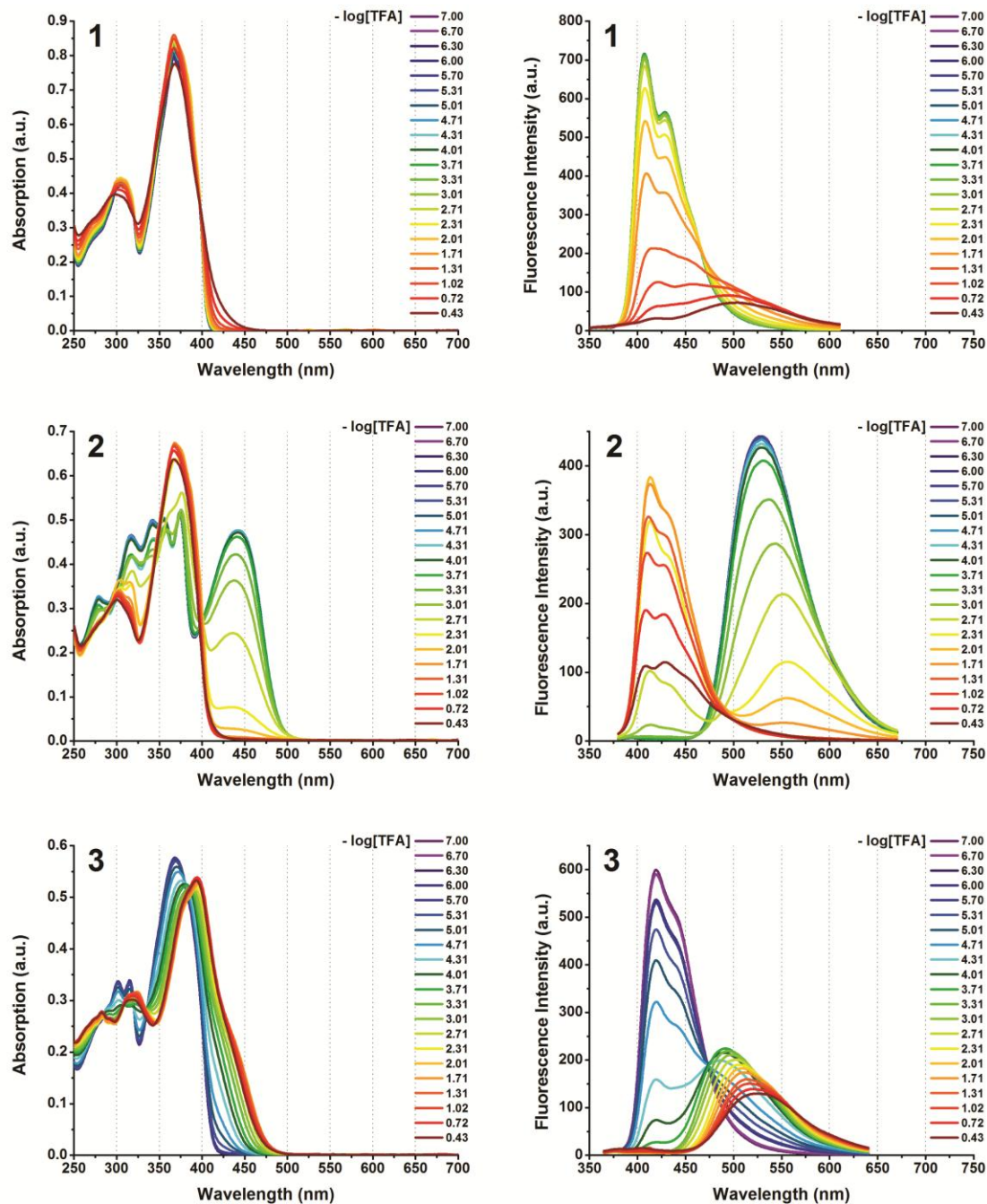


**Figure 2.8** Changes in UV/Vis absorption (left) and emission (right) spectra of cruciforms **1–3** in  $\text{CH}_2\text{Cl}_2$  in response to protonation with TFA. Excitation wavelengths: 320 (**1**), 350 (**2**), and 335 (**3**) nm.



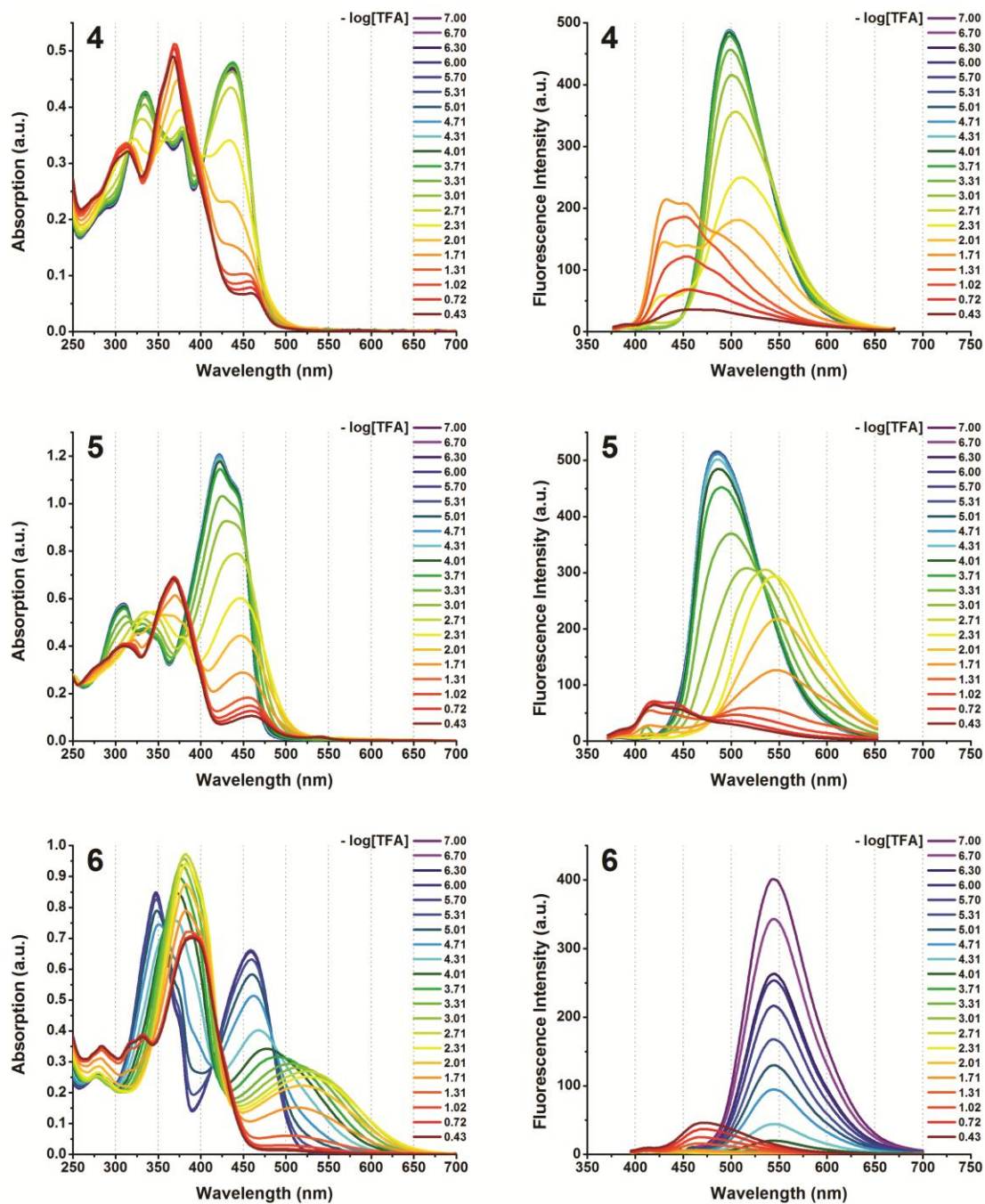


**Figure 2.9** Changes in UV/Vis absorption (left) and emission (right) spectra of cruciforms **4–6** in  $\text{CH}_2\text{Cl}_2$  in response to protonation with TFA. Excitation wavelengths: 350 (**4**), 341 (**5**), and 356 (**6**) nm.

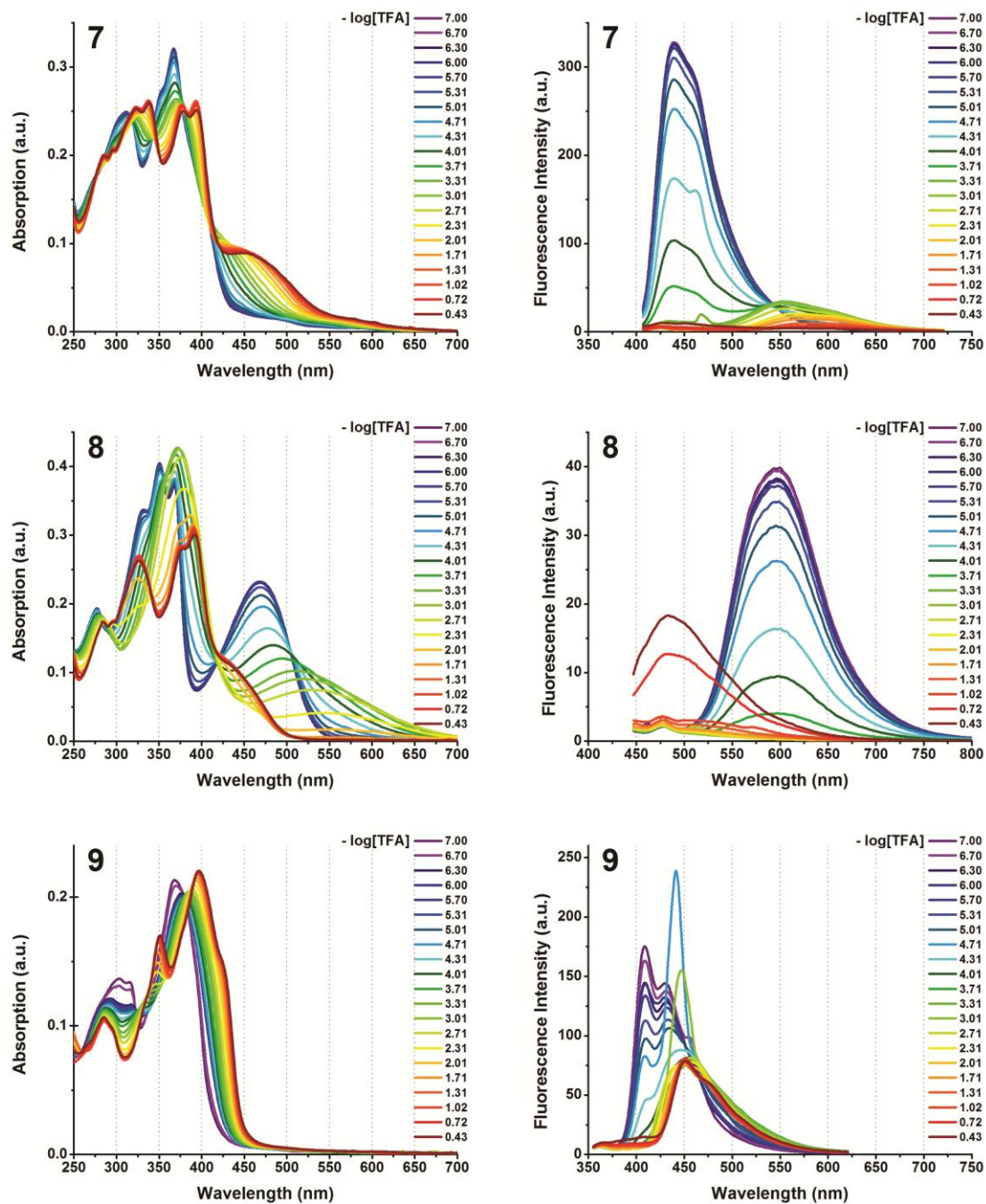


**Figure 2.10** Changes in UV/Vis absorption (left) and emission (right) spectra of cruciforms **7–9** in  $\text{CH}_2\text{Cl}_2$  in response to protonation with TFA. Excitation wavelengths: 377 (**7**), 417 (**8**), and 325 (**9**) nm.

TFA ( $pK_a = 0.2$ ). In the emission spectra of compounds **3** and **9**, a significant red shift was observed around  $-\log[\text{TFA}] = 3.71$ , consistent with pyridine protonation.<sup>52</sup>

The spectra of cruciforms **4** and **5**, which have partially separated FMOs, are quite diagnostic. Protonation of **4** occurs on the dimethylamino group, causing a pronounced blue shift in both absorption and emission spectra, that is consistent with stabilization of its HOMO. In **5**, a slight red shift in both absorption and emission, most apparent at  $-\log[\text{TFA}] = 2.31$ , is followed by a more pronounced blue shift with continued acidification. Such behavior is consistent with the initial protonation along the horizontal dimethylamino groups, which should stabilize the LUMO, and secondary protonation along the vertical axis, which should strongly stabilize the more localized HOMO.

Cruciform **2**, with its strongly separated FMOs, is protonated at its dimethylamino groups positioned along the vertical axis. Upon protonation, stabilization of the HOMO is apparent from the blue shifts in both absorption and emission spectra. As in **1**, the blue-shifted emission is partially quenched in very acidic solutions, which I attribute to the onset of protonation of oxazole rings. Cruciform **7** exhibits a rather moderate red shift in absorption and quenching of fluorescence upon protonation; the former effect is consistent with dominant protonation along its LUMO-bearing horizontal axis, but is puzzlingly unpronounced—given the strong spatial separation of calculated FMOs. Together with the results on protonation of **5**, this observation would suggest that both pyridyl and dimethylamino groups are more basic when positioned along the cruciforms' horizontal axes. This effect is probably caused by the influence of the HOMO–1 orbital which donates electron density to the substituents positioned along the horizontal axes,

and is especially relevant in the case of electron-donating 4-(*N,N*-dimethylamino)phenyl substituents.

Finally, spectra of donor–acceptor cruciforms **6** and **8** reveal a distinct two-step optical response to protonation. Initially, protonation causes a red shift in absorption spectra of both compounds, most pronounced at  $-\log[\text{TFA}] = 3.01$ . Quenching of emission from both compounds suggests that the initial protonated species is non-fluorescent. The red shift is explained by the initial protonation of the pyridine nitrogen atoms in both cruciforms, regardless of their positioning on horizontal or vertical axis. These results stand in contrast to those of Bunz<sup>16n</sup> and Haley,<sup>12g</sup> who observed that *N,N*-dibutylanilines protonate before pyridines. This difference may be caused by the stronger stabilization of protonated pyridines through conjugation with the 4-substituent (vs. protonated anilines).<sup>53</sup> With continued acidification, both **6** and **8** recover their fluorescence, which is now blue-shifted. Absorption maxima are also blue shifted, indicative of a second protonation along the electron-rich HOMO-bearing axis.

All observed protonation-induced optical changes could be fully reversed by addition of a base such as Et<sub>3</sub>N.

## 2.3 Conclusions and Outlook

In summary, a family of benzobisoxazole-based cruciform-shaped conjugated molecules have been synthesized and exhaustively characterized. These materials are characterized by modular FMOs, which can be localized on different portions of the molecule by design. While this behavior parallels that observed previously in Bunz' distyrylbis(arylethynyl)benzenes and Haley's tetrakis(arylethynyl)benzenes, benzobis-



oxazole cruciforms have at least three additional features that warrant their further study. First, benzobisoxazole core has four lone-pair electrons that are possibly protonated in acidic condition and could participate in hydrogen bonding interaction with H-bond donor molecules. Next, the horizontal and vertical axes of these cruciforms are electronically quite different, and their arrangement enforces a certain degree of frontier orbital separation that is independent of substitution due to the inductive effect of oxygens and nitrogens on the center of cruciforms. This "inherent" FMO separation in **1–9** is quite moderate, and intervention of substituents is still needed to produce systems with highly localized HOMOs and LUMOs. Finally, four arms are evenly positioned around the central benzobisoxazole in 90 ° angle between two conjugated circuits: therefore, the charge transfer being dependent upon the distance between donor and acceptor can evenly occur from one terminal to two adjacent terminals. This structural feature could not be achieved using benzene-based cruciforms of Haley and Bunz groups.

These results open several avenues of future investigation. Synthetically, incorporation of different donor and acceptor groups, as well as modification of their arrangement around cruciforms' axes would be of interest.<sup>12e,12g</sup> In addition, more sophisticated functionalities could be included in the structures of these molecules to render their molecular recognition properties specific for individual cationic, anionic, and neutral analytes. Cruciforms **1–9** are potentially appealing as materials with non-linear optical properties and semiconducting properties.<sup>7a,54</sup> On a conceptual note, other substructures could be designed as central cores of future molecular cruciforms that would exhibit even larger inherent separation of FMOs—perhaps entirely independent of substitution.

## 2.4 Experimental Section

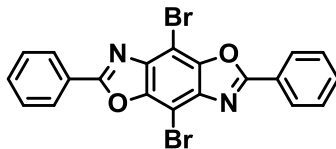
### 2.4.1 General Experimental Methods

Reagents and solvents were purchased from commercial suppliers and used without further purification. Compounds  $\text{PdCl}_2(\text{PPh}_3)_2$ <sup>55</sup> and 2,5-diamino-3,6-dibromohydroquinone (**10**)<sup>44a</sup> were prepared according to literature procedures. Microwave-assisted reactions were performed in a Biotage Initiator 2.0 microwave reactor, producing monochromatic microwave radiation with the frequency of 2.45 GHz.

Mass spectral measurements were performed by the Mass Spectrometry Facility of the Department of Chemistry and Biochemistry at the University of Texas at Austin. NMR spectra were obtained on JEOL ECX-400 and ECA-500 spectrometers, with working frequencies (for  $^1\text{H}$  nuclei) of 400 and 500 MHz, respectively. All  $^{13}\text{C}$  NMR spectra were recorded with simultaneous decoupling of  $^1\text{H}$  nuclei.  $^1\text{H}$  NMR chemical shifts are reported in ppm units relative to the residual signal of the solvent ( $\text{CDCl}_3$ : 7.26 ppm,  $\text{DMSO}-d_6$ : 2.50 ppm). All NMR spectra were recorded at 25 °C. Infrared spectra were recorded on a Perkin-Elmer Spectrum 100 FT-IR spectrophotometer using Pike MIRacle Micrometer pressure clamp. UV-Vis and fluorescence spectra were recorded on a Perkin-Elmer Lambda 25 UV/Vis spectrophotometer and a Perkin-Elmer Fluorescence Analyzer LS-45 fluorimeter, respectively.

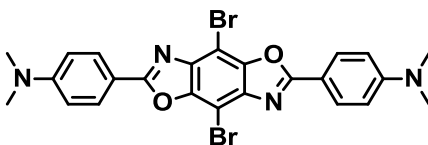
Column chromatography was carried out on silica gel 60, 32–63 mesh. Analytical TLC was performed on Merck aluminum-backed silica gel plates.

#### 2.4.2 Synthesis of 2,6-Diphenyl-4,8-dibromobenzo[1,2-*d*;4,5-*d'*]bisoxazole (**14**)



Benzoic acid (**11**, 902 mg, 7.38 mmol) and compound **10** (1.00 g, 3.36 mmol) were mixed with polyphosphoric acid (14.0 g) in a 100 mL round-bottom flask equipped with a Friedrich condenser. The mixture was heated at 150 °C for 25 h, and was then cooled, neutralized with aqueous 1M NaOH solution, and filtered. The dark solid was washed with H<sub>2</sub>O, EtOH, and then Et<sub>2</sub>O. The solid was air-dried to give 1.45 g (92 %, 3.08 mmol) of crude **14** (mp >350 °C, with decomposition). Due to its extremely low solubility, this material was only partially characterized and then used without further purification. **14**: IR (neat): 1608 (w), 1564 (m), 1490 (w), 1453 (w), 1319 (m), 1223 (m), 1054 (m), 1025 (m), 974 (m), 912 (m), 873 (m), 773 (m), 719 (m), 693 (s), 683 (s) cm<sup>-1</sup>. <sup>1</sup>H NMR (CDCl<sub>3</sub>, 500 MHz):  $\delta$  8.37 (m, 4H), 7.58 (m, 6H) ppm. <sup>13</sup>C NMR (CDCl<sub>3</sub>, 125 MHz):  $\delta$  164.8, 147.2, 139.9, 132.6, 129.3, 128.4, 126.4, 92.1 ppm. HRMS (ESI/[M+H]<sup>+</sup>) calcd. for C<sub>20</sub>H<sub>11</sub>Br<sub>2</sub>N<sub>2</sub>O<sub>2</sub>: 468.9187. Found: 468.9181.

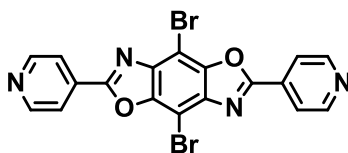
#### 2.4.3 Synthesis of 2,6-Di(*p*-(*N,N*-dimethylamino)phenyl)-4,8-dibromobenzo[1,2-*d*;4,5-*d'*]bisoxazole (**15**)



In a 100 mL round-bottom flask equipped with a Friedrich condenser, compound **10** (1.00 g, 3.36 mmol) and 4-(*N,N*-dimethylamino)benzoic acid (**12**, 1.22 g, 7.38 mmol)

were mixed with polyphosphoric acid (14.0 g) and stirred for 24 h at 160 °C. The mixture was then cooled, neutralized with aqueous 1M NaOH solution, and filtered. The dark solid was washed with H<sub>2</sub>O, EtOH, and then Et<sub>2</sub>O. After air-drying, the solid was dissolved in 9:1 CH<sub>2</sub>Cl<sub>2</sub>/MeOH mixture (200 mL), and then passed through a short silica gel column. The solvent was removed in vacuo to give 1.68 g (90%, 3.02 mmol) of **15** (mp >350 °C, with decomposition). **15**: IR (neat): 1612 (s), 1514 (s) 1372 (m), 1316 (m), 1224 (m), 1185 (s), 1055 (m), 904 (m), 870 (m), 812 (m) cm<sup>-1</sup>. <sup>1</sup>H NMR (CDCl<sub>3</sub>, 400 MHz):  $\delta$  8.19 (d, <sup>3</sup>J<sub>H-H</sub>=9.2 Hz, 4H), 6.77 (d, <sup>3</sup>J<sub>H-H</sub>=9.2 Hz, 4H), 3.10 (s, 12H) ppm. Because of the low solubility of **15**, a satisfactory <sup>13</sup>C NMR spectrum could not be obtained. HRMS (ESI/[M+H]<sup>+</sup>) calcd. for C<sub>24</sub>H<sub>21</sub>Br<sub>2</sub>N<sub>4</sub>O<sub>2</sub>: 555.0031. Found: 555.0026.

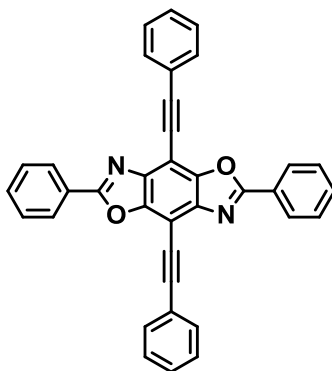
#### 2.4.4 Synthesis of 2,6-Dipyridin-4-yl-4,8-dibromobenzo[1,2-*d*;4,5-*d'*]bisoxazole (**16**)



In a 100 mL round-bottom flask equipped with a Friedrich condenser, compound **10** (2.45 g, 8.22 mmol) and isonicotinic acid (**13**, 3.07 g, 24.7 mmol) were mixed with polyphosphoric acid (20.0 g). The mixture was heated to 170 °C, and stirred at that temperature for 25 h. After cooling, the suspension was neutralized with cold aqueous 1M NaOH solution, and filtered. The dark solid was washed with H<sub>2</sub>O, EtOH, and then Et<sub>2</sub>O. After air-drying, the solid was dissolved in 9:1 CH<sub>2</sub>Cl<sub>2</sub>/MeOH mixture (200 mL), and then passed through a short silica gel column. Product was eluted using a CH<sub>2</sub>Cl<sub>2</sub>/MeOH/Et<sub>3</sub>N mixture (18:2:1). Solvent was removed in vacuo to give 2.09 g

(54%, 4.42 mmol) of **16** (mp >350 °C, with decomposition). **16**: IR (neat): 1608 (w), 1576 (m), 1548 (m), 1490 (w), 1414 (s), 1357 (w), 1322 (m), 1279 (w), 1230 (s), 1060 (s), 990 (m), 971 (w), 920 (w), 876 (m), 830 (s), 740 (w), 723 (w), 697 (s), 687 (s) cm<sup>-1</sup>. <sup>1</sup>H NMR (THF-*d*<sub>8</sub>, 500 MHz): δ 8.86 (d, <sup>3</sup>*J*<sub>H-H</sub> = 5.7 Hz, 4H), 8.18 (d, <sup>3</sup>*J*<sub>H-H</sub> = 5.7 Hz, 4H) ppm. <sup>13</sup>C NMR (THF-*d*<sub>8</sub>, 125 MHz): δ 163.9, 152.2, 148.6, 141.3, 134.0, 121.9, 93.6 ppm. HRMS (ESI/[M+H]<sup>+</sup>) calcd. for C<sub>18</sub>H<sub>9</sub>Br<sub>2</sub>N<sub>4</sub>O<sub>2</sub>: 470.9092. Found: 470.9087.

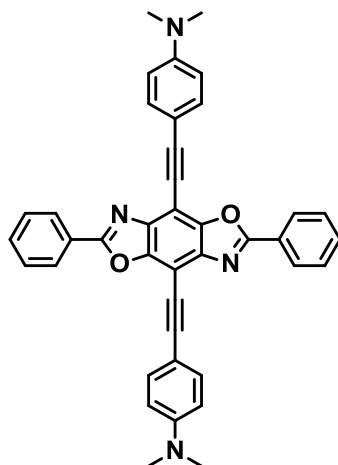
#### 2.4.5 Synthesis of Cruciform 1



Phenylacetylene (**17**, 391 mg, 3.83 mmol) was added to a thick-walled microwave pressure vial that contained a mixture of compound **14** (300 mg, 0.638 mmol), PdCl<sub>2</sub>(PPh<sub>3</sub>)<sub>2</sub> (90 mg, 0.13 mmol), CuI (24 mg, 0.13 mmol), Et<sub>3</sub>N (5 mL), and MeCN (5 mL). The vial was sealed and exposed to microwave irradiation for 3 h at 100 °C. After cooling, solvents were removed under reduced pressure, and the crude solid was purified by column chromatography, eluting first with pure CH<sub>2</sub>Cl<sub>2</sub>, and then successively with CH<sub>2</sub>Cl<sub>2</sub>/MeOH mixtures in 97:3, 19:1, and 9:1 ratios. The solvent was removed under reduced pressure to give 270 mg (83%, 0.527 mmol) of **1** (mp 305 °C, with decomposition). **1**: UV-Vis (CH<sub>2</sub>Cl<sub>2</sub>): λ<sub>max</sub> (log ε) = 304 (6.62), 367 (6.90) nm. IR (neat):

3067 (w), 2221 (w), 1609 (w), 1562 (m), 1488 (m), 1451 (m), 1383 (w), 1340 (m), 1278 (m), 1079 (w), 1062 (m), 1027 (m), 977 (m), 918 (m), 777 (m), 755 (m), 723 (m), 697 (s), 687 (s)  $\text{cm}^{-1}$ .  $^1\text{H}$  NMR ( $\text{CDCl}_3$ , 500 MHz):  $\delta$  8.42 (m, 4H), 7.80 (m, 4H), 7.58 (m, 6H), 7.46 (m, 6H) ppm.  $^{13}\text{C}$  NMR ( $\text{CDCl}_3$ , 125 MHz):  $\delta$  164.8, 149.0, 141.1, 132.4, 132.3, 129.4, 129.2, 128.7, 128.4, 126.8, 123.0, 100.5, 98.9, 80.0 ppm. LRMS (ESI/[M+H] $^+$ ) calcd. for  $\text{C}_{36}\text{H}_{21}\text{N}_2\text{O}_2$ : 513.15. Found: 513.33. HRMS calcd. for  $\text{C}_{36}\text{H}_{21}\text{N}_2\text{O}_2$ : 513.1603. Found: 513.1601. Anal. calcd. for  $\text{C}_{36}\text{H}_{20}\text{N}_2\text{O}_2$ : C, 84.36; H, 3.93; N, 5.47. Found: C, 84.01; H, 3.52; N, 5.39.

#### 2.4.6 Synthesis of Cruciform 2

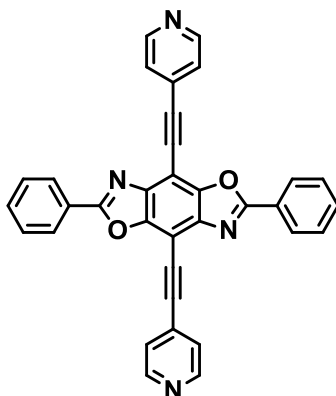


In a nitrogen-flushed round-bottom flask, anhydrous  $\text{K}_2\text{CO}_3$  (1.06 g, 7.66 mmol) was added to a solution of 2-[4-(*N,N*-dimethylamino)phenyl]trimethylsilylethyne<sup>56</sup> (832 mg, 3.83 mmol) in a mixture of MeOH (5 mL) and THF (5 mL). After stirring for 30 min, the reaction mixture was filtered through celite. The solvent was removed under reduced pressure, to yield crude 4-ethynyl-*N,N*-dimethylaniline (**18**), which was used

without purification in the next step. To minimize manipulations of this somewhat sensitive compound, we assumed a 95% yield for this reaction.

The entire amount of **18**, prepared as above described, was added to a thick-walled microwave pressure vial that contained a mixture of compound **14** (300 mg, 0.638 mmol), PdCl<sub>2</sub>(PPh<sub>3</sub>)<sub>2</sub> (90 mg, 0.13 mmol), CuI (24 mg, 0.13 mmol), Et<sub>3</sub>N (5 mL), and MeCN (5 mL). The vial was sealed and exposed to microwave irradiation for 3 h at 100 °C. After cooling, solvents were removed under reduced pressure, and the crude solid was purified by column chromatography, eluting first with pure CH<sub>2</sub>Cl<sub>2</sub>, and then successively with CH<sub>2</sub>Cl<sub>2</sub>/MeOH mixtures in 97:3, 19:1, and 9:1 ratios. The solvent was removed under reduced pressure to give 338 mg (88%, 0.565 mmol) of pure **2** (mp >350 °C, with decomposition). **2**: UV-Vis (CH<sub>2</sub>Cl<sub>2</sub>):  $\lambda_{\text{max}}$  (log  $\epsilon$ ) = 279 (6.51), 317 (6.66), 342 (6.69), 356 (6.70), 374 (6.71), 443 (6.67) nm. IR (neat): 2890 (w), 2853 (w), 2801 (w), 2211 (w), 1606 (s), 1563 (m), 1543 (m), 1512 (m), 1489 (m), 1452 (m), 1366 (m), 1353 (m), 1341 (m), 1315 (w), 1280 (m), 1227 (m), 1184 (s), 1169 (m), 1028 (m), 976 (m), 946 (m), 917 (m), 813 (s), 779 (m), 722 (m), 698 (s), 686 (s) cm<sup>-1</sup>. <sup>1</sup>H NMR (CDCl<sub>3</sub>, 500 MHz):  $\delta$  8.42 (m, 4H), 7.67 (d, <sup>3</sup>J<sub>H-H</sub> = 9.2 Hz, 4H), 7.56 (m, 6H), 6.74 (d, <sup>3</sup>J<sub>H-H</sub> = 9.2 Hz, 4H), 3.06 (s, 12H) ppm. <sup>13</sup>C NMR (CDCl<sub>3</sub>, 125 MHz):  $\delta$  164.4, 150.8, 148.8, 141.5, 133.6, 132.0, 129.0, 128.3, 127.0, 111.9, 109.7, 102.9, 102.3, 78.5, 40.4 ppm. LRMS (ESI/[M+H]<sup>+</sup>) calcd. for C<sub>40</sub>H<sub>31</sub>N<sub>4</sub>O<sub>2</sub>: 599.24. Found: 599.33. HRMS calcd. for C<sub>40</sub>H<sub>31</sub>N<sub>4</sub>O<sub>2</sub>: 599.2447. Found: 599.2440. Anal. calcd. for C<sub>40</sub>H<sub>30</sub>N<sub>4</sub>O<sub>2</sub>: C, 80.25; H, 5.05; N, 9.36. Found: C, 79.13; H, 4.52; N, 9.10. Despite three separate attempts, satisfactory elemental analysis for C and H could not be obtained.

### 2.4.7 Synthesis of Cruciform **3**



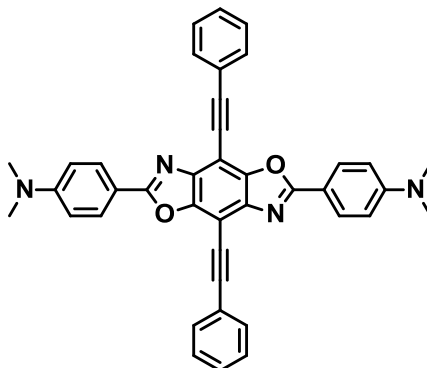
In a nitrogen-flushed round-bottom flask, anhydrous  $\text{K}_2\text{CO}_3$  (1.06 g, 7.66 mmol) was added to a solution of 2-[4-(pyridinyl)]trimethylsilylethyne<sup>57</sup> (671 mg, 3.83 mmol) in a mixture of MeOH (5 mL) and THF (5 mL). After stirring for 30 min, the reaction mixture was filtered through celite. The solvent was removed under reduced pressure, to yield crude 4-ethynylpyridine (**19**), which was used without purification in the next step. To minimize manipulations of this somewhat sensitive compound, we assumed a 95% yield for this reaction.

The entire amount of **19**, prepared as above described, was added to a thick-walled microwave pressure vial that contained a mixture of compound **14** (300 mg, 0.638 mmol),  $\text{PdCl}_2(\text{PPh}_3)_2$  (90 mg, 0.13 mmol), CuI (24 mg, 0.13 mmol),  $\text{Et}_3\text{N}$  (5 mL), and MeCN (5 mL). The vial was sealed and exposed to microwave irradiation for 3 h at 90 °C. After cooling, solvents were removed under reduced pressure, and the crude solid was purified by column chromatography, eluting first with pure  $\text{CH}_2\text{Cl}_2$ , and then successively with  $\text{CH}_2\text{Cl}_2/\text{MeOH}$  mixtures in 97:3, 19:1, and 9:1 ratios. The solvent was removed under reduced pressure to give 202 mg (62%, 0.392 mmol) of **3** (mp >350 °C, with decomposition). **3**: UV-Vis ( $\text{CH}_2\text{Cl}_2$ ):  $\lambda_{\text{max}}$  (log  $\varepsilon$ ) = 302 (6.52), 315 (6.52), 368



(6.76) nm. IR (neat): 2927 (w), 2854 (w), 2220 (w), 1606 (s), 1591 (s), 1561 (m), 1538 (w), 1486 (m), 1451 (m), 1407 (m), 1340 (m), 1280 (m), 1224 (m), 1210 (m), 1177 (w), 1160 (w), 1079 (m), 1064 (m), 1028 (m), 999 (w), 982 (m), 918 (m), 821 (s), 795 (m), 780 (m), 724 (m), 700 (s), 688 (s), 627 (m)  $\text{cm}^{-1}$ .  $^1\text{H}$  NMR ( $\text{CDCl}_3$ , 400 MHz):  $\delta$  8.72 (d,  $^3J_{\text{H-H}} = 4.1$  Hz, 4H), 8.38 (m, 4H), 7.63 (d,  $^3J_{\text{H-H}} = 6.0$  Hz, 4H), 7.58 (m, 6H) ppm.  $^{13}\text{C}$  NMR ( $\text{CDCl}_3$ , 100 MHz):  $\delta$  165.2, 150.1, 149.0, 141.4, 132.6, 130.9, 129.2, 128.4, 126.4, 126.1, 98.4, 97.5, 84.0 ppm. LRMS (ESI/[M+H] $^+$ ) calcd. for  $\text{C}_{34}\text{H}_{19}\text{N}_4\text{O}_2$ : 515.14. Found: 515.2. HRMS calcd. for  $\text{C}_{34}\text{H}_{19}\text{N}_4\text{O}_2$ : 515.1508. Found: 515.1500. Anal. calcd for  $\text{C}_{34}\text{H}_{18}\text{N}_4\text{O}_2 \cdot \frac{1}{4}\text{CH}_2\text{Cl}_2$ : C, 76.78; H, 3.48; N, 10.46. Found: C, 77.19; H, 3.67; N, 10.46.

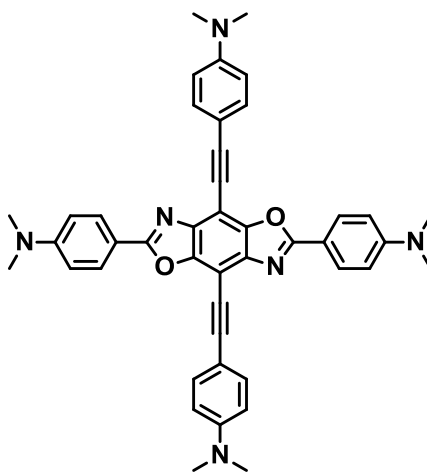
#### 2.4.8 Synthesis of Cruciform 4



Phenylacetylene (**17**, 33.0 mg, 3.24 mmol) was added to a thick-walled microwave pressure vial that contained a mixture of compound **15** (300 mg, 0.539 mmol),  $\text{PdCl}_2(\text{PPh}_3)_2$  (76 mg, 0.11 mmol), CuI (21 mg, 0.11 mmol),  $\text{Et}_3\text{N}$  (5 mL), and MeCN (5 mL). The vial was sealed and exposed to microwave irradiation for 3 h at 100  $^\circ\text{C}$ . After cooling, solvents were removed under reduced pressure, and the crude solid was purified by column chromatography, eluting first with pure  $\text{CH}_2\text{Cl}_2$ , and then

successively with CH<sub>2</sub>Cl<sub>2</sub>/MeOH mixtures in 97:3, 19:1, and 9:1 ratios. The solvent was removed under reduced pressure to give 232 mg (72%, 0.388 mmol) of cruciform **4** (mp >350 °C, with decomposition). **4**: UV-Vis (CH<sub>2</sub>Cl<sub>2</sub>):  $\lambda_{\text{max}}$  (log  $\epsilon$ ) = 335 (6.62), 378 (6.53), 437 (6.67) nm. IR (neat): 2904 (w), 2220 (w), 1607 (s), 1585 (m), 1509 (s), 1487 (w), 1444 (m), 1436 (m), 1368 (m), 1355 (m), 1337 (m), 1281 (w), 1185 (s), 1065 (m), 976 (m), 944 (w), 910 (m), 815 (m), 762 (m), 741 (m), 691 (m) cm<sup>-1</sup>. <sup>1</sup>H NMR (CDCl<sub>3</sub>, 400 MHz):  $\delta$  8.25 (d, <sup>3</sup>*J*<sub>H-H</sub> = 9.2 Hz, 4H), 7.79 (m, 4H), 7.43 (m, 6H), 6.79 (d, <sup>3</sup>*J*<sub>H-H</sub> = 9.2 Hz, 4H), 3.10 (s, 12H) ppm. <sup>13</sup>C NMR (CDCl<sub>3</sub>, 100 MHz):  $\delta$  165.6, 152.7, 148.8, 140.8, 132.4, 129.8, 129.0, 128.6, 123.4, 113.9, 111.7, 99.5, 97.3, 80.7, 40.4 ppm. LRMS (ESI/[M+H]<sup>+</sup>) calcd. for C<sub>40</sub>H<sub>31</sub>N<sub>4</sub>O<sub>2</sub>: 599.24. Found: 599.33. HRMS calcd. for C<sub>40</sub>H<sub>31</sub>N<sub>4</sub>O<sub>2</sub>: 599.2447. Found: 599.2444. Anal. calcd. for C<sub>40</sub>H<sub>30</sub>N<sub>4</sub>O<sub>2</sub> • 1/3CH<sub>2</sub>Cl<sub>2</sub>: C, 77.26; H, 4.93; N, 8.94. Found: C, 77.67; H, 4.62; N, 8.78.

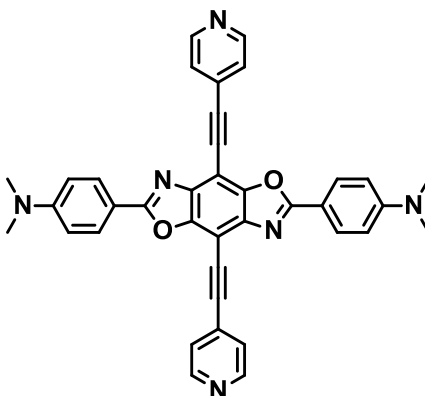
## 2.4.9 Synthesis of Cruciform 5



Compound **18** (261 mg, 1.80 mmol) was added to a thick-walled pressure vessel that contained a mixture of compound **15** (100 mg, 0.180 mmol), PdCl<sub>2</sub>(PPh<sub>3</sub>)<sub>2</sub> (25 mg,

0.036 mmol), CuI (7 mg, 0.04 mmol), *i*-Pr<sub>2</sub>NH (2 mL), and MeCN (2 mL). The vessel was sealed and the mixture was heated for 7 d at 120 °C. After cooling, solvents were removed under reduced pressure, and the crude solid was purified by column chromatography, eluting first with pure CH<sub>2</sub>Cl<sub>2</sub>, and then successively with CH<sub>2</sub>Cl<sub>2</sub>/MeOH mixtures in 97:3, 19:1, and 9:1 ratios. The solvent was removed under reduced pressure to give 51.0 mg (41%, 0.0745 mmol) of cruciform **5** (mp >350 °C, with decomposition). **5**: UV-Vis (CH<sub>2</sub>Cl<sub>2</sub>):  $\lambda_{\text{max}}$  (log  $\epsilon$ ) = 310 (6.76), 334 (6.67), 421 (7.08) nm. IR (neat): 2910 (w), 2212 (w), 1607 (s), 1586 (w), 1540 (w), 1509 (s), 1445 (w), 1364 (m), 1339 (m), 1284 (w), 1230 (w), 1184 (m), 1066 (w), 975 (w), 945 (w), 911 (w), 814 (m), 741(w), 695 (w) cm<sup>-1</sup>. <sup>1</sup>H NMR (CDCl<sub>3</sub>, 500 MHz):  $\delta$  8.25 (d, <sup>3</sup>*J*<sub>H-H</sub> = 9.2 Hz, 4H), 7.66 (d, <sup>3</sup>*J*<sub>H-H</sub> = 8.6 Hz, 4H), 6.79 (d, <sup>3</sup>*J*<sub>H-H</sub> = 8.6 Hz, 4H), 6.73 (d, <sup>3</sup>*J*<sub>H-H</sub> = 9.2 Hz, 4H), 3.09 (s, 12H), 3.04 (s, 12H) ppm. Because of the low solubility of cruciform **5**, a satisfactory <sup>13</sup>C NMR spectrum could not be obtained. LRMS (ESI/[M+H]<sup>+</sup>) calcd. for C<sub>44</sub>H<sub>41</sub>N<sub>6</sub>O<sub>2</sub>: 685.32. Found: 685.50. HRMS calcd. for C<sub>44</sub>H<sub>41</sub>N<sub>6</sub>O<sub>2</sub>: 685.3291. Found: 685.3289. Anal. calcd. for C<sub>44</sub>H<sub>40</sub>N<sub>6</sub>O<sub>2</sub> • 2CH<sub>2</sub>Cl<sub>2</sub>: C, 64.64; H, 5.19; N, 9.83. Found: C, 64.62; H, 5.41; N, 9.74.

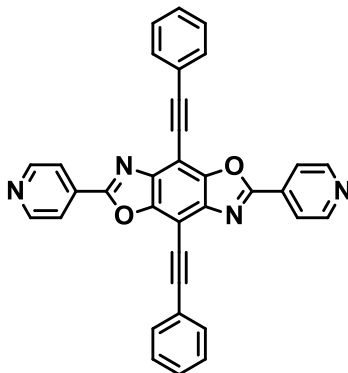
#### 2.4.10 Synthesis of Cruciform 6



Compound **19** (56 mg, 0.54 mmol) was added to a thick-walled microwave pressure vial that contained a mixture of compound **15** (100 mg, 0.18 mmol), PdCl<sub>2</sub>(PPh<sub>3</sub>)<sub>2</sub> (25 mg, 0.036 mmol), CuI (7.0 mg, 0.036 mmol), Et<sub>3</sub>N (2 mL), and MeCN (2 mL). The vial was sealed and exposed to microwave irradiation for 3 h at 120 °C. After cooling, solvents were removed under reduced pressure, and the crude solid was purified by column chromatography, eluting first with pure CH<sub>2</sub>Cl<sub>2</sub>, and then successively with CH<sub>2</sub>Cl<sub>2</sub>/MeOH mixtures in 97:3, 19:1, and 9:1 ratios. The solvents were removed under reduced pressure to give 32 mg (30%, 0.053 mmol) of compound **6** (mp >350 °C, with decomposition). **6**: UV-Vis (CH<sub>2</sub>Cl<sub>2</sub>):  $\lambda_{\text{max}}$  (log  $\epsilon$ ) = 347 (6.92), 458 (6.81) nm. IR (neat): 2907 (w), 2224 (w), 1608 (s), 1593 (m), 1508 (s), 1488 (w), 1448 (w), 1434 (w), 1408 (w), 1365 (m), 1337 (m), 1282 (w), 1224 (w), 1192 (m), 1170 (w), 1074 (m), 980 (m), 944 (w), 913 (m), 820 (s), 743 (m), 698 (w) cm<sup>-1</sup>. <sup>1</sup>H NMR (CDCl<sub>3</sub>, 500 MHz):  $\delta$  8.71 (d, <sup>3</sup>*J*<sub>H-H</sub> = 5.8 Hz, 4H), 8.23 (d, <sup>3</sup>*J*<sub>H-H</sub> = 9.2 Hz, 4H), 7.64 (d, <sup>3</sup>*J*<sub>H-H</sub> = 5.8 Hz, 4H), 6.80 (d, <sup>3</sup>*J*<sub>H-H</sub> = 9.2 Hz, 4H), 3.11 (s, 12H) ppm. <sup>13</sup>C NMR (CDCl<sub>3</sub>, 125 MHz):  $\delta$  166.0, 153.0, 150.1, 147.6, 141.1, 137.6, 129.9, 126.1, 113.4, 111.7, 85.0, 40.3 (one peak is missing; poor solubility of this compound precluded the collection of a better

$^{13}\text{C}$  NMR spectrum). LRMS (ESI/[M+H] $^{+}$ ) calcd. for  $\text{C}_{38}\text{H}_{29}\text{N}_6\text{O}_2$ : 601.23. Found: 601.30. HRMS calcd. for  $\text{C}_{38}\text{H}_{29}\text{N}_6\text{O}_2$ : 601.2352. Found: 601.2343. Anal. calcd. for  $\text{C}_{38}\text{H}_{28}\text{N}_6\text{O}_2 \cdot \frac{1}{3}\text{CH}_2\text{Cl}_2$ : C, 73.20; H, 4.59; N, 13.36. Found: C, 73.02; H, 4.17; N, 13.26.

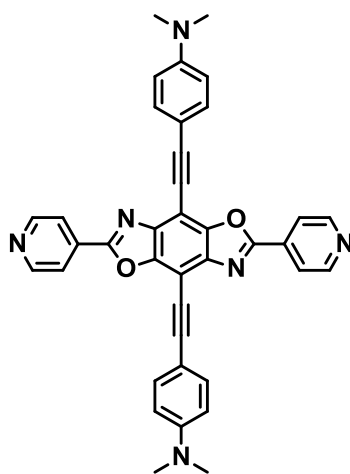
#### 2.4.11 Synthesis of Cruciform **7**



Phenylacetylene (**17**, 95  $\mu\text{L}$ , 0.85 mmol) was added to a thick-walled microwave pressure vial that contained a mixture of compound **16** (100 mg, 0.212 mmol),  $\text{PdCl}_2(\text{PPh}_3)_2$  (30 mg, 0.042 mmol),  $\text{CuI}$  (8 mg, 0.04 mmol),  $\text{Et}_3\text{N}$  (2 mL), and  $\text{MeCN}$  (2 mL). The vial was sealed and exposed to microwave irradiation for 3 h at 100  $^{\circ}\text{C}$ . After cooling, solvents were removed under reduced pressure, and the crude solid was purified by column chromatography, eluting first with pure  $\text{CH}_2\text{Cl}_2$ , and then successively with  $\text{CH}_2\text{Cl}_2/\text{MeOH}$  mixtures in 97:3, 19:1, and 9:1 ratios. The solvent was removed under reduced pressure to give 28 mg (26%, 0.054 mmol) of pure **7** (mp  $>350$   $^{\circ}\text{C}$ , with decomposition). **7**: UV-Vis ( $\text{CH}_2\text{Cl}_2$ ):  $\lambda_{\text{max}}$  (log  $\epsilon$ ) = 311 (6.40), 367 (6.51) nm. IR (neat): 3061 (w), 2214 (w), 1597 (m), 1576 (m), 1546 (m), 1489 (m), 1442 (m), 1414 (m), 1394 (w), 1339 (m), 1283 (m), 1216 (w), 1064 (m), 1028 (w), 991 (m), 981 (m), 924 (m), 831 (m), 755 (s), 691 (s)  $\text{cm}^{-1}$ .  $^1\text{H}$  NMR ( $\text{CDCl}_3$ , 500 MHz):  $\delta$  8.89 (br s, 4H), 8.25 (br d,  $^3J_{\text{H-H}}$

$\text{H} = 4.0 \text{ Hz}$ , 4H), 7.80 (m, 4H), 7.47 (m, 4H) ppm. Because of the poor solubility of **7**, a satisfactory  $^{13}\text{C}$  NMR spectrum could not be obtained. HRMS (ESI/[M+H] $^{+}$ ) calcd. for  $\text{C}_{34}\text{H}_{19}\text{N}_4\text{O}_2$ : 515.1508. Found: 515.1502. Anal. calcd for  $\text{C}_{34}\text{H}_{18}\text{N}_4\text{O}_2 \cdot \text{CH}_2\text{Cl}_2$ : C, 70.12; H, 3.36; N, 9.35. Found: C, 70.17; H, 2.96; N, 7.80. Despite three separate attempts, a satisfactory elemental analysis for N could not be obtained.

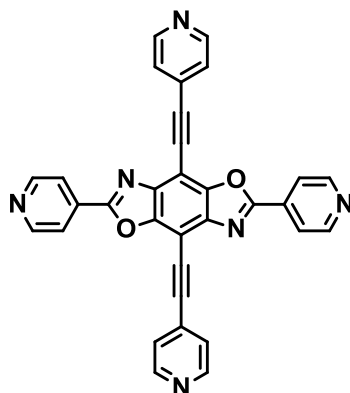
#### 2.4.12 Synthesis of Cruciform **8**



Compound **18** (157 mg, 1.10 mmol) was added to a thick-walled microwave pressure vial that contained a mixture of compound **16** (100 mg, 0.212 mmol),  $\text{PdCl}_2(\text{PPh}_3)_2$  (30 mg, 0.042 mmol), CuI (8 mg, 0.04 mmol),  $\text{Et}_3\text{N}$  (2 mL), and MeCN (2 mL). The vial was sealed and exposed to microwave irradiation for 3 h at 110  $^{\circ}\text{C}$ . After cooling, solvents were removed under reduced pressure, and the crude solid was purified by column chromatography, eluting first with pure  $\text{CH}_2\text{Cl}_2$ , and then successively with  $\text{CH}_2\text{Cl}_2/\text{MeOH}$  mixtures in 97:3, 19:1, and 9:1 ratios. The solvent was removed under reduced pressure to give 27 mg (21%, 0.045 mmol) of compound **8** (mp  $>350$   $^{\circ}\text{C}$ , with decomposition). **8**: UV-Vis ( $\text{CH}_2\text{Cl}_2$ ):  $\lambda_{\text{max}}$  (log  $\epsilon$ ) = 277 (6.28), 332 (6.52), 350 (6.60),

368 (6.57), 468 (6.36) nm. IR (neat): 2891 (w), 2120 (w), 1606 (s), 1578 (w), 1544 (m), 1518 (m), 1486 (w), 1445 (w), 1415 (w), 1356 (m), 1287 (w), 1229 (w), 1186 (m), 1168 (m), 1130 (w), 1063 (w), 991 (w), 980 (w), 946 (w), 927 (w), 817 (m), 740 (w), 725 (w), 699 (w), 690 (w)  $\text{cm}^{-1}$ .  $^1\text{H}$  NMR ( $\text{CDCl}_3$ , 500 MHz):  $\delta$  8.87 (d,  $^3J_{\text{H-H}} = 6.3$  Hz, 4H), 8.25 (d,  $^3J_{\text{H-H}} = 6.3$  Hz, 4H), 7.66 (d,  $^3J_{\text{H-H}} = 9.2$  Hz, 4H), 6.75 (d,  $^3J_{\text{H-H}} = 9.2$  Hz, 4H), 3.07 (s, 12H) ppm. Because of the poor solubility of **8**, a satisfactory  $^{13}\text{C}$  NMR spectrum could not be obtained. LRMS (ESI/[M+H] $^+$ ) calcd. for  $\text{C}_{38}\text{H}_{28}\text{N}_6\text{O}_2$ : 601.23. Found: 601.30. HRMS calcd. for  $\text{C}_{38}\text{H}_{29}\text{N}_6\text{O}_2$ : 601.2352. Found: 601.2350. Anal. calcd. for  $\text{C}_{38}\text{H}_{28}\text{N}_6\text{O}_2 \cdot \text{CH}_2\text{Cl}_2$ : C, 68.32; H, 4.41; N, 12.26. Found: C, 69.67; H, 4.04; N, 12.46. Inclusion of dichloromethane was confirmed by an X-ray crystal structure. Despite repeated attempts, a satisfactory elemental analysis for C could not be obtained.

#### 2.4.13 Synthesis of Cruciform **9**



Compound **19** (262 mg, 2.54 mmol) was added to a thick-walled microwave pressure vial that contained a mixture of compound **16** (300 mg, 0.635 mmol),  $\text{PdCl}_2(\text{PPh}_3)_2$  (89 mg, 0.13 mmol), CuI (24 mg, 0.13 mmol), *i*-Pr $_2$ NH (4 mL), and MeCN (4 mL). The vial was sealed and exposed to microwave irradiation for 4 h at 115  $^\circ\text{C}$ .

After cooling, solvents were removed under reduced pressure, and the crude solid was purified by column chromatography, eluting first with pure CH<sub>2</sub>Cl<sub>2</sub>, and then successively with CH<sub>2</sub>Cl<sub>2</sub>/MeOH mixtures in 97:3, 19:1, and 9:1 ratios. The solvent was removed under reduced pressure to give 28 mg (8.5%, 0.054 mmol) of pure **9** (mp >350 °C, with decomposition). **9**: UV-Vis (CH<sub>2</sub>Cl<sub>2</sub>):  $\lambda_{\text{max}}$  (log  $\epsilon$ ) = 304 (6.18), 315 (6.18), 367 (6.34) nm. IR (neat): 3040 (w), 2221 (w), 1591 (s), 1575 (m), 1545 (m), 1486 (w), 1409 (m), 1384 (w), 1339 (m), 1318 (w), 1283 (w), 1228 (w), 1207 (w), 1061 (m), 992 (m), 984 (m), 922 (m), 829 (s), 817 (s), 740 (m), 726 (m), 699 (m), 689 (m) cm<sup>-1</sup>. <sup>1</sup>H NMR (CDCl<sub>3</sub>, 400 MHz):  $\delta$  8.91 (d, <sup>3</sup>*J*<sub>H-H</sub> = 6.0 Hz, 4H), 8.76 (d, <sup>3</sup>*J*<sub>H-H</sub> = 6.0 Hz, 4H), 8.25 (d, <sup>3</sup>*J*<sub>H-H</sub> = 6.0 Hz, 4H), 7.65 (d, <sup>3</sup>*J*<sub>H-H</sub> = 6.0 Hz, 4H) ppm. <sup>13</sup>C NMR (CDCl<sub>3</sub>, 100 MHz):  $\delta$  163.2, 151.2, 150.3, 149.3, 141.8, 133.4, 130.4, 126.0, 121.6, 99.6, 98.5, 83.1 ppm. LRMS (ESI/[M+H]<sup>+</sup>) calcd. for C<sub>32</sub>H<sub>17</sub>N<sub>6</sub>O<sub>2</sub>: 517.13. Found: 517.20.



## Chapter Three

### Identification of Carboxylic Acids, Organoboronic Acids, Phenols, Amines, Ureas, and Tetrabutylammonium Salts with Cruciform **6**<sup>58</sup>

#### 3.1 Introduction

The discriminative sensory responses of fluorophores or chromophores to various target molecules have been employed in the fields of biological, analytical, material, and environmental chemistry to visualize the qualitative and/or the quantitative information.<sup>59</sup> A colorimetric sensor array method is one of the powerful way to detect and to differentiate between chemically diverse analytes.<sup>60</sup> Using this methodology, each member of a chemical family having same functional group can be coded by a single fluorophore.<sup>16b</sup> This chapter will describe the fingerprinting of each member of six chemical families using fluorimetric sensor arrays based on benzobisoxazole cruciforms described in Chapter 2. Carboxylic acids, boronic acids, phenols, amines, ureas, and tetrabutylammonium salts are selected as groups of analytes considering their importance in organic chemistry and the huge industrial and pharmaceutical demand.

In organic chemistry, carboxylic acids occupy a central place among carbonyl compounds. They are not only important themselves, but also serve as starting materials for preparing numerous acyl derivatives such as esters, amides, and acid chlorides. A 2010 US compilation lists 37 carboxylic acids among the top-200 brand-name drugs including three among the top-ten prescribed drugs.<sup>61</sup> Carboxylic acids and their esters

are also trace ingredients in foods and alcoholic beverages.<sup>62</sup> Boronic acids are extensively used in organic synthesis and medicinal chemistry because of their versatility as synthetic intermediates in the preparation of complex molecules. Boronic acids also have biological applications, such as inhibition of serine proteases by forming boronate esters with the 1,2- and 1,3-diols of saccharides.<sup>63</sup> The important feature of neutral boronic acid that causes the reversible formation of a boronate ester is an electron-deficiency of boron atom having three  $\sigma$ -bonds and an empty  $p$ -orbital, and interacting with electron-rich species. Based on this property, organoboronic acids have also been employed as fluorescent sensors for saccharides,<sup>59f,64</sup> anions,<sup>65</sup> and other nucleophilic analytes.<sup>66</sup> Phenols widely occur in throughout nature including plants algae, fungi, and mammals. Additionally, the tremendous amount of phenols are used in the industrial synthesis of dyes, pesticides, disinfectants, flavors, fragrances, and explosives.<sup>67</sup> Phenols are also important components in the structures of 35 drugs among the top-200 brand-name drugs in a 2010 US compilation list. Nitrogen-containing compounds—amines and ureas—are the major components of the drugs in the compilation list: 159 out of 200 have amine and/or urea functional moieties. Amines widely occur throughout both plants and animals, e.g. trimethylamine occurs in animal tissues and is partially responsible for the distinctive odor of many fishes. A lone pair of electrons on nitrogen atom in amine molecules causes both basicity and nucleophilicity of the molecules, so many of amine compounds exist in ammonium salt form and show high solubility in water. Quaternary ammonium salts are well known and widely used chemicals in numerous applications, as disinfectants, surfactants, antistatic agents, catalysts, *etc.*<sup>68</sup> The properties of quaternary ammonium salts depend on the chain length and functional groups, and on the anion.<sup>69</sup>

Recently, Bunz' group has shown that the fluorescent response of distyrylbis(aryl-ethynyl)benzene cruciforms to protonation strongly depends on the nature of the carboxylic acid.<sup>16c</sup> A battery of three closely related sensors in six different solvents was sufficient to unambiguously identify ten carboxylic acids with similar  $pK_a$  values and closely related structures. They also reported the possible use of aldehyde cruciforms as dosimeters for primary and secondary amines which can form imines and enamines with aldehyde functional group and give different optical response.<sup>5b</sup>

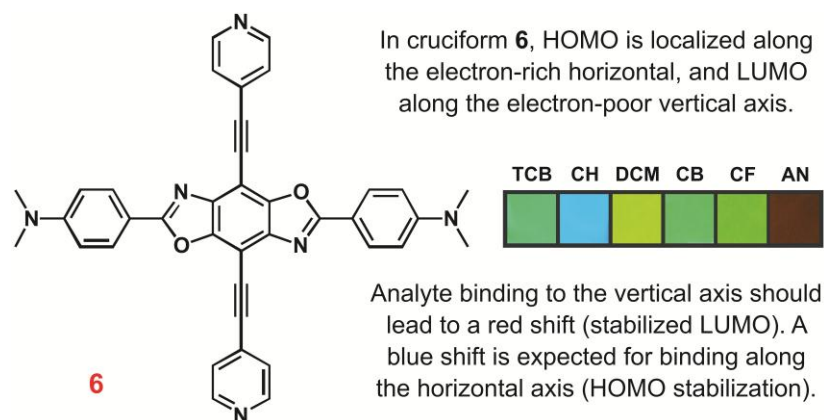


**Figure 3.1** Cruciform **6** is the fluorescent sensor used in this study. The panel on the right shows emission colors of **6** in various solvents ( $\lambda_{\text{excitation}} = 365 \text{ nm}$ ; shutter speed 0.5 s).

As shown in the previous chapter, cruciform **6** presented the most localized HOMO/LUMO and a distinct two-step optical response to protonation. Also, **6** has multiple interaction sites, that is, two aniliny, two pyridiny, and two oxazole nitrogens. In this chapter, I will show the possibility of using cruciform **6** as a sensor for the

discrimination of carboxylic acids and boronic acids. As mentioned in previous paragraph, boronic acids can be used as sensors for electron-rich species such as alcohols, anions, and other nucleophiles. Non-fluorescent boronic acids can also be used as sensors through the indicator displacement strategy,<sup>59f,70</sup> wherein the boronic acid transiently binds—and thus quenches—a fluorescent indicator. Upon its displacement by a better-binding analyte, the indicator recovers its fluorescence, which can be measured and correlated with the analyte concentration. This methodology often allows simplifications in the synthesis of the sensor, but can be qualitatively limited to the emission responses of the indicator. Using this concept the incorporated sensory system of **6** with boronic acid was employed to identify phenols, amines, ureas, and tetraammonium salts.

## 3.2 Results and Discussion

### 3.2.1 Optimization of Ratio between Fluorescent Sensor **6** and Analytes

We first investigated the interaction of a carboxylic acid and a boronic acid with **6** to obtain the concentration-dependent response of **6** to both acids. Figure 3.2 shows the dependence of emission color responses on the concentrations of cruciform **6** and two representative analytes, **C6** and **B5**. Concentration of the analytes was varied first (rows 2–5), from 0.0017 g L<sup>-1</sup> to 17 g L<sup>-1</sup>—when analytes started precipitating. While the response of **6** to **B5** was almost indistinguishable from the emission colors of pure **6** until the concentration of **B5** reached 1.7 g L<sup>-1</sup>, carboxylic acid **C6** induced changes at much lower levels (0.017 g L<sup>-1</sup>). Next, concentration of **6** was varied from approx. 1.1×10<sup>-9</sup> M to 1.1×10<sup>-4</sup> M (rows 6–11), while the analyte concentration was kept constant at 17 g L<sup>-1</sup>.

Poor solubility of cruciform **6** prevented the examination of concentrations higher than  $1.1 \times 10^{-4}$  M. At low concentrations of **6**, excess of analytes is more than sufficient to fully bind to **6**, but **6**'s fluorescence is so weak that these changes are barely observable (rows 6–8 for **C6** and 6–7 for **B5**). In the region we deemed analytically useful (row 9 for **C6** and rows 8 and 9 for **B5**), dramatic emission color changes are observed. Finally, as the concentration of cruciform **6** is increased further (rows 10 and 11), emission colors in the case of **C6** revert almost fully to those of pure **6**. This observation suggests that the excess of weak acid **C6** is now insufficient to fully protonate **6**. On the other hand,

Row #	Emission Colors ( <b>C6</b> )					Cruciform <b>6</b> [mol L <sup>-1</sup> ]	Analyte [g L <sup>-1</sup> ]	Emission Colors ( <b>B5</b> )				
	TCB	CH	DCM	CB	AN			TCB	CH	DCM	CB	AN
1						$1.1 \times 10^{-6}$	—					
2						$1.1 \times 10^{-6}$	0.0017					
3						$1.1 \times 10^{-6}$	0.017					
4						$1.1 \times 10^{-6}$	0.17					
5						$1.1 \times 10^{-6}$	1.7					
6						$1.1 \times 10^{-9}$	17					
7						$1.1 \times 10^{-8}$	17					
8						$1.1 \times 10^{-7}$	17					
9						$1.1 \times 10^{-6}$	17					
10						$1.1 \times 10^{-5}$	17					
11						$1.1 \times 10^{-4}$	17					

**Figure 3.2** Investigation of the dependence of fluorescence emission colors of **6** ( $\lambda_{\text{excitation}} = 365$  nm; shutter speed 0.5 s) on the concentrations of **6** and representative analytes **C6** and **B5**. The conditions used in Figure 3.3 and Figure 3.5 are highlighted in the red frame.

emission colors of **6** + **B5** are still clearly distinct from those of pure **6**, but not so from each other. In addition, **6** + **B5** may be exhibiting concentration-induced quenching at these high concentrations since its emission appears qualitatively dimmer than that at lower concentrations of **6**. At the highest concentration (row 11), observation is further complicated by partial precipitation of **6** and both examined analytes. Overall, the final choice of concentrations for **6** ( $1.1 \times 10^{-6}$  M) and analytes ( $17 \text{ g L}^{-1}$ ) is among the optimal ones for standardized analytes of both compound classes: some other ratios would also perform well for carboxylic or boronic acids taken separately. Lower detection limits for both carboxylic and boronic acids are estimated at  $0.017 \text{ g L}^{-1}$  and  $1.7 \text{ g L}^{-1}$ , respectively, while the upper limit is determined chiefly by solubilities of **6** and corresponding analytes.

### 3.2.2 Qualitative Discrimination of Carboxylic Acids with Fluorescent Sensor **6**

Using the determined optimal concentration ratio, I performed the discrimination of carboxylic acids. Even a cursory examination of the panel of emission colors in Figure 3.3 shows dramatic differences among the studied analytes, as no two compounds have the same emission color in all five examined solvents. In general, exposure of **6** to carboxylic acids **C1–C12** resulted in blue shifts in its emission. In light of the previous chapter, this observation suggests that the initial protonation occurs at pyridine (red shift), but that excess acid ultimately also protonates the dimethylamino group, leading to a more pronounced blue shift. Analytes **C3** and **C8** lead to almost complete quenching of

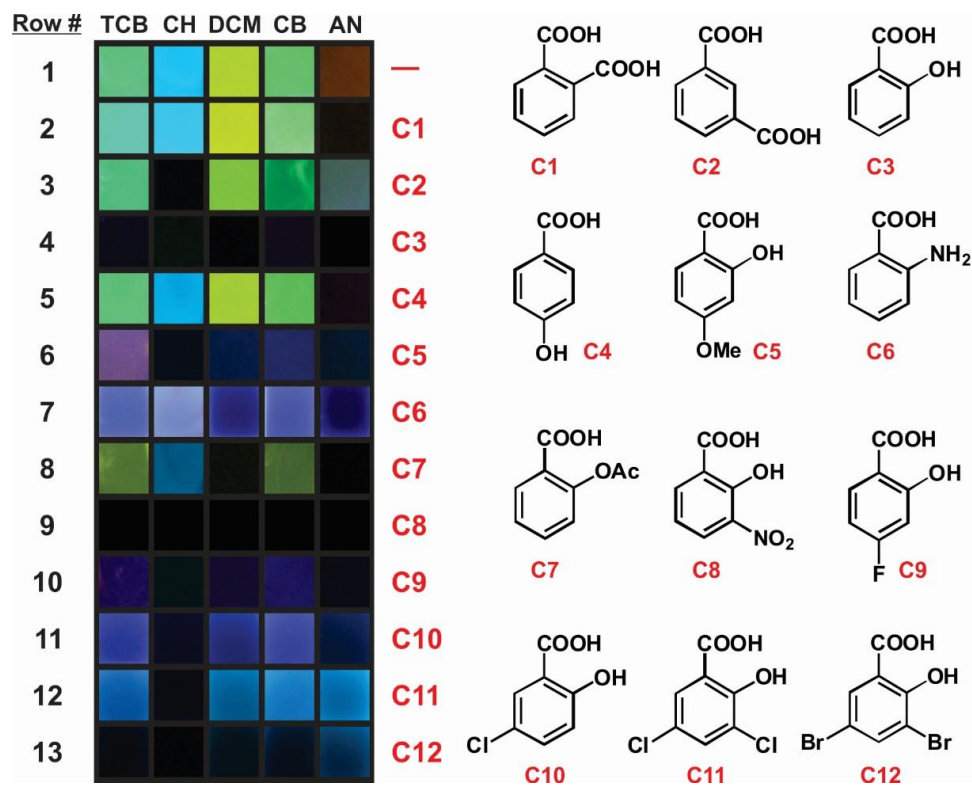


**Figure 3.3** Identification of substituted benzoic acids **C1–C12** (right) using cruciform

**6**. Emission colors of **6** upon exposure to excess analytes are shown in left panel

( $\lambda_{\text{excitation}} = 365 \text{ nm}$ ; shutter speed 0.5 s; “—” indicates the blank).

fluorescence of **6** in all solvents. Quenching of fluorescence by salicylic acid (**C3**) had been precendented;<sup>71</sup> in the case of electron-poor nitrosalicylic acid **C8**, the quenching was ascribed to the electron-transfer from the charge-separated excited state of **6** onto **C8** as a good acceptor.<sup>59g</sup>

These obvious distinctions were next put on quantitative footing. Emission colors were converted into numerical values using Colour Contrast Analyzer<sup>72</sup> software, which extracted *R*(ed), *G*(reen), and *B*(lue) values for each individual acid in each of the five

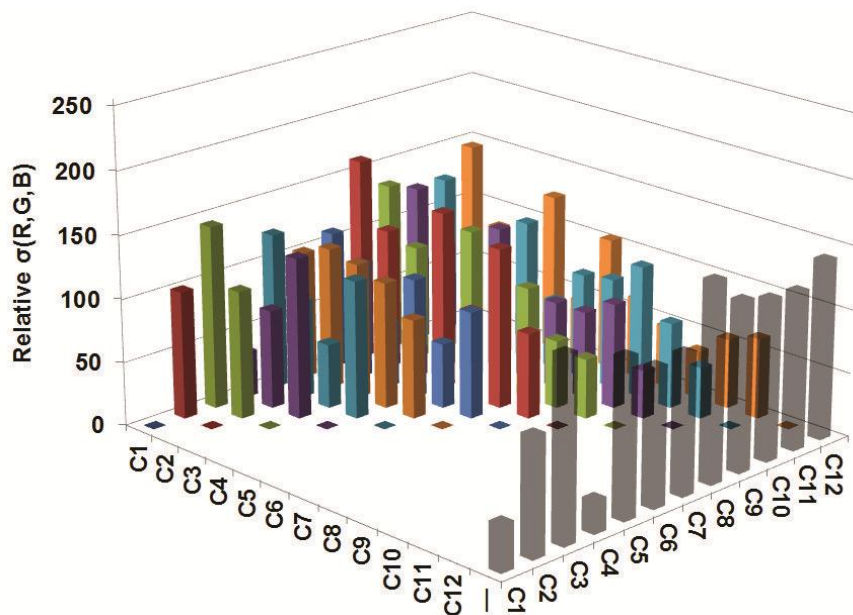


**Figure 3.4** The correlation diagram shows standard deviations of *R/G/B* values for **C1–C12** (summed over five solvents), relative to all other analytes. The semi-transparent bars in the row marked with “—” indicate standard deviations relative to the blank solution of **6**, summed over all five solvents. Maximum possible value of  $\sigma$  is 255.

solvents. Thus, every analyte was initially assigned 15 numbers: *R*, *G*, and *B* values for each of the 5 solvents. For each compound–solvent combination, a standard deviation ( $\sigma$ )<sup>73</sup> of that compound’s *R/G/B* values was obtained from the corresponding values for the blank solution of **6**. For example,  $\sigma_{C1@AN}$ —which characterizes acid **C1** in AN, is derived as:

$$\sigma_{C1@AN} = \sqrt{\frac{(R_{C1}^{AN} - R_6^{AN})^2 + (G_{C1}^{AN} - G_6^{AN})^2 + (B_{C1}^{AN} - B_6^{AN})^2}{3}} \quad (1)$$



where  $R_{C1}^{AN}$  and  $R_6^{AN}$  represent  $R$ -values for **6** + **C1** and **6** in AN, respectively (and analogously for  $G$  and  $B$  values).

No statistically significant correlation was observed between the  $pK_a$  values<sup>74</sup> of **C1–C12** and their  $\sigma$  values in any of the five examined solvents. Interestingly, such a correlation was also absent within the subset of substituted salicylic acids **C3**, **C5**, and **C8–C12**, even though  $\sigma$  values for this subset were clustered away from all other examined acids in both DCM (145.44–171.59) and CH (154.43–184.17).

Judicious statistical evaluation of differences in emission colors among individual acids was performed, with the aim of establishing whether this method can be used to distinguish them. Thus, for each combination of two carboxylic acids, relative standard deviations  $\sigma'$  were calculated, and defined as, for the example of **C1** vs. **C2**:

$$\sigma'_{C1@C2} = \sqrt{\frac{\sum_{solv}^i [(R_{C1}-R_{C2})^2 + (G_{C1}-G_{C2})^2 + (B_{C1}-B_{C2})^2]}{3*i}} \quad (2)$$

Each such number defines the relationship between two acids across all examined solvents. These relative standard deviations are plotted in Figure 3.4. To highlight the distinction between individual analytes and the blank sample of **6**, those standard deviations were also plotted in the row of semitransparent value bars marked with “—”. This graph suggests that all the investigated analytes can be distinguished from each other and from the blank solution of **6**, as the correlation value drops to zero only for the auto-correlation data points.

### 3.2.3 Qualitative Discrimination of Organoboronic Acids with Fluorescent Sensor

6

Organoboronic acids **B1–B9** were examined next, using the same methodology as for the carboxylic acids. Again, very dramatic changes in fluorescence emission colors were observed (Figure 3.5). In the majority of cases, emission colors were red-shifted, suggesting dominant stabilization of the LUMO through a stronger pyridine-boron interaction.  $^1\text{H}$  NMR spectroscopic titration of **6** with **B5** confirmed this hypothesis, as dramatic shifts in the pyridine signals of **6** occurred first, and were followed by shifts in

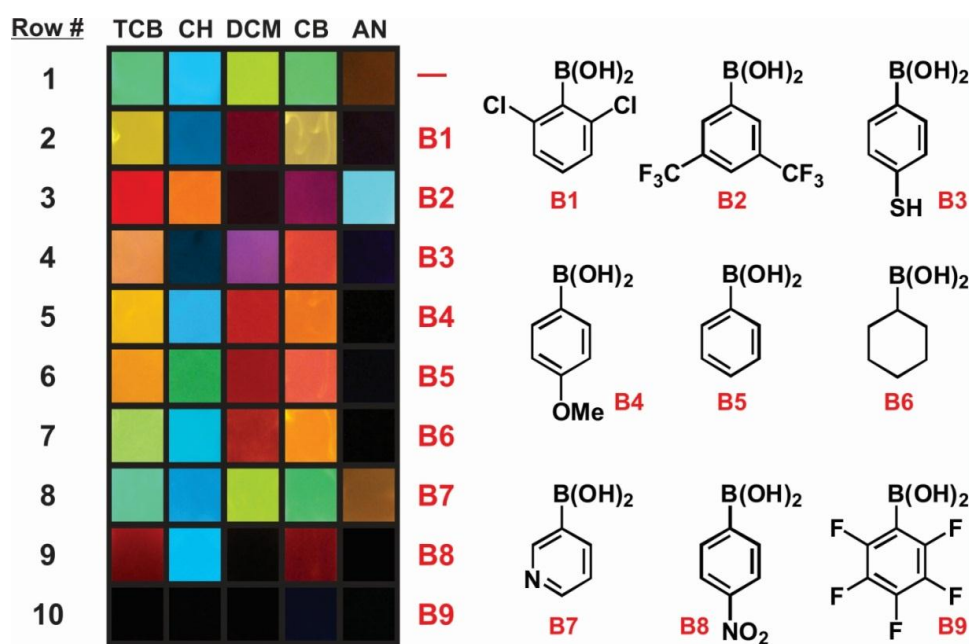


**Figure 3.5** Identification of boronic acids **B1–B9** (right) using cruciform **6**. Emission colors of **6** upon exposure to excess analytes are shown in left panel ( $\lambda_{\text{excitation}} = 365$  nm; shutter speed 0.5 s; “—” indicates the blank).

the signals of the 4-(*N,N*-dimethylamino)phenyl group at significantly higher concentration of **B5**. While all nine boronic acids can be distinguished from each other, emission of the **6/B7** combination is not sufficiently different from the emission of pure **6**—presumably because the pyridine moiety of **B7** (which is in excess) replaces the pyridine of **6** in binding to boron. Pentafluorophenylboronic acid (**B9**) causes unselective quenching of fluorescence of **6** in all solvents (much like carboxylic acids **C3** and **C8** described above), which can be explained by electron-transfer from the excited state of **6** onto acceptor **B9**.<sup>59g</sup>

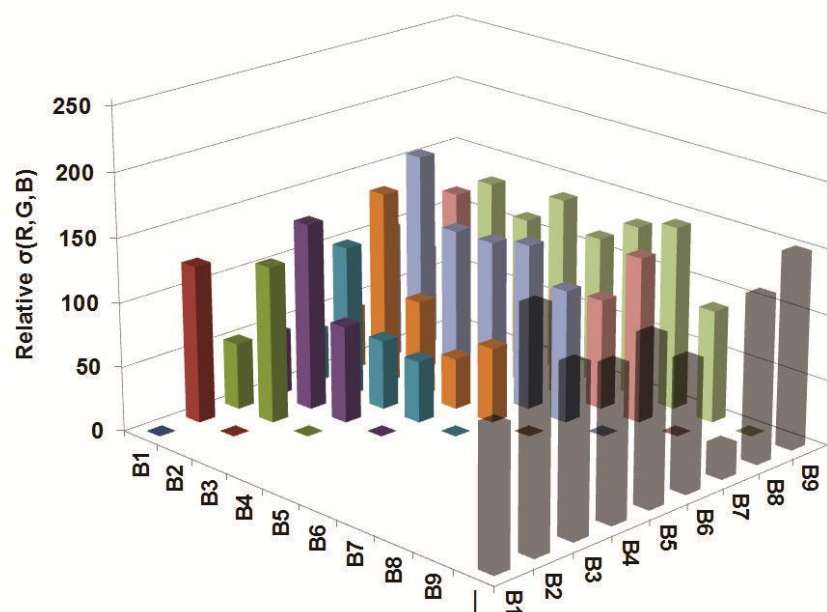


**Figure 3.6** The correlation diagram shows standard deviations of *R/G/B* values for **B1–B9** (summed over five solvents), relative to all other analytes. The semi-transparent bars in the row marked with “—” indicate standard deviations relative to the blank solution of **6**, summed over all five solvents. Maximum possible value of  $\sigma$  is 255.

### 3.2.4 Qualitative Discrimination of Substituted Phenols with a Hybrid Sensing System

Since fluorescent boronic acids have been used as sensors for sugars,<sup>64</sup> anions,<sup>65</sup> and other nucleophilic analytes,<sup>66</sup> I was curious to examine the effects that analyte binding to boron<sup>75</sup> would exert over the emission colors of complexes of **6** and boronic acids. The mechanism of this optical response involves both indicator displacement and

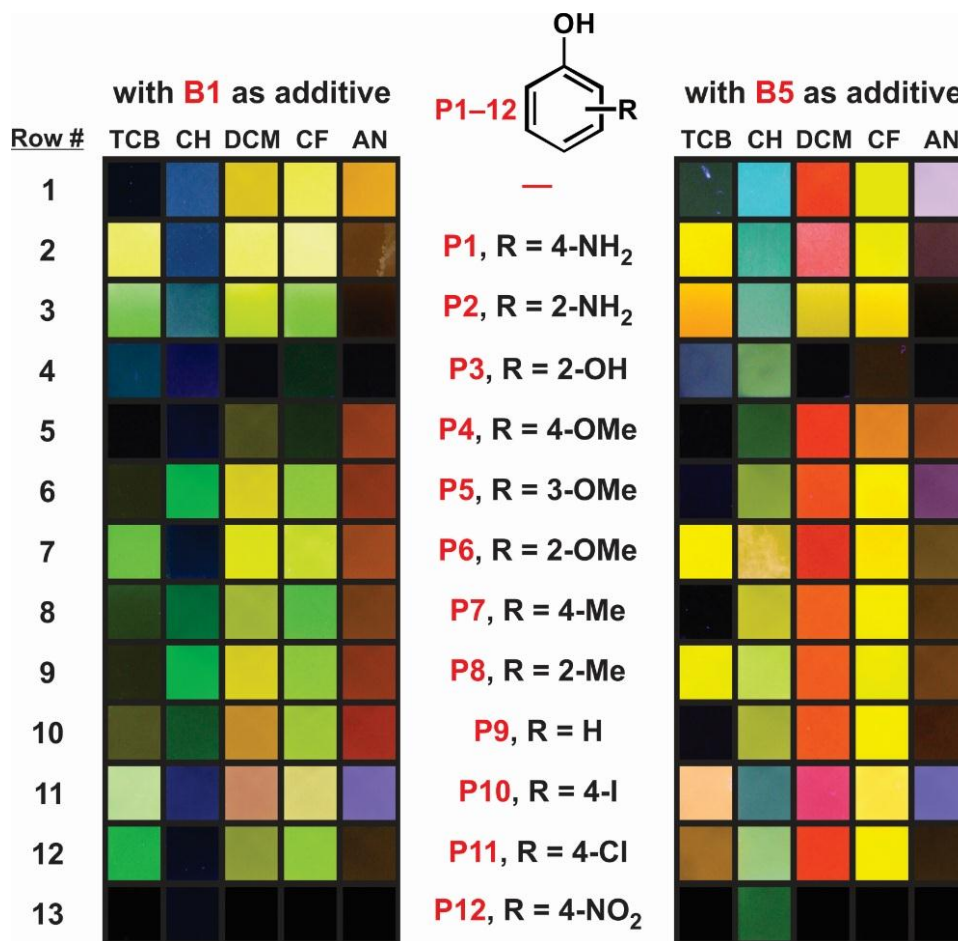


**Figure 3.7** Identification of phenols **P1–P12** (center) using a combination of cruciform **6** and boronic acids **B1** (left) and **B5** (right).  $\lambda_{\text{excitation}} = 365 \text{ nm}$ ; shutter speed 0.5 s.

fluorescence modulation pathways. First, I speculated that an inexpensive non-fluorescent boronic acid could be used to bind to a phenol, and that the associated change in electron density on the boron could be sensed by cruciform **6** as the fluorescent responder. To evaluate this hypothesis, 0.02 M solutions of non-fluorescent boronic acids **B1** and **B5** in TCB, CH, DCM, chloroform (CF), and AN were prepared. Each solution was treated with a small amount of cruciform **6**, to set the final  $\text{ArB(OH)}_2$  : **6** molar ratio to 20,000 : 1. These solutions<sup>76</sup> were then exposed to an approximately fivefold molar excess of phenols **P1–P12** (Figure 3.7 center) relative to boronic acid. Fluorescence

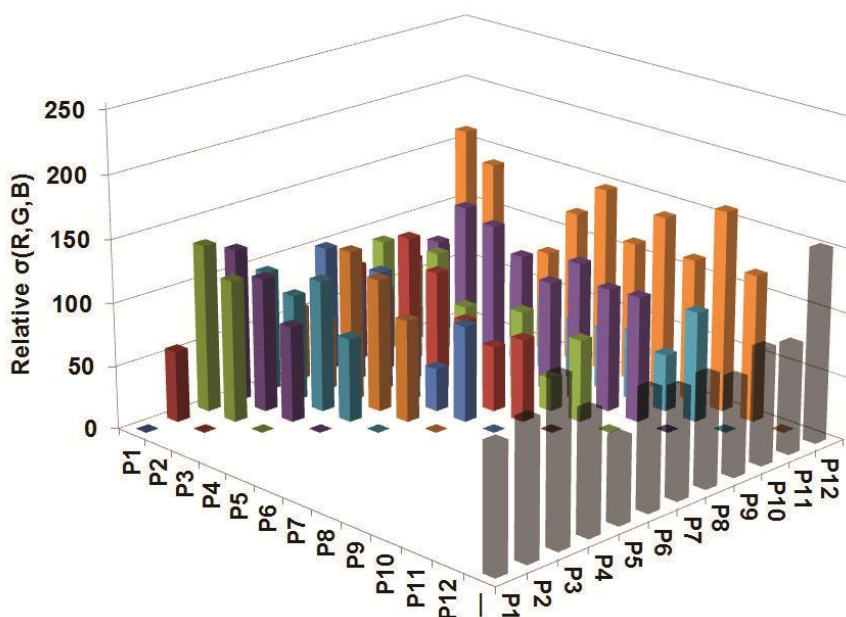


**Figure 3.8** The correlation diagram shows standard deviations of  $R/G/B$  values for **P1–P12** (summed over ten solvents), relative to all other analytes. The semi-transparent bars in the row marked with “—” indicate standard deviations relative to the blank solution of **6** + **B1/B5**, summed over all ten solvents. Maximum possible value of  $\sigma$  is 255.

emission photographs were recorded, and a numerical analysis analogous to the one performed for carboxylic and organoboronic acids was conducted. The results, summarized in Figure 3.8, clearly show that all twelve phenols can be discerned from each other and from the blank solution of **6** + **B1/B5**. Remarkably, even subtle structural differences—such as those among the three positional isomers of methoxyphenol—are identifiable. The presence of boronic acid additives is indispensable in eliciting changes in the fluorescence of **6** in response to phenolic analytes. With  $pK_a$  values above 8.00, electron-rich and electron-neutral phenols are insufficiently acidic to protonate **6** and thus

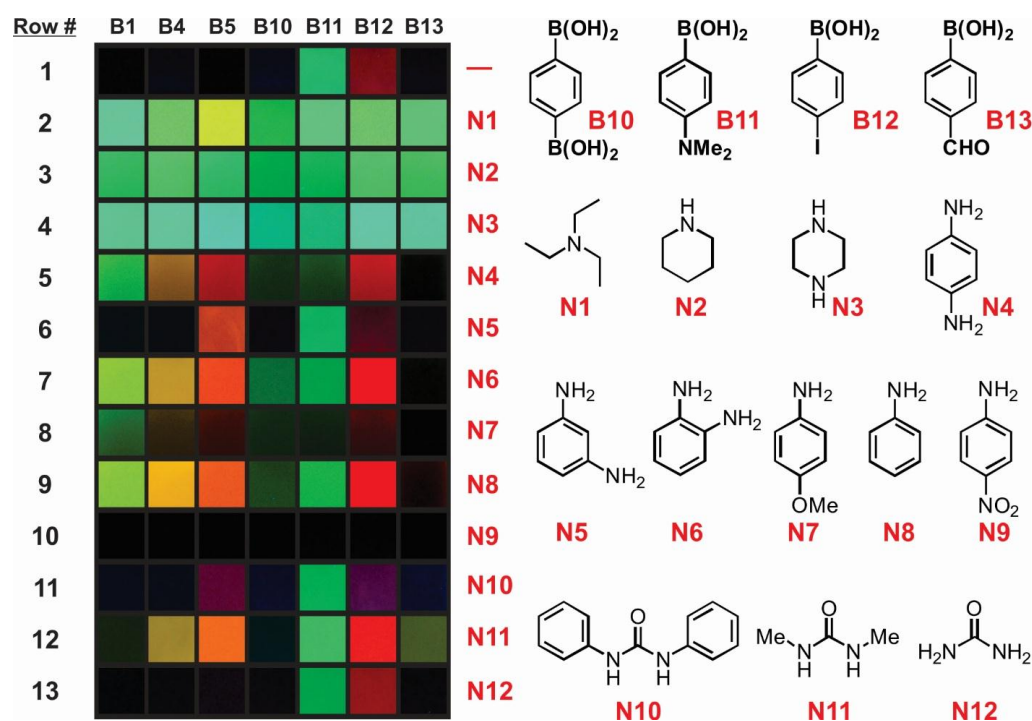


**Figure 3.9** Row #1 shows emission colors of complexes of cruciform **6** and boronic acids **B1**, **B4**, **B5**, and **B10–B13** in TCB as the solvent. Rows #2–13 show the emission colors resulting from the exposure of these complexes to the specified organic nitrogen compounds. Molar ratio of **6** vs. boronic acids was ~1:20,000,  $\lambda_{\text{excitation}}$  was 365 nm, and shutter speed was 0.5 s.

cause negligible shifts in emission colors. On the other hand, electron-poor nitrophenols, while sufficiently acidic, completely and unselectively quench the fluorescence of **6**.<sup>59g,75</sup>

### 3.2.5 Qualitative Discrimination of Amines and Ureas with a Hybrid Sensing System

After demonstrating the ability of the hybrid fluorescent sensor system to discriminate among weakly acidic phenols, I speculated that the same system could sense other nucleophilic analytes that could interact with electron-deficient boron nuclei of coordinated boronic acids. This hypothesis was tested first on nitrogen-containing organic compounds, including amines and ureas (Figure 3.9, right) with the same methodology as the one used for the discrimination of phenols. A  $10^{-6}$  M solution of cruciform **6** in TCB was first exposed to a ~20,000-fold excess of boronic acids **B1**, **B4**, **B5**, and **B10–B13**. Emission colors of the complexes developed instantaneously and were photographed in a darkroom setup. All but two boronic acids (**B11** and **B12**) quenched the fluorescence of **6** (Figure 3.9, row #1). Subsequently, 2 mL aliquots of these seven stock solutions were transferred to cuvettes and exposed to 40 mg of analytes shown in Figure 3.9. Photographs of the developed emission colors are shown in Figure 3.9, rows #2–13. Several trends are apparent. Analytes more basic than pyridine-based cruciform **6** (rows # 2–4)<sup>77</sup> appear to simply regenerate the fluorescence of pure **6**, manifesting indicator displacement behavior. On the other hand, less basic analytes appear to modulate the strength of the complex between **6** and boronic acids,<sup>78</sup> resulting in a change in fluorescence color. Finally, boronic acid **B11** appears to be self-complexed: it

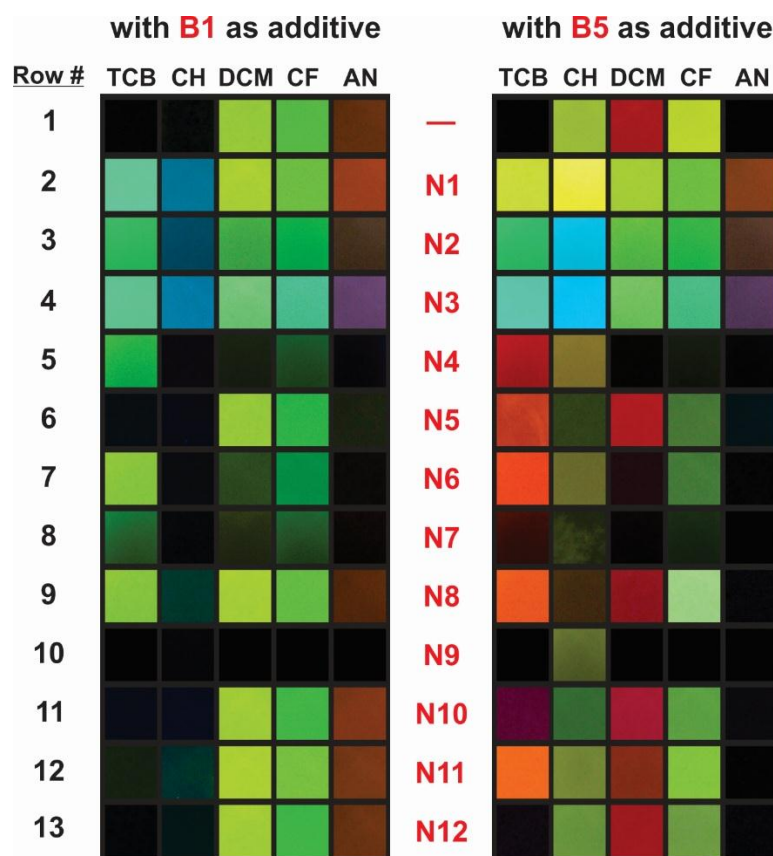


**Figure 3.10** Row #1 shows emission colors of complexes of cruciform **6** and boronic acids **B1** (left) and **B5** (right) in five different solvents. Rows #2–13 show the emission colors resulting from the exposure of these complexes to the specified amine analytes.  $\lambda_{\text{excitation}}$  was 365 nm and shutter speed was 0.5 s.

does not significantly affect the fluorescence of **6**, regardless of whether an analyte is present. Overall, qualitative distinction among analytes in rows # 2–13 could be achieved in some, but not all cases.

Next, we varied the solvent in which emission colors were observed; cruciform **6** and its complexes with boronic acids—**B1** and **B5**— were studied as additives to **6**, and the fluorescence response was examined in five solvents: TCB, CH, DCM, CF, and AN.



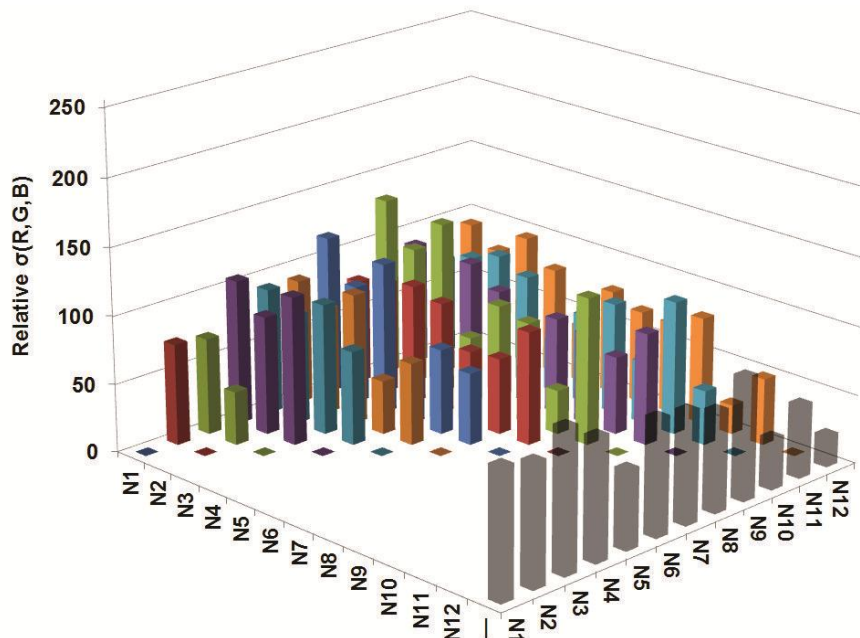


**Figure 3.11** The correlation diagram shows standard deviations of  $R/G/B$  values for **N1–N12** (summed over ten solvents), relative to all other analytes. The semi-transparent bars in the row marked with “—” indicate standard deviations relative to the blank solution of **6** + **B1/B5**, summed over all ten solvents. Maximum possible value of  $\sigma$  is 255.

Results are summarized in the two panels shown in Figure 3.10. Similarly to the solvent variation experiments, amines more basic than the pyridine-based cruciform **6** show emission colors that suggest at least partial expulsion of **6** from its boronic acid complexes (Figure 3.10, rows #2–4). On the other hand, less basic analytes show a diverse range of emission colors. This diversity was sufficient to permit qualitative discrimination between these species, based on the fact that no two of them will have all ten identical emission colors. This notion was confirmed by the statistical analysis of the numeric  $R/G/B$  values of emission colors, which is shown in Figure 3.11.

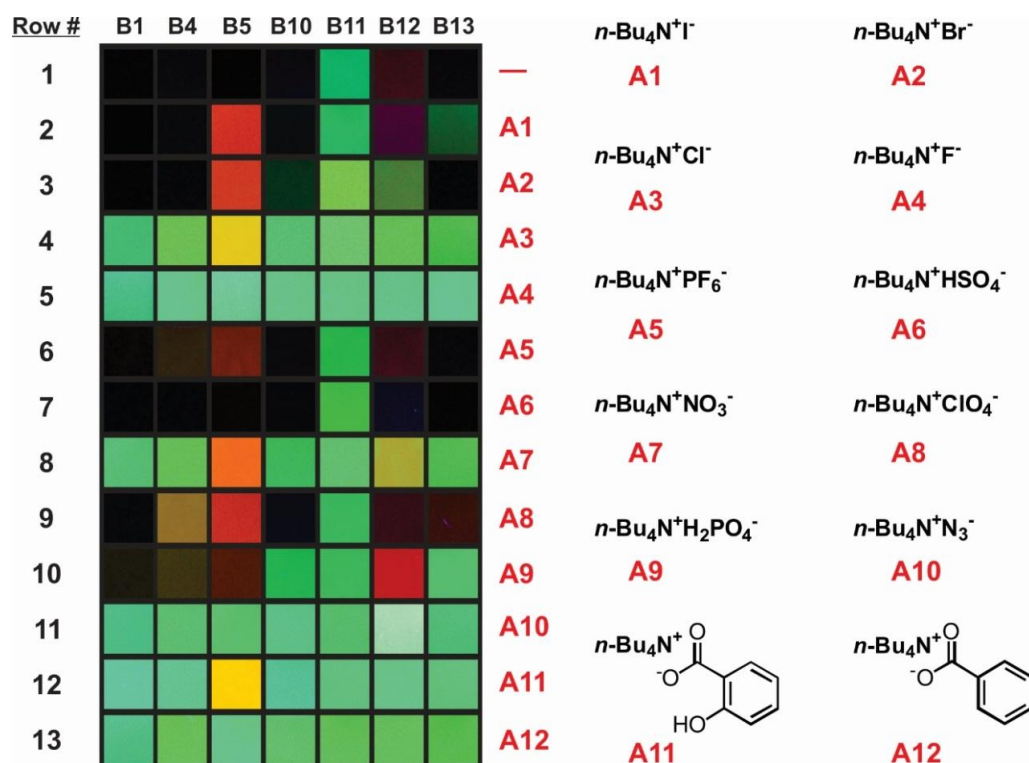


**Figure 3.12** Row #1 shows emission colors of complexes of cruciform **6** and boronic acids **B1**, **B4**, **B5**, and **B10–B13** in TCB as the solvent. Rows #2–13 show the emission colors resulting from the exposure of these complexes to the specified anions, added as their tetrabutylammonium (TBA) salts. Molar ratio of **6** vs. boronic acids was ~1:20,000,  $\lambda_{\text{excitation}}$  was 365 nm, and shutter speed was 0.5 s.

### 3.2.6 Qualitative Discrimination of Anions with a Hybrid Sensing System

Following the successful demonstration that organic nitrogen compounds can be qualitatively identified using cruciform **6** in tandem with boronic acid additives, small organic and inorganic anions were examined next. These analytes are of broad significance in environmental, physiological, and industrial applications.<sup>16k,79</sup> The

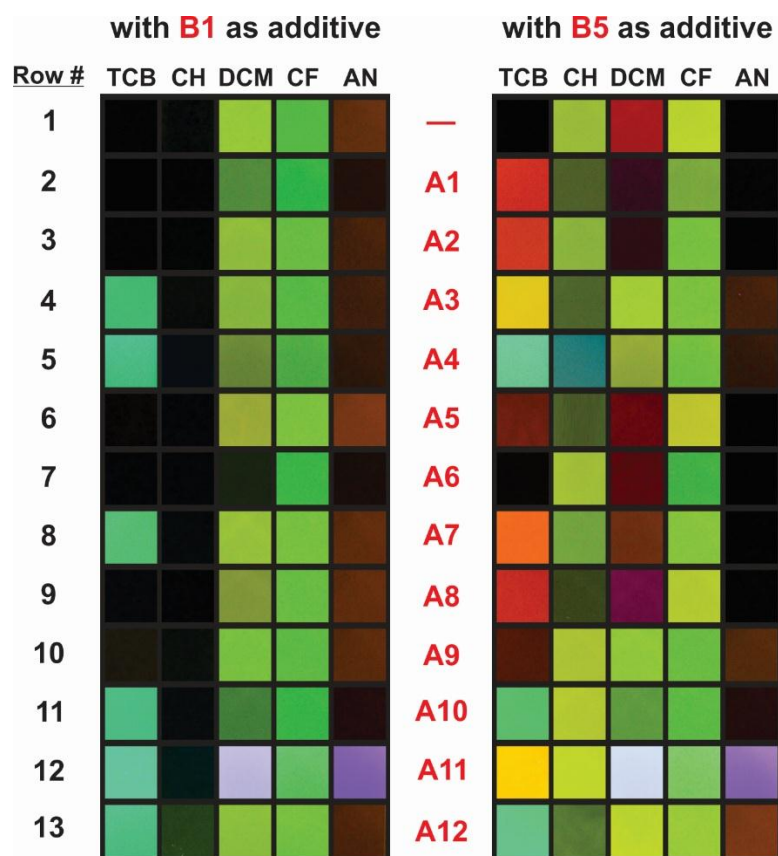


**Figure 3.13** Row #1 shows emission colors of complexes of cruciform **6** and boronic acids **B1** (left) and **B5** (right) in five different solvents. Rows #2–13 show the emission colors resulting from the exposure of these complexes to the specified anions analytes.  $\lambda_{\text{excitation}}$  was 365 nm and shutter speed was 0.5 s.

methodology used was analogous to the one described for the analysis of organic amines and ureas. The results of the anion analysis are shown in Figures 3.12 and Figure 3.13. Again, basic anions such as fluoride or benzoate lead to the apparent decomplexation of **6** from the boronic acid (Figure 3.12, rows #5 and #13). The qualitative discrimination between the different anions is possible and statistically significant, as shown in Figure 3.15.

The use of this hybrid sensing system, coupled with the photographic identification of emission responses allows rapid screening of potential sensors for a given analyte. In this context, the behavior of complexes of **6** with **B1**, **B4**, **B5**, and **B10–B13** in TCB was particularly intriguing: initially quenched fluorescence of these complexes was restored upon exposure to analytes. Such OFF→ON behavior<sup>80</sup> is desirable in sensing applications because of the enhanced contrast. I thus investigated whether the **6**•**B5** complex could be used as a quantitative sensor for chloride anions. The results of the titration of the 1:20,000 mixture of **6** and **B5** in TCB with concentrated

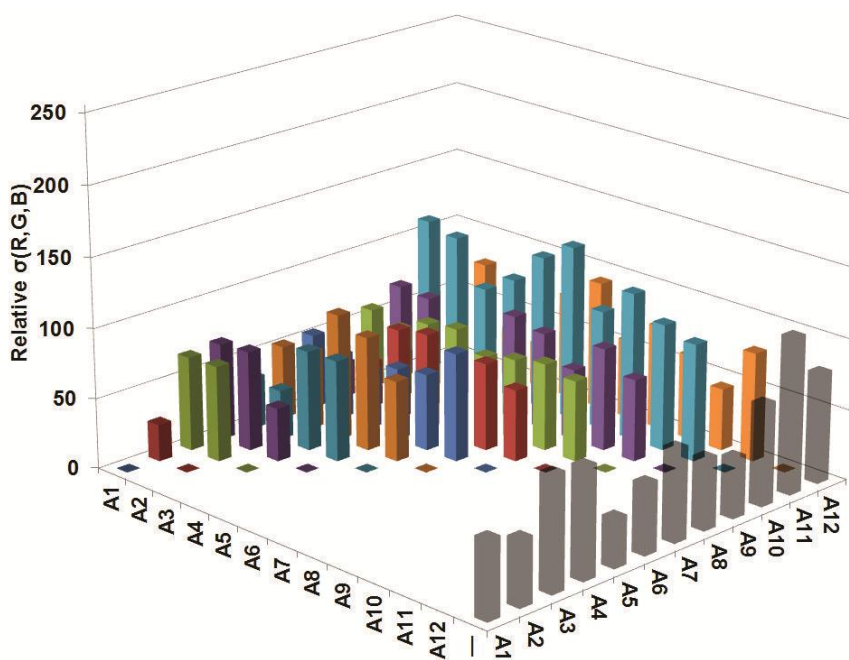


**Figure 3.14** The correlation diagram shows standard deviations of *R/G/B* values for **A1–A12** (summed over ten solvents), relative to all other analytes. The semi-transparent bars in the row marked with “—” indicate standard deviations relative to the blank solution of **6** + **B1/B5**, summed over all ten solvents. Maximum possible value of  $\sigma$  is 255.

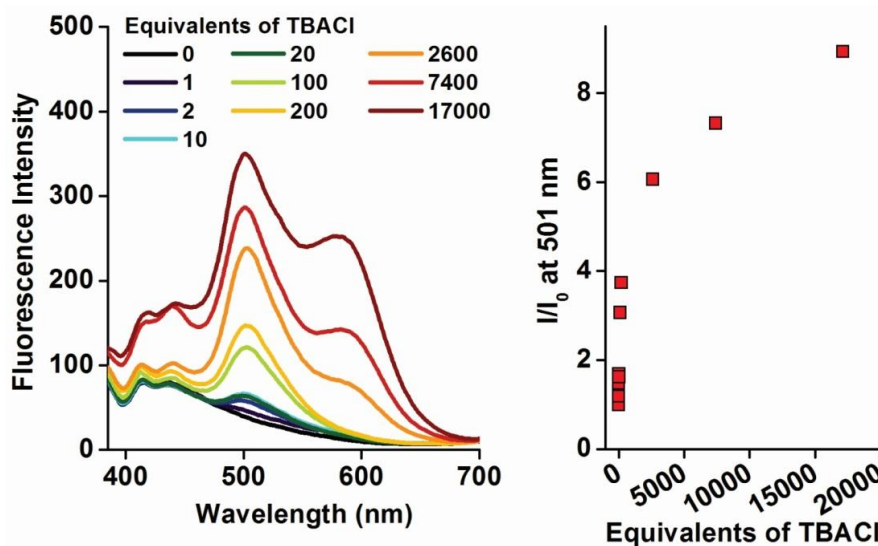


**Figure 3.15** On the left, stacked fluorescence emission spectra for the titration of a mixture of **6** and **B5** (1:20,000 molar ratio) with TBACl.  $\lambda_{\text{excitation}}$  was 365 nm, excitation slit width and emission slit width were 10 nm. On the right, enhancement in the emission intensity of a **6**·**B5** solution (at 501 nm) is plotted as a function of added TBACl. Equivalents of TBACl are given relative to the amount of cruciform **6**.

solutions of tetrabutylammonium chloride (TBACl) are shown in Figure 3.15. A calibration curve (Figure 3.15 right) suggests an exponential correlation ( $R^2=0.911$ ) between the fluorescence enhancement and the amount of added TBACl.

### 3.3 Conclusions and Outlook

The results presented in this chapter show that effective discrimination of twelve carboxylic and nine boronic acids from each other can be achieved using differences in the fluorescence response of cruciform **6** to these species. Furthermore, we have

developed a self-assembled two-component fluorescent sensing system which can respond to diverse analytes through either fluorescence modulation or indicator displacement pathways. Using this hybrid sensor system, structurally related phenols can be distinguished—which is a potentially broadly applicable result. Moreover, the use of the cruciform fluorophore/boronic acids sensing system was successfully expanded to the discrimination of organic nitrogen compounds (amines and ureas) and small organic/inorganic anions. However, further improvements of this sensing system are also need to enhance the intensity of optical response of the fluorophore to analytes, which is dependent on the concentration. The low solubility of cruciform **6** somewhat prevented the discrimination of analytes in lower concentration than 17 g/L. Another improvement can be achieved by changing the sensing media. Instead of liquid phase, the sensing system in solid phase possibly makes more practical application to the identification of both liquid and gas analytes. Overall, this "vicarious sensing" strategy could allow rapid screening and optimization of new sensors for many chemically diverse species, given the available diversity of cruciform structures and potential additives.

### **3.4 Experimental Section**

#### **3.4.1 General Methods**

Carboxylic acids **C1–C12** (and **C13–C16**, *vide infra*), organoboronic acids **B1–B13**, phenols **P1–P12** (and **P13–P14**, *vide infra*), nitrogen containing compounds **N1–N12**, and tetrabutylammonium salts **A1–A11** were purchased from commercial suppliers and used without further purification. Tetrabutylammonium benzoate was prepared

according to literature procedure.<sup>81</sup> Reagent-grade solvents were used as received. Cruciform **6** was prepared according to the procedure described in Chapter 2.

Photographs of emission colors were taken using a FujiFilm FinePix S9000

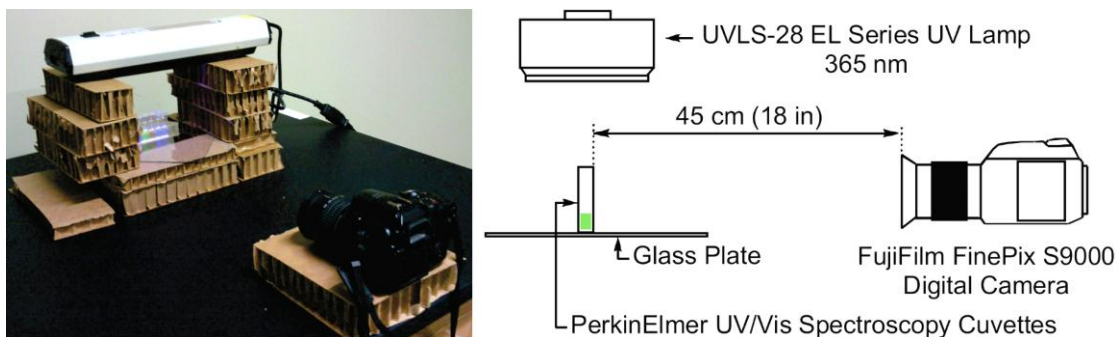


**Figure 3.16** Dark room setup for taking emission color photographs.

digital camera, with a shutter speed of 0.5 s. A handheld UVLS-28 EL series UV lamp ( $\lambda_{\text{excitation}}=365$  nm) was used as the light source. All photographs were taken in a dark windowless room, with a 45 cm (18 in) distance between the sample cuvettes and the camera lens. A photograph and the schematics of the photography setup are shown in Figure 3.16.

### 3.4.2 Discrimination of C1–C16, B1–B9, and P11–P14 Using Solutions of Cruciform **6**

For each analyte, five individual solutions were prepared by dissolving 50 mg of the analyte in 3 mL each of AN, TCB, DCM, CH, and CB. Thus, the resultant concentration of analytes in these solutions was  $\sim 16.7$  g L<sup>-1</sup>. Next, 1.8 mL of these solutions was transferred into a 10×10 mm quartz cuvette, followed by a 20  $\mu$ L injection of the  $1.0 \times 10^{-4}$  M solution of cruciform **6** in DCM ( $2.0 \times 10^{-9}$  mol). The mixed solution

was stirred using a disposable pipette. This procedure was repeated for each of the five solvents, and a five-cuvette set was then placed on glass plate and irradiated by a handheld UV lamp (365 nm). A digital photograph was immediately taken.

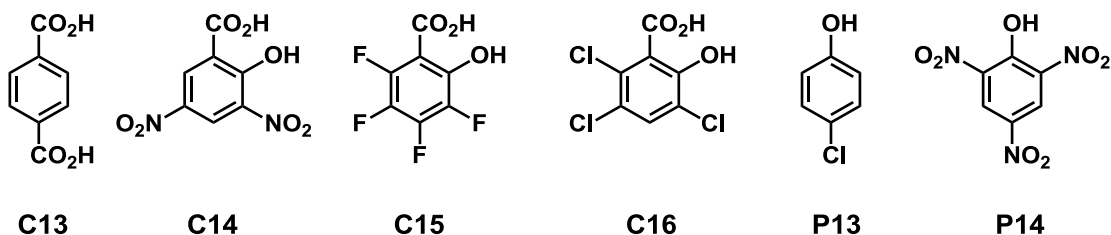


**Figure 3.17** Analytes **C12–C16** and **P13–P14**. **C12–C16** and **P11–P14** were also analyzed using cruciform **6** as the sole sensor.

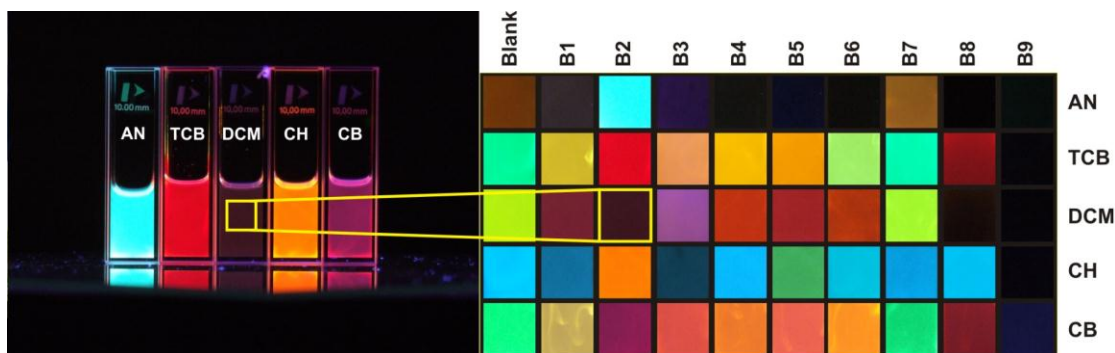


**Figure 3.18** The original photo of emission colors of solutions of **6/B2** mixture in five different solvents in UV/Vis spectroscopy cuvettes (left) and the panel of all boronic acids' emission colors in five solvents (right).

### 3.4.3 Calculation of RGB Changes

From each of the digital photographs of emission colors, representative segments were cut out using Adobe PhotoShop. These cut-outs were arranged into panels (as



shown in Figure 3.18) using CorelDRAW X5, and then exported into TIFF files. Figure 3.19 shows the complete panels of emission colors of pure cruciform **6** exposed to carboxylic (**C1–C16**) and boronic (**B1–B9**) acids, and phenols **P11–P14**.

Numeric values for R(ed), G(reen), and B(lue) colors were extracted from the emission color panels using freely downloadable program Colour Contrast Analyzer.<sup>46</sup> These values were extracted for each analyte in each solvent, and were then statistically treated

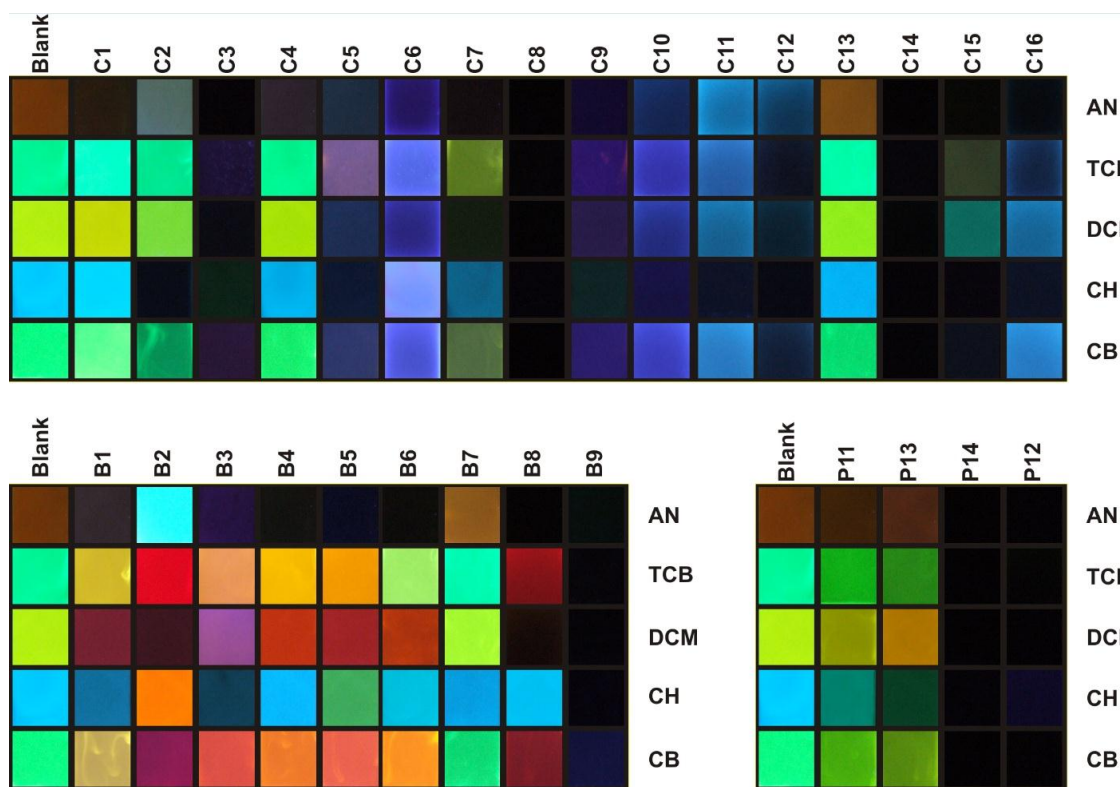


**Figure 3.19** Panels with the photographs of the emission colors observed when the solutions of cruciform **6** were exposed to carboxylic acids **C1–C16** (top), boronic acids **B1–B9** (bottom left), and phenols **P11–P14** (bottom right), and irradiated at 365 nm.

and compared to other analytes and the blank solutions of each experiment using Microsoft Excel.

To evaluate the correlation between the R/G/B values of different analytes within the same compound class, we also calculated relative standard deviations  $\sigma$ . For arbitrary compounds **X** and **Y**, this  $\sigma'_{X@Y}$  was defined as:

$$\sigma'_{X@Y} = \sqrt{\frac{\sum_{solvent}^i (R_X - R_Y)^2 + (G_X - G_Y)^2 + (B_X - B_Y)^2}{3 \cdot i}} \quad (3)$$

Importantly, these relative standard deviations are not solvent-specific, as they statistically treat R/G/B differences across all examined solvents. Thus, a single number—plotted in the graphs in Figure 3.4 (for carboxylic acid analytes), Figure 3.6 (for boronic acids analytes), Figure 3.8 (for phenol analytes with boronic acid additives),

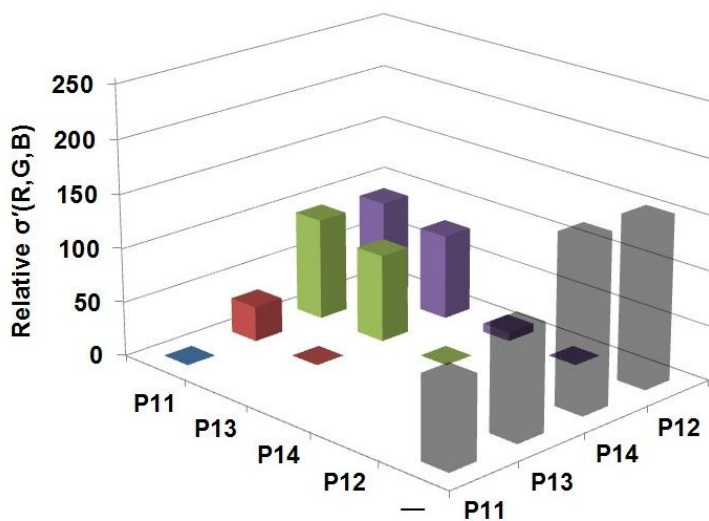


**Figure 3.20** Correlation of  $\sigma'$  values for R/G/B values of phenols **P11–P14** using cruciform **6** as the sole sensor. Correlation with the blank sample is given in the row of semi-transparent bars marked with "—".

Figure 3.11 (for amine and urea analytes with boronic acid additives), Figure 3.14 (for anionic analytes with boronic acid additives), and Figure 3.20 (for **P11–P14** without boronic acid additive)—describe a difference between the two analytes.

#### **3.4.4 Discrimination of P1–P12 with Solutions of Cruciform 6 Combined with B1 or B5**

Each of the phenol analytes **P1–P12** was treated with ten separate sensing solutions. First, five solutions were prepared by dissolving 2,6-dichlorophenylboronic acid (**B1**, 76.3 mg, 0.40 mmol) in 20 mL of  $1.0 \times 10^{-6}$  M solutions of cruciform **6** in AN, TCB, CH, DCM, and CF, successively. Second, five solutions were prepared by dissolving phenylboronic acid (**B5**, 48.8 mg, 0.40 mmol) in 20 mL of  $1.0 \times 10^{-6}$  M solutions of cruciform **6** in AN, TCB, CH, DCM, and CF, successively. In each of these ten sensor solutions, the molar ratio between cruciform **6** and the boronic acid was 1 : 20,000. Sensing solutions were left to stand for 7 h, before dissolving ten samples of 20 mg each of phenol derivatives **P1–P12** in 1 mL of each of the sensing solutions. The final molar ratios of **6** : boronic acid : phenol varied between 1 : 20,000 : 90,500 to 1 : 20,000 : 213,000. All photos were taken 4 h after the corresponding phenol/(**B1** or **B5**)/**6** solutions were prepared. Two five-cuvette sets (one for **B1**, one for **B5** additive) were placed on glass plate, irradiated at 365 nm by a handheld UV lamp, and immediately photographed.

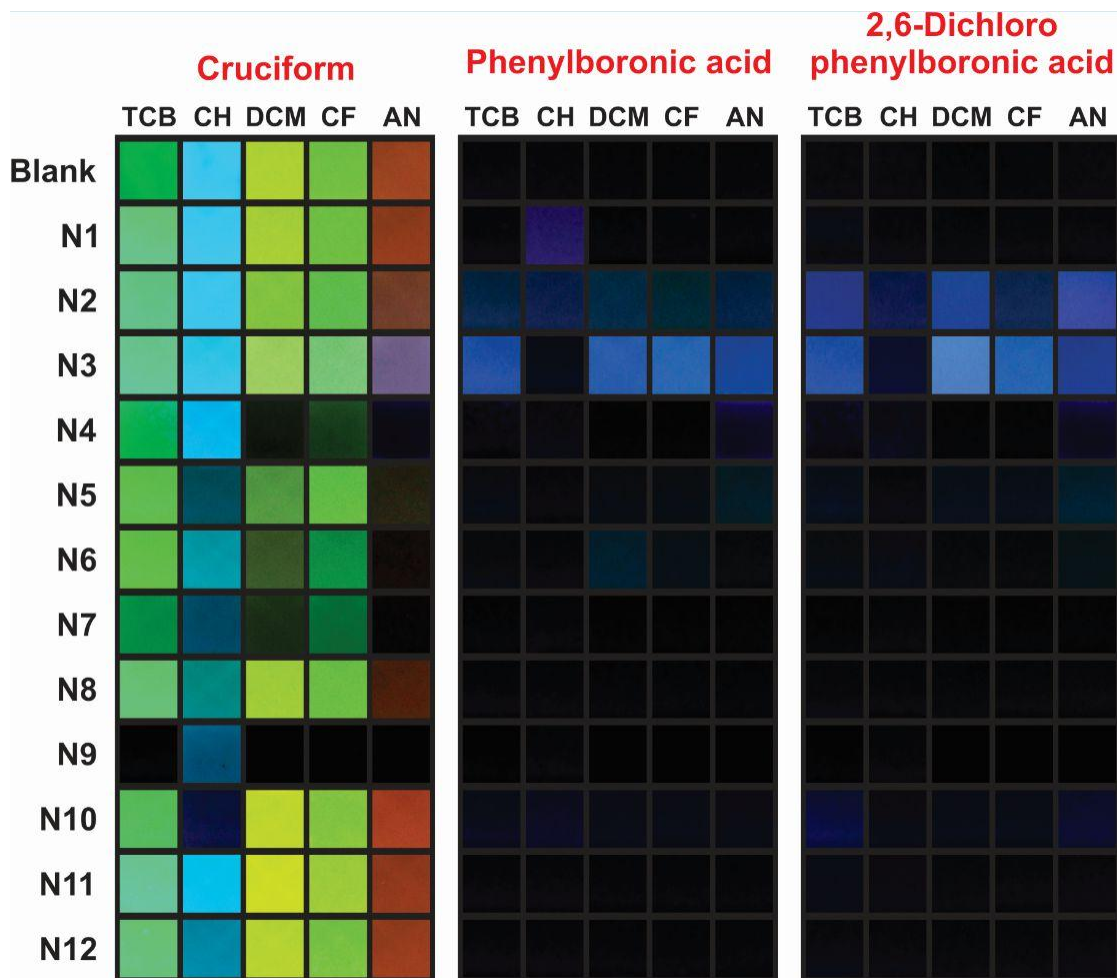


**Figure 3.21** In three control experiments, amine and urea analytes were exposed to the solutions of only cruciform **6** (no boronic acids, left), only **B5** (no cruciform, middle), or only **B1** (no cruciform, right). The photographic workup was the same as in the above described experiments.

### 3.4.5 Discrimination of Amines and Ureas Using Cruciform 6 and Boronic Acid Additives: Boronic Acid Variation

Seven solutions of cruciform **6**/boronic acids **B1**, **B4**, **B5**, **B10–B13** were prepared by dissolving 2,6-dichlorophenylboronic acid (**B1**, 229 mg, 1.2 mmol), 4-

methoxyphenylboronic acid (**B4**, 182 mg, 1.2 mmol), phenylboronic acid (**B5**, 145 mg, 1.2 mmol), 1,4-benzenediboronic acid (**B10**, 199 mg, 1.2 mmol), 4-(*N,N*-dimethylamino)phenylboronic acid (**B11**, 198 mg, 1.2 mmol), 4-iodophenylboronic acid (**B12**, 297 mg, 1.2 mmol), or 4-formylbenzeneboronic acid (**B13**, 180 mg, 1.2 mmol) in 60 mL of  $1.0 \times 10^{-6}$  M solutions of cruciform **6** in TCB.

Each of the cruciform/boronic acid solutions was used immediately after the preparation to dissolve seven samples of 40 mg each of amines and ureas. For each analyte, aliquots of the seven prepared analyte/boronic acid/**6** solutions were transferred to a set of seven quartz cuvettes. These seven cuvettes were placed on a glass plate, exposed to 365 nm of UV light by a handheld UV lamp, and immediately photographed.

### **3.4.6 Discrimination of Amines and Ureas Using Cruciform 6 and Boronic Acid Additives: Solvent Variation**

Each of the examined amines and ureas was treated with ten separate sensing solutions. First, five solutions were prepared by dissolving 2,6-dichlorophenylboronic acid (**B1**, 152.6 mg, 0.80 mmol) in 40 mL of  $1.0 \times 10^{-6}$  M solutions of cruciform **6** in AN, TCB, CH, DCM, and CF. Second, five solutions were prepared by dissolving phenylboronic acid (**B5**, 97.6 mg, 0.80 mmol) in 40 mL of  $1.0 \times 10^{-6}$  M solutions of cruciform **6** in AN, TCB, CH, DCM, and CF. In each of these ten sensor solutions, the molar ratio between the cruciform **6** and boronic acid was 1 : 20,000. Immediately after the preparation, 2 mL of each of the sensing solutions was used dissolve ten samples of

40 mg each of amines and ureas. The final molar ratios of **6** : boronic acid : amine/urea varied between 1 : 20,000 : 333,000 and 1 : 20,000 : 94,000.

For each analyte, aliquots of the ten prepared analyte/boronic acid/**6** solutions were transferred to separate quartz cuvettes. These two five-cuvette sets (one for **1/B1**, one for **1/B5**) were placed on glass plate, irradiated at 365 nm by a handheld UV lamp, and immediately photographed.

#### **3.4.7 Discrimination of Anions Using Cruciform 6 and Boronic Acid Additives: Boronic Acid Variation**

Seven solutions of cruciform **6**/boronic acids **B1**, **B4**, **B5**, **B10–B13** were prepared by dissolving 2,6-dichlorophenylboronic acid (**B1**, 229 mg, 1.2 mmol), 4-methoxyphenylboronic acid (**B4**, 182 mg, 1.2 mmol), phenylboronic acid (**B5**, 145 mg, 1.2 mmol), 1,4-benzenediboronic acid (**B10**, 199 mg, 1.2 mmol), 4-(*N,N*-dimethylamino)phenylboronic acid (**B11**, 198 mg, 1.2 mmol), 4-iodophenylboronic acid (**B12**, 297 mg, 1.2 mmol), or 4-formylbenzeneboronic acid (**B13**, 180 mg, 1.2 mmol) in 60 mL of  $1.0 \times 10^{-6}$  M solutions of cruciform **6** in TCB.

Each of the cruciform/boronic acid solutions was used immediately after the preparation to dissolve seven samples of 40 mg each of anions. For each analyte, aliquots of the seven prepared analyte/boronic acid/**6** solutions were transferred to a set of seven quartz cuvettes. These seven cuvettes were placed on glass plate, irradiated by a handheld UV lamp ( $\lambda_{\text{exc}}=365$  nm), and immediately photographed.

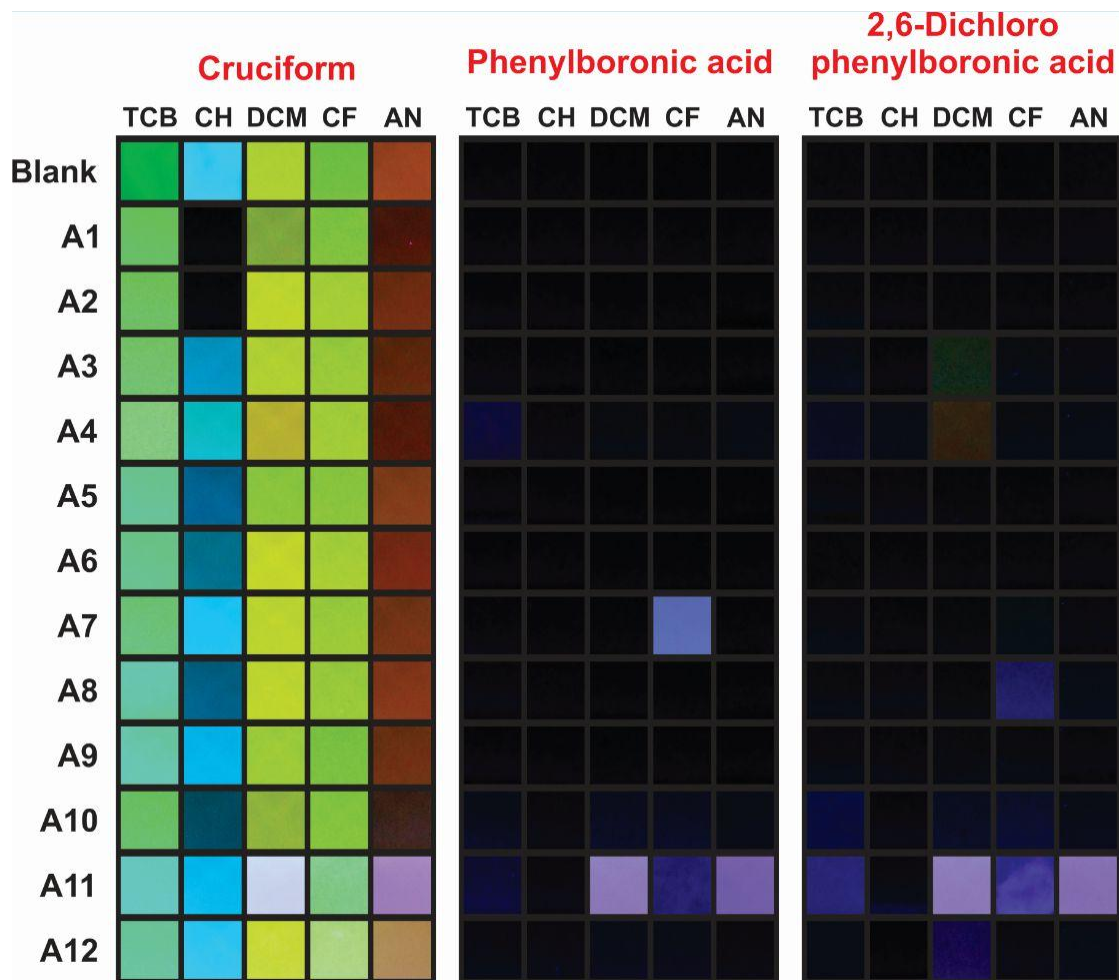


**Figure 3.22** In three control experiments, anion analytes were exposed to the solutions of only cruciform **6** (no boronic acids, left), only **B5** (no cruciform, middle), or only **B1** (no cruciform, right). The photographic workup was the same as in the above described experiments.

### 3.4.8 Discrimination of Anions Using Cruciform 6 and Boronic Acid Additives: Solvent Variation

Each of the examined anions was treated with ten separate sensing solutions. First, five solutions were prepared by dissolving 2,6-dichlorophenylboronic acid (**B1**, 152.6

mg, 0.80 mmol) in 40 mL of  $1.0 \times 10^{-6}$  M solutions of cruciform **6** in AN, TCB, CH, DCM, and CF. Second, five solutions were prepared by dissolving phenylboronic acid (**B5**, 97.6 mg, 0.80 mmol) in 40 mL of  $1.0 \times 10^{-6}$  M solutions of cruciform **6** in AN, TCB, CH, DCM, and CF. In each of these ten sensor solutions, the molar ratio between the boronic acid and cruciform **6** was 20,000 : 1. Immediately after the preparation, 2 mL of each of the sensing solutions was used to dissolve ten samples of 40 mg each of anions shown. The final molar ratios of **6** : boronic acid : amine/urea varied between 1 : 20,000 : 76,500 and 1 : 20,000 : 51,600.

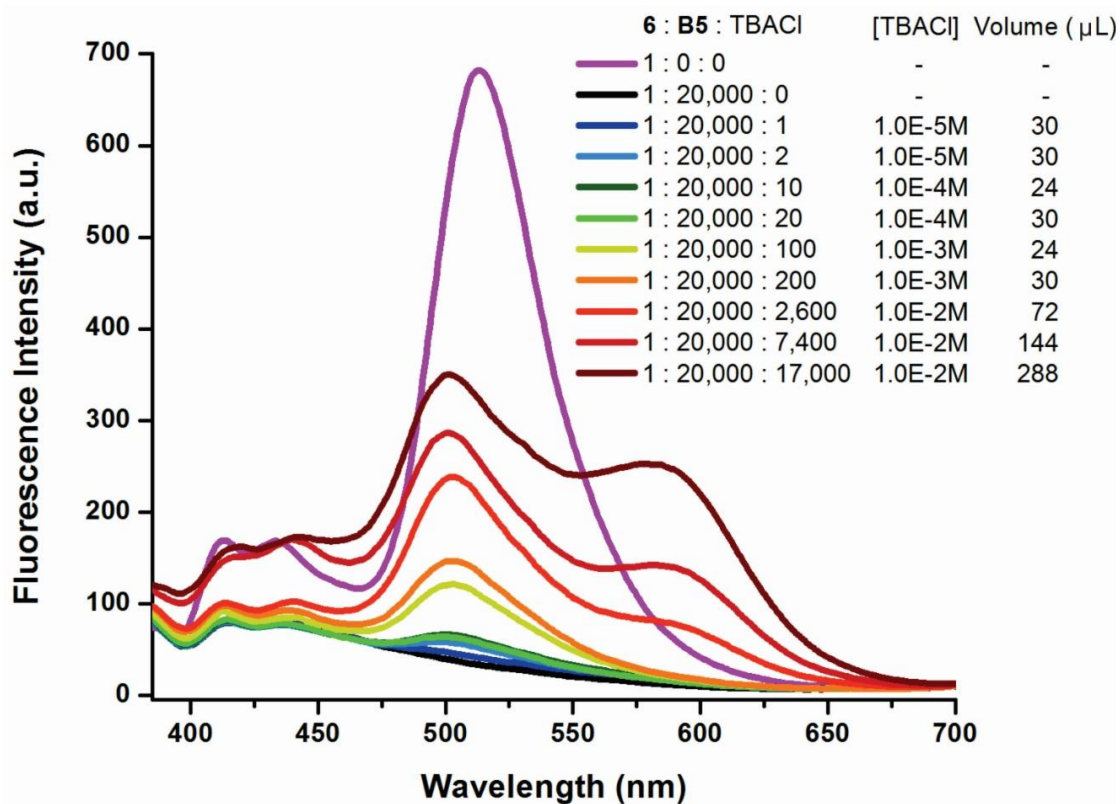


**Figure 3.24** Fluorescence emission spectra for the titration of solution of **6/B5** in TCB with a concentrated solution of TBACl. Excitation wavelength is 365 nm, excitation slit width is 10 nm, and emission slit width is 10 nm.



For each analyte, aliquots of the ten prepared analyte/boronic acid/**6** solutions were transferred to separate quartz cuvettes. These two five-cuvette sets (one for **6/B1**, one for **6/B5**) were placed on glass plate, irradiated at 365 nm by a handheld UV lamp, and immediately photographed.

### 3.4.9 Fluorescence Titration of a Mixture of **6** and **B5** with TBACl

A Perkin-Elmer Fluorescence Spectrometer LS-55 was used for the fluorescence titration a solution of **6** and **B5** with TBACl. The concentration of cruciform **6** in the titrated solution was about  $1.0 \times 10^{-7}$  M, and the ratio of **6** : **B5** was 1: 20,000.

To prepare 0.01 M stock solution of TBACl in TCB, TBACl (278 mg, 2.54 mmol) was added to 30 mL of TCB solvent in 100 mL volumetric flask, and then the flask was filled with additional TCB to the graduation. Ten-, hundred-, and thousand-fold diluted solutions of the stock solution,  $1.0 \times 10^{-3}$  M,  $1.0 \times 10^{-4}$  M, and  $1.0 \times 10^{-5}$  M, were also prepared.

A quartz cuvette with a maximum volume of 4 mL was filled with 3 mL of  $1.0 \times 10^{-7}$  M solution of **6** in TCB to select the excitation and emission slit widths, to see the emission intensity as well. After taking the emission spectrum of cruciform **6** solution, the cuvette was filled with 3 mL of **6/B5** solution, and then treated with volumes of TBACl solutions shown in Figure 3.24 with a micro syringe. Because the ratio of added TBACl ranged from 1 to 17,000 equivalents (relative to **6**), four different stock

solutions of TBACl, with progressively higher concentrations had to be used. These concentrations are indicated in the legend to Figure 3.24.

## Chapter Four

### Structural Studies of Benzobisoxazole Cruciforms' Organization in the Solid State<sup>82</sup>

#### 4.1 Introduction

An apparent omission in the studies of cruciforms described in Chapter 1 is the lack of structural analysis using X-ray crystallography—the ultimate way to obtain structural information in detail. As we have seen in Chapter 1, the main streams of cruciform research flowed into the study of the structure-property relationship through the introduction of various donors/acceptors to cruciform's end-groups and the use of cruciform scaffold as dendrimeric core decorated with functional moieties. Considering the history of this area started since mid-1990s in earnest,<sup>28a,b</sup> a comprehensive picture of factors that favor certain assembly patterns within a class appears to be lacking although several crystal structures of molecular cruciforms have been reported.<sup>12i,16f.,16j,16p-q,42a,83</sup>

Because of their appealing electronic properties and well-defined rigid geometries, molecular cruciforms are promising synthons for the construction of ordered solid-state functional assemblies based on e.g. metal organic frameworks (MOFs),<sup>84</sup> covalent organic frameworks (COFs),<sup>85</sup> or discrete porous molecular cages.<sup>86</sup> As mentioned in Chapter 1, the first use of cruciform spacer into MOF construction has very recently been reported by Yaghi's group,<sup>17a</sup> and they employed cruciform **94** to create zirconium-based MOF-535. From this perspective, the examination of cruciforms' crystal structures is of eminent importance. In this chapter, the supramolecular solid-state

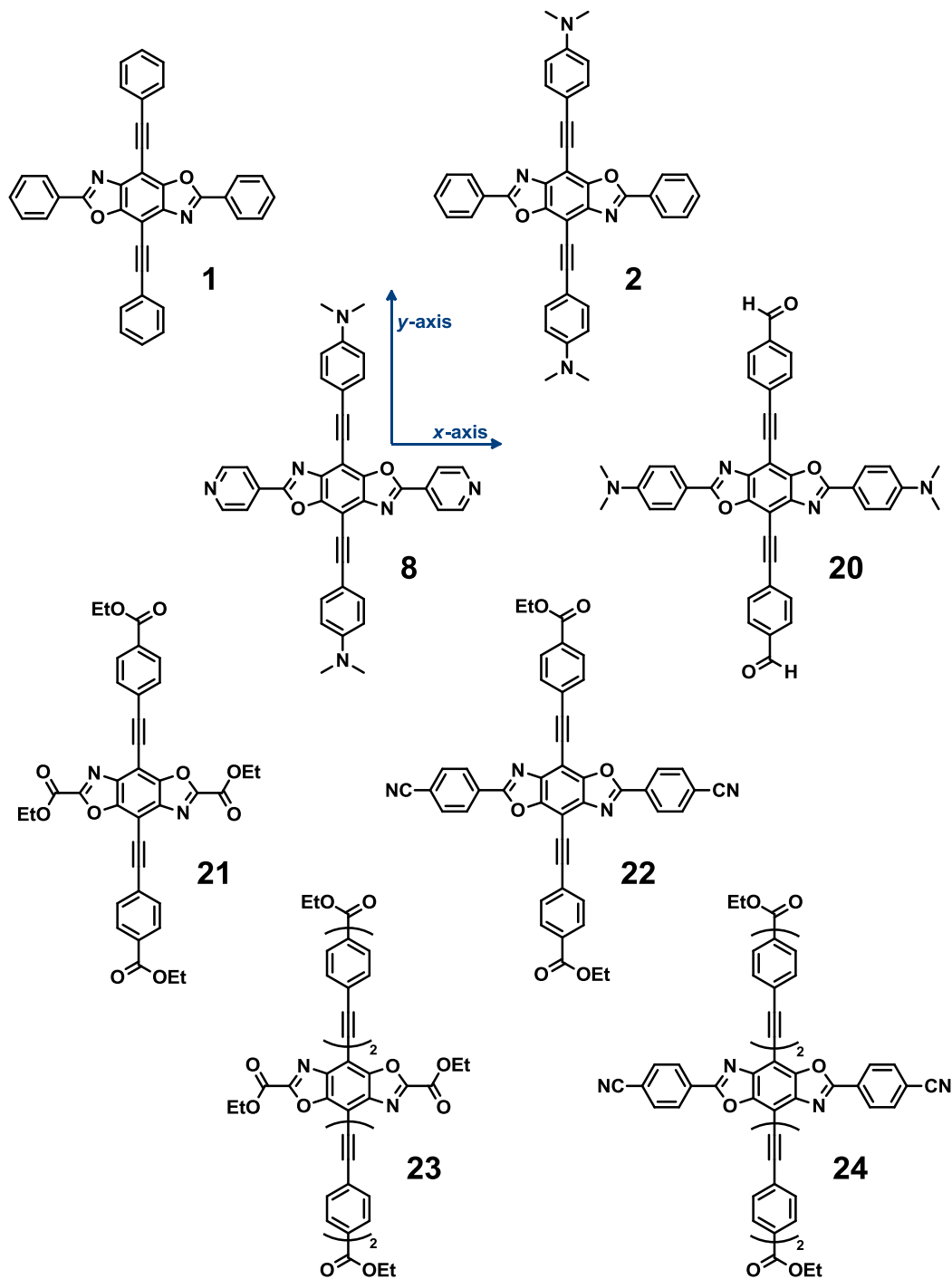
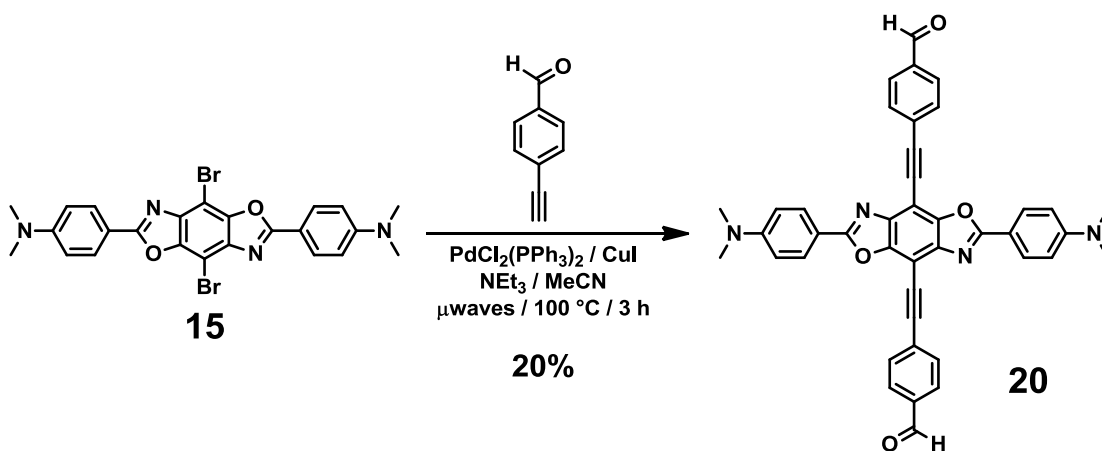


**Chart 4.1** Benzo[1,2-*d*:4,5-*d'*]bixazole (BBO)-centered cruciform fluorophores.

The *x* and *y* axes are defined as illustrated for cruciform **8**.

structures of eight benzobisoxazole cruciforms **1**, **2**, **8**, and **20–24** (Chart 4.1) in which horizontal (*x*) and vertical (*y*) axes intersect at a  $\sim 90^\circ$  angle are described in detail. The length of the *x*-axis was varied between  $\sim 6.3$  Å in compounds **21** and **23**—where the terminal substituent is directly attached to the BBO system, and  $\sim 14.7$  Å in compounds **1**, **2**, **5**, **20**, **22**, and **24**, in which 1,4-phenylene linkers separate the BBO core from the terminal substituents. Similarly, cruciforms with two different lengths of *y*-axis were



**Scheme 4.1** Synthesis of new cruciform **20**.

examined: compounds **1**, **2**, **5**, and **20–22**, with a  $\sim 16.6$  Å long *y*-axis had a single phenylethynylene unit separating the BBO core from the terminal substituent on either side. Longer cruciforms **23** and **24** were decorated with twice longer intervening linkers, resulting in the total length along *y*-axis of approx. 30.2 Å. Specifically, this chapter will highlight: (1) the synthesis and spectroscopic characterization of novel benzobisoxazole cruciforms **20**; (2) crystal structures of cruciforms **1**, **2**, **8**, and **20**, as well as the previously synthesized compounds **21–24**,<sup>87</sup> and (3) the comparison of molecular and supramolecular structures of the series of eight cruciforms.

**Table 4.1** Crystallographic data for Cruciforms **1**, **2**, **8**, and **20**.

Compound reference	Cruciform <b>1</b>	Cruciform <b>2</b>	Cruciform <b>8</b>	Cruciform <b>20</b>
Chemical formula	C <sub>36</sub> H <sub>20</sub> N <sub>2</sub> O <sub>2</sub>	C <sub>40</sub> H <sub>30</sub> N <sub>4</sub> O <sub>2</sub>	C <sub>46</sub> H <sub>30</sub> Cl <sub>4</sub> N <sub>4</sub> O <sub>6</sub>	C <sub>44</sub> H <sub>34</sub> Cl <sub>4</sub> N <sub>4</sub> O <sub>4</sub>
Formula Mass	512.54	598.68	876.54	739.63
Crystal system	Trigonal	Monoclinic	Monoclinic	Triclinic
<i>a</i> /Å	40.527(3)	16.3473(14)	20.440(4)	9.0410(18)
<i>b</i> /Å	40.527(3)	8.9927(8)	5.8011(11)	10.560(2)
<i>c</i> /Å	4.3741(5)	23.966(2)	30.416(6)	11.850(2)
$\alpha$ /°	90	90	90	65.99(3)
$\beta$ /°	90	94.853(2)	108.933(5)	79.99(3)
$\gamma$ /°	120	90	90	88.69(3)
Unit cell volume/Å <sup>3</sup>	6221.6(9)	3510.5(5)	3411.3(11)	1016.3(4)
Temperature/K	223(2)	223(2)	223(2)	293(2)
Space group	<i>R</i> $\bar{3}$	<i>C</i> 2/ <i>c</i>	<i>C</i> 2/ <i>c</i>	<i>P</i> 1
No. of formula units per unit cell, <i>Z</i>	9	4	4	1
Radiation type	Mo-K $\alpha$	Mo-K $\alpha$	Mo-K $\alpha$	Mo-K $\alpha$
Absorption coefficient, $\mu$ /mm <sup>-1</sup>	0.077	0.071	0.235	0.339
No. of reflections measured	21017	16338	11258	10511
No. of independent reflections	3157	4013	3842	4619
<i>R</i> <sub>int</sub>	0.0899	0.0623	0.1109	0.0458
<i>R</i> <sub>I</sub> ( <i>I</i> > 2 $\sigma$ ( <i>I</i> ))	0.069	0.0722	0.0659	0.0869
<i>wR</i> ( <i>F</i> <sup>2</sup> ) ( <i>I</i> > 2 $\sigma$ ( <i>I</i> ))	0.1007	0.1963	0.1477	0.2320
<i>R</i> <sub>I</sub> (all data)	0.1226	0.1108	0.147	0.1831
<i>wR</i> ( <i>F</i> <sup>2</sup> ) (all data)	0.1077	0.2200	0.2044	0.2945
Goodness of fit on <i>F</i> <sup>2</sup>	1.727	1.009	0.908	1.028

## 4.2 Results and Discussion

### 4.2.1 Synthesis of Materials

New cruciform **20** was prepared (Scheme 4.1) through a Sonogashira coupling<sup>47</sup> of precursors **15** described in Chapter 1 with 4-ethynylbenzaldehyde.<sup>88</sup> After routine purification, the dark red powder was obtained in 20% yield. The details of a synthetic

**Table 4.2** Crystallographic data for Cruciforms **21–24**.

Compound reference	Cruciform <b>21</b> <sup>a</sup>	Cruciform <b>22</b> <sup>a</sup>	Cruciform <b>23</b> <sup>a</sup>	Cruciform <b>24</b>
Chemical formula	C <sub>40</sub> H <sub>34</sub> N <sub>4</sub> O <sub>10</sub>	C <sub>46</sub> H <sub>30</sub> Cl <sub>4</sub> N <sub>4</sub> O <sub>6</sub>	C <sub>54</sub> H <sub>40</sub> Cl <sub>4</sub> N <sub>2</sub> O <sub>10</sub>	C <sub>60</sub> H <sub>34</sub> N <sub>4</sub> O <sub>6</sub>
Formula Mass	730.71	876.54	1018.68	906.91
Crystal system	Triclinic	Triclinic	Triclinic	Triclinic
<i>a</i> /Å	7.5375(11)	3.8598(5)	8.9868(15)	7.4382(9)
<i>b</i> /Å	8.5549(12)	14.4562(17)	9.9983(17)	17.0249(19)
<i>c</i> /Å	14.7035(21)	18.4857(22)	14.506(3)	20.224(2)
$\alpha$ /°	101.088(2)	105.228(2)	99.874(3)	96.374(9)
$\beta$ /°	98.465(2)	94.344(2)	93.339(3)	97.194(9)
$\gamma$ /°	92.660(2)	93.861(2)	107.320(3)	94.166(8)
Unit cell volume/Å <sup>3</sup>	917.6(2)	988.3(2)	1217.6(4)	2515.4(5)
Temperature/K	223(2)	223(2)	193(2)	100(2)
Space group	<i>P</i> 1	<i>P</i> 1	<i>P</i> 1	<i>P</i> 1
No. of formula units per unit cell, <i>Z</i>	1	1	1	2
Radiation type	Mo-K $\alpha$	Mo-K $\alpha$	Mo-K $\alpha$	Cu-K $\alpha$
Absorption coefficient, $\mu$ /mm <sup>-1</sup>	0.096	0.357	0.306	0.631
No. of reflections measured	4097	5050	9381	28 025
No. of independent reflections	2699	3470	4259	8696
<i>R</i> <sub>int</sub>	0.0350	0.0535	0.0272	0.0575
<i>R</i> <sub><i>I</i></sub> ( <i>I</i> > 2 $\sigma$ ( <i>I</i> ))	0.0453	0.0501	0.0808	0.0799
<i>wR</i> ( <i>F</i> <sup>2</sup> ) ( <i>I</i> > 2 $\sigma$ ( <i>I</i> ))	0.1164	0.1200	0.1864	0.2156
<i>R</i> <sub><i>I</i></sub> (all data)	0.0896	0.0811	0.1090	0.1112
<i>wR</i> ( <i>F</i> <sup>2</sup> ) (all data)	0.1490	0.1418	0.2001	0.2316
Goodness of fit on <i>F</i> <sup>2</sup>	1.022	1.025	1.021	1.046

<sup>a</sup> See also ref. 87

procedure is in the Experimental Section. Compound **20** is highly fluorescent in solution, and dimly red fluorescent in solid state when irradiated with a 356 nm handheld UV lamp.

## 4.2.2 X-Ray Crystal Structure Analysis

### 4.2.2.1 Cruciform **1**<sup>32</sup>

Compound **1** crystallizes in the  $R\bar{3}$  space group, with nine molecules of **1** in the unit cell. Solvent ( $\text{CHCl}_3$ ) molecules appear to surround the crystallographic  $c$ -axis, but are disordered to such an extent that subtraction of their electron density (using the PLATON/SQUEEZE<sup>89</sup> routine) from the final refined structure was necessary. The crystal structure of **1** (Figure 4.1A) reveals an essentially planar molecule, with minimal distortions of peripheral phenyl rings relative to the average plane of the BBO nucleus: the phenyl rings oriented along the  $x$ -axis are at a  $5.7^\circ$  angle relative to the molecule's core, while the vertical phenyl rings define a  $5.9^\circ$  angle with the core. The angle between the horizontal and the vertical axis is  $86.8^\circ$ , defined by the centroids of (a) the vertical phenyl ring, (b) the benzene ring of the benzobisoxazole core, and (c) the horizontal phenyl ring. The triple bonds of **1** are virtually undeformed, with  $\text{C}\equiv\text{C}-\text{C}$  angles of  $178.8^\circ$  and  $179.3^\circ$ . While the molecular structure of **1** generally resembles those of **8** and **20–22**, its supramolecular organization in the crystal is entirely different. Molecules of **1** are stacked in an offset arrangement into infinite columns, with a  $3.44 \text{ \AA}$  interplanar distances between molecules of **1** (Figure 4.1B). Six of these columns, which alternate in the direction of their tilt, surround a three-fold rotation axis. Through its phenyl rings on the  $y$ -axis, each cruciform is shared between two of these six-column assemblies, forming the complete three-dimensional structure. The six molecules of **1** that surround the three-fold axis establish short  $[\text{N}_{\text{oxazole}} \cdots \text{H}-\text{C}_{\text{sp}2}]$  contacts ( $2.58 \text{ \AA}$ ) between the BBO nitrogen atoms of one cruciform and the *para*-hydrogen atoms on the horizontal phenyl rings on



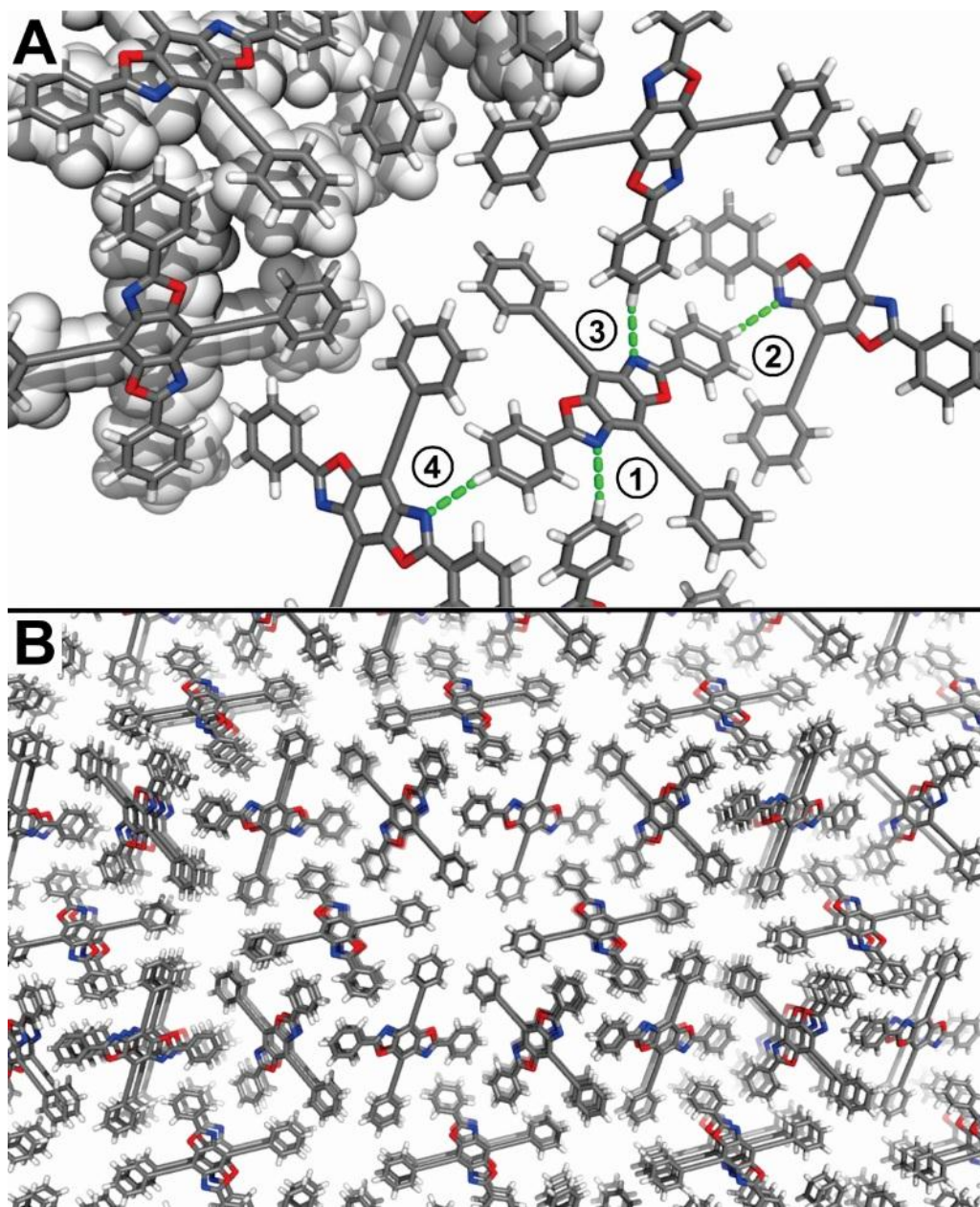


**Figure 4.1** (A) Crystal structure of **1** with intermolecular hydrogen bonds highlighted in green. *Contacts 1–4* are identical and characterized by the following geometry:  $\text{N}\cdots\text{H}$  2.58 Å,  $\text{N}\cdots\text{C}$  3.60 Å,  $\text{N}\cdots\text{H}-\text{C}$  155.3°. (B) The three-dimensional structure of compound **1** consists of six alternating stacks of molecules (interplanar distance of 3.44 Å) organized around a three-fold rotation axis. C—gray, H—white, N—blue, and O—red.

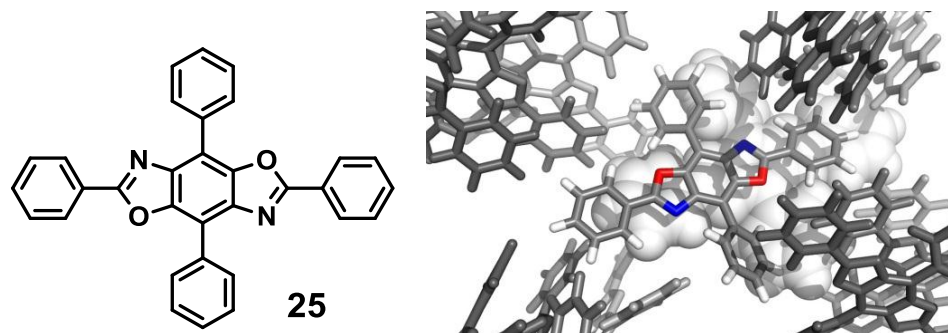


**Figure 4.2** Schematic and crystal structures of cruciform **25**, previously studied by Nuckolls et al.

adjacent cruciforms. Contacts between the cruciforms and solvent ( $\text{CHCl}_3$ ) presumably occur along the channels surrounding the three-fold rotation axis—but more specific data could not be obtained, because of the prohibitively large disorder of solvent molecules.

Intriguingly, cruciform **25** (Figure 4.2, left)—previously characterized by Nuckolls *et al.*<sup>42a</sup>—does not share the organizational motives of **1**. It is significantly deplanarized (Figure 4.2, right): the phenyl rings along its  $y$ -axis distort out of the BBO plane by  $34.7^\circ$  and  $29.1^\circ$ , while those along the  $x$ -axis form angles of  $13.1^\circ$  and  $2.4^\circ$  with the central BBO core. The supramolecular organization of **25** is dominated by edge-to-face  $[\text{C}-\text{H}\cdots\pi]$  contacts between the peripheral benzene rings. Both of these observations point to the importance of the sterically undemanding  $-\text{C}\equiv\text{C}-$  linkers in the organization of **1**: they allow the molecule to adopt an essentially planar structure, and make the central BBO core available for short contacts that presumably play the role in the assembly of the three-dimensional structure.

#### 4.2.2.2 Cruciform **2**<sup>32</sup>

Cruciform **2** crystallizes in the  $C2/c$  space group, with four molecules of **2** in the unit cell, and one half of a molecule in the asymmetric unit. Similarly to compound **1**,  $\text{CHCl}_3$  solvent molecules were too disordered to be successfully modelled and were subtracted using the PLATON/SQUEEZE routine. Among the eight cruciforms studied, compound **2** is most significantly deplanarized (Figure 4.3): the electron-rich benzene

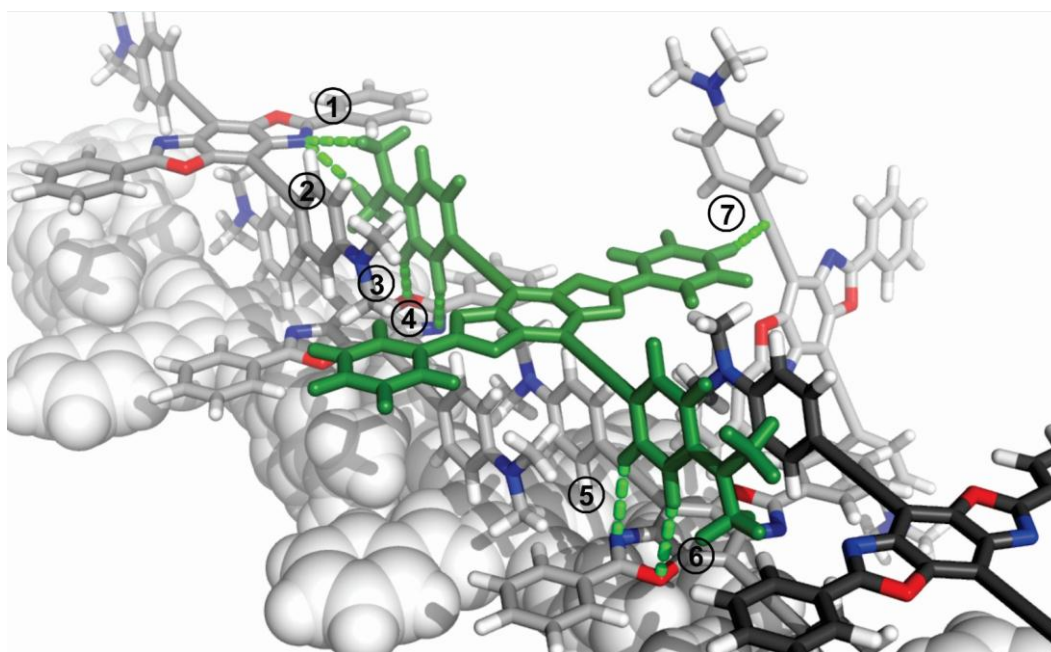


**Figure 4.3** Crystal structure of **2** with short intermolecular contacts highlighted in green. *Contact 1*:  $\text{H}\cdots\text{N}$  3.01 Å,  $\text{C}\cdots\text{N}$  4.05 Å,  $\text{C}-\text{H}\cdots\text{N}$  158.8°. *Contact 2*:  $\text{H}\cdots\text{N}$  3.00 Å,  $\text{C}\cdots\text{N}$  4.04 Å,  $\text{C}-\text{H}\cdots\text{N}$  159.3°. *Contact 3*:  $\text{H}\cdots\text{O}$  2.74 Å,  $\text{C}\cdots\text{O}$  3.75 Å,  $\text{C}-\text{H}\cdots\text{O}$  154.1°. *Contact 4*:  $\text{H}\cdots\text{N}$  2.78 Å,  $\text{C}\cdots\text{N}$  3.53 Å,  $\text{C}-\text{H}\cdots\text{N}$  125.6°. *Contact 5*:  $\text{H}\cdots\text{N}$  2.70 Å,  $\text{C}\cdots\text{N}$  3.58 Å,  $\text{C}-\text{H}\cdots\text{N}$  137.3°. *Contact 6*:  $\text{H}\cdots\text{O}$  2.66 Å,  $\text{C}\cdots\text{O}$  3.70 Å,  $\text{C}-\text{H}\cdots\text{O}$  160.1°. *Contact 7*:  $\text{H}\cdots(\text{C}\equiv\text{C}_{\text{centroid}})$  2.86 Å,  $\text{C}\cdots(\text{C}\equiv\text{C}_{\text{centroid}})$  3.91 Å,  $\text{C}-\text{H}\cdots(\text{C}\equiv\text{C}_{\text{centroid}})$  162.7°. C—gray, H—white, N—blue, and O—red.

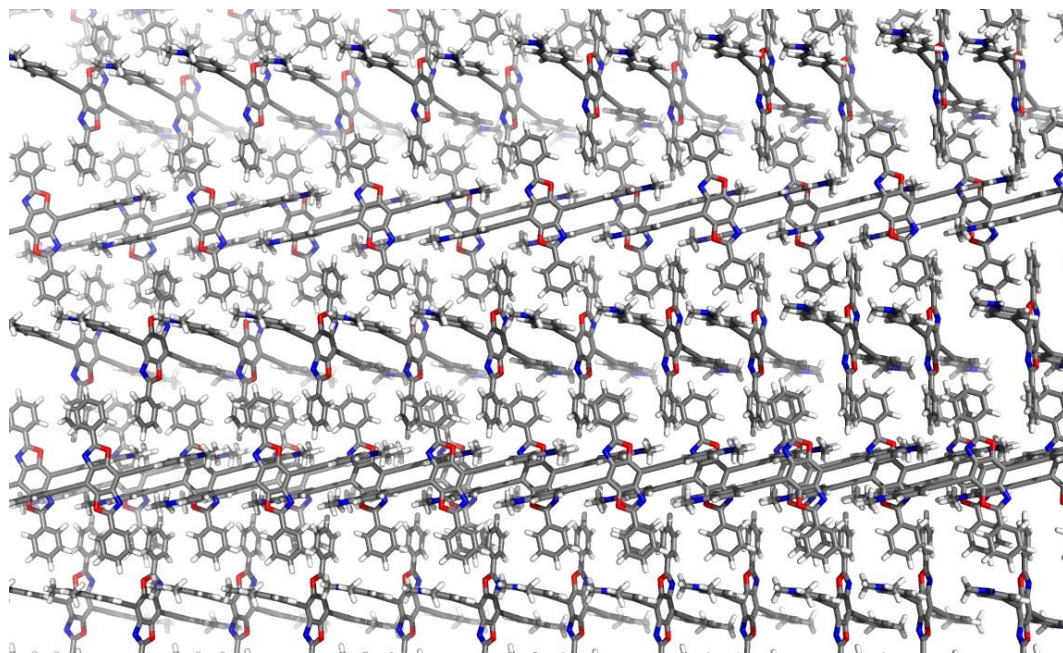


**Figure 4.4** Molecules of **2** are lined up in one-dimensional tapes that organize into two-dimensional layers through  $[\text{O}_{\text{oxazole}} \cdots \text{H}-\text{C}]$  and  $[\text{N}_{\text{oxazole}} \cdots \text{H}-\text{C}]$  contacts between the adjacent tapes. Adjacent two-dimensional sheets define an angle of  $63.3^\circ$ . C—gray, H—white, N—blue, and O—red.

rings positioned along the cruciforms y-axis distort by  $82.1^\circ$  relative to the central BBO core. This almost perpendicular arrangement translates into a packing pattern that dramatically differs from those observed in the other seven cruciforms. Through a  $[\pi \cdots \pi]$  interaction between the 4-(*N,N*-dimethylamino)phenyl rings (interplanar distance of  $3.65 \text{ \AA}$ ), cruciform **2** is organized into infinite one-dimensional tapes. Within these tapes, short  $[\text{N}_{\text{oxazole}} \cdots \text{H}-\text{C}_{\text{sp}3}]$  contacts are established between the oxazole nitrogen atom of one cruciform and the hydrogens on the  $-\text{NMe}_2$  group in the adjacent cruciform (contacts 1 and 2 in Figure 4.3,  $3.00$  and  $3.01 \text{ \AA}$ ). Each of the cruciforms mediates contact with a parallel tape running underneath in Figure 4.3, through two  $[\text{O}_{\text{oxazole}} \cdots \text{H}-\text{C}_{\text{sp}2}]$  and two



[N<sub>oxazole</sub>...H-C<sub>sp2</sub>] hydrogen bonds (contacts 3–6 in Figure 4.3). Such two-dimensional stacking of tapes forms "cruciform walls", in which individual cruciforms' *x*-axes are positioned perpendicularly to the two-dimensional layer. The adjacent layer is rotated by 63.3° relative to the first one, and this two-layer motif repeats throughout the three-dimensional crystal (Figure 4.4). The two adjacent cruciform walls are in apparent contact through the [C<sub>sp2</sub>-H... $\pi$ ]<sup>90</sup> interaction of *para*-hydrogen atoms on the horizontal phenyl rings in one layer's cruciforms with the triple bonds of the adjacent layer's cruciforms (contact 7 in Figure 4.3).

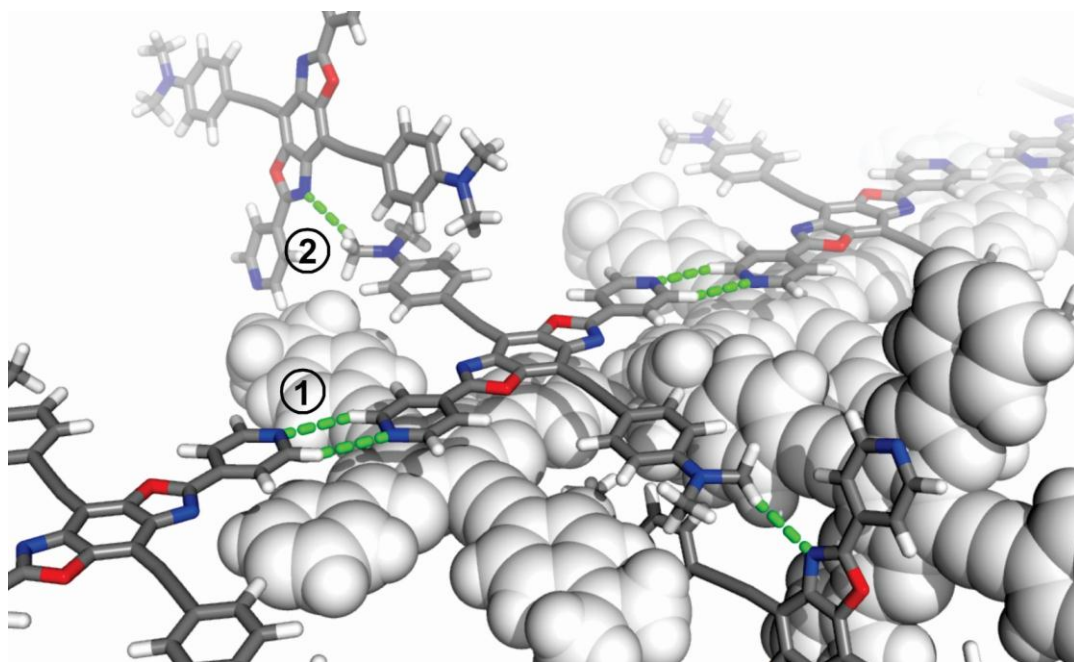


**Figure 4.5** Crystal structure of **8** with short intermolecular contacts highlighted in green. Solvent molecules are omitted. *Contact 1*: H...N 2.80 Å, C...N 3.73 Å, C-H...N 143.2°. *Contact 2*: H...N 2.64 Å, C...N 3.62 Å, C-H...N 148.7°. C—gray, H—white, N—blue, O—red, and Cl—green.

#### 4.2.2.3 Cruciform **8**<sup>32</sup>

Compound **8** also crystallizes in the  $C2/c$  space group, with four molecules of **8** and four molecules of  $\text{CH}_2\text{Cl}_2$  in the unit cell; the asymmetric unit contains half a molecule of **8** and half a  $\text{CH}_2\text{Cl}_2$  molecule. Structural replacement of the phenyl groups along the  $x$ -axis of cruciform **2** with 4-pyridyl moieties in compound **8** results in the replanarization of the latter (Figure 4.5). Vertically positioned phenyl rings of **8** distort by  $9.5^\circ$  from the plane of central BBO moiety, while the horizontal remain essentially coplanar—distorted by  $3.5^\circ$ . Triple bonds of **8** are slightly bent, with  $\text{C}\equiv\text{C}-\text{C}$  bond angles of  $173.2^\circ$  and  $178.6^\circ$ . Each molecule of **8** engages into  $[\pi\cdots\pi]$  stacking interactions with two adjacent molecules (Figure 4.5 and 4.6B); these stacks are offset and characterized by  $3.31\text{ \AA}$  interplanar distance. Stacks of **8** are connected to each other via pairwise  $[\text{N}_{\text{pyridine}}\cdots\text{H}-\text{C}_{\text{sp}2}]$  contacts ( $2.80\text{ \AA}$ , contact 1 in Figure 4.5), producing—analogously to the superstructure of **2**—a two-dimensional sheet that contains cruciforms'  $x$ -axes, but is perpendicular to their  $y$ -axes. The adjacent sheet is rotated by  $69.6^\circ$  with respect to the first one—and connected to it via a series of  $[\text{N}_{\text{oxazole}}\cdots\text{H}-\text{C}_{\text{sp}3}]$  contacts (contact 2 in Figure 4.5)—and this arrangement repeats throughout the crystal.

Notably, the ordered molecules of  $\text{CH}_2\text{Cl}_2$  solvent play an important role in the superstructure of **8** (Figure 4.6A). Each solvent molecule connects four neighbouring cruciforms through the formation of (a) two  $[\text{Cl}\cdots\text{H}-\text{C}_{\text{sp}2}]$  contacts between chlorines in  $\text{CH}_2\text{Cl}_2$  and hydrogen atoms *ortho*- to  $-\text{NMe}_2$  groups in two molecules of **8** (contact 3 in Figure 4.6A,  $2.90\text{ \AA}$ ) and (b) two  $[\text{C}_{\text{sp}3}-\text{H}\cdots\pi]^{90}$  contacts between the hydrogen atoms of

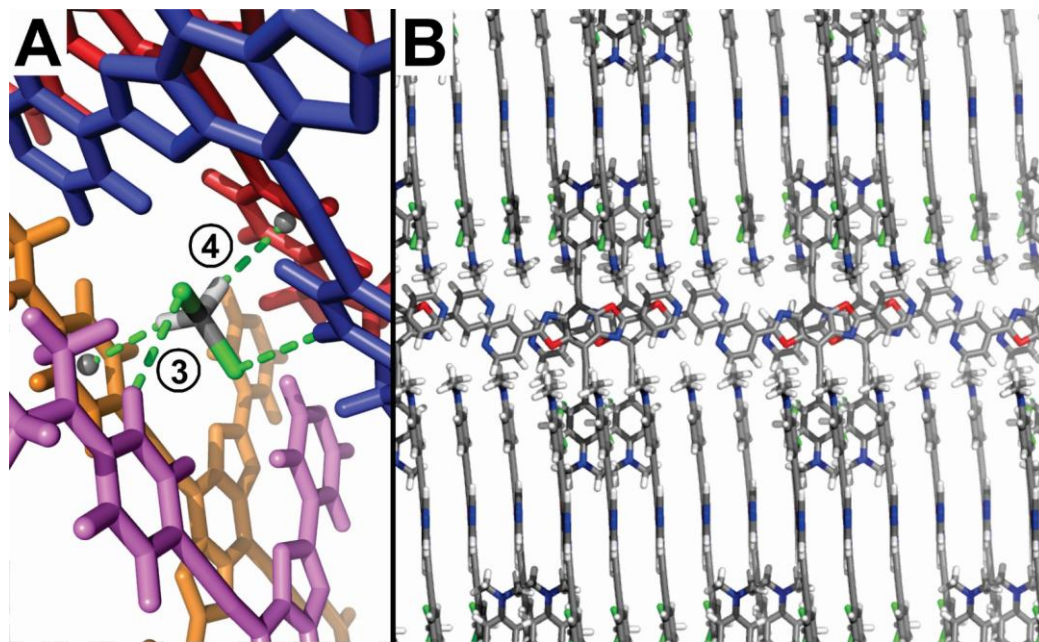


**Figure 4.6** (A) The association of  $\text{CH}_2\text{Cl}_2$  solvent molecules with four adjacent molecules of cruciform **8**. *Contact 3*:  $\text{Cl}\cdots\text{H}$  2.90 Å,  $\text{Cl}\cdots\text{C}$  3.88 Å,  $\text{C}-\text{Cl}\cdots\text{H}$  95.4°,  $\text{Cl}\cdots\text{H}-\text{C}$  149.5°. *Contact 4*:  $\text{H}\cdots\text{Ph}_{\text{centroid}}$  2.48 Å,  $\text{C}\cdots\text{Ph}_{\text{centroid}}$  3.51 Å,  $\text{C}-\text{H}\cdots\text{Ph}_{\text{centroid}}$  157.4°. (B) Compound **8** packs into one-dimensional tapes that organize into two-dimensional layers through  $[\pi\cdots\pi]$  stacking with a distance of 3.31 Å. The adjacent sheets define a 69.6° angle, and are in contact with each other through *contact 2* from Figure 4.5. C—gray, H—white, N—blue, O—red, and Cl—green.

$\text{CH}_2\text{Cl}_2$  and the electron-rich phenyl rings along the y-axis of two molecules of **8** (contact 4 in Figure 4.6A, with  $\text{H}\cdots\text{Ph}_{\text{centroid}}$  distance of 2.48 Å).

#### 4.2.2.4 Cruciform **20**

Compound **20** crystallizes in the  $P\bar{1}$  space group, with an asymmetric unit that contains half a molecule of **20** and one disordered molecule of  $\text{CH}_2\text{Cl}_2$ . This cruciform

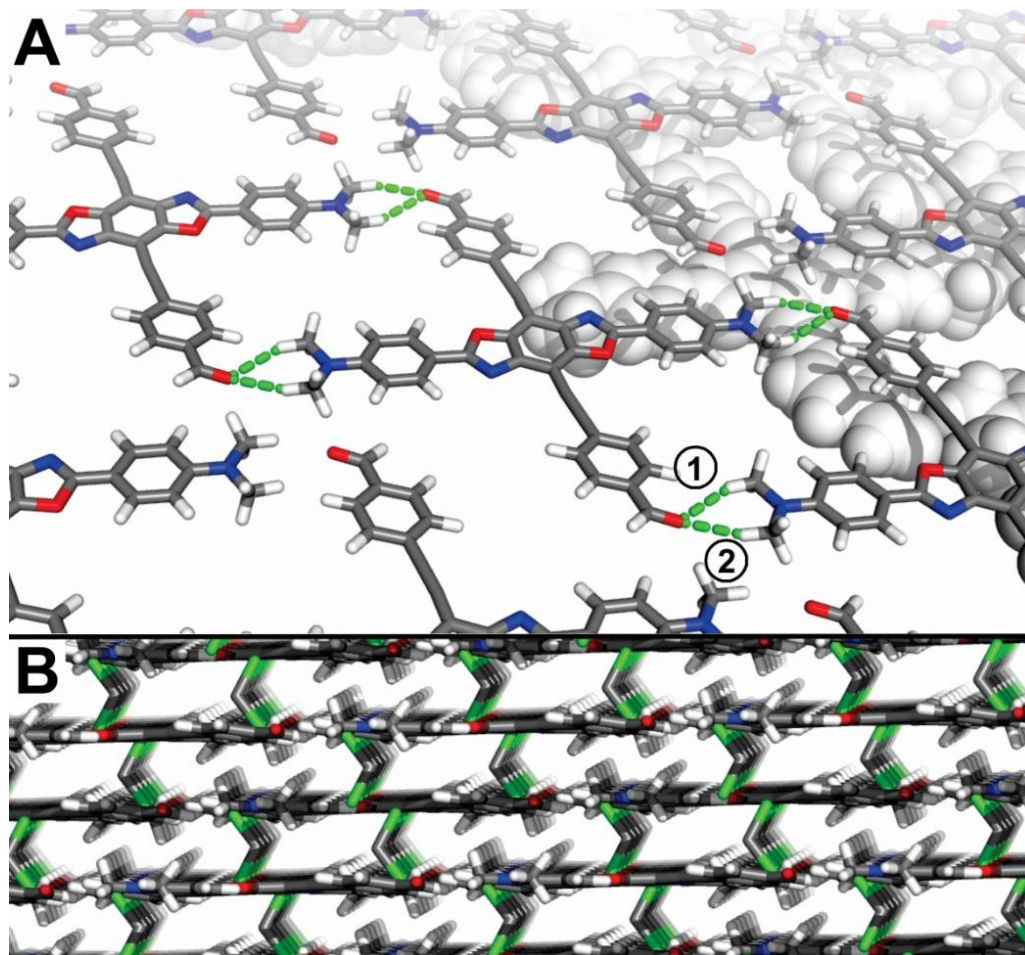


**Figure 4.7** (A) Crystal structure of **20** with short intermolecular contacts highlighted in green. Solvent molecules are omitted. *Contact 1*:  $\text{O} \cdots \text{H}$  2.50 Å,  $\text{O} \cdots \text{C}$  3.54 Å,  $\text{O} \cdots \text{H}-\text{C}$  158.5°,  $\text{C}=\text{O} \cdots \text{H}$  130.0°. *Contact 2*:  $\text{O} \cdots \text{H}$  2.51 Å,  $\text{O} \cdots \text{C}$  3.55 Å,  $\text{O} \cdots \text{H}-\text{C}$  162.3°,  $\text{C}=\text{O} \cdots \text{H}$  167.3°. (B) Compound **20** packs into two-dimensional sheets that organize into the three-dimensional structure through  $[\pi \cdots \pi]$  stacking with an interplanar distance of 3.64 Å. Disordered solvent ( $\text{CH}_2\text{Cl}_2$ ) molecules hydrogen bond to **20**, assisting in the assembly of this layered structure. C—gray, H—white, N—blue, O—red, and Cl—green.



(Figure 4.7A) is slightly deplanarized, with benzene rings positioned along the *y*-axis distorting from the central BBO plane by 10.0°, and those along the horizontal axis deplanarized by just 3.6°. Triple bonds are close to linear, with the corresponding C≡C–C bond angles of 174.7° and 179.8°. The cruciform organizes into two-dimensional sheets through short contacts between the aldehyde carbonyl and the hydrogen atoms in both methyl groups of the –NMe<sub>2</sub> functionality. The short contacts are characterized by H···O distances of 2.50 and 2.51 Å (contacts 1 and 2 in Figure 4.7A). In contrast to cruciforms **21** and **22**, compound **20** does not involve its aromatic hydrogens in the formation of the sheet superstructures—although some short contacts between aryl hydrogens and the disordered solvent are apparent. Planes of cruciform molecules stack into the three-dimensional structure via [ $\pi\cdots\pi$ ] contacts with an average interplanar distance of 3.64 Å (Figure 4.7B).

#### 4.2.2.5 Cruciform **21**<sup>87</sup>

Compound **21** crystallizes in the  $P\bar{1}$  space group, with an asymmetric unit that contains half a molecule of **21** and one disordered molecule of MeCN. The solid-state structure of cruciform **21** (Figure 4.8A) reveals an almost planar molecule. Deplanarization is apparent in the pendant ethyl groups, the terminal benzene rings on the bisethynylbenzene axis twist out of the central BBO plane by just 5.2°. Carbon–carbon triple bonds are essentially linear, with C–C≡C angles of 177.3–177.5°. Excluding solvent molecules, each molecule of **21** closely contacts sixteen of its neighbours, through hydrophobic interaction among terminal ethyl groups, eight C–H···O interactions and [ $\pi\cdots\pi$ ] stacking. Ester moieties on the horizontal axis of the

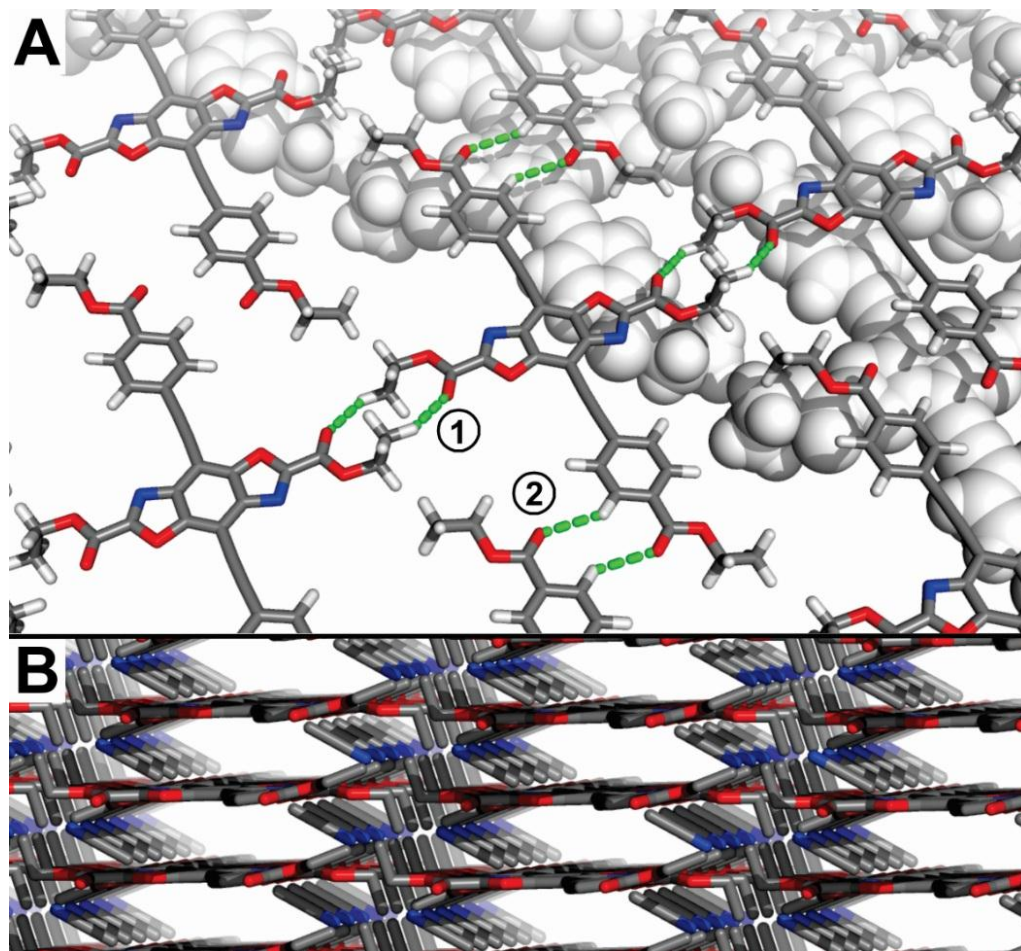


**Figure 4.8** (A) Crystal structure of **21** with intermolecular short contacts highlighted in green. Solvent molecules are omitted. *Contact 1*: H $\cdots$ O 2.58 Å, C $\cdots$ O 3.48 Å, C–H $\cdots$ O 138.6°, C=O $\cdots$ H 153.2°. *Contact 2*: H $\cdots$ O 2.60 Å, C $\cdots$ O 3.41 Å, C–H $\cdots$ O 130.8°, C=O $\cdots$ H 126.9°. (B) Compound **21** packs into two-dimensional sheets that are organized into three-dimensional structure through  $[\pi\cdots\pi]$  stacking with an interplanar distance of 3.29 Å. Hydrogen atoms are omitted. C—gray, H—white, N—blue, and O—red.

cruciform establish short  $[C=O\cdots H-C_{sp^3}]$  contacts (contact 1 in Figure 4.8A, 2.58 Å)<sup>91</sup> with their counterparts on the neighbouring molecules. Simultaneously, ester groups

positioned along the cruciform's *y*-axis engage into pairwise weak  $[C=O\cdots H-C_{sp2}]$  hydrogen bonds<sup>92</sup> (contact 2 in Figure 4.8A, 2.60 Å) with the hydrogen atoms on the adjacent cruciform's benzene rings. Ester groups on the *y*-axis of compound **21** also engage in close contacts with MeCN solvent molecules (not shown in Figure 4.8). Contacts 1 and 2 are symmetry-related through inversion centers and appear responsible for organizing the molecules of **21** into a corrugated two-dimensional supramolecular sheet. These sheets are further organized into a three-dimensional network through  $[\pi\cdots\pi]$  stacking interactions, with the interplanar distance of 3.29 Å (Figure 4.8B).

#### 4.2.2.6 Cruciform **22**<sup>87</sup>

Compound **22** also crystallizes in the  $P\bar{1}$  space group, with half a molecule of **21** and one disordered molecule of CH<sub>2</sub>Cl<sub>2</sub> in the asymmetric unit. In the solid state, molecules of **22** (Figure 4.9A) also show deplanarization of the benzene rings positioned along the *y*-axis of the molecule, which distort by 29.1° out of the plane of the central BBO core. Carbon–carbon triple bonds are essentially linear, with C–C≡C angles in the 175.9–178.8° range. The supramolecular structure of **22** is highly reminiscent of that of **21**, as this cruciform packs into well-ordered two-dimensional sheets with an all-parallel orientation of individual molecules. Four unique contacts can be identified within these supramolecular sheets (shown in green in Figure 4.9A): (a) the pairwise  $[C\equiv N\cdots H-C_{sp2}]$  contacts (2.54 Å) between the cyano groups on the benzene ring of one cruciform and the *o*-hydrogen atom of another; (b) the  $[C=O\cdots H-C_{sp2}]$  contact (2.41 Å) between the ester carbonyl on the *y*-axis of one cruciform and a hydrogen atom of the benzene ring on the *x*-axis of its neighbour and (c)/(d) two bifurcating  $[C\equiv N\cdots H-C_{sp3}]$  contacts between the

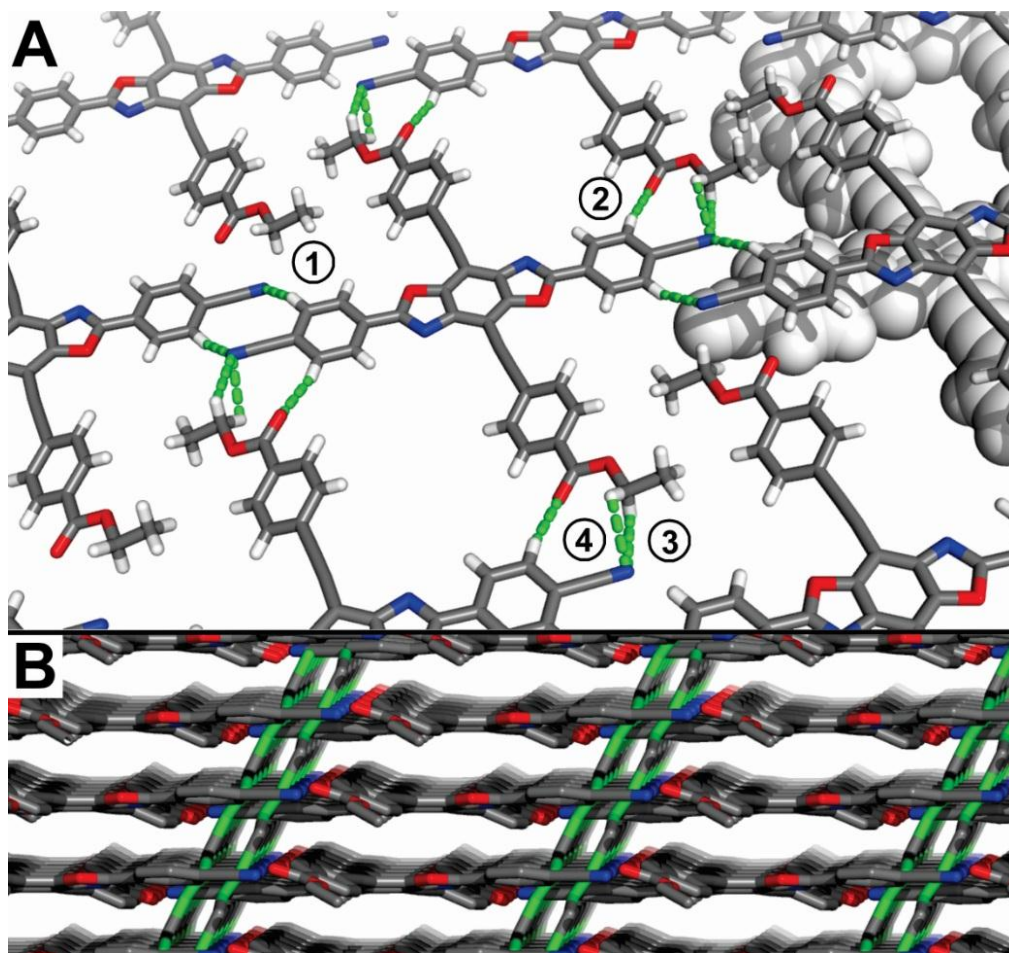


**Figure 4.9** (A) Crystal structure of **22** with short intermolecular contacts highlighted in green. Solvent molecules are omitted. *Contact 1*:  $\text{H}\cdots\text{N}$  2.54 Å,  $\text{C}\cdots\text{N}$  3.48 Å,  $\text{C}-\text{H}\cdots\text{N}$  144.8°,  $\text{H}\cdots\text{N}\equiv\text{C}$  112.9°. *Contact 2*:  $\text{H}\cdots\text{O}$  2.41 Å,  $\text{C}\cdots\text{O}$  3.45 Å,  $\text{C}-\text{H}\cdots\text{O}$  160.9°,  $\text{H}\cdots\text{O}=\text{C}$  148.5°. *Contact 3*:  $\text{H}\cdots\text{N}$  2.85 Å,  $\text{C}\cdots\text{N}$  3.20 Å,  $\text{C}-\text{H}\cdots\text{N}$  98.8°,  $\text{H}\cdots\text{N}\equiv\text{C}$  108.9°. *Contact 4*:  $\text{H}\cdots\text{N}$  2.72 Å,  $\text{C}\cdots\text{N}$  3.20 Å,  $\text{C}-\text{H}\cdots\text{N}$  105.9°,  $\text{H}\cdots\text{N}\equiv\text{C}$  94.6°. (B) Compound **22** packs into corrugated two-dimensional sheets that organize into three-dimensional structure through  $[\pi\cdots\pi]$  stacking with the interplanar distance of 3.30 Å. Hydrogen atoms are omitted and solvent molecules appear connected to each other because of chlorine atoms' disorder. C—gray, H—white, N—blue, O—red, and Cl—green.

ester's methylene groups of one and cyano groups of the other cruciform (2.72 and 2.85 Å). The corrugated two-dimensional sheets organize into a three-dimensional structure (Figure 4.9B) through  $[\pi \cdots \pi]$  stacking characterized by the average interplanar distance of 3.30 Å. Within this closely packed structure, molecules of **22** from adjacent layers also establish a series of close contacts with massively disordered solvent ( $\text{CH}_2\text{Cl}_2$ ) molecules.

#### 4.2.2.7 Cruciform **23**<sup>87</sup>

The final two cruciforms—**23** and **24**—have been endowed with an extended *y*-axis to probe the effect of this structural variation on the molecular structure and supramolecular organization. Cruciform **23** crystallizes in  $P\bar{1}$  space group, with half a molecule of **23** in the asymmetric unit, along with a disordered molecule of  $\text{CH}_2\text{Cl}_2$  solvent. In the solid state, molecules of **23** (Figure 4.10A) are oriented around an inversion center, with the disorder in the BBO core making oxazole nitrogens and oxygens indistinguishable. The molecule is largely planar, with significant deplanarization occurring in the pendant ethyl groups and the terminal benzene rings, which are twisted out of the central molecular plane by 25.2°. Molecules of **23** assume a gently undulating conformation with an angle of 167.8° between the centroids of three benzene rings. This shape is brought about by the distortion of its  $\text{C}\equiv\text{C}$  triple bonds: the  $\text{C}\equiv\text{C}-\text{C}$  angles reside in the 173.8–178.1° range. The supramolecular organization is once again dominated by the two-dimensional sheets, which reveal two sets of inter-cruciform short contacts: (a) the pairwise association of the horizontally positioned  $-\text{COOEt}$  groups, via a 2.43 Å  $[\text{C}_{sp^3}-\text{H}\cdots\text{O}]$  hydrogen bond (contact 1 in Figure 4.10A) and (b) the 2.53 Å



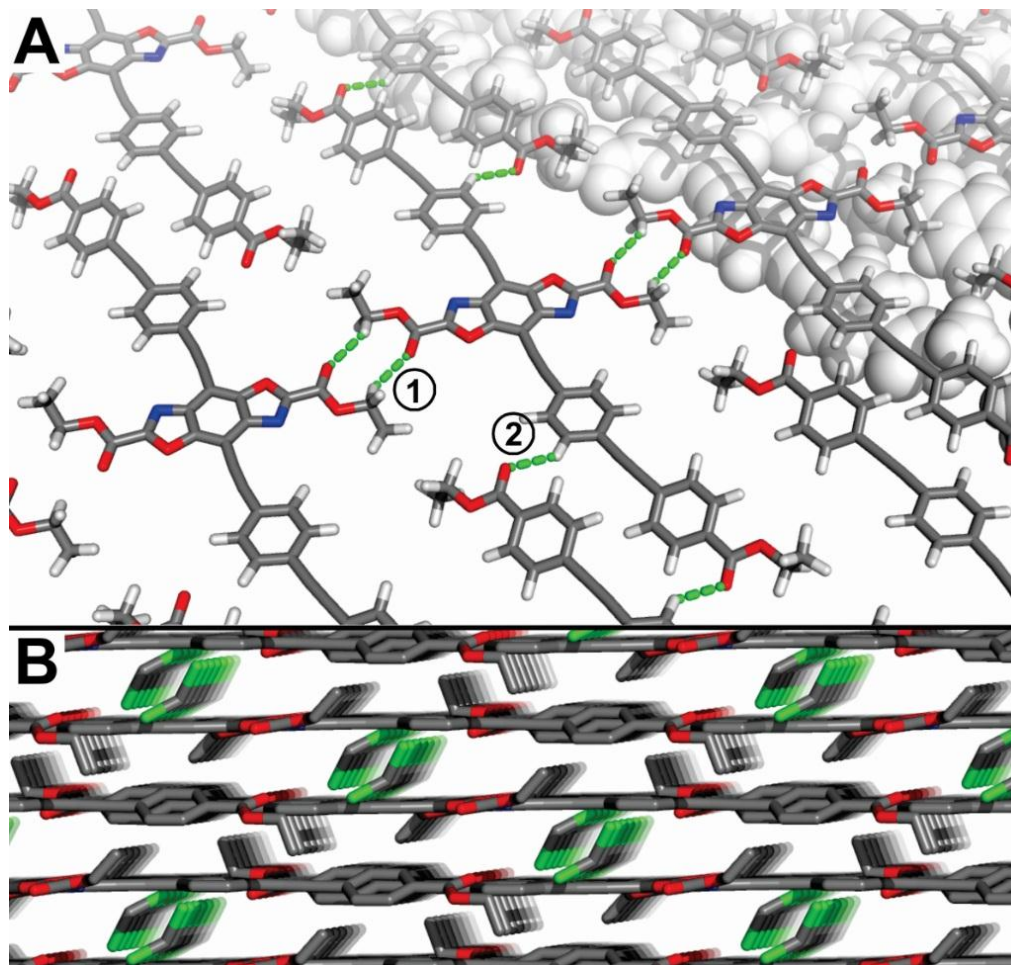


**Figure 4.10** (A) Crystal structure of **23** with intermolecular hydrogen bonds highlighted in green. *Contact 1*: O...H 2.44 Å, O...C 3.32 Å, C=O...H 151.3°, O...H-C 138.1°. *Contact 2*: H...O 2.53 Å, C...O 3.43 Å, C-H...O 139.2°, H...O=C 123.2°. (B) Compound **23** packs into corrugated two-dimensional sheets that organize into the three-dimensional structure through [π...π] stacking at an average distance of 3.24 Å. Hydrogen atoms are omitted. C—gray, H—white, N—blue, O—red, and Cl—green.

contact between the carbonyl oxygen along the vertical axis of **23** and one of the hydrogen atoms on the internal benzene ring of the vertical axis (contact 2 in Figure 4.10A). In addition, the disordered solvent molecules appear to be engaged in several short contacts with neighboring cruciforms via both their H and Cl atoms (not shown). Much like in the crystal structures of **20**, **21**, and **22**, two-dimensional sheets of **23**

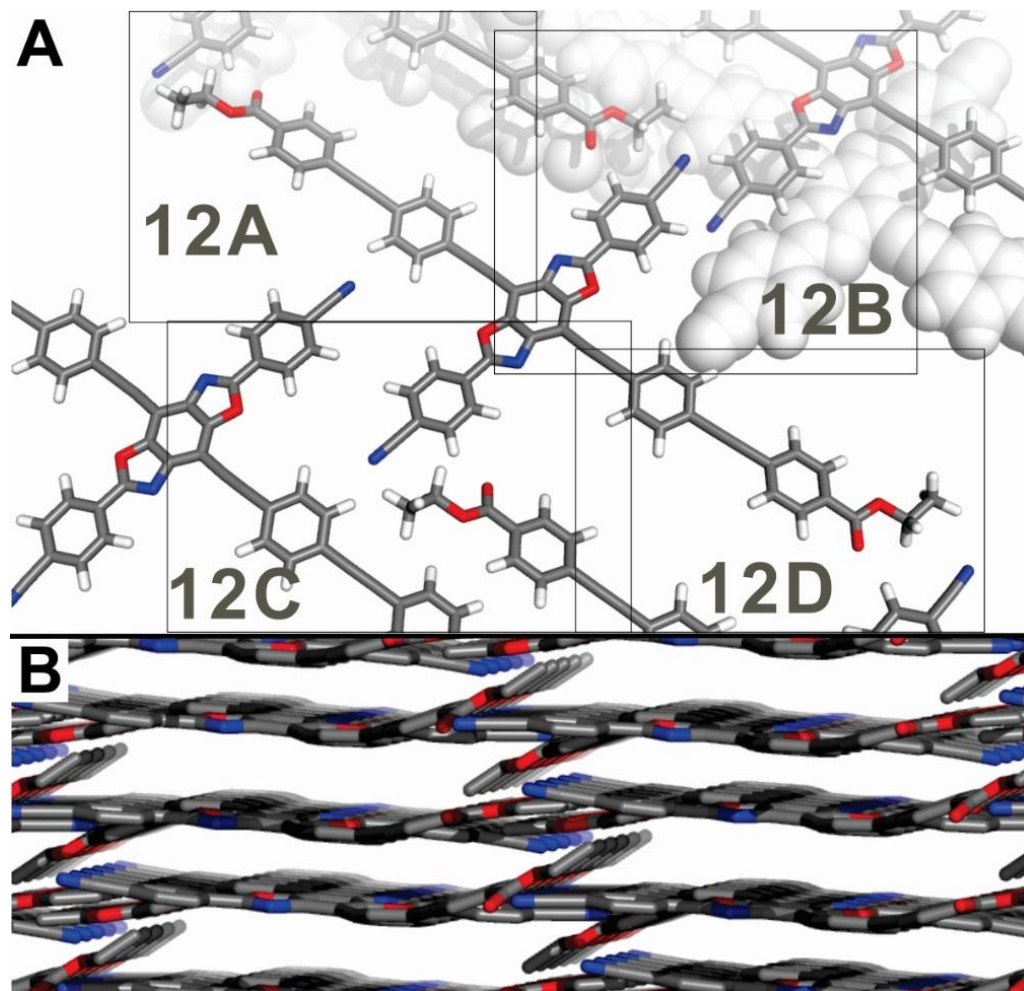


**Figure 4.11** (A) Crystal structure of cruciform **24**, and the designations of cruciform's "quadrants". (B) Compound **24** packs into corrugated two-dimensional sheets that organize into the three-dimensional structure through  $[\pi\cdots\pi]$  stacking. C—gray, H—white, N—blue, and O—red.

apparently  $[\pi \cdots \pi]$  stack into a three-dimensional crystal, with an interplanar distance of 3.24 Å.

#### 4.2.2.8 Cruciform **24**

The largest examined cruciform was **24**, whose crystal structure is also the most complex. Cruciform **24** crystallizes in the  $P\bar{1}$  space group, with one molecule in the asymmetric unit. Disordered  $\text{CH}_2\text{Cl}_2$  solvent was present in the crystal, but could not be satisfactorily modeled and its electron density was subtracted using the SQUEEZE routine. In the solid state, molecules of **24** show a highly deformed structure (Figure 4.11A), especially along the cruciforms' y-axis. The inner benzene rings distort by  $10.1^\circ$  and  $8.6^\circ$  relative to the plane of the central BBO core, while the outer benzene rings on the y-axis deplanarize even further, to  $23.0^\circ$  and  $19.2^\circ$ , respectively. Triple bonds are moderately distorted from linearity, with  $\text{C}\equiv\text{C}-\text{C}$  angles in the  $174.4\text{--}179.0^\circ$  range. Because one entire molecule of **24** constitutes the asymmetric unit, each cruciform engages in sixteen short contacts, eight of which are unique. The situation is additionally complicated by the deplanarized structure of **24**, which means that even though layered sheet structure is apparent (Figure 4.12D, also *vide infra*), each molecule contacts other cruciforms from both its own and adjacent layers. For clarity, these contacts are organized into four sections, one for each quadrant of the molecule (Figure 4.12A–D). Thus, the "northwest" quadrant (Figure 4.12A) reveals two unique short contacts: (1)  $[\text{C}=\text{O} \cdots \text{H}-\text{C}_{sp2}]$  contact between the ester's carbonyl group and the hydrogen atom *ortho*- to the  $-\text{CN}$  group on the horizontal axis of the adjacent molecule, and (2) the  $[\text{C}\equiv\text{N} \cdots \text{H}-\text{C}_{sp2}]$  contact between the hydrogen on the inner benzene ring of the cruciform's vertical



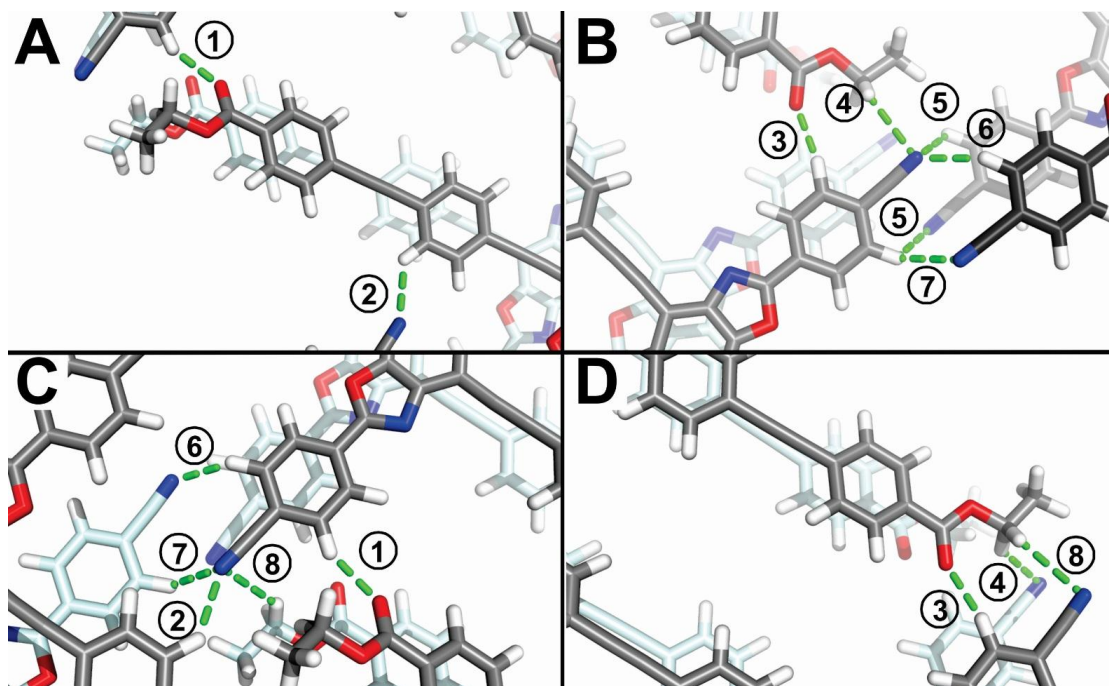


**Figure 4.12** (A) The "northwest" quadrant of **24**. *Contact 1*: O $\cdots$ H 2.26 Å, O $\cdots$ C 3.26 Å, H $\cdots$ O–C 152.2°, C=O $\cdots$ H 137.1°. *Contact 2*: H $\cdots$ N 2.53 Å, C $\cdots$ N 3.37 Å, C–H $\cdots$ N 133.4°, H $\cdots$ N $\equiv$ C 151.1°. (B) The "northeast" quadrant of **24**. *Contact 3*: O $\cdots$ H 2.24 Å, O $\cdots$ C 3.31 Å, O $\cdots$ H–C 167.1°, C=O $\cdots$ H 153.7°. *Contact 4*: N $\cdots$ H 2.78 Å, N $\cdots$ C 3.57 Å, N $\cdots$ H–C 129.4°, C $\equiv$ N $\cdots$ H 96.4°. *Contact 5*: N $\cdots$ H 2.74 Å, N $\cdots$ C 3.29 Å, N $\cdots$ H–C 111.4°, C $\equiv$ N $\cdots$ H 123.9°. *Contact 6*: N $\cdots$ H 2.55 Å, N $\cdots$ C 3.48 Å, N $\cdots$ H–C 142.0°, C $\equiv$ N $\cdots$ H 130.1°. *Contact 7*: H $\cdots$ N 2.67 Å, C $\cdots$ N 3.50 Å, C–H $\cdots$ N 132.3°, H $\cdots$ N $\equiv$ C 120.8°. (C) The "southwest" quadrant of **24**. *Contact 8*: N $\cdots$ H 2.76 Å, N $\cdots$ C 3.64 Å, N $\cdots$ H–C 137.4°, C $\equiv$ N $\cdots$ H 77.1°. (D) The "southeast" quadrant of **24**. C—gray, H—white, N—blue, and O—red.

axis and the –CN nitrogen of the adjacent cruciform (contacts 1 and 2 in Figure 4.12A, 2.26 and 2.53 Å, respectively). The "northeast" quadrant of the molecule (Figure 4.12B) points to five additional unique short contacts: (3) the [C<sub>sp2</sub>–H $\cdots$ O=C] association which

is constitutionally analogous to contact 1 in Figure 4.9B, but is not symmetry-equivalent (contact 3, 2.24 Å); (4) the  $[C\equiv N\cdots H-C_{sp3}]$  contact between the cruciform's  $-CN$  group and methylene hydrogens in the neighboring molecule's  $-COOEt$  group (contact 4, 2.78 Å); (5)/(6) two  $[C\equiv N\cdots H-C_{sp2}]$  short contacts between the cruciform's  $-CN$  group and the hydrogens *ortho*- to the  $-CN$  group in two other cruciforms (contacts 5 and 6, 2.74 and 2.55 Å, respectively), and (7) another  $[C_{sp2}-H\cdots N\equiv C]$  short contact—constitutionally analogous to contacts 5 and 6, but symmetry non-equivalent (contact 7, 2.67 Å). The "southwest" quadrant (Figure 4.12C) repeats several of the just discussed contacts, along an additional unique contact (8), established between the cruciform's  $-CN$  group and methylene hydrogens in the neighboring molecule's  $-COOEt$  functionality (this contact is constitutionally, but not symmetrically, equivalent to contact 4 in Figure 4.12B). Finally, the "southeast" quadrant (Figure 4.12D) replicates contacts 3, 4, and 8 previously discussed. Overall, molecules stack into strongly undulating two-dimensional sheets (Figure 4.11B), wherein two adjacent sheets are related through inversion symmetry.

### 4.2.3 Discussion

Comparison of crystal structures of cruciforms **1**, **2**, **8**, and **20–24** reveals several key similarities across the series. All examined cruciforms are largely unstrained, with their bond angles minimally deformed within the crystal. Even the readily deformed<sup>95</sup> carbon–carbon triple bonds are essentially unaffected by the crystal packing: the most distorted one, observed in **8**, has the  $C\equiv C-C$  angle of  $173.2^\circ$ , bent by a mere  $6.8^\circ$  from the ideal linear geometry. However, in larger cruciforms **23** and **24**, such small individual

**Table 4.3** The geometric parameters of the short [C–H···X] contacts (X=N, O)observed in the crystal structures of **1**, **2**, **8**, **20–24**.

Cruciform	H···A (Å)	D···A (Å)	D–H···A (°)	H···A–C (°)	D/ <i>sp</i> <sup>x</sup>	A/ <i>sp</i> <sup>x</sup>
<b>24</b>	2.24	3.31	167.1	153.7	C/ <i>sp</i> <sup>2</sup>	O/ <i>sp</i> <sup>2</sup>
<b>24</b>	2.26	3.26	152.2	137.1	C/ <i>sp</i> <sup>2</sup>	O/ <i>sp</i> <sup>2</sup>
<b>22</b>	2.40	3.45	160.9	148.4	C/ <i>sp</i> <sup>2</sup>	O/ <i>sp</i> <sup>2</sup>
<b>23</b>	2.43	3.32	138.0	151.2	C/ <i>sp</i> <sup>3</sup>	O/ <i>sp</i> <sup>2</sup>
<b>20</b>	2.50	3.54	158.7	130.0	C/ <i>sp</i> <sup>3</sup>	O/ <i>sp</i> <sup>2</sup>
<b>20</b>	2.51	3.56	161.9	167.0	C/ <i>sp</i> <sup>3</sup>	O/ <i>sp</i> <sup>2</sup>
<b>22</b>	2.53	3.48	144.7	112.9	C/ <i>sp</i> <sup>2</sup>	N/ <i>sp</i>
<b>23</b>	2.53	3.43	139.2	123.2	C/ <i>sp</i> <sup>2</sup>	O/ <i>sp</i> <sup>2</sup>
<b>24</b>	2.53	3.37	133.4	151.1	C/ <i>sp</i> <sup>2</sup>	N/ <i>sp</i>
<b>24</b>	2.55	3.48	142.0	130.1	C/ <i>sp</i> <sup>2</sup>	N/ <i>sp</i>
<b>21</b>	2.58	3.48	138.6	153.2	C/ <i>sp</i> <sup>3</sup>	O/ <i>sp</i> <sup>2</sup>
<b>1</b>	2.58	3.60	155.3	—	C/ <i>sp</i> <sup>2</sup>	N/ <i>sp</i> <sup>2</sup>
<b>21</b>	2.60	3.41	130.8	126.9	C/ <i>sp</i> <sup>2</sup>	O/ <i>sp</i> <sup>2</sup>
<b>8</b>	2.64	3.62	148.7	—	C/ <i>sp</i> <sup>3</sup>	N/ <i>sp</i> <sup>2</sup>
<b>2</b>	2.66	3.70	160.1	—	C/ <i>sp</i> <sup>2</sup>	O/ <i>sp</i> <sup>3</sup>
<b>24</b>	2.67	3.50	132.3	120.8	C/ <i>sp</i> <sup>2</sup>	N/ <i>sp</i>
<b>2</b>	2.69	3.74	161.1	—	C/ <i>sp</i> <sup>2</sup>	C/ <i>sp</i>
<b>2</b>	2.70	3.58	137.3	—	C/ <i>sp</i> <sup>2</sup>	N/ <i>sp</i> <sup>2</sup>
<b>22</b>	2.72	3.20	105.8	94.5	C/ <i>sp</i> <sup>3</sup>	N/ <i>sp</i>
<b>2</b>	2.74	3.75	154.1	—	C/ <i>sp</i> <sup>2</sup>	O/ <i>sp</i> <sup>3</sup>
<b>24</b>	2.74	3.29	111.4	123.9	C/ <i>sp</i> <sup>2</sup>	N/ <i>sp</i>
<b>24</b>	2.76	3.64	137.4	77.2	C/ <i>sp</i> <sup>3</sup>	N/ <i>sp</i>
<b>2</b>	2.78	3.53	125.6	—	C/ <i>sp</i> <sup>2</sup>	N/ <i>sp</i> <sup>2</sup>
<b>24</b>	2.78	3.57	129.4	96.4	C/ <i>sp</i> <sup>3</sup>	N/ <i>sp</i>
<b>8</b>	2.80	3.73	143.2	—	C/ <i>sp</i> <sup>2</sup>	N/ <i>sp</i> <sup>2</sup>
<b>22</b>	2.84	3.20	98.7	108.9	C/ <i>sp</i> <sup>3</sup>	N/ <i>sp</i>
<b>2</b>	3.00	4.04	159.3	—	C/ <i>sp</i> <sup>3</sup>	N/ <i>sp</i> <sup>2</sup>
<b>2</b>	3.01	4.05	158.8	—	C/ <i>sp</i> <sup>3</sup>	N/ <i>sp</i> <sup>2</sup>

deviations add up and these cruciforms deviate significantly from their idealized structures. At the same time, triple bonds are not encumbered by substitution and the rotation around them is free,<sup>94</sup> allowing these cruciforms to adopt a variety of

conformations in the crystal. Perhaps surprisingly, only cruciform **2** takes advantage of this conformational freedom and significantly deplanarizes by distorting its benzene rings positioned along the y-axis into an almost perpendicular conformation with respect to the remainder of the molecule. All other cruciforms are much closer to coplanarity, with their y-axes distorted by less than 30° from the plane of the central BBO core.

Within the series, supramolecular structures of all eight cruciforms appear to include solvent molecules—MeCN, CH<sub>2</sub>Cl<sub>2</sub>, or CHCl<sub>3</sub>. Because of the presumed solvent loss (and, possibly, other factors), three of the structures necessitated subtraction of electron density associated with the highly disordered solvent, while the other five could be modelled with explicit inclusion of solvent molecules. However, only cruciform **8** crystallized with an ordered molecule of solvent. Examination of this structure, and of the parts of disordered solvent molecules in other structures, suggests that the chlorinated solvent molecules engage into short [C–H···Cl] contacts with cruciforms, typically occupying the voids left over by the title molecules.

Five of the examined cruciforms—compounds **20–24**—form largely analogous superstructures: two-dimensional sheets of closely packed cruciforms, which then stack into a three-dimensional structure mediated by  $[\pi \cdots \pi]$  interactions. This organizing motif is highly versatile, as both the lengths of x- and y-axes, and the terminal functionalities have been widely varied within this mini-series of five compounds. Superstructures of cruciforms **2** and **8** share some general elements—both compounds form one-dimensional  $[\pi \cdots \pi]$  stacks of molecules which connect via [C–H···O/N] contacts first into two-dimensional sheets, and then into a three-dimensional assembly of these sheets.

Cruciform **1** remains unique within this set in its supramolecular organization around the rotation axis. Intriguingly, the five cruciforms that share the sheet-like superstructures all have carbonyl groups, whose only supramolecular associations are with weakly polarized C–H bonds in neighbouring molecules. Are these contacts suggestive of weak hydrogen bonding? Two factors point toward such a conclusion. First, the supramolecular structure persists across the mini-series of five compounds, despite the introduction of various other functional groups, and the variations in lengths of cruciforms' *x*- and *y*-axes. Additionally, the summary of geometric parameters of short contacts observed in the structures of eight cruciforms (Table 4.2) reveals that the contacts between hydrogen and oxygen atoms are notably shorter than those between hydrogen and nitrogen. Such a trend is consistent with the strengths of corresponding hydrogen bonds; if the short contacts were just a consequence of crystal packing, it would have been expected that they would not show such an ordering. Admittedly, other factors could play a role in this trichotomy of supramolecular assemblies, most notably the influence of solvents. All three solvents used in the crystallization of eight cruciforms (MeCN, CH<sub>2</sub>Cl<sub>2</sub>, and CHCl<sub>3</sub>) are capable of engaging in specific supramolecular associations. However, the significant disorder observed in the solvent molecules in all structures (except that of **8**) suggests that solvents are weakly and non-specifically bound in most cases. In situations when solvent molecules could be analyzed, they appear to mostly fill the voids left over by the parent molecules, without critically contributing to one structural pattern or the other. Additionally discouraging of this proposition is the fact that sheet-like superstructures of various cruciforms were obtained from a variety of solvents, and, conversely, that

different cruciforms crystallized from the same solvent yielded different crystal packing patterns.

### 4.3 Conclusion and Outlook

We have synthesized and characterized a set of eight BBO-centred cruciforms, in which the substituents along their *x*- and *y*-axes were varied pairwise among the electron-rich 4-(*N,N*-dimethylamino)phenyl group, electron poor 4-pyridyl, 4-(formyl)phenyl, and 4-(carboxyethyl)phenyl functionalities, and electron-neutral phenyl group. Crystal structures of compounds in this series reveal expected molecular geometries with  $\sim 90^\circ$  junctions between cruciforms' horizontal and vertical axes. At a molecular level, two sources of desymmetrization were noted: (1) the deplanarization of (typically) *y*-axis substituents from the plane of the central BBO core, and (2) the slight bending of alkyne triple bonds, which endowed longer cruciforms with an undulating overall structure. The supramolecular assembly of benzobisoxazole cruciforms is dominated by  $[\pi \cdots \pi]$  stacking and weak  $[\text{C}-\text{H} \cdots \text{O}]/[\text{C}-\text{H} \cdots \text{N}]$  hydrogen bonds, the former apparently mediating the formation of two-dimensional sheet structures in cases where cruciforms possess carbonyl groups. To confirm these supramolecular interactions in solid state, one should study more about the isostructural cruciform that has different heterocyclic core such as benzobisimidazole, benzodithiophene, and benzobisthiazole. In addition to this direct comparison, the indirect comparison with "L-shaped" benzoxazoles can also be helpful to the further understanding of the driving force of cruciform's 3D structure. This preliminary study will be useful for the application of BBO cruciform as rigid 2D spacer

to the construction of synthesized porous materials, MOFs and COFs. Furthermore, the decoration of the end-groups of BBO cruciform with strong hydrogen-bond donors/acceptors, e.g. guanine bases, will possibly give relatively stable, but reversible 2D or 3D network of BBO cruciform.

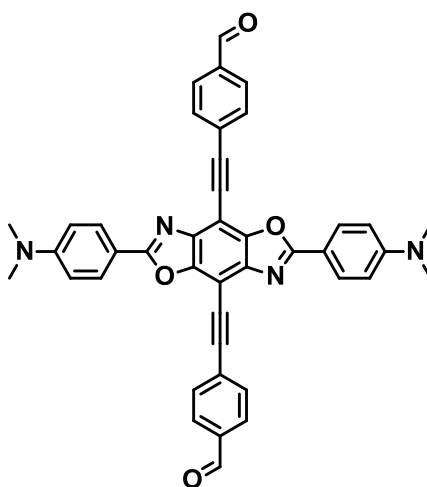
## **4.4 Experimental Section**

### **4.4.1 General Procedures**

All reactions were performed under nitrogen atmosphere in oven-dried glassware. Reagents were purchased from commercial suppliers and used without further purification. Solvents were used as received, except *N,N*-dimethylformamide (DMF), which was dried over activated alumina in an mBraun Solvent Purification System. Triethylamine (Et<sub>3</sub>N) was distilled over KOH pellets and degassed by a 15-minute nitrogen purge prior to use. Microwave-assisted reactions were performed in a Biotage Initiator 2.0 microwave reactor, producing monochromatic microwave radiation with the frequency of 2.45 GHz. Column chromatography was carried out on silica gel 60, 32–63 mesh. Analytical TLC was performed on Merck aluminium-backed silica-gel plates. Melting points measurements were performed in open capillary tubes, using Mel-Temp Thermo Scientific apparatus. UV/Vis spectra were recorded on a Perkin-Elmer Lambda 25 UV/Vis spectrophotometer. Infrared spectra were recorded on a Perkin-Elmer Spectrum 100 FT-IR spectrophotometer using Pike MIRacle Micrometer pressure clamp. NMR spectra were obtained on JEOL ECX-400 and ECA-500 spectrometers, with working frequencies (for <sup>1</sup>H nuclei) of 400 and 500 MHz, respectively. All <sup>13</sup>C-NMR

spectra were recorded with simultaneous decoupling of  $^1\text{H}$  nuclei.  $^1\text{H}$ -NMR chemical shifts are reported in ppm units relative to the residual signal of the  $\text{CDCl}_3$  solvent (7.26 ppm). All NMR spectra were recorded at 25 °C. Mass spectral measurements were performed by the Mass Spectrometry Facility of the Department of Chemistry and Biochemistry at the University of Texas at Austin. Elemental analyses were conducted by Intertek USA, Inc.

#### 4.4.2 Synthesis of Cruciform 20



Compound 4-ethynylbenzaldehyde<sup>88</sup> (281 mg, 2.16 mmol) was added to a thick-walled microwave pressure vial that contained a mixture of compound **15**<sup>32</sup> (Scheme 4.1; 300 mg, 0.539 mmol),  $\text{PdCl}_2(\text{PPh}_3)_2$ <sup>55</sup> (76 mg, 0.11 mmol), CuI (20 mg, 0.11 mmol),  $\text{Et}_3\text{N}$  (5 mL), and MeCN (5 mL). The vial was sealed and exposed to microwave irradiation for 3 h at 100 °C. After cooling, solvents were removed under reduced pressure, and the crude solid was purified by column chromatography, eluting first with



pure CH<sub>2</sub>Cl<sub>2</sub>, and then successively with CH<sub>2</sub>Cl<sub>2</sub>/MeOH mixtures in 97:3, 19:1, and 9:1 ratios. The solvent was removed under reduced pressure to give 71 mg (20%, 0.11 mmol) of product (mp >350 °C, with decomposition). Single crystals of compound **20** were formed by layering its CH<sub>2</sub>Cl<sub>2</sub> solution with pentane. UV-Vis (CH<sub>2</sub>Cl<sub>2</sub>):  $\lambda_{\text{max}}$  (log  $\epsilon$ ) = 367 (6.84), 397 (6.71), 456 (6.62) nm. IR (neat): 2215, 1699, 1609, 1507, 1339, 1189, 978, 913, 823 cm<sup>-1</sup>. <sup>1</sup>H NMR (CDCl<sub>3</sub>, 500 MHz):  $\delta$  10.08 (s, 2H), 8.24 (d, <sup>3</sup>*J*<sub>H-H</sub> = 8.6 Hz, 4H), 7.96 (d, <sup>3</sup>*J*<sub>H-H</sub> = 8.6 Hz, 4H), 7.93 (d, <sup>3</sup>*J*<sub>H-H</sub> = 8.6 Hz, 4H), 6.79 (d, <sup>3</sup>*J*<sub>H-H</sub> = 8.6 Hz, 4H), 3.11 (s, 12H) ppm. <sup>13</sup>C NMR (CDCl<sub>3</sub>, 500 MHz):  $\delta$  191.56, 165.71, 152.70, 148.61, 140.79, 135.78, 132.66, 129.67, 129.61, 129.29, 113.31, 111.48, 98.40, 96.94, 84.39, 40.14 ppm. HRMS (CI/[M]<sup>+</sup>) calcd. for C<sub>42</sub>H<sub>30</sub>N<sub>4</sub>O<sub>4</sub>: 654.2267. Found: 654.2271. Anal. calcd. for C<sub>42</sub>H<sub>30</sub>N<sub>4</sub>O<sub>4</sub> • CH<sub>2</sub>Cl<sub>2</sub> (molecular formula derived from the single-crystal X-ray structure): C, 69.83; H, 4.36; N, 7.57. Found: C, 70.64; H, 4.24; N, 7.75.

## Chapter Five

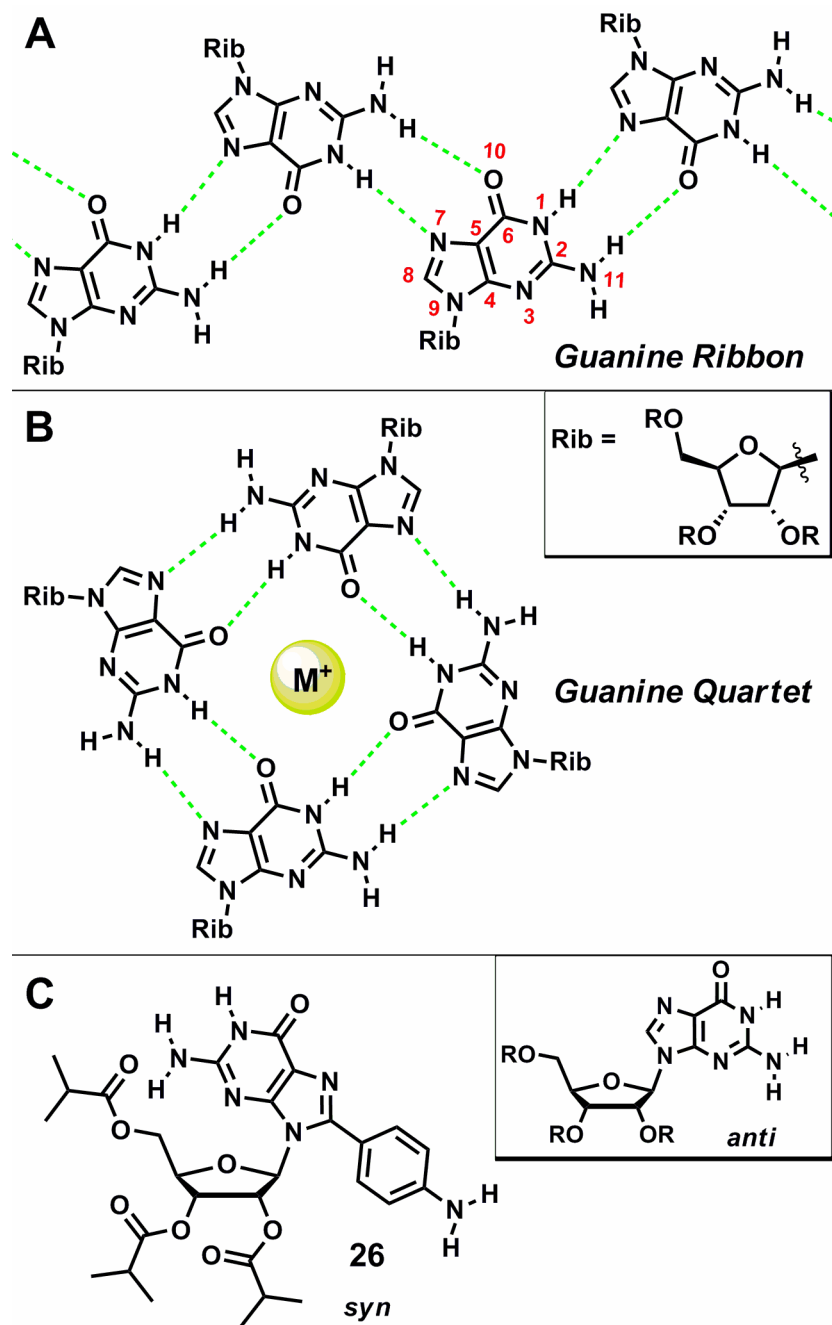
### Synthesis and Structural Analysis of 8-Arylethynyl Substituted Guanosine

#### Derivatives<sup>95</sup>

##### 5.1 Introduction

Self-assembly is a very promising strategy for the preparation of materials with novel functions and structures. My research was aimed at the synthesis and characterization of porous materials (and their model structures) based on the strong hydrogen bonding of derivatives of DNA nucleobase guanosine. Guanosine is unique among DNA components by its propensity for self-assembly into tetrameric superstructures known as guanine quadruplexes. These moieties can be used as square-shaped building blocks as "self-assembled cruciform" in the construction of porous structures. In this last chapter, I will show that the guanine, one of DNA and RNA nucleobases, has a possibility as a candidate of a terminal ornament to decorate benzobisoxazole cruciforms.

Naturally occurring DNA and RNA nucleobases, as well as their synthetic derivatives, are commonly used motifs in supramolecular chemistry<sup>96</sup> on account of their low cost and well-established propensity for intermolecular association through hydrogen bonding and  $[\pi \cdots \pi]$  stacking. In addition, ribose- and deoxyribose-substituted nucleobases—known respectively as nucleosides and deoxynucleosides—are readily available chiral (and enantiopure) building blocks. Among the five nucleobases, guanine



**Scheme 5.1** Guanine derivatives can assemble into infinite guanine ribbons (A) or discrete guanine quartets (B). The latter superstructure is typically templated by a metal cation; compound **26** (C), however, forms guanine quartet superstructures without a templating cation.

has the most diverse supramolecular chemistry, as it can self-assemble into discrete dimers and tetramers, or extended ribbon- and helix-shaped structures.<sup>97</sup> The most common mode of guanine self-assembly is an infinite *guanine ribbon*, stabilized by pairs of [C6–O10···H–N11] and [N7···H–N1] hydrogen bonds (Scheme 5.1A). Alternatively, discrete *guanine quartets*<sup>98</sup> (Scheme 5.1B) can be formed when four guanine nuclei organize into a cyclic tetramer through four [C6–O10···H–N1] and four [N7···H–N11]

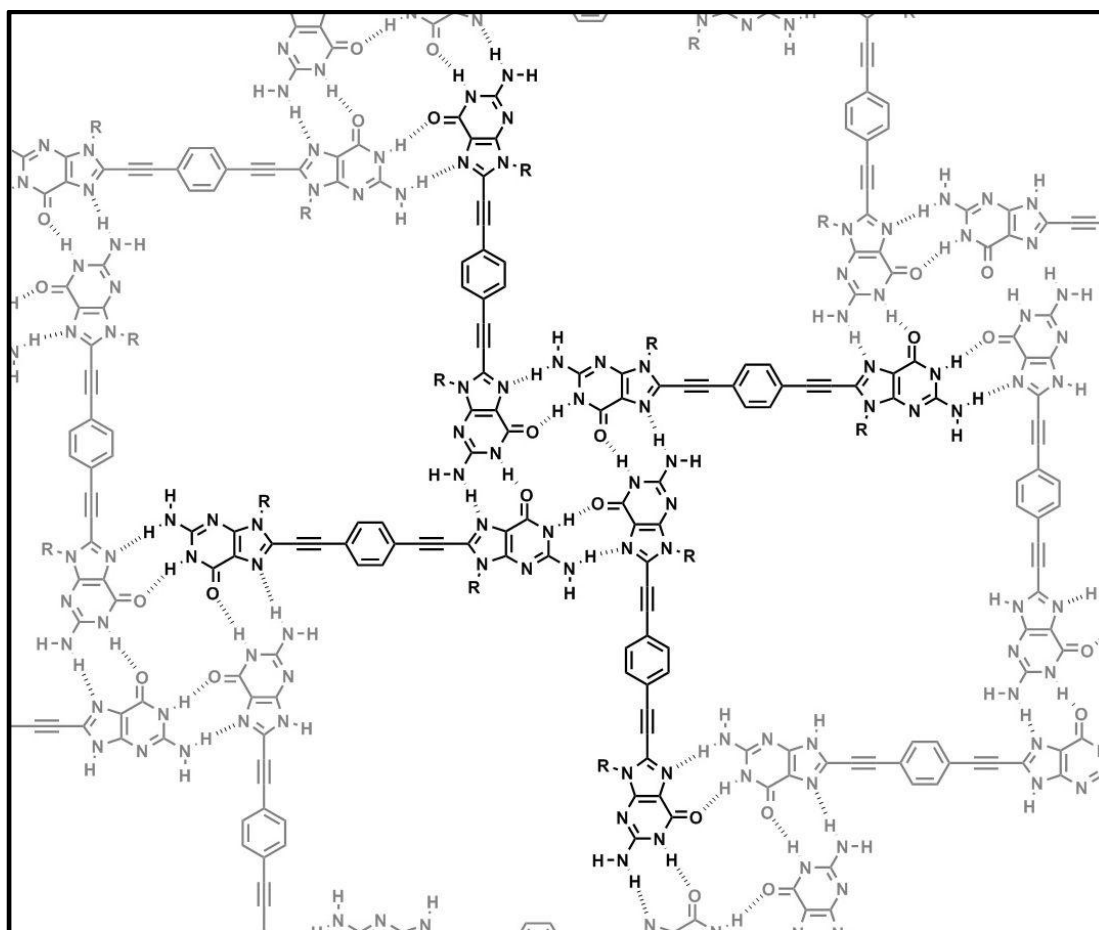


**Figure 5.1** Proposed 2D network of linearly linked bisguanosine derivatives.

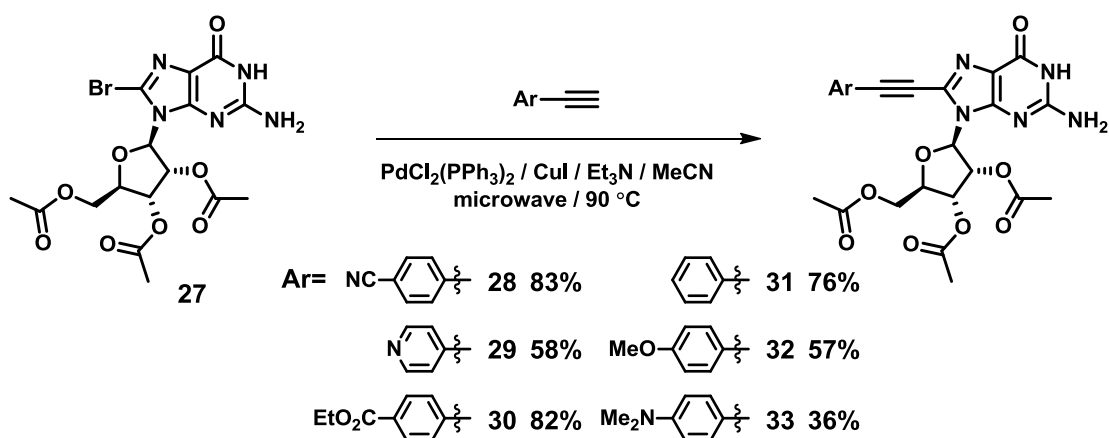
hydrogen bonds. Guanine quartets' symmetry, convergent geometry, and ability to complex cations make it a versatile and often used component of functional

supramolecular assemblies,<sup>97</sup> including ion transporters,<sup>99</sup> gelators,<sup>100</sup> liquid crystals,<sup>101</sup> drug-delivery vehicles,<sup>102</sup> and DNA-based molecular machines.<sup>103</sup>

What determines whether a given guanine derivative will assemble into a ribbon or a quartet superstructure? Traditionally, guanine quartets were favored only in the presence of a templating metal cation (*e.g.* K<sup>+</sup>) that would be pseudo-chelated by the four carbonyl oxygens of the quartet structure. However, in a seminal 2000 report, Sessler and coworkers<sup>104</sup> challenged this view by demonstrating that compound **26** (Scheme 5.1C) forms a quartet superstructure without metal cation assistance. The authors postulated that steric effects were responsible for the switch. The presence of a (4-dimethylamino)phenyl substituent in the 8-position of the guanine ring system distorted the ribose substituent into an unprecedented *syn*-orientation with respect to the guanine (torsion angle of 42.5°),<sup>105</sup> apparently forcing the formation of the quartet. My work was inspired by this pioneering report of guanosine quartet without metal cation, and therefore focused on the design of building blocks with guanine moieties which can self-assembled into 2D or 3D architecture. Possible 2D network of linearly linked bisguanosine derivatives is shown in Figure 5.1. To reach to this ultimate goal, I have started from the study of monosubstituted guanosine derivatives, followed by bisguanosine derivatives, in which two guanosines are connected with a linear linker.

In this chapter, the synthesis of six monosubstituted guanosine derivatives **28–33** coupled with arylethynyl group at 8-position of guanine base and nine bisguanosine derivatives **34–42** and three bisguanine derivatives **43–45** with linear linkers in different length. The synthesis of linear linkers is shown in the Experimental Section 5.4. I present

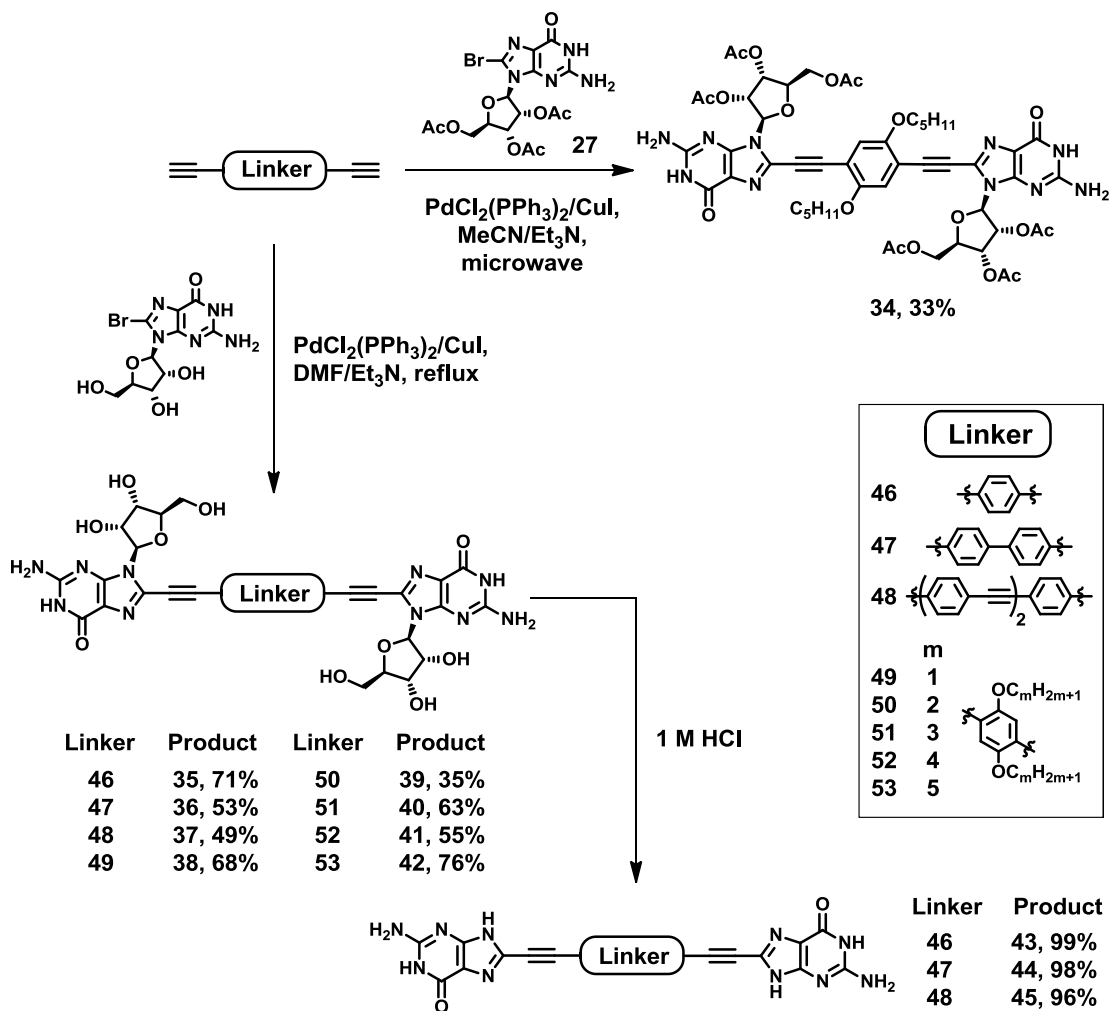
the crystal structures of two 8-alkynyl substituted guanine derivatives **28** and **29** (Scheme 5.2) which organize into highly twisted hydrogen bonded ribbons, despite the presence of a substituent in the 8-position. We explain this return to ribbon superstructures as a consequence of  $[\pi \cdots \pi]$  interactions between the electron-poor arylethynyl substituents and electron-rich guanine nuclei, which were enabled by the optimal match between the dimensions of **28/29** and the pitch of the guanine ribbon.



**Scheme 5.2** Synthesis of alkynylated guanosine derivatives **28–33**.

Within the guanine ring system, carbon C8 represents the only position that can be substituted without disturbing any of the hydrogen-bonding functionalities;  $sp^2$ -character of this carbon makes it amenable to transition metal-catalyzed carbon–carbon bond forming reactions. Much recent interest has been devoted to the study of 8-alkynyl substituted guanine derivatives; the electronic properties and rigid geometry of the  $\text{C}\equiv\text{C}$  triple bond in these compounds make them appealing precursors to fluorescent monitors of DNA conformations,<sup>106</sup> hydrogen-bonded porous materials,<sup>107</sup> organic nanoparticles,<sup>108</sup> and novel supramolecular ensembles.<sup>109</sup> However, there is only one

report about the solid-state organization of guanine derivatives with an 2-(trimethylsilyl)ethynyl-unit on C8 this class of modified guanines, as revealed by a October 2012 search of Cambridge Structural Database (CSD).<sup>110</sup>



**Scheme 5.3** Synthesis of nine bisguanosine derivatives **34–42** and three bisguanine derivatives **43–45**.

## 5.2 Results and Discussion

### 5.2.1 Synthesis of Compounds 28–45

The synthesis of the target compounds was straightforward and utilized Sonogashira coupling<sup>73</sup> as the key reaction step that coupled terminal alkynyl substituents with 8-bromoguanosine<sup>111</sup> or 8-bromo-2',3',5'-tri-*O*-acetylguanosine **27**.<sup>112</sup> All the TMS protected terminal acetylenes except phenylacetylene (for **31**) and *p*-diethynylbenzene **46** were also obtained by the same coupling reaction between (trimethylsilyl)acetylene and the counterpart of each substituent (see Experimental Section). Scheme 5.2 outlines the synthesis of monoguanosine derivatives **28–33**, which were synthesized as model compounds for bis- and tetra-guanosine derivatives. Sonogashira coupling reactions of 8-bromo-2',3',5'-tri-*O*-acetylguanosine **27** with acetylene in MeCN solvent produced soluble products **28–33** in polar aprotic solvents including chlorinated solvents. The yields of the products varied from 36% to 83%, and were presumably compromised by electronically unfavorable matches between electron-rich alkylhalide and electron-rich arylacetylenes. Scheme 5.3 summarized the synthesis of bisguanosine derivatives **34–42** and bisguanine derivatives **43–45**, which were synthesized as middle step to the final goal. Sonogashira coupling reactions of 8-bromo-2',3',5'-tri-*O*-acetylguanosine **27** with 1,4-diethynyl-2,5-bis(pentoxy)benzene **53** in MeCN solvent gave the product **34** in 33% yield, which can be dissolved in polar aprotic solvents including chlorinated solvents. The same coupling reaction of bromoguanosine with linkage compounds **46–53** yielded sparingly soluble bisguanosine compounds **35–42** due to multiple hydrogen-bond donors and acceptors in their structures. The yields of



these eight compounds varied from 35% to 76%. Three of bisguanine derivatives **43–45** were obtained in high yields through hydrolysis reaction of **35–37** in 1 M HCl aqueous solution. Single crystals of **28** and **29** were formed by layering their CHCl<sub>3</sub> solutions (8 mg mL<sup>-1</sup> for **28**; 4 mg mL<sup>-1</sup> for **29**) with pentane (**28**) or hexane (**29**). Compounds **28** and **29** crystallize in *P*2<sub>1</sub>2<sub>1</sub>2<sub>1</sub> space group, and are almost isostructural. Each compound crystallizes with two disordered molecules of CHCl<sub>3</sub> per molecule of guanine derivative.

### 5.2.2 X-Ray Crystal Structure Analysis

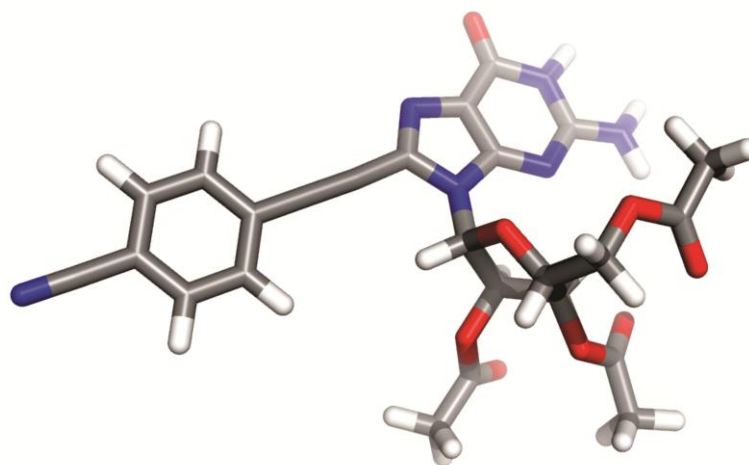


**Figure 5.2** Crystal structure of **28**. C—gray, H—white, N—blue, and O—red.

The crystal structure of compound **28** (Figure 5.2) is characterized by the *syn*-conformation of the ribose substituent relative to the guanine nucleus, with a 10.5° torsional angle between the guanine and ribose moieties.<sup>105</sup> The cyano-substituted phenyl ring is disordered over two closely related orientations (only one is shown in Figure 5.2),

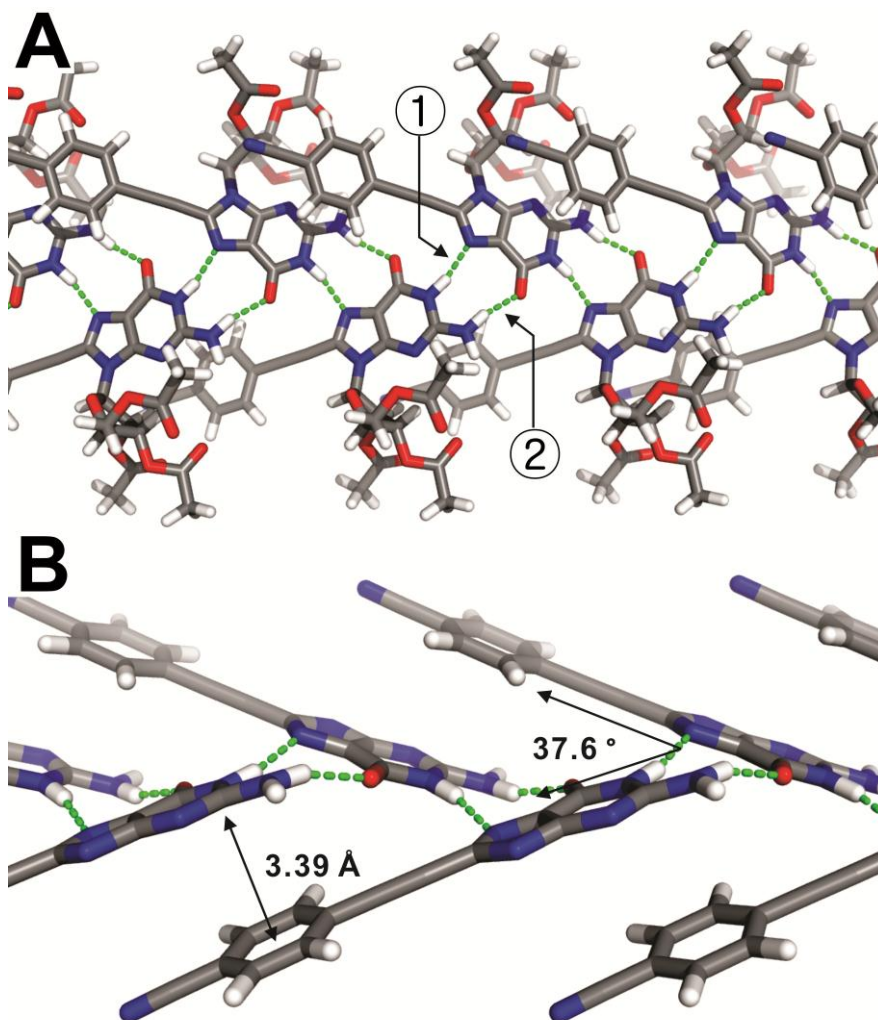


**Figure 5.3** (A) Top view of twisted hydrogen-bonded guanine ribbon within the superstructure of **28**. Hydrogen bonds are highlighted in green. *Contact 1*: N $\cdots$ H 2.09 Å, N $\cdots$ N 2.95 Å, N–H $\cdots$ N 167.6°. *Contact 2*: O $\cdots$ H 1.98 Å, O $\cdots$ N 2.92 Å, N–H $\cdots$ O 161.1°, C=O $\cdots$ H 128.9°. (B) Side view of a twisted guanine ribbon (ribose substituents removed for clarity) highlights the 37.6° angle between the planes of adjacent guanine nuclei, and a 3.39 Å distance between parallel planes, consistent with  $[\pi\cdots\pi]$  stacking. Disordered solvent (CHCl<sub>3</sub>) molecules are omitted. C—gray, H—white, N—blue, O—red.

and the triple bond is slightly bent, with  $\text{C}\equiv\text{C}-\text{C}$  angles ranging between  $173.8^\circ$  and  $179.5^\circ$  (across both orientations). Aryl and guanine moieties are essentially coplanar—interplanar angle is  $7.0^\circ$ . The supramolecular structure of **28** (Figure 5.3A) reveals infinite guanine ribbons, wherein each guanine nucleus acts as a hydrogen bond<sup>113</sup> donor in two interactions, and as an acceptor in another two (see caption to Figure. 5.3 for distances and angles). Hydrogen-bonded guanine ribbons in the superstructure of **28** are twisted, as illustrated in the side-view in Figure 5.3B. The angle defined by the planes of adjacent hydrogen-bonded guanine rings is  $37.6^\circ$ , representing the most highly twisted

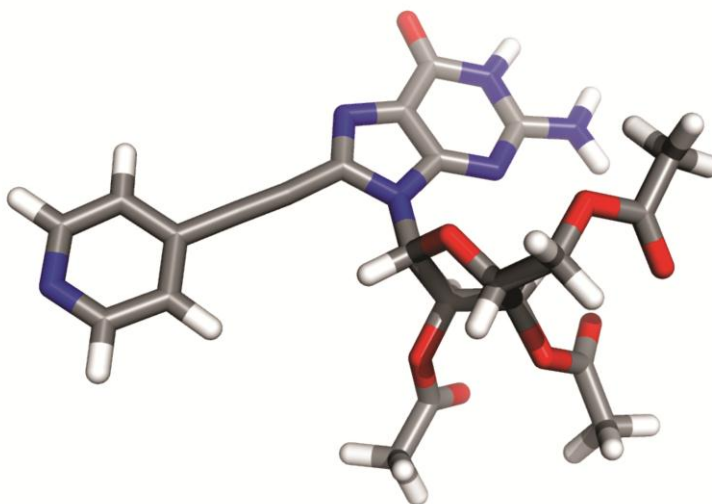


**Figure 5.4** Crystal structure of **29**. C—gray, H—white, N—blue, and O—red.

guanine ribbon reported to date.<sup>114</sup> Molecules of **28** reside in two alternating sets of parallel planes and the distance between two adjacent planes in each set is  $3.39 \text{ \AA}$ . This distance is consistent with a  $[\pi \cdots \pi]$  slipped-stacked interaction between the electron-poor 4-cyanophenyl ring and the electron-rich guanine nucleus.<sup>115</sup> Pyridine derivative **29** is virtually isostructural with **28** (Figure 5.4 and 5.5). The molecular structure shows

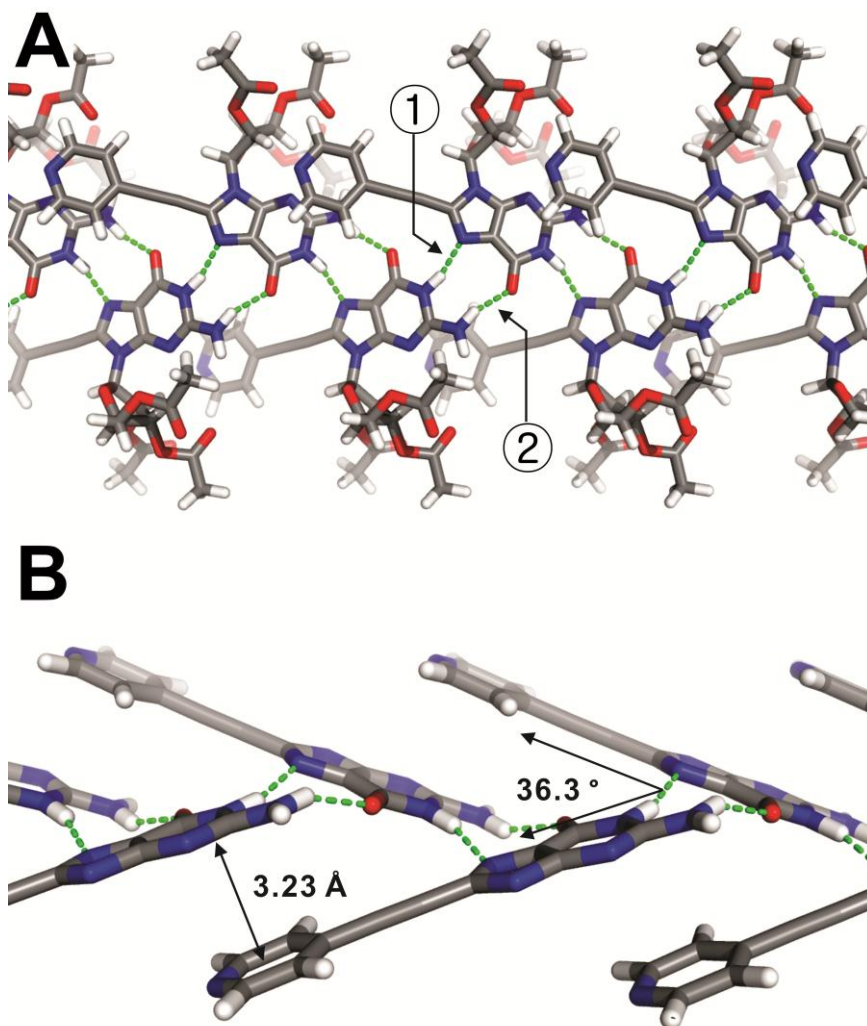


**Figure 5.5** (A) Top view of twisted hydrogen-bonded guanine ribbon within the superstructure of **29**. Hydrogen bonds are highlighted in green. *Contact 1*: N $\cdots$ H 2.10 Å, N $\cdots$ N 2.95 Å, N–H $\cdots$ N 164.3°. *Contact 2*: O $\cdots$ H 2.09 Å, O $\cdots$ N 2.89 Å, N–H $\cdots$ O 153.5°, C=O $\cdots$ H 130.2°. (B) Side view of a twisted guanine ribbon (ribose substituents removed for clarity) highlights the 36.3° angle between the planes of adjacent guanine nuclei, and a 3.23 Å distance between parallel planes, consistent with  $[\pi\cdots\pi]$  stacking. Disordered solvent ( $\text{CHCl}_3$ ) molecules are omitted. C—gray, H—white, N—blue, O—red.

disorder only in the solvent molecules. The triple bond in **29** is slightly bent ( $\text{C}\equiv\text{C}-\text{C}$  angles are  $174.7^\circ$  and  $178.7^\circ$ ), pyridine and guanine moieties are at a low  $4.0^\circ$  angle relative to each other, and guanine and ribose are *syn* to each other (torsional angle  $7.2^\circ$ ).<sup>105</sup> Just like in the case of **28**, compound **29** organizes into infinite guanine ribbons, stabilized by  $[\text{N1}-\text{H}\cdots\text{N7}]$  ( $2.10 \text{ \AA}$ ) and  $[\text{N11}-\text{H}\cdots\text{O10}-\text{C6}]$  ( $2.09 \text{ \AA}$ ) hydrogen bonds. Analogous to **28**, these ribbons are twisted, with adjacent guanine planes defining an angle of  $36.3^\circ$ , and parallel (every other) planes positioned at a distance of  $3.23 \text{ \AA}$ .

Given the structural similarity between Sessler's compound **26** and my derivatives **28** and **29**, the difference in their supramolecular organization is unexpected. Since all three systems are characterized by complex substituents in the 8-position and the *syn*-relationship between the ribose and guanine moieties, some more subtle structural variations must be responsible for the switch to ribbon structures in **28** and **29**.<sup>116</sup> We propose that the combination of geometric and electronic factors stabilizes the twisted ribbon superstructure relative to the guanine quartet. Figures 5.3 and 5.5 suggest efficient  $[\pi\cdots\pi]$  stacking between the alternating guanine nuclei and electron-poor arylethynyl substituents. This is a reasonable proposition for **28** and **29**, since their electron-poor cyanophenyl and pyridyl groups should be electronically complementary to the electron-rich guanine; in **26**, the electronics would be mismatched, since (4-dimethylamino)phenyl substituent would be electron-rich as well. In addition, geometric factors play a role: the  $\sim 4 \text{ \AA}$  long  $-\text{C}\equiv\text{C}-$  unit in **28** and **29** projects their pendant substituents into an optimal position to stack with the guanine nucleus two sites away in the emerging ribbon superstructure. The shorter linker length in **26** would not have allowed such a match. Finally, the steric bulk of the acyl group on the ribose substituents—acetyl (**28/29**) vs.

isobutyryl (**26**)—might be contributing to the observed absence of  $[\pi \cdots \pi]$  stacking in **26**, as its (4-dimethylamino)phenyl group effectively gets buried amongst the large isobutyryl groups from the neighboring molecules.<sup>117</sup>

### 5.3 Conclusion and Outlook

In summary, I have synthesized new monoguanosine, bisguanosine, and bisguanine derivatives through Sonogashira coupling halogenated guanosine derivatives with terminal alkynes. The low solubility of guanosine derivatives in organic solvents was overcome by protecting hydroxyl groups of ribose subunit with acetylation for compounds **28–34**. Crystallographic data was obtained for compound **28** and **29**, whose solid-state structures reveal hydrogen-bonded ribbon superstructures despite the presence of a substituent in the 8-position. These results suggest that the balance between guanine ribbon and quartet superstructures is more subtle than previously thought, with both steric and electronic factors playing a role.

For the future work, the guanine-based porous materials, there are three points to be duly considered. (a) Solubility of both cruciform and guanosine derivative is the first issue. Many cruciform compounds introduced in previous chapters have long aliphatic chains to increase their solubility. As shown in this chapter, three acetyl groups were introduced to dissolve monoguanosine derivatives in organic solvents because of their sparse solubility caused by strong hydrogen-bonding interaction and  $\pi$ - $\pi$  interaction between guanine bases. (b) The length of linker between cruciform core and guanine base must be longer than that of compounds **1–9** to give porosity to the self-assembled

structure as shown in Figure 5.1, therefore, the flexibility of ethynyl linker have to be taken into account. (c) Dimensional expansion from 2D to 3D can also be a challenging task.

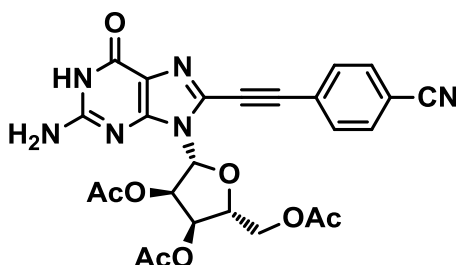
## 5.4 Experimental Section

### 5.4.1 General Methods

All reactions were performed under nitrogen atmosphere in oven-dried glassware. Reagents were purchased from commercial suppliers and used without further purification. Solvents were used as received, except tetrahydrofuran (THF) and *N,N*-dimethylformamide (DMF), which were dried over activated alumina in an mBraun Solvent Purification System. Triethylamine (Et<sub>3</sub>N) was distilled over KOH pellets and degassed by a 15 min nitrogen purge prior to use. Compounds 8-bromoguanosine,<sup>111</sup> 8-bromo-2',3',5'-tri-*O*-acetylguanosine<sup>112</sup> and PdCl<sub>2</sub>(PPh<sub>3</sub>)<sub>2</sub><sup>55</sup> were prepared according to literature procedures. Microwave-assisted reactions were performed in a Biotage Initiator 2.0 microwave reactor, producing monochromatic microwave radiation with the frequency of 2.45 GHz. Melting points measurements were performed in open capillary tubes, using Mel-Temp Thermo Scientific apparatus, and are uncorrected. Microanalyses were conducted by Intertek USA, Inc. Mass spectral measurements were performed by the Mass Spectrometry Facility of the Department of Chemistry and Biochemistry at the University of Texas at Austin. NMR spectra were obtained on Bruker QE-300, JEOL ECX-400 and ECA-500 spectrometers, with working frequencies (for <sup>1</sup>H nuclei) of 300, 400, and 500 MHz, respectively. All <sup>13</sup>C-NMR spectra were recorded with simultaneous

decoupling of  $^1\text{H}$  nuclei.  $^1\text{H}$ -NMR chemical shifts are reported in ppm units relative to the residual signal of the solvent ( $\text{CDCl}_3$ , 7.26 ppm and  $\text{DMSO}-d_6$ , 2.50 ppm). Unless otherwise specified, all NMR spectra were recorded at 25 °C. Infrared spectra were recorded on a Perkin-Elmer Spectrum 100 FT-IR spectrophotometer using Pike MIRacle Micrometer pressure clamp. UV-Vis spectra were recorded on a Perkin-Elmer Lambda 25 UV/Vis spectrophotometer. Column chromatography was carried out on silica gel 60, 32–63 mesh. Analytical TLC was performed on Merck aluminum-backed silica-gel plates.

#### 5.4.2 Synthesis of Compound 28

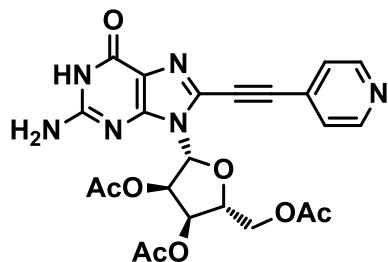


In a nitrogen flushed round-bottom flask,  $\text{K}_2\text{CO}_3$  (423 mg, 3.07 mmol) was added to methanol (3 mL), THF (3 mL), and 4-[(trimethylsilyl)ethynyl]-benzonitrile<sup>118</sup> (306 mg, 1.54 mmol). After stirring for 30 min, the reaction mixture was filtered through celite. The crude mixture was added to a thick-walled microwave pressure vial containing a mixture of 8-bromo-2',3',5'-tri-*O*-acetylguanosine (**27**, 500 mg, 1.02 mmol),  $\text{PdCl}_2(\text{PPh}_3)_2$  (144 mg, 0.205 mmol),  $\text{CuI}$  (39 mg, 0.21 mmol),  $\text{Et}_3\text{N}$  (5 mL), and MeCN (5 mL). The vial was sealed and exposed to microwave irradiation for 3 h at 90 °C. After cooling, solvents were removed under reduced pressure and the crude solid was purified by column chromatography, eluting first with pure  $\text{CH}_2\text{Cl}_2$ , then with a  $\text{CH}_2\text{Cl}_2/\text{MeOH}$



(97:3) mixture, and finally with a 19:1 CH<sub>2</sub>Cl<sub>2</sub>/MeOH mixture. After removal of the solvent, the product was obtained as a yellow solid (mp >150 °C, with decomposition) in 83% yield (452 mg, 0.846 mmol). Single crystals of **28** were obtained by layering a chloroform solution of **29** (8 mg/mL) with pentane (crystals formed in 2 days). UV-Vis (CH<sub>2</sub>Cl<sub>2</sub>):  $\lambda_{\text{max}}$  (log $\epsilon$ ) = 266 (6.23), 348 (6.30) nm. IR (neat): 3710 (w), 3461 (w), 2968 (w), 2230 (w), 2130 (w), 1739 (s), 1367 (s), 1229 (s), 1033 (w) cm<sup>-1</sup>. <sup>1</sup>H NMR (CDCl<sub>3</sub>, 500 MHz):  $\delta$  11.90 (br s, 1H), 7.74 (d, <sup>3</sup>J<sub>H-H</sub> = 8.0 Hz, 2H), 7.68 (d, <sup>3</sup>J<sub>H-H</sub> = 8.0 Hz, 2H), 6.90 (br s, 2H), 6.19 (dd, <sup>3</sup>J<sub>H-H</sub> = 5.7 Hz, <sup>3</sup>J<sub>H-H</sub> = 3.4 Hz, 1H), 6.13 (d, <sup>3</sup>J<sub>H-H</sub> = 3.4 Hz, 1H), 6.08 (dd, <sup>3</sup>J<sub>H-H</sub> = 6.3 Hz, <sup>3</sup>J<sub>H-H</sub> = 5.7 Hz, 1H), 4.50 (dd, <sup>2</sup>J<sub>H-H</sub> = 12.0 Hz, <sup>3</sup>J<sub>H-H</sub> = 4.0 Hz, 1H), 4.38 (m, 1H), 4.30 (dd, <sup>2</sup>J<sub>H-H</sub> = 12.0 Hz, <sup>3</sup>J<sub>H-H</sub> = 5.7 Hz, 1H), 2.14 (s, 3H), 2.12 (s, 3H), 1.97 (s, 3H) ppm. <sup>13</sup>C NMR (CDCl<sub>3</sub>, 125 MHz):  $\delta$  170.87, 169.64 (2C), 158.44, 154.49, 151.22, 132.73, 132.36, 130.27, 125.92, 118.32, 118.16, 113.05, 93.09, 87.43, 81.80, 79.50, 72.90, 70.28, 62.92, 20.81, 20.75 (2C) ppm. HRMS (ESI): Calcd for C<sub>25</sub>H<sub>23</sub>N<sub>6</sub>O<sub>8</sub><sup>+</sup>: 535.1572. Found: 535.1566. Anal. calcd for C<sub>25</sub>H<sub>22</sub>N<sub>6</sub>O<sub>8</sub>: C, 56.18; H, 4.15; N, 15.72. Found: C, 55.67; H, 4.67; N, 12.97.

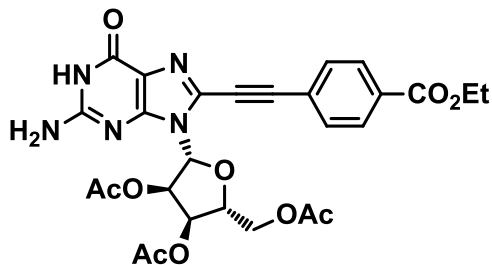
### 5.4.3 Synthesis of Compound 29



The entire amount of 4-ethynylpyridine prepared with 4-[(trimethylsilyl)-ethynyl]pyridine<sup>57</sup> (646 mg, 3.69 mmol) as described above was added to a thick-walled

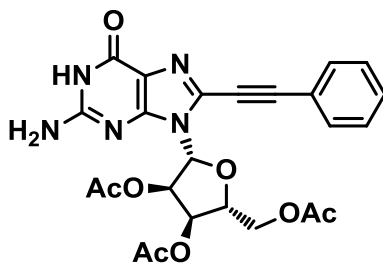
microwave pressure vial that contained a mixture of 8-bromo-2',3',5'-tri-*O*-acetylguanosine (**27**, 900 mg, 1.84 mmol), PdCl<sub>2</sub>(PPh<sub>3</sub>)<sub>2</sub> (259 mg, 0.369 mmol), CuI (70 mg, 0.37 mmol), Et<sub>3</sub>N (5 mL), and MeCN (5 mL). The vial was sealed and exposed to microwave irradiation for 3 h at 90 °C. After cooling, solvents were removed under reduced pressure, and the crude solid was purified by column chromatography, eluting first with pure CH<sub>2</sub>Cl<sub>2</sub>, and then successively with CH<sub>2</sub>Cl<sub>2</sub>/MeOH mixtures in 97:3, 19:1, and 9:1 ratios. After removal of the solvent, the product was obtained as a yellow solid (mp >127 °C, with decomposition) in 58% yield (546 mg, 1.07 mmol). Single crystals of **29** were obtained by layering a chloroform solution of **29** (4 mg/mL) with hexane (crystals formed in 7 d). UV-Vis (CH<sub>2</sub>Cl<sub>2</sub>): λ<sub>max</sub> (logε) = 267 (5.90), 336 (6.15) nm. IR (neat): 3467 (w), 3155 (w), 2227 (w), 1754 (s), 1729 (s), 1705 (s), 1366 (s), 1244 (s) cm<sup>-1</sup>. <sup>1</sup>H NMR (CDCl<sub>3</sub>, 400 MHz): δ 12.03 (br s, 1H), 8.69 (d, <sup>3</sup>J<sub>H-H</sub> = 5.9 Hz, 2H), 7.52 (d, <sup>3</sup>J<sub>H-H</sub> = 5.9 Hz, 2H), 6.69 (br s, 2H), 6.21 (dd, <sup>3</sup>J<sub>H-H</sub> = 5.9 Hz, <sup>3</sup>J<sub>H-H</sub> = 3.7 Hz, 1H), 6.15 (d, <sup>3</sup>J<sub>H-H</sub> = 3.7 Hz, 1H), 6.12 (dd, <sup>3</sup>J<sub>H-H</sub> = 5.9 Hz, <sup>3</sup>J<sub>H-H</sub> = 5.9 Hz, 1H), 4.54 (dd, <sup>2</sup>J<sub>H-H</sub> = 11.9 Hz, <sup>3</sup>J<sub>H-H</sub> = 3.7 Hz, 1H), 4.41 (ddd, <sup>3</sup>J<sub>H-H</sub> = 5.9 Hz, <sup>3</sup>J<sub>H-H</sub> = 5.9 Hz, <sup>3</sup>J<sub>H-H</sub> = 3.7 Hz, 1H), 4.33 (dd, <sup>2</sup>J<sub>H-H</sub> = 11.9 Hz, <sup>3</sup>J<sub>H-H</sub> = 5.9 Hz, 1H), 2.14 (s, 3H), 2.14 (s, 3H), 2.01 (s, 3H) ppm. <sup>13</sup>C NMR (CDCl<sub>3</sub>, 125 MHz): δ 170.10, 169.62, 169.53, 156.06, 154.54, 151.07, 150.17, 128.27, 127.76, 125.33, 117.76, 90.63, 86.59, 82.46, 79.21, 78.92, 71.78, 69.76, 62.83, 20.42, 20.32 ppm. HRMS (ESI): Calcd for C<sub>23</sub>H<sub>23</sub>N<sub>6</sub>O<sub>8</sub><sup>+</sup>: 511.1572. Anal. calcd for C<sub>23</sub>H<sub>22</sub>N<sub>6</sub>O<sub>8</sub>: C, 54.12; H, 4.34; N, 16.46. Found: C, 53.20; H, 4.03; N, 16.04.

#### 5.4.4 Synthesis of Compound 30



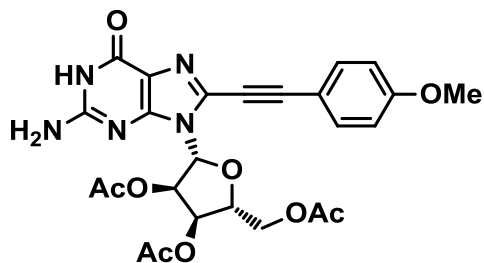
The entire amount of ethyl 4-(ethynyl)benzoate prepared with ethyl 4-[2-(trimethylsilyl)ethynyl]benzoate<sup>119</sup> (379 mg, 1.54 mmol) as described above was added to a thick-walled microwave pressure vial that contained a mixture of 8-bromo-2',3',5'-tri-*O*-acetylguanosine (**27**, 500 mg, 1.02 mmol), PdCl<sub>2</sub>(PPh<sub>3</sub>)<sub>2</sub> (144 mg, 0.21 mmol), CuI (40 mg, 0.21 mmol), Et<sub>3</sub>N (5 mL), and MeCN (5 mL). The vial was sealed and exposed to microwave irradiation for 3 h at 90 °C. After cooling, solvents were removed under reduced pressure and the crude solid was purified by column chromatography, eluting first with CH<sub>2</sub>Cl<sub>2</sub>, then 3% MeOH/CH<sub>2</sub>Cl<sub>2</sub>, and finally with 5% MeOH/CH<sub>2</sub>Cl<sub>2</sub> to collect the product. After removal of the solvent, the product was obtained as a yellow solid (mp >200 °C, with decomposition) in 82% yield (488 mg, 0.84 mmol). UV-Vis (CH<sub>2</sub>Cl<sub>2</sub>): λ<sub>max</sub> (logε) = 270 (6.23), 343 (6.38) nm. IR (neat): 3462 (w), 3316 (w), 2989 (w), 2218 (w), 1748 (s), 1716 (s), 1689 (s), 1370 (s), 1241 (s) cm<sup>-1</sup>. <sup>1</sup>H NMR (CDCl<sub>3</sub>, 400 MHz): δ 11.78 (br s, 1H), 7.98 (d, <sup>3</sup>J<sub>H-H</sub> = 8.2 Hz, 2H), 7.63 (d, <sup>3</sup>J<sub>H-H</sub> = 8.2 Hz, 2H), 6.85 (br s, 2H), 6.35 (m, 1H), 6.20 (d, <sup>3</sup>J<sub>H-H</sub> = 3.7 Hz, 1H), 6.13 (dd, <sup>3</sup>J<sub>H-H</sub> = 5.9 Hz, <sup>3</sup>J<sub>H-H</sub> = 5.5 Hz, 1H), 4.54 (br m, 1H), 4.29–4.43 (m, 4H), 2.12 (s, 3H), 2.09 (s, 3H), 2.00 (s, 3H), 1.39 (t, <sup>3</sup>J<sub>H-H</sub> = 7.3 Hz, 3H) ppm. <sup>13</sup>C NMR (CDCl<sub>3</sub>, 100 MHz): δ 170.81, 169.62, 169.45, 165.69, 158.22, 154.30, 151.35, 131.86, 131.03, 130.66, 129.56, 125.50, 117.88, 93.74, 87.27, 80.83, 79.61, 72.59, 70.36, 62.95, 61.39, 20.74, 20.62, 20.56, 14.32 ppm.

#### 5.4.5 Synthesis of Compound 31



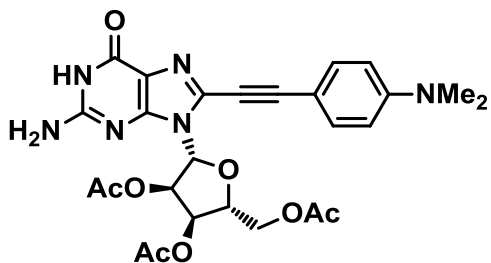
A mixture of 8-bromo-2',3',5'-tri-*O*-acetylguanosine (**27**, 1.00 g, 2.05 mmol), phenylacetylene (459  $\mu$ L, 4.10 mmol),  $\text{PdCl}_2(\text{PPh}_3)_2$  (288 mg, 0.410 mmol), CuI (78 mg, 0.41 mmol),  $\text{Et}_3\text{N}$  (5 mL), and MeCN (5 mL) was sealed in a thick-walled microwave pressure vial and exposed to microwave irradiation for 3 h at 90  $^\circ\text{C}$ . After cooling, solvents were removed under reduced pressure and the crude solid was purified by column chromatography, eluting first with  $\text{CH}_2\text{Cl}_2$ , then 3% MeOH/ $\text{CH}_2\text{Cl}_2$ , and finally with 5% MeOH/ $\text{CH}_2\text{Cl}_2$  to collect the product. After removal of the solvent, the product was obtained as pale-yellow solid (mp  $>150$   $^\circ\text{C}$ , with decomposition) in 76% yield (796 mg, 1.56 mmol). UV-Vis ( $\text{CH}_2\text{Cl}_2$ ):  $\lambda_{\text{max}}$  (log $\epsilon$ ) = 323 (6.30) nm. IR (neat): 3331 (w), 3158 (w), 2221 (w), 1747 (s), 1687 (s), 1369 (s), 1231 (s)  $\text{cm}^{-1}$ .  $^1\text{H}$  NMR ( $\text{DMSO}-d_6$ , 400 MHz):  $\delta$  10.98 (br s, 1H), 7.67 (m, 2H), 7.49 (m, 3H), 6.72 (br s, 2H), 6.08 (d,  $^3J_{\text{H-H}} = 4.6$  Hz, 1H), 6.01 (dd,  $^3J_{\text{H-H}} = 6.4$  Hz,  $^3J_{\text{H-H}} = 4.6$  Hz, 1H), 5.64 (dd,  $^3J_{\text{H-H}} = 6.4$  Hz,  $^3J_{\text{H-H}} = 6.4$  Hz, 1H), 4.43 (dd,  $^3J_{\text{H-H}} = 11.9$  Hz,  $^3J_{\text{H-H}} = 3.7$  Hz, 1H), 4.36 (ddd,  $^3J_{\text{H-H}} = 6.4$  Hz,  $^3J_{\text{H-H}} = 5.9$  Hz,  $^3J_{\text{H-H}} = 3.7$  Hz, 1H), 4.19 (dd,  $^3J_{\text{H-H}} = 11.9$  Hz,  $^3J_{\text{H-H}} = 6.4$  Hz, 1H), 2.11 (s, 3H), 2.08 (s, 3H), 1.92 (s, 3H) ppm.  $^{13}\text{C}$  NMR ( $\text{DMSO}-d_6$ , 100 MHz):  $\delta$  170.10, 169.56, 169.49, 156.05, 154.36, 150.96, 131.73, 130.13, 129.05, 128.71, 120.25, 117.33, 93.38, 86.44, 78.93, 78.67, 71.54, 69.75, 62.75, 20.39, 20.33, 20.29 ppm.

#### 5.4.6 Synthesis of Compound 32



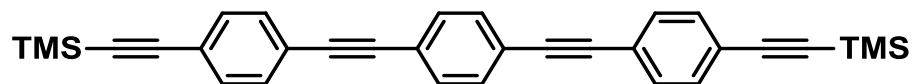
The entire amount of 4-ethynylanisole prepared with 4-[2-(trimethylsilyl)-ethynyl]anisole<sup>120</sup> (837 mg, 4.10 mmol) as described above was added to a thick-walled microwave pressure vial that contained a mixture of 8-bromo-2',3',5'-tri-*O*-acetylguanosine (**27**, 1.00 g, 2.05 mmol), PdCl<sub>2</sub>(PPh<sub>3</sub>)<sub>2</sub> (289 mg, 0.410 mmol), CuI (78 mg, 0.41 mmol), Et<sub>3</sub>N (5 mL), and MeCN (5 mL). The vial was sealed and exposed to microwave irradiation for 3 h at 90 °C. After cooling, solvents were removed under reduced pressure and the crude solid was purified by column chromatography, eluting first with CH<sub>2</sub>Cl<sub>2</sub>, then 3% MeOH/CH<sub>2</sub>Cl<sub>2</sub>, and finally with 5% MeOH/CH<sub>2</sub>Cl<sub>2</sub> to collect the product. After removal of the solvent, the product was obtained as white solid (mp >150 °C, with decomposition) in 57% yield (625 mg, 1.16 mmol). UV-Vis (CH<sub>2</sub>Cl<sub>2</sub>): λ<sub>max</sub> (logε) = 324 (6.43), 344 (6.30) nm. IR (neat): 3340 (w), 2215 (w), 1750 (s), 1688 (s), 1371 (s), 1239 (s) cm<sup>-1</sup>. <sup>1</sup>H NMR (CDCl<sub>3</sub>, 400 MHz): δ 11.89 (br s, 1H), 7.56 (d, <sup>3</sup>J<sub>H-H</sub> = 8.7 Hz, 2H), 6.88 (d, <sup>3</sup>J<sub>H-H</sub> = 8.7 Hz, 2H), 6.85 (br s, 2H), 6.26 (dd, <sup>3</sup>J<sub>H-H</sub> = 5.5 Hz, <sup>3</sup>J<sub>H-H</sub> = 4.1 Hz, 1H), 6.20 (d, <sup>3</sup>J<sub>H-H</sub> = 4.1 Hz, 1H), 6.07 (dd, <sup>3</sup>J<sub>H-H</sub> = 5.9 Hz, <sup>3</sup>J<sub>H-H</sub> = 5.5 Hz, 1H), 4.52 (dd, <sup>3</sup>J<sub>H-H</sub> = 11.0 Hz, <sup>3</sup>J<sub>H-H</sub> = 2.7 Hz, 1H), 4.28–4.39 (m, 2H), 3.82 (s, 3H), 2.10 (s, 3H), 2.09 (s, 3H), 1.99 (s, 3H) ppm. <sup>13</sup>C NMR (CDCl<sub>3</sub>, 100 MHz): δ 170.88, 169.51, 169.48, 160.76, 158.39, 154.17, 151.25, 133.86, 131.53, 117.51, 114.26, 112.98, 95.09, 87.04, 79.46, 77.00, 72.53, 70.31, 62.92, 55.46, 20.75, 20.64, 20.59 ppm.

#### 5.4.7 Synthesis of Compound 33



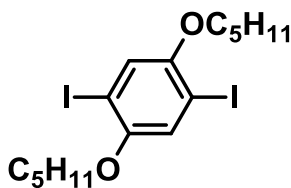
The entire amount of *N,N*-dimethyl-4-(ethynyl)aniline prepared with *N,N*-dimethyl-4-[(trimethylsilyl)ethynyl]aniline<sup>56</sup> (890 mg, 4.10 mmol) as described above was added to a thick-walled microwave pressure vial that contained a mixture of 8-bromo-2',3',5'-tri-*O*-acetylguanosine (**27**, 1.00 g, 2.05 mmol), PdCl<sub>2</sub>(PPh<sub>3</sub>)<sub>2</sub> (289 mg, 0.410 mmol), CuI (78 mg, 0.41 mmol), Et<sub>3</sub>N (5 mL), and MeCN (5 mL). The vial was sealed and exposed to microwave irradiation for 3 h at 90 °C. After cooling, solvents were removed under reduced pressure and the crude solid was purified by column chromatography, eluting first with CH<sub>2</sub>Cl<sub>2</sub>, then 3% MeOH/CH<sub>2</sub>Cl<sub>2</sub>, 5% MeOH/CH<sub>2</sub>Cl<sub>2</sub> and finally with 10% MeOH/CH<sub>2</sub>Cl<sub>2</sub> to collect the product. After removal of the solvent, the product was obtained as brown solid (mp >142 °C, with decomposition) in 36% yield (410 mg, 0.742 mmol). UV-Vis (CH<sub>2</sub>Cl<sub>2</sub>): λ<sub>max</sub> (log ε) = 351 (6.46) nm. IR (neat): 3322 (w), 2203 (w), 1751 (s), 1690 (s), 1369 (s), 1235 (s) cm<sup>-1</sup>. <sup>1</sup>H NMR (CDCl<sub>3</sub>, 400 MHz): δ 11.96 (br s, 1H), 7.49 (d, <sup>3</sup>J<sub>H-H</sub> = 8.7 Hz, 2H), 6.67 (br s, 2H), 6.66 (d, <sup>3</sup>J<sub>H-H</sub> = 8.7 Hz, 2H), 6.18–6.26 (m, 2H), 6.02 (dd, <sup>3</sup>J<sub>H-H</sub> = 5.9 Hz, <sup>3</sup>J<sub>H-H</sub> = 5.5 Hz, 1H), 4.52 (m, 1H), 4.30–4.39 (m, 2H), 3.02 (s, 6H), 2.11 (s, 3H), 2.10 (s, 3H), 2.01 (s, 3H) ppm. <sup>13</sup>C NMR (CDCl<sub>3</sub>, 100 MHz): δ 170.97, 169.59, 169.48, 158.51, 154.02, 151.33, 150.99, 133.54, 132.34, 117.54, 111.72, 107.19, 96.91, 86.94, 79.52, 76.43, 72.40, 70.42, 62.98, 40.21, 20.83, 20.72, 20.65 ppm.

#### 5.4.8 Synthesis of 1,4-Bis[2-[4-[2-(trimethylsilyl)ethynyl]phenyl]ethynyl]benzene



Triethylamine (15 mL) in 100 mL Schlenk flask was degassed for 15 min and then *p*-diethynylbenzene (250 mg, 1.98 mmol), PdCl<sub>2</sub>(PPh<sub>3</sub>)<sub>2</sub> (28 mg, 0.040 mmol), CuI (4 mg, 0.02 mmol), and 4-bromo-1-(2-(trimethylsilyl)ethynyl)benzene<sup>123</sup> (1.00 g, 3.96 mmol) were added. The mixture was refluxed for 18 h under nitrogen gas. The mixture was filtered out, concentrated *in vacuo*, and diluted with ethyl acetate (100 mL). The mixture was washed with water (2×100 mL) and brine (100 mL). The solvent was removed *in vacuo*, and the crude solid was purified using column chromatography, eluting with hexane to collect the product. After removal of the solvent, the product was obtained as a pale yellow solid in 42% yield (396 mg, 0.841 mmol). <sup>1</sup>H NMR (CDCl<sub>3</sub>, 300 MHz):  $\delta$  7.50 (s, 4H), 7.45 (s, 8H), 0.26 (s, 18H) ppm.

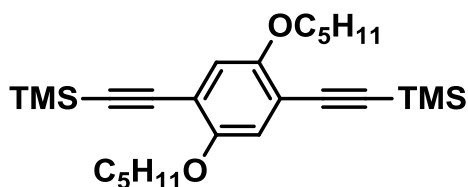
#### 5.4.9 Synthesis of 1,4-Diiodo-2,5-dipentoxybenzene



In a round-bottom flask, 2,5-diiodobenzene-1,4-diol<sup>122</sup> (500 mg, 1.38 mmol), 1-bromopentane (525  $\mu$ L, 4.15 mmol), and potassium carbonate (573 mg, 4.15 mmol) were added and dissolved in acetone (5 mL) and refluxed for 20 h. The mixture was

concentrated, and purified by column chromatography, eluting with hexane/ethyl acetate (4:1) to collect the product. Concentration afforded 587 mg (1.17 mmol, 84%) of product.  $^1\text{H}$  NMR ( $\text{CDCl}_3$ , 500 MHz):  $\delta$  7.17 (s, 2H), 3.93 (t,  $^3J_{\text{H-H}} = 6.9$  Hz, 4H), 1.78 (m, 4H), 1.53 (m, 4H), 0.98 (t,  $^3J_{\text{H-H}} = 7.4$  Hz, 6H) ppm.

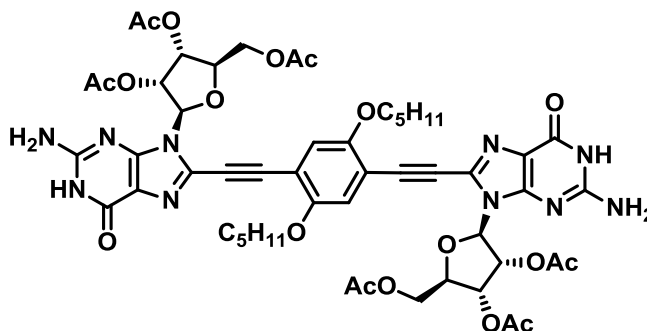
#### 5.4.10 Synthesis of 1,4-Dipentoxy-2,5-bis[2-(trimethylsilyl)ethynyl]benzene



A mixture of 1,4-diiodo-2,5-dimethoxybenzene (500 mg, 1.28 mmol), (trimethylsilyl)acetylene (1.40 mL, 9.96 mmol),  $\text{PdCl}_2(\text{PPh}_3)_2$  (140 mg, 0.20 mmol),  $\text{CuI}$  (38 mg, 0.20 mmol),  $\text{Et}_3\text{N}$  (1.0 mL), and  $\text{MeCN}$  (9.0 mL) was sealed in a thick-walled microwave pressure vial and exposed to microwave irradiation for 3 h at 85 °C. After cooling, solvents were removed under reduced pressure and the crude solid was purified by column chromatography, eluting with a hexane/ $\text{CH}_2\text{Cl}_2$  (2:1) mixture to collect the product in 73% yield (320 mg, 0.72 mmol).  $^1\text{H}$  NMR ( $\text{CDCl}_3$ , 500 MHz):  $\delta$  6.89 (s, 2H), 3.94 (t,  $^3J_{\text{H-H}} = 6.3$  Hz, 4H), 1.79 (m, 4H), 1.48 (m, 4H), 1.39 (m, 4H), 0.93 (t,  $^3J_{\text{H-H}} = 7.4$  Hz, 6H), 0.25 (s, 18H) ppm.



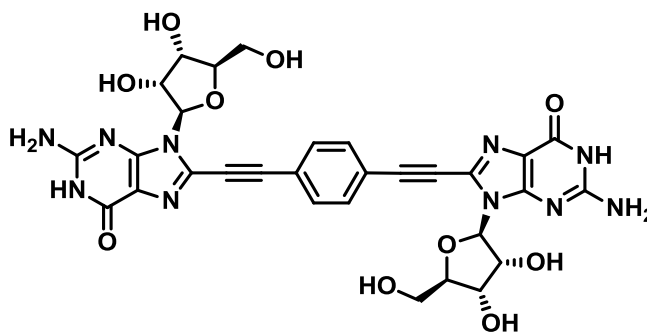
#### 5.4.11 Synthesis of Compound 34



In a nitrogen-flushed round-bottom flask,  $\text{K}_2\text{CO}_3$  (187 mg, 1.36 mmol) was added to MeOH (3 mL), THF (3 mL), and 1,4-dipentoxy-2,5-bis[2-(trimethylsilyl)-ethynyl]benzene (200 mg, 0.45 mmol). After stirring for 30 min, the reaction mixture was filtered through celite. The solvent was removed under reduced pressure. The crude mixture was added to thick-walled microwave pressure vial that already contained mixture of 8-bromo-2',3',5'-tri-*O*-acetylguanosine (529 mg, 1.08 mmol),  $\text{PdCl}_2(\text{PPh}_3)_2$  (32 mg, 0.045 mmol), CuI (9 mg, 0.05 mmol),  $\text{Et}_3\text{N}$  (5 mL), and MeCN (5 mL). The vial was sealed and exposed to microwave irradiation for 4 h at 90 °C. After cooling, solvents were removed under reduced pressure, and the crude solid was purified by column chromatography, eluting first with  $\text{CH}_2\text{Cl}_2$ , then 3% MeOH/ $\text{CH}_2\text{Cl}_2$ , 5% MeOH/ $\text{CH}_2\text{Cl}_2$  and finally with 10% MeOH/ $\text{CH}_2\text{Cl}_2$  to collect the product. After removal of the solvent, the product was obtained as a yellow solid in 33% yield (168 mg, 0.151 mmol).  $^1\text{H}$  NMR (DMSO- $d_6$ , 500 MHz):  $\delta$  11.03 (br s, 2H), 7.31 (s, 2H), 6.74 (br s, 4H), 6.15 (d,  $^3J_{\text{H-H}} = 3.4$  Hz, 2H), 5.98 (dd,  $^3J_{\text{H-H}} = 6.3$  Hz,  $^3J_{\text{H-H}} = 3.8$  Hz, 2H), 5.71 (dd,  $^3J_{\text{H-H}} = 6.9$  Hz,  $^3J_{\text{H-H}} = 6.3$  Hz, 2H), 4.44 (dd,  $^3J_{\text{H-H}} = 11.5$  Hz,  $^3J_{\text{H-H}} = 3.4$  Hz, 2H), 4.31 (m, 2H), 4.22 (dd,  $^3J_{\text{H-H}} = 11.5$  Hz,  $^3J_{\text{H-H}} = 6.9$  Hz, 2H), 4.02–4.16 (m, 4H), 2.11 (s, 6H), 2.05 (s, 6H), 1.96 (s,

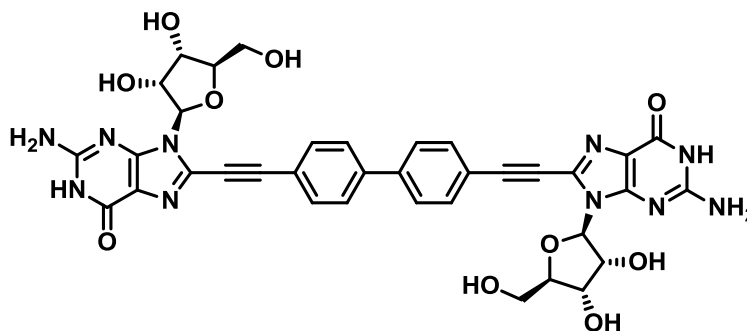
6H), 1.71–1.83 (m, 4H), 1.32–1.46 (m, 8H), 0.89 (t,  $^3J_{\text{H-H}} = 6.9$  Hz, 6H) ppm.  $^{13}\text{C}$  NMR (DMSO- $d_6$ , 125 MHz):  $\delta$  170.05, 169.37, 156.10, 154.33, 153.34, 150.79, 129.04, 117.71, 116.27, 112.05, 90.34, 87.15, 84.21, 79.40, 79.18, 71.97, 70.05, 69.04, 63.09, 28.19, 27.62, 27.42, 21.80, 20.38, 20.25, 20.17 ppm.

#### 5.4.12 Synthesis of Compound 35



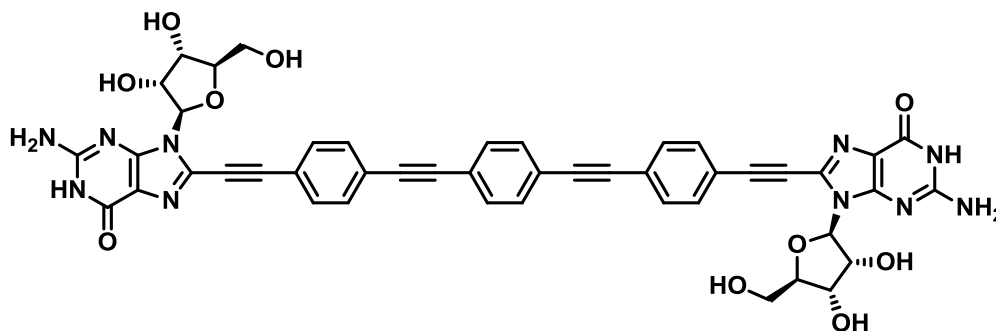
The mixture of 8-bromoguanosine (5.01 g, 13.6 mmol), *p*-diethynylbenzene (580  $\mu\text{L}$ , 4.52 mmol),  $\text{PdCl}_2(\text{PPh}_3)_2$  (65 mg, 0.093 mmol), and  $\text{CuI}$  (18 mg, 0.093 mmol) was added to degassed DMF (100 mL), and then  $\text{Et}_3\text{N}$  (2.52 mL) was added to the flask. After stirring for 4 d, the reaction mixture was concentrated *in vacuo*, filtrated, and washed with hot water and acetone to give 2.20 g of product (3.20 mmol, 71%).  $^1\text{H}$  NMR (DMSO- $d_6$ , 300 MHz):  $\delta$  10.92 (br s, 2H), 7.72 (s, 4H), 6.45 (br s, 4H), 5.88 (d,  $^3J_{\text{H-H}} = 6.3$  Hz, 2H), 5.50 (d,  $^3J_{\text{H-H}} = 6.3$  Hz, 2H), 5.15 (d,  $^3J_{\text{H-H}} = 5.1$  Hz, 2H), 4.90–5.10 (m, 4H), 4.10–4.20 (m, 2H), 3.83–3.93 (m, 2H), 3.50–3.70 (m, 4H) ppm.  $^{13}\text{C}$  NMR (DMSO- $d_6$ , 75 MHz):  $\delta$  162.34, 156.11, 154.13, 151.30, 132.99, 132.03, 121.68, 117.81, 92.03, 88.32, 85.75, 82.03, 71.05, 70.50, 61.99 ppm. HRMS (ESI/[M+H] $^+$ ) Calcd for  $\text{C}_{30}\text{H}_{29}\text{N}_{10}\text{O}_{10}$ : 689.2063. Found: 689.2063.

#### 5.4.13 Synthesis of Compound 36



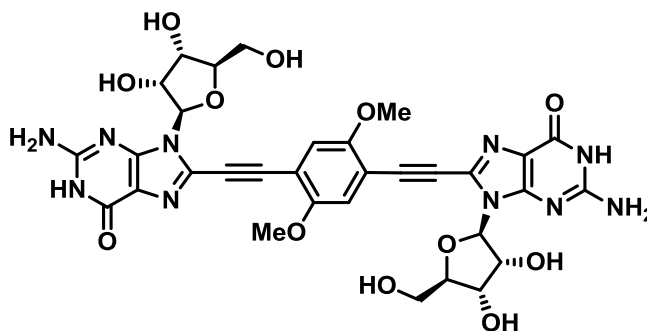
In a nitrogen-flushed round-bottom flask,  $\text{K}_2\text{CO}_3$  (121 mg, 0.875 mmol) was added to MeOH (3 mL), THF (3 mL), and 4,4'-[2-(trimethylsilyl)-ethynyl]biphenyl<sup>123</sup> (100 mg, 0.289 mmol). After stirring for 30 min, the reaction mixture was filtered through celite. The solvent was removed under reduced pressure. The crude mixture was added to round-bottomed flask equipped with condenser that already contained mixture of 8-bromoguanosine (235 mg, 0.649 mmol),  $\text{PdCl}_2(\text{PPh}_3)_2$  (4 mg, 0.006 mmol), CuI (0.6 mg, 0.003 mmol), and degassed  $\text{Et}_3\text{N}/\text{DMF}$  (1:9). The reaction mixture was heated at reflux for 5 d. After cooling down, the mixture was concentrated *in vacuo* to remove  $\text{Et}_3\text{N}$ , filtered, and washed with hot water and acetone to give 116 mg of product (0.15 mmol, 53%).  $^1\text{H}$  NMR ( $\text{DMSO}-d_6$ , 75 MHz):  $\delta$  10.91 (br s, 2H), 7.98 (m, 4H), 7.74 (m, 4H), 6.63 (br s, 4H), 5.90 (br s, 2H), 5.51 (br s, 2H), 5.17 (br s, 2H), 4.97 (br s, 4H), 4.17 (br s, 2H), 3.89 (br s, 2H), 3.65 (br s, 2H), 3.56 (br s, 2H) ppm. LRMS Calcd for  $\text{C}_{36}\text{H}_{32}\text{N}_{10}\text{O}_{10}$ : 764.7. Found: 763.4.

#### 5.4.14 Synthesis of Compound 37



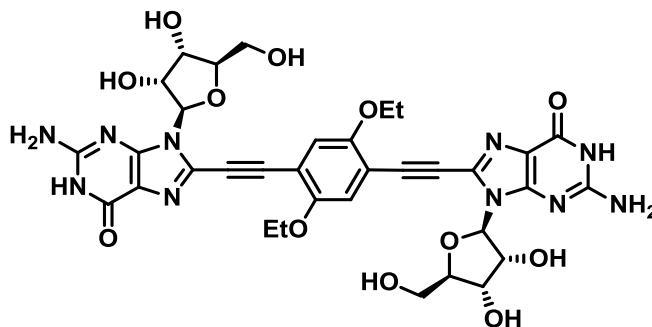
In a nitrogen-flushed round-bottom flask,  $\text{K}_2\text{CO}_3$  (89 mg, 0.64 mmol) was added to MeOH (3 mL), THF (3 mL), and 1,4-bis[2-[4-[2-(trimethylsilyl)ethynyl]phenyl]ethynyl]benzene (100 mg, 0.212 mmol). After stirring for 30 min, the reaction mixture was filtered through celite. The solvent was removed under reduced pressure. The crude mixture was added to round-bottomed flask equipped with condenser that already contained mixture of 8-bromoguanosine (173 mg, 0.478 mmol),  $\text{PdCl}_2(\text{PPh}_3)_2$  (3 mg, 0.004 mmol), CuI (0.4 mg, 0.002 mmol), and 20 mL of degassed  $\text{Et}_3\text{N}/\text{DMF}$  (1:9). The reaction mixture was heated at reflux for 5 d. After cooling down, the mixture was concentrated *in vacuo* to remove  $\text{Et}_3\text{N}$ , filtered, and washed with hot water and acetone to give 92 mg of product (0.10 mmol, 49%).  $^1\text{H}$  NMR ( $\text{DMSO}-d_6$ , 300 MHz):  $\delta$  10.91 (br s, 2H), 7.69 (br s, 12H), 6.64 (br s, 4H), 5.90 (br s, 2H), 5.51 (br s, 2H), 5.16 (br s, 2H), 4.97 (br s, 4H), 4.16 (br s, 2H), 3.89 (br s, 2H), 3.65 (br s, 2H), 3.54 (br s, 2H) ppm. HRMS (ESI/[M+H] $^+$ ) Calcd for  $\text{C}_{46}\text{H}_{34}\text{N}_{10}\text{O}_{10}$ : 443.1231. Found: 443.1235.

#### 5.4.15 Synthesis of Compound 38



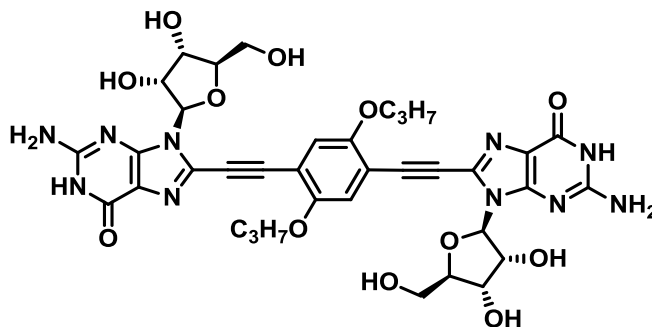
In a nitrogen-flushed round-bottom flask,  $\text{K}_2\text{CO}_3$  (127 mg, 0.919 mmol) was added to a mixture of MeOH (3 mL), THF (3 mL), and 1,4-dimethoxy-2,5-bis[2-(trimethylsilyl)-ethynyl]benzene<sup>124</sup> (100 mg, 0.303 mmol). After stirring for 30 min, the reaction mixture was filtered through celite. The solvent was removed under reduced pressure. The crude mixture was added to round-bottomed flask equipped with condenser that already contained mixture of 8-bromoguanosine (329 mg, 0.908 mmol),  $\text{PdCl}_2(\text{PPh}_3)_2$  (4 mg, 0.006 mmol), CuI (1 mg, 0.006 mmol), and 20 mL of degassed  $\text{Et}_3\text{N}/\text{DMF}$  (1:9). The reaction mixture was heated at reflux for 4 d. After cooling down, the mixture was concentrated *in vacuo* to remove  $\text{Et}_3\text{N}$ , filtered, and washed with hot water and acetone to give 153 mg of product (0.204 mmol, 68%).  $^1\text{H}$  NMR ( $\text{DMSO}-d_6$ , 400 MHz):  $\delta$  10.99 (br s, 2H), 7.28 (s, 2H), 6.66 (br s, 4H), 5.96 (d,  $^3J_{\text{H-H}} = 6.4$  Hz, 2H), 5.45 (d,  $^3J_{\text{H-H}} = 6.0$  Hz, 2H), 4.90–5.16 (m, 6H), 4.17 (m, 2H), 3.91 (s, 6H), 3.88 (m, 2H), 3.65 (m, 2H), 3.52 (m, 2H) ppm.

#### 5.4.16 Synthesis of Compound 39



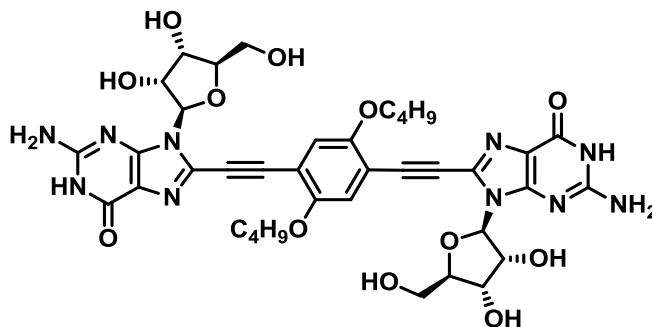
In a nitrogen-flushed round-bottom flask,  $\text{K}_2\text{CO}_3$  (116 mg, 0.839 mmol) was added to a mixture of MeOH (3 mL), THF (3 mL), and 1,4-diethoxy-2,5-bis[2-(trimethylsilyl)ethynyl]benzene<sup>125</sup> (100 mg, 0.279 mmol). After stirring for 30 min, the reaction mixture was filtered through celite. The solvent was removed under reduced pressure. The crude mixture was added to a round-bottomed flask equipped with condenser that already contained a mixture of 8-bromoguanosine (303 mg, 0.836 mmol),  $\text{PdCl}_2(\text{PPh}_3)_2$  (4 mg, 0.006 mmol), CuI (1 mg, 0.006 mmol), and 20 mL of degassed  $\text{Et}_3\text{N}/\text{DMF}$  (1:9). The reaction mixture was refluxed for 4 d. After cooling down, the mixture was concentrated *in vacuo* to remove  $\text{Et}_3\text{N}$ , filtered, and washed with hot water and acetone to give 75 mg of product (0.10 mmol, 35%).  $^1\text{H}$  NMR ( $\text{DMSO}-d_6$ , 500 MHz):  $\delta$  10.89 (br s, 2H), 7.25 (s, 2H), 6.62 (br s, 4H), 5.95 (d,  $^3J_{\text{H-H}} = 5.7$  Hz, 2H), 5.45 (d,  $^3J_{\text{H-H}} = 6.3$  Hz, 2H), 5.04 (d,  $^3J_{\text{H-H}} = 4.6$  Hz, 2H), 4.99 (dd,  $^3J_{\text{H-H}} = 11.5$  Hz,  $^3J_{\text{H-H}} = 6.3$  Hz, 2H), 4.93 (t,  $^3J_{\text{H-H}} = 5.7$  Hz, 2H), 4.10–4.23 (m, 6H), 3.86 (m, 2H), 3.63 (m, 2H), 3.52 (m, 2H), 1.40 (t,  $^3J_{\text{H-H}} = 6.9$  Hz, 6H) ppm.

#### 5.4.17 Synthesis of Compound 40



In a nitrogen-flushed round-bottom flask,  $\text{K}_2\text{CO}_3$  (107 mg, 0.774 mmol) was added to a mixture of MeOH (3 mL), THF (3 mL), and of 1,4-dipropoxy-2,5-bis[2-(trimethylsilyl)-ethynyl]benzene<sup>126</sup> (100 mg, 0.258 mmol). After stirring for 30 min, the reaction mixture was filtered through celite. The solvent was removed under reduced pressure. The crude mixture was added to round-bottomed flask equipped with condenser that already contained mixture of 8-bromoguanosine (281 mg, 0.776 mmol),  $\text{PdCl}_2(\text{PPh}_3)_2$  (4 mg, 0.005 mmol), CuI (1 mg, 0.005 mmol), and 20 mL of degassed  $\text{Et}_3\text{N}/\text{DMF}$  (1:9). The reaction mixture was refluxed for 5 d. After cooling down, the mixture was concentrated *in vacuo* to remove  $\text{Et}_3\text{N}$ , filtered, and washed with hot water and acetone to give 132 mg of product (0.164 mmol, 63%).  $^1\text{H}$  NMR ( $\text{DMSO}-d_6$ , 400 MHz):  $\delta$  10.88 (br s, 2H), 7.26 (s, 2H), 6.59 (br s, 4H), 5.93 (d,  $^3J_{\text{H-H}} = 6.4$  Hz, 2H), 5.43 (d,  $^3J_{\text{H-H}} = 6.0$  Hz, 2H), 5.04 (d,  $^3J_{\text{H-H}} = 5.0$  Hz, 2H), 4.97 (dd,  $^3J_{\text{H-H}} = 6.0$  Hz,  $^3J_{\text{H-H}} = 6.0$  Hz, 2H), 4.92 (t,  $^3J_{\text{H-H}} = 6.4$  Hz, 2H), 4.18 (m, 2H), 4.06 (m, 4H), 3.85 (m, 2H), 3.63 (m, 2H), 3.52 (m, 2H), 1.79 (m, 4H), 1.00 (t,  $^3J_{\text{H-H}} = 7.3$  Hz, 6H) ppm.

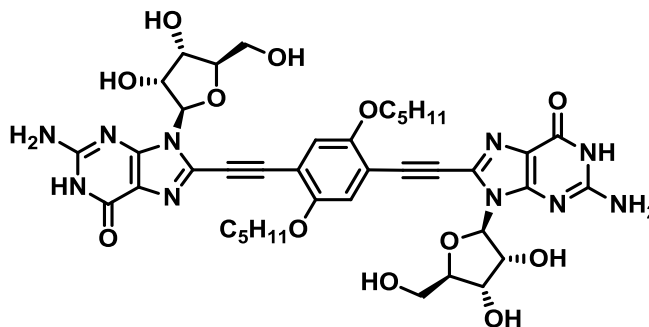
#### 5.4.18 Synthesis of Compound 41



In a nitrogen-flushed round-bottom flask,  $\text{K}_2\text{CO}_3$  (100 mg, 0.723 mmol) was added to a mixture of methanol (3 mL), THF (3 mL), and 1,4-dibutoxy-2,5-bis[2-(trimethylsilyl)ethynyl]benzene<sup>124</sup> (100 mg, 0.241 mmol). After stirring for 30 min, the reaction mixture was filtered through celite. The solvent was removed under reduced pressure. The crude mixture was added to round-bottomed flask equipped with condenser that already contained mixture of 8-bromoguanosine (262 mg, 0.723 mmol),  $\text{PdCl}_2(\text{PPh}_3)_2$  (4 mg, 0.005 mmol), CuI (1 mg, 0.005 mmol), and 15 mL of degassed  $\text{Et}_3\text{N}/\text{DMF}$  (1:9). The reaction mixture was refluxed for 6 d. After cooling down, the mixture was concentrated *in vacuo* to remove  $\text{Et}_3\text{N}$ , filtered, and washed with hot water and acetone to give 110 mg of product (0.132 mmol, 53%).  $^1\text{H}$  NMR ( $\text{DMSO}-d_6$ , 400 MHz):  $\delta$  10.89 (br s, 2H), 7.26 (s, 2H), 6.60 (br s, 4H), 5.93 (d,  $^3J_{\text{H-H}} = 6.0$  Hz, 2H), 5.42 (d,  $^3J_{\text{H-H}} = 6.0$  Hz, 2H), 5.03 (d,  $^3J_{\text{H-H}} = 4.6$  Hz, 2H), 4.97 (dd,  $^3J_{\text{H-H}} = 6.4$  Hz,  $^3J_{\text{H-H}} = 6.0$  Hz, 2H), 4.93 (dd,  $^3J_{\text{H-H}} = 6.4$  Hz,  $^3J_{\text{H-H}} = 5.5$  Hz, 2H), 4.18 (m, 2H), 4.10 (m, 4H), 3.86 (m, 2H), 3.65 (m, 2H), 3.52 (m, 2H), 1.78 (m, 4H), 1.47 (m, 4H), 0.94 (t,  $^3J_{\text{H-H}} = 7.3$  Hz, 6H) ppm.

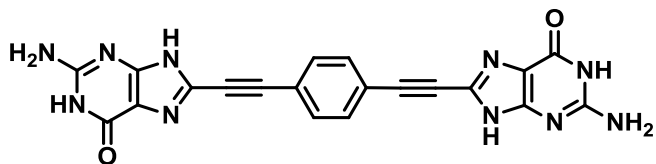


#### 5.4.19 Synthesis of Compound 42



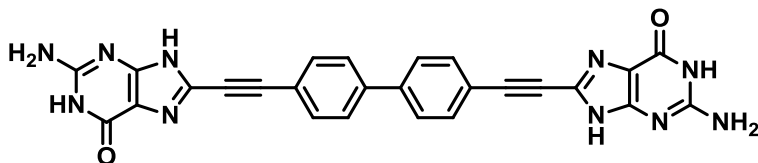
In a nitrogen-flushed round-bottom flask,  $\text{K}_2\text{CO}_3$  (94 mg, 0.68 mmol) was added to a mixture of MeOH (3 mL), THF (3 mL), and 1,4-dipentoxo-2,5-bis[2-(trimethylsilyl)ethynyl]benzene (100 mg, 0.226 mmol). After stirring for 30 min, the reaction mixture was filtered through celite. The solvent was removed under reduced pressure. The crude mixture was added to round-bottomed flask equipped with condenser that already contained mixture of 8-bromoguanosine (254 mg, 0.701 mmol),  $\text{PdCl}_2(\text{PPh}_3)_2$  (4 mg, 0.005 mmol), CuI (1 mg, 0.005 mmol), and 15 mL of degassed  $\text{Et}_3\text{N}/\text{DMF}$  (1:9). The reaction mixture was refluxed for 6 d. After cooling down, the mixture was concentrated *in vacuo* to remove  $\text{Et}_3\text{N}$ , filtered, and washed with hot water and acetone to give 148 mg of product (0.172 mmol, 76%).  $^1\text{H}$  NMR ( $\text{DMSO}-d_6$ , 500 MHz):  $\delta$  10.89 (br s, 2H), 7.26 (s, 2H), 6.58 (br s, 4H), 5.93 (d,  $^3J_{\text{H-H}} = 6.3$  Hz, 2H), 5.42 (d,  $^3J_{\text{H-H}} = 6.3$  Hz, 2H), 5.03 (d,  $^3J_{\text{H-H}} = 5.2$  Hz, 2H), 4.97 (m, 2H), 4.93 (m, 2H), 4.18 (m, 2H), 4.09 (m, 4H), 3.86 (m, 2H), 3.65 (m, 2H), 3.52 (m, 2H), 1.79 (m, 4H), 1.37 (m, 8H), 0.89 (m, 6H) ppm.

#### 5.4.20 Synthesis of Compound 43



Compound **35** (200 mg, 0.290 mmol) was suspended in 20 mL of 1 M HCl aqueous solution and stirred at 100 °C for 3 h. The reaction mixture was cooled, neutralized with sat. NaHCO<sub>3</sub> solution and left at 0 °C for 2 h. The precipitate was filtered, washed with water and acetone to give 123 mg of product (0.290 mmol, 99%). <sup>1</sup>H NMR (DMSO-*d*<sub>6</sub>, 300 MHz):  $\delta$  13.04 (br s, 2H), 10.71 (br s, 2H), 7.63 (s, 4H), 6.52 (br s, 4H) ppm. HRMS (ESI/[M+H]<sup>+</sup>) Calcd for C<sub>20</sub>H<sub>13</sub>N<sub>10</sub>O<sub>2</sub> : 425.1220. Found: 425.1217.

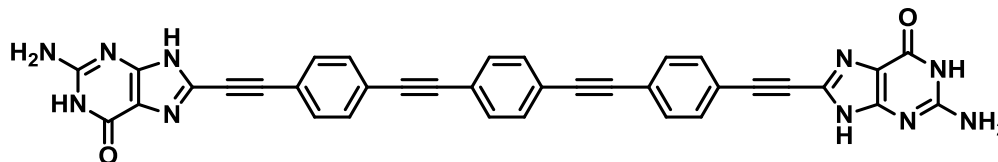
#### 5.4.21 Synthesis of Compound 44



Compound **36** (50 mg, 0.065 mmol) was suspended in 5 mL of 1 M HCl aqueous solution and stirred at 100 °C for 3 h. The reaction mixture was cooled, neutralized with sat. NaHCO<sub>3</sub> solution and left at 0 °C for 2 h. The precipitate was filtered, washed with water and acetone to give 32 mg of product (0.064 mmol, 98%). <sup>1</sup>H NMR (DMSO-*d*<sub>6</sub>, 300 MHz):  $\delta$  10.79 (br s, 2H), 10.71 (br s, 2H), 7.85 (d, <sup>3</sup>J<sub>H-H</sub> = 8.42 Hz, 4H), 7.70 (d,

$^3J_{\text{H-H}} = 8.42 \text{ Hz}$ , 4H), 6.53 (br s, 2H) ppm. HRMS (ESI/[M+H]<sup>+</sup>) Calcd for C<sub>26</sub>H<sub>17</sub>N<sub>10</sub>O<sub>2</sub>: 501.1532. Found: 501.1530.

#### 5.4.22 Synthesis of Compound 45



Compound **37** (50 mg, 0.056 mmol) was suspended in 5 mL of 1 M HCl aqueous solution and stirred at 100 °C for 3 h. The reaction mixture was cooled, neutralized with sat. NaHCO<sub>3</sub> solution and left at 0 °C for 2 h. The precipitate was filtered, washed with water and acetone to give 34 mg of product (0.054 mmol, 96%). <sup>1</sup>H NMR (DMSO-*d*<sub>6</sub>, 300 MHz):  $\delta$  10.88 (br s, 1H), 7.66 (s, 12H), 6.64 (br s, 3H) ppm. HRMS (ESI/[M+H]<sup>+</sup>) Calcd for C<sub>36</sub>H<sub>183</sub>N<sub>10</sub>O<sub>2</sub> : 311.0807. Found: 311.0812.

#### 5.4.23 Crystal Data for Compound 28

Empirical formula	C <sub>27</sub> H <sub>24</sub> Cl <sub>6</sub> N <sub>6</sub> O <sub>8</sub>
Formula weight	773.22
Temperature	223(2) K
Wavelength	0.71073 Å
Crystal system	Orthorhombic

Space group	$P2_12_12_1$	
Unit cell dimensions	$a = 9.726(8) \text{ \AA}$	$\alpha = 90.00^\circ$
	$b = 10.525(2) \text{ \AA}$	$\beta = 90.00^\circ$
	$c = 34.007(2) \text{ \AA}$	$\gamma = 90.00^\circ$
Volume	$3481.5(4) \text{ \AA}^3$	
Z	4	
Density (calculated)	$1.475 \text{ Mg/m}^3$	
Absorption coefficient	$0.548 \text{ mm}^{-1}$	
$F(000)$	1576	
Crystal size	$0.45 \times 0.30 \times 0.08 \text{ mm}$	
Theta range for data collection	$1.20 \text{ to } 23.54^\circ$	
Index ranges	$-10 \leq h \leq 11, 0 \leq k \leq 11, 0 \leq l \leq 38$	
Reflections collected	15676	
Independent reflections	5190 [ $R_{\text{int}} = 0.062$ ]	
Completeness to $\theta = 23.54^\circ$	100.0 %	
Absorption correction	Empirical	
Max. and min. transmission	0.9892 and 0.7299	
Refinement method	Full-matrix least-squares on $F^2$	
Data / restraints / parameters	3072 / 0 / 389	
Goodness-of-fit on $F^2$	1.038	
Final R indices [ $I > 2\sigma(I)$ ]	$R_1 = 0.059, wR_2 = 0.169$	
R indices (all data)	$R_1 = 0.096, wR_2 = 0.206$	
Largest diff. peak and hole	$+0.61 \text{ and } -0.33 \text{ e}^-/\text{\AA}^3$	

#### 5.4.24 Crystal Data for Compound 29

Empirical formula	$\text{C}_{25}\text{H}_{24}\text{Cl}_6\text{N}_6\text{O}_8$	
Formula weight	749.20	
Temperature	223(2) K	
Wavelength	0.71073 Å	
Crystal system	Orthorhombic	
Space group	$P2_12_12_1$	
Unit cell dimensions	$a = 9.754(1)$ Å	$\alpha = 90.00^\circ$
	$b = 10.353(1)$ Å	$\beta = 90.00^\circ$
	$c = 31.859(3)$ Å	$\gamma = 90.00^\circ$
Volume	$3217.4(6)$ Å <sup>3</sup>	
<i>Z</i>	4	
Density (calculated)	1.547 Mg/m <sup>3</sup>	
Absorption coefficient	0.590 mm <sup>-1</sup>	
<i>F</i> (000)	1528	
Crystal size	0.45×0.20×0.05 mm	
Theta range for data collection	1.28 to 23.64 °	
Index ranges	$-10 \leq h \leq 11, 0 \leq k \leq 11, 0 \leq l \leq 35$	
Reflections collected	13581	
Independent reflections	4782 [ $R_{\text{int}} = 0.079$ ]	
Completeness to theta = 23.64 °	99.3 %	
Absorption correction	Empirical	
Max. and min. transmission	0.9957 and 0.7244	

Refinement method	Full-matrix least-squares on $F^2$
Data / restraints / parameters	2814 / 0 / 415
Goodness-of-fit on $F^2$	1.218
Final $R$ indices [ $I > 2\sigma(I)$ ]	$R_1 = 0.058$ , $wR_2 = 0.124$
$R$ indices (all data)	$R_1 = 0.120$ , $wR_2 = 0.169$
Largest diff. peak and hole	+0.44 and $-0.41 \text{ e}^-/\text{\AA}^3$

## References

- [1] (a) Valeur, B.; Berberan-Santos, M. N. *Molecular Fluorescence*, 2<sup>nd</sup> ed.; Wiley-VCH: Weinheim, 2012. (b) Muller, P. *Pure Appl. Chem.* **1994**, *66*, 1077–1184.
- [2] (a) Dsouza, R. N.; Pischel, U.; Nau, W. M. *Chem. Rev.* **2011**, *111*, 7941–7980. (b) Merino, E. *Chem. Soc. Rev.* **2011**, *40*, 3835–3853. (c) Hagfeldt, A.; Boschloo, G.; Sun, L.; Kloo, L.; Pettersson, H. *Chem. Rev.* **2010**, *110*, 6595–6663. (d) Wang, L.-Y.; Chen, Q.-W.; Zhai, G.-H.; Wen, Z.-Y.; Zhang, Z.-X. *Dyes Pigments* **2007**, *72*, 357–362. (e) Delaire, J. A.; Nakatani, K. *Chem. Rev.* **2000**, *100*, 1817–1845. (f) Reichardt, C. *Chem. Rev.* **1994**, *94*, 2319–2358. (g) Fabian, J. *Chem. Rev.* **1992**, *92*, 1197–1226; (h) Rattee, I. D. *Chem. Soc. Rev.* **1972**, *1*, 145–162.
- [3] (a) Lin, Y.; Li, Y.; Zhan, X. *Chem. Soc. Rev.* **2012**, *41*, 4245–4272. (b) Kanibolotsky, A. L.; Perepichka, I. F.; Skabara, P. J. *Chem. Soc. Rev.* **2010**, *39*, 2695–2728. (c) Pron, A.; Gawrys, P.; Zagorska, M.; Djurado, D.; Demadrille, R. *Chem. Soc. Rev.* **2010**, *39*, 2577–2632. (d) Wu, J.; Pisula, W.; Müllen, K. *Chem. Rev.* **2007**, *107*, 718–747. (e) Roncali, J. *Acc. Chem. Res.* **2000**, *33*, 147–156.
- [4] (a) Kertesz, M.; Choi, C. H.; Yang, S. *Chem. Rev.* **2005**, *105*, 3448–3481. (b) Ajayaghosh, A. *Chem. Soc. Rev.* **2003**, *32*, 181–191. (c) Jug, K.; Hiberty, P. C.; Shaik, S. *Chem. Rev.* **2001**, *101*, 1477–1500. (d) Roncali, J. *Chem. Rev.* **1997**, *97*, 173–205.
- [5] (a) Homnick P. J.; Lahti, P. M. *Phys. Chem. Chem. Phys.* **2012**, *14*, 11961–11968. (b) Yoshizawa, K. *Acc. Chem. Res.* **2012**, *45*, 1612–1621. (c) Chen, Z.; Lohr, A.; Saha-Möller, C. R.; Würthner, F. *Chem. Soc. Rev.* **2010**, *39*, 2577–2632. (d) Dutta, T.; Woody,

K. B.; Parkin, S. R.; Watson, M. D.; Gierschner, J. *J. Am. Chem. Soc.* **2009**, *131*, 17321–17327. (e) Hissler, M.; Dyer, P. W.; Réau, R. *Coord. Chem. Rev.* **2003**, *244*, 1–44. (f) Fowler, P. W.; Hansen, P.; Caporossi, G.; Soncini, A. *Chem. Phys. Lett.* **2001**, *342*, 105–112. (g) Brooker, L. G. S.; White, F. L.; Sprague, R. H.; Dent, Jr. S. G.; Van Zandt, G. *Chem. Rev.* **1947**, *41*, 325–351.

[6] (a) Beharry, A. A.; Woolley, G. A. *Chem. Soc. Rev.* **2011**, *40*, 4422–4437. (b) Joly, D.; Tondelier, D.; Deborde, V.; Geffroy, B.; Hissler, M.; Réau, R. *New J. Chem.* **2010**, *34*, 1603–1611. (c) Perepichka, I. F.; Perepichka, D. F.; Meng, H.; Wudl, F. *Adv. Mater.* **2005**, *17*, 2281–2305. (d) Berggren, B.; Inganäs, O.; Gustafsson, G.; Rasmusson, J.; Andersson, M. R.; Hjertberg, T.; Wennerström, O. *Nature* **1994**, *372*, 444–446.

[7] (a) Wang, C.; Dong, H.; Hu, W.; Liu, Y.; Zhu, D. *Chem. Rev.* **2012**, *112*, 2208–2267. (b) Platt, A. D.; Kendrick, M. J.; Loth, M.; Anthony, J. E.; Ostroverkhova, O. *Phys. Rev. B* **2011**, *84*, 235209. (c) Klauk, H. *Chem. Soc. Rev.* **2010**, *39*, 2643–2666.

[8] (a) Du, J.; Hu, M.; Fan, J.; Peng, X. *Chem. Soc. Rev.* **2012**, *41*, 4511–4535. (b) Boens, N.; Leen, V.; Dehaen, W. *Chem. Soc. Rev.* **2012**, *41*, 1130–1172. (c) Zhou, Y.; Yoon, J. *Chem. Soc. Rev.* **2012**, *41*, 52–67. (d) Chen, X.; Tian, X.; Shin, I.; Yoon, J. *Chem. Soc. Rev.* **2011**, *40*, 4783–4804. (e) Moragues, M. E.; Martínez-Máñez, R.; Sancenón, F. *Chem. Soc. Rev.* **2011**, *40*, 2593–2643. (f) Zhou, Y.; Xu, Z.; Yoon, J. *Chem. Soc. Rev.* **2011**, *40*, 2222–2235.

[9] (a) Haid, S.; Marszalek, M.; Mishra, A.; Wielopolski, M.; Teuscher, J.; Moser, J.; Humphry-Baker, R.; Zakeeruddin, S. M.; Grätzel, M.; Bäuerle, P. *Adv. Funct. Mater.* **2012**, *22*, 1291–1302. (b) Clifford, J. N.; Martínez-Ferrero, E.; Viterisi, A.; Palomares, E.



*Chem. Soc. Rev.* **2011**, *40*, 1635–1646. (c) Bouachrine, M.; Bouzzine, SM.; Hamidi, M.; Lère-Porte, J-P.; Serein-Spirau, F.; Sotiropoulos, J. M.; Miqueu, K. *J. Mater. Environ. Sci.* **2010**, *1*, 78–83. (d) Cheng, Y.-J.; Yang, S.-H.; Hsu, C.-S. *Chem. Rev.* **2009**, *109*, 5868–5923.

[10] (a) Anthony, J.; Boldi, A. M.; Rubin, Y.; Hobi, M.; Gramlich, V.; Knobler, C. B.; Seiler, P.; Diederich, F. *Helv. Chim. Acta.* **1995**, *78*, 13–45. (b) Tolosa, J.; Solntsev, K. M.; Tolbert, L. M.; Bunz, U. H. F. *J. Org. Chem.* **2010**, *75*, 523–534. (c) Jung, K. H.; Bae, S. Y.; Kim, K. H.; Cho, M. J.; Lee, K.; Kim, Z. H.; Choi, D. H.; Lee, D. H.; Chung, D. S.; Park, C. E. *Chem. Commun.* **2009**, 5290–5292.

[11] (a) Narita, T.; Takase, M.; Nishinaga, T.; Iyoda, M.; Kamada, K.; Ohta, K. *Chem. Eur. J.* **2010**, *16*, 12108–12113. (b) Rupert, B. L.; Mitchell, W. J.; Ferguson, A. J.; Köse, M. E.; Rance, W. L.; Rumbles, G.; Ginley, D. S.; Shaheen, S. e.; Kopidakis, N. *J. Mater. Chem.* **2009**, *19*, 5311–5324. (c) Huang, G.; Sun, Y.-Q.; Xu, Z.; Zellerb, M.; Hunterb, A. D. *Dalton Trans.* **2009**, 5083–5093. (d) Shoji, T.; Ito, S.; Toyota, K.; Yasunami, M.; Morita, N. *Chem. Eur. J.* **2008**, *14*, 8398–8408. (e) Kivala, M.; Stanoeva, T.; Michinobu, T.; Frank, B.; Gescheidt, G.; Diederich, F. *Chem. Eur. J.* **2008**, *14*, 7638–7647. (f) Constable, E. C.; Gusmeroli, D.; Housecroft, C. E.; Neuburger, M.; Schaffner, S. *Polyhedron* **2006**, *25*, 421–428. (g) Müller, P. U.; Akpo, C. C.; Stöckelhuber, K. W.; Weber, E. *Adv. Colloid Interface Sci.* **2005**, *114–115*, 291–302. (h) Amoroso, A. J.; Thompson, A. M. W. C.; Maher, J. P.; McCleverty, J. A.; Ward, M. D. *Inorg. Chem.* **1995**, *34*, 4828–4835.

[12] (a) Chase, D. T.; Young, B. S.; Haley, M. M. *J. Org. Chem.* **2011**, *76*, 4043–4051. (b) Ohta, K.; Yamada, S.; Kamada, K.; Slepko, A. D.; Hegmann, F. A.; Tykwinski, R. R.; Shirtcliff, L. D.; Haley, M. M.; Salek, P.; Gel'mukhanov, F.; Ågren, H. *J. Phys. Chem. A* **2011**, *115*, 105–117. (c) Spitler, E. L.; Haley, M. M. *Tetrahedron* **2008**, *64*, 11469–11474. (d) Samori, S.; Tojo, S.; Fujitsuka, M.; Spitler, E. L.; Haley, M. M.; Majima, T. *J. Org. Chem.* **2008**, *73*, 3551–3558. (e) Spitler, E. L.; Monson, J. M.; Haley, M. M. *J. Org. Chem.* **2008**, *73*, 2211–2223. (f) Samori, S.; Tojo, S.; Fujitsuka, M.; Spitler, E. L.; Haley, M. M.; Majima, T. *J. Org. Chem.* **2007**, *72*, 2785–2793. (g) Spitler, E. L.; Shirtcliff, L. D.; Haley, M. M. *J. Org. Chem.* **2007**, *72*, 86–96. (h) Slepko, A. D.; Hegmann, F. A.; Tykwinski, R. R.; Kamada, K.; Ohta, K.; Marsden, J. A.; Spitler, E. L.; Miller, J. J.; Haley, M. M. *Opt. Lett.* **2006**, *31*, 3315–3317. (i) Marsden, J. A.; Miller, J. J.; Shirtcliff, L. D.; Haley, M. M. *J. Am. Chem. Soc.* **2005**, *127*, 2464–2476. (j) Miller, J. J.; Marsden, J. A.; Haley, M. M. *Synlett* **2004**, 165–168.

[13] Zhang, X.-B.; Feng, J.-K.; Ren, A.-M.; Sun, C.-C. *Opt. Mater.* **2007**, *29*, 955–962.

[14] (a) Tong, G. S. M.; Ghosh, P. K.; Che, C.-M. *Angew. Chem. Int. Ed.* **2010**, *49*, 9206–9209. (b) García, F.; Fernández, G.; Sánchez, L. *Chem. Eur. J.* **2009**, *15*, 6740–6747. (c) Rupert, B. L.; Mitchell, W. J.; Ferguson, A. J.; Köse, M. E.; Rance, W. L.; Rumbles, G.; Ginley, D. S.; Shaheen, S. E.; Kopidakis, N. *J. Mater. Chem.* **2009**, *19*, 5311–5324. (d) Shoji, T.; Ito, S.; Toyota, K.; Yasunami, M.; Morita, N. *Chem. Eur. J.* **2008**, *14*, 8398–8408. (e) Caskey, D. C.; Yamamoto, T.; Addicott, C.; Shoemaker, R. K.; Vacek, J.; Hawkrig, A. M.; Muddiman, D. C.; Kottas, G. S.; Michl, J.; Stang, P. J. *J.*

*Am. Chem. Soc.* **2008**, *130*, 7620–7628. (f) Ito, S.; Akimoto, K.; Kawakami, J.; Tajiri, A.; Shoji, T.; Satake, H.; Morita, N. *J. Org. Chem.* **2007**, *72*, 162–172. (g) Manimaran, B.; Thanasekaran, P.; Rajendran, T.; Liao, R.-T.; Liu, Y.-H.; Lee, G.-H.; Peng, S.-M.; Rajagopal, S.; Lu, K.-L. *Inorg. Chem.* **2003**, *42*, 4795–4797.

[15] (a) Villagómez, C. J.; Sasaki, T.; Tour, J. M.; Grill, L. *J. Am. Chem. Soc.* **2010**, *132*, 16848–16854. (b) Godoy, J.; Vives, G.; Tour, J. M. *ACS Nano* **2011**, *5*, 85–90.

[16] (a) Gard, M. N.; Zuccherro, A. J.; Kuzmanich, G.; Oelsner, C.; Guldi, D.; Dreuw, A.; Bunz, U. H. F.; Garcia-Garibay, M. A. *Org. Lett.* **2012**, *14*, 1000–1003. (b) Patze, C.; Broedner, K.; Rominger, F.; Trapp, O.; Bunz, U. H. F. *Chem. Eur. J.* **2011**, *17*, 13720–13725. (c) Davey, E. A.; Zuccherro, A. J.; Trapp, O.; Bunz, U. H. F. *J. Am. Chem. Soc.* **2011**, *133*, 7716–7718. (d) McGrier, P. L.; Solntsev, K. M.; Zuccherro, A. J.; Miranda, O. R.; Rotello, V. M.; Tolbert, L. M.; Bunz, U. H. F. *Chem. Eur. J.* **2011**, *17*, 3112–3119. (e) Tolosa, J.; Solntsev, K. M.; Tolbert, L. M.; Bunz, U. H. F. *J. Org. Chem.* **2010**, *75*, 523–534. (f) Tolosa, J.; Bunz, U. H. F. *Chem. Asian J.* **2009**, *4*, 270–276. (g) Zuccherro, A. J.; Shiels, R. A.; McGrier, P. L.; To, M. A.; Jones, C. W.; Bunz, U. H. F. *Chem. Asian J.* **2009**, *4*, 262–269. (h) Tolosa, J.; Zuccherro, A. J.; Bunz, U. H. F. *J. Am. Chem. Soc.* **2008**, *130*, 6498–6506. (i) McGrier, P. L.; Solntsev, K. M.; Miao, S.; Tolbert, L. M.; Miranda, O. R.; Rotello, V. M.; Bunz, U. H. F. *Chem. Eur. J.* **2008**, *14*, 4503–4510. (j) Hauck, M.; Schönhaber, J.; Zuccherro, A. J.; Hardcastle, K. I.; Müller, T. J. J.; Bunz, U. H. F. *J. Org. Chem.* **2007**, *72*, 6714–6725. (k) Brombosz, S. M.; Zuccherro, A. J.; Phillips, R. L.; Vazquez, D.; Wilson, A.; Bunz, U. H. F. *Org. Lett.* **2007**, *9*, 4519–4522. (l) Gerhardt, W. W.; Zuccherro, A. J.; South, C. R.; Bunz, U. H. F.; Weck, M. *Chem. Eur. J.* **2007**, *13*,

4467–4474. (m) McGrier, P. L.; Solntsev, K. M.; Schönhaber, J.; Brombosz, S. M.; Tolbert, L. M.; Bunz, U. H. F. *Chem. Commun.* **2007**, 2127–2129. (n) Zuccherro, A. J.; Wilson, J. N.; Bunz, U. H. F. *J. Am. Chem. Soc.* **2006**, *128*, 11872–11881. (o) Gerhardt, W. W.; Zuccherro, A. J.; Wilson, J. N.; South, C. R.; Bunz, U. H. F.; Weck, M. *Chem. Commun.* **2006**, 2141–2143. (p) Wilson, J. N.; Smith, M. D.; Enkelmann, V.; Bunz, U. H. F. *Chem. Commun.* **2004**, 1700–1701. (q) Wilson, J. N.; Hardcastle, K. I.; Josowicz, M.; Bunz, U. H. F. *Tetrahedron* **2004**, *60*, 7157–7167. (r) Wilson, J. N.; Bunz, U. H. F. *J. Am. Chem. Soc.* **2005**, *127*, 4124–4125. (s) Wilson, J. N.; Josowicz, M.; Wang, Y.; Bunz, U. H. F. *Chem. Commun.* **2003**, 2962–2963.

[17] (a) Morris, W.; Voloskiy, B.; Demir, S.; Gándara, F.; McGrier, P. L.; Furukawa, H.; Cascio, D.; Stoddart, J. F.; Yaghi, O. M. *Inorg. Chem.* **2012**, *51*, 6443–6445. (b) Mangalum, A.; Gilliard, R. J. Jr.; Hanley, J. M.; Parker, A. M.; Smith, R. C. *Org. Biomol. Chem.* **2010**, *8*, 5620–5627. (c) Grunder, S.; Huber, R.; Wu, S.; Schönenberger, C.; Calame, M.; Mayor, M. *Eur. J. Org. Chem.* **2010**, 833–845. (d) Grunder, S.; Huber, R.; Horhoiu, V.; González, M. T.; Schönenberger, C.; Calame, M.; Mayor, M. *J. Org. Chem.* **2007**, *72*, 8337–8344. (e) Egbe, D. A. M.; Tekin, E.; Birckner, E.; Pivrikas, A.; Sariciftci, N. S.; Schubert, U. S. *Macromolecules* **2007**, *40*, 7786–7794.

[18] (a) Sun, Y.-H.; Zhao, K.; Wang, C.-K.; Luo, Y.; Ren, Y.; Tao, X.-T.; Jiang, M.-H. *J. Mol. Struct. Theochem.* **2004**, *682*, 185–189. (b) Ren, Y.; Xin, Q.; Tao, X.-T.; Wang, L.; Yu, X.-Q.; Yang, J.-X.; Jiang, M.-H. *Chem. Phys. Lett.* **2005**, *414*, 253–258. (c) Rumi, M.; Pond, S. J. K.; Meyer-Friedrichsen, T.; Zhang, Q.; Bishop, M.; Zhang, Y.; Barlow, S.; Marder, S. R.; Perry, J. W. *J. Phys. Chem. C* **2008**, *112*, 8061–8071. (d) Jiu,

P.-W.; Zhao, K.; Han, G.-C. *Chem. Phys. Lett.* **2011**, *514*, 226–233. (e) Wang, L.; Tao, X.-T.; Yang, J.-X.; Xu, G.-B.; Ren, Y.; Liu, Y.; Yan, Y.-X.; Liu, Z.; Jiang, M.-H. *Synthetic Met.* **2006**, *156*, 141–145.

[19] (a) Shirman, T.; Kaminker, R.; Freman, D.; van der Boom, M. E. *ACS Nano* **2011**, *5*, 6553–6563. (b) Lin, J.-L.; Chen, C.-W.; Sun, S.-S.; Lees, A. J. *Chem. Commun.* **2011**, *47*, 6030–6032. (c) Kaminker, R.; Popovitz-Biro, R.; van der Boom, M. E. *Angew. Chem. Int. Ed.* **2011**, *50*, 3224–3226. (d) Kaminker, R.; Motiei, L.; Gulino, A.; Fragalá, I.; Shimon, L. J. W.; Evmenenko, G.; Dutta, P.; Iron, M. A.; van der Boom, M. E. *J. Am. Chem. Soc.* **2010**, *132*, 14554–14561. (e) Kaminker, R.; Lahav, M.; Motiei, L.; Vartanian, M.; Popovitz-Biro, R.; Iron, M. A.; van der Boom, M. E. *Angew. Chem. Int. Ed.* **2010**, *49*, 1218–1221. (f) Caskey, D. C.; Yamamoto, T.; Addicott, C.; Shoemaker, R. K.; Vacek, J.; Hawkrigde, A. M.; Muddiman, D. C.; Kottas, G. S.; Michl, J.; Stang, P. J. *J. Am. Chem. Soc.* **2008**, *130*, 7620–7628. (g) Wang, L.; Tao, X.-t.; Shi, J.-h.; Yu, X.-q.; Jiang, M.-h. *J. Phys. Chem. B* **2006**, *110*, 19711–19716. (h) Wang, L.; Tao, X.-T.; Yang, J.-X.; Yu, W.-T.; Ren, Y.; Xin, Q.; Liu, Z.; Jiang, M.-H. *J. Solid State Chem.* **2004**, *177*, 4293–4299.

[20] (a) Hoang, M. H.; Nguyen, D. N.; Choi, D. H. *Adv. Nat. Sci. Nanosci. Nanotechnol.* **2011**, *2*, 045006. (b) Wilks, R. G.; Chang, G. S.; Kim, K. H.; Choi, D. H.; Moewes, A. *J. Elect. Spect. Related Phenom.* **2011**, *184*, 355–359. (c) El-Khouly, M. E.; Choi, D. H.; Fukuzumi, S. *J. Photochem. Photobiol. A, Chem.* **2011**, *218*, 17–25. (d) Kim, M. H.; Cho, M. J.; Kim, K. H.; Hoang, M. H.; Lee, T. W.; Jin, J.-I.; Kang, N. S.; Yu, J.-W.; Choi, D. H. *Org. Electron.* **2009**, *10*, 1429–1441. (e) Kim, D. C.; Kang, N. S.;

Yu, J. W.; Cho, M. J.; Kim, K. H.; Choi, D. H. *Synthetic Met.* **2009**, *159*, 396–400. (f) Hoang, M. H.; Cho, M. J.; Kim, D. C.; Kim, K. H.; Shin, J. W.; Cho, M. Y.; Joo, J. -S.; Choi, D. H. *Org. Electron.* **2009**, *10*, 607–617. (g) Lee, T. W.; Kim, D. C.; Kang, N. S.; Yu, J. W.; Cho, M. J.; Kim, K. H.; Choi, D. H. *Chem. Lett.* **2008**, *37*, 866–867. (h) Cho, M. Y.; Kim, S. J.; Han, Y. D.; Park, D. H.; Kim, K. H.; Choi, D. H.; Joo, J. *Adv. Funct. Mater.* **2008**, *18*, 2905–2912. (i) Cho, M. Y.; Kang, H. S.; Kim, K.; Kim, S. J.; Joo, J.; Kim, K. H.; Cho, M. J.; Choi, D. H. *Coll. Surf. A, Physicochem. Eng. Aspects* **2008**, *313–314*, 431–434. (j) Kim, K. H.; Chi, Z.; Cho, M. J.; Jin, J.-I.; Cho, M. Y.; Kim, S. J.; Joo, J.; Choi, D. H. *Chem. Mater.* **2007**, *19*, 4925–4932. (k) Kim, K. H.; Chi, Z.; Cho, M. J.; Jin, J. -I.; Cho, M. Y.; Kim, S. J.; Joo, J.; Choi, D. H. *Synthetic Met.* **2007**, *157*, 497–501. (l) Kim, K. H.; Chi, Z.; Cho, M. J.; Choi, D. H.; Kang, H. S.; Cho, M. Y.; Joo, J.-S. *Appl. Phys. Lett.* **2006**, *89*, 202109.

[21] (a) Kim, Y.-G.; Christian-Pandya, H.; Ananthakrishnan, N.; Niazimbetova, Z. I.; Thompson, B. C.; Galvin, M. E.; Reynolds, J. R. *Sol. Energy Mater. Sol. Cells* **2008**, *92*, 307–312. (b) Christian-Pandya, H. K.; Niazimbetova, Z. I.; Beyer, F. L.; Galvin, M. E. *Chem. Mater.* **2007**, *19*, 993–1001. (c) Fratiloiu, S.; Senthilkumar, K.; Grozema, F. C.; Christian-Pandya, H.; Niazimbetova, Z. I.; Bhandari, Y. J.; Galvin, M. E.; Siebbeles, L. D. A. *Chem. Mater.* **2006**, *18*, 2118–2129. (d) Niazimbetova, Z. I.; Christian, H. Y.; Bhandari, Y. J.; Beyer, F. L.; Galvin, M. E. *J. Phys. Chem. B* **2004**, *108*, 8673–8681. (e) Niazimbetova, Z. I.; Menon, A.; Galvin, M. E.; Evans, D. H. *J. Electroanal. Chem.* **2002**, *529*, 43–50.

- [22] (a) Du, C.-J. F.; Hart, H. *J. Org. Chem.* **1987**, *52*, 4311–4314. (b) Tao, W.; Nesbitt, S.; Heck, R. F. *J. Org. Chem.* **1990**, *55*, 63–69. (c) Meier, H.; Fetten, M. *Tetrahedron Lett.* **2000**, *41*, 1535–1538.
- [23] (a) Kim, J. E.; Song, S.-Y.; Shim, H.-K. *Synthetic Met.* **2001**, *121*, 1665–1666. (b) Gerold, J.; Holzenkamp, U.; Meier, H. *Eur. J. Org. Chem.* **2001**, 2757–2763. (c) Holmes, B. T.; Padgett, C. W.; Pennington, W. T. *Acta Cryst.* **2003**, *C59*, o114–o116. (d) Kang, H.; Zhu, P.; Yang, Y.; Facchetti, A.; Marks, T. J. *J. Am. Chem. Soc.* **2004**, *126*, 15974–15975. (e) Kang, H.; Evmenenko, G.; Dutta, P.; Clays, K.; Song, K.; Marks, T. J. *J. Am. Chem. Soc.* **2006**, *128*, 6194–6205. (f) Chang, D. W.; Dai, L. *J. Mater. Chem.* **2007**, *17*, 364–371. (g) Chang, D. W.; Choi, H.-J.; Jung, S.-M.; Dai, L.; Baek, J.-B. *J. Mater. Chem.* **2012**, *22*, 13365–13373. (h) Winter, A.; Friebe, C.; Hager, M. D.; Schubert, U. S. *Eur. J. Org. Chem.* **2009**, 801–809. (i) Siebert, R.; Akimov, D.; Schmitt, M.; Winter, A.; Schubert, U. S.; Dietzek, B.; Popp, J. *ChemPhysChem* **2009**, *10*, 910–919. (j) Gohy, J.-F.; Chipier, M.; Guillet, P.; Fustin, C.-A.; Hoeppener, S.; Winter, A.; Hoogenboom, R.; Schubert, U. S. *Soft Matter* **2009**, *5*, 2954–2961. (k) Lengkeek, N. A.; Boulos, R. A.; McKinley, A. J.; Riley, T. V.; Martinac, B.; Stewart, S. G. *Aust. J. Chem.* **2011**, *64*, 316–323.
- [24] Hori, Y.; Noda, K.; Kobayashi, S.; Taniguchi, H. *Tetrahedron Lett.* **1969**, *40*, 3563–3566.
- [25] Hauptmann, V. H. *Angew. Chem.* **1975**, *87*, 490–491.
- [26] Rubin, V. Y.; Knobler, C. B.; Diederich, F. *Angew. Chem.* **1991**, *103*, 708–710.

- [27] Posner, G. H.; Loomis, G. L.; Sawaya, H. S. *Tetrahedron Lett.* **1975**, *16*, 1373–1376.
- [28] (a) Diederich, F.; Philp, D.; Seiler, P. *J. Chem. Soc., Chem. Commun.* **1994**, 205–208. (b) Anthony, J.; Boldi, A. M.; Rubin, Y.; Hobi, M.; Gramlich, V.; Knobler, C. B.; Seiler, P.; Diederich, F. *Helv. Chim. Acta* **1995**, *78*, 13–45. (c) Boudon, C.; Gisselbrecht, J. P.; Gross, M.; Anthony, J.; Boldi, A. M.; Faust, R.; Lange, T.; Philp, D.; Van Loon, J.-D.; Diederich, F. *J. Electroanal. Chem.* **1995**, *394*, 187–197. (d) Philp, D.; Gramlich, V.; Seiler, P.; Diederich, F. *J. Chem. Soc. Perkin Trans. 2* **1995**, 875–886. (e) Bosshard, C.; Spreiter, R.; Günter, P.; Tykwinski, R. R.; Schreiber, M.; Diederich, F. *Adv. Mater.* **1996**, *8*, 231–234. (f) Tykwinski, R. R.; Schreiber, M.; Carlón, R. P.; Diederich, F.; Gramlich, V. *Helv. Chim. Acta* **1996**, *79*, 2249–2281. (g) Hilger, A.; Gisselbrecht, J.-P.; Tykwinski, R. R.; Boudon, C.; Schreiber, M.; Martin, R. E.; Lüthi, H. P.; Gross, M.; Diederich, F. *J. Am. Chem. Soc.* **1997**, *119*, 2069–2078. (h) Gobbi, L.; Seiler, P.; Diederich, F. *Angew. Chem. Int. Ed.* **1999**, *38*, 674–678. (i) Mitzel, F.; Boudon, C.; Gisselbrecht, J.-P.; Seiler, P.; Gross, M.; Diederich, F. *Helv. Chim. Acta* **2004**, *87*, 1130–1157.
- [29] Theologitis, M.; Screttas, G. C.; Raptis, S. G.; Papadopoulos, M. G. *Intern. J. Quantum Chem.* **1999**, *72*, 177–187.
- [30] Bourne, S. A.; Nash, K. L. G.; Toda, F. *J. Mol. Struct.* **1999**, *474*, 223–233.
- [31] Koentjoro, O. F.; Zuber, P.; Puschmann, H.; Goeta, A. E.; Howard, J. A. K.; Low, P. J. *J. Organometal. Chem.* **2003**, *670*, 178–187.



- [32] Lim, J.; Albright, T. A.; Martin, B. R.; Miljanić, O. Š. *J. Org. Chem.* **2011**, *76*, 10207–10219.
- [33] (a) *Functional Organic Materials: Syntheses, Strategies and Applications*; Müller, T. J. J., Bunz, U. H. F., Eds.; Wiley-VCH: Weinheim, 2007. (b) *Electronic Materials, the Oligomer Approach*; Müllen, K., Wegner, G., Eds.; Wiley-VCH: Weinheim, 1998. (c) Fukui, K. *Science* **1982**, *218*, 747–754.
- [34] For examples of non-cruciform structures with spatially separated FMOs, see: (a) Fahrni, C. J.; Yang, L.; VanDerveer, D. G. *J. Am. Chem. Soc.* **2003**, *125*, 3799–3812. (b) Huang, H.-H.; Prabhakar, Ch.; Tang, K.-C.; Chou, P.-T.; Huang, G.-J.; Yang, J.-S. *J. Am. Chem. Soc.* **2011**, *133*, 8028–8039.
- [35] (a) Koenen, J.-M.; Bilge, A.; Allard, S.; Alle, R.; Meerholz, K.; Scherf, U. *Org. Lett.* **2009**, *11*, 2149–2152. (b) Pina, J.; Seixas de Melo, J.; Burrows, H. D.; Galbrecht, F.; Bilge, A.; Kudla, C. J.; Scherf, U. *J. Phys. Chem. B* **2008**, *112*, 1104–1111. (c) Zen, A.; Bilge, A.; Galbrecht, F.; Alle, R.; Meerholz, K.; Grenzer, J.; Neher, D.; Scherf, U.; Farrell, T. *J. Am. Chem. Soc.* **2006**, *128*, 3914–3915. (d) Bilge, A.; Zen, A.; Forster, M.; Li, H.; Galbrecht, F.; Nehls, B. S.; Farrell, T.; Neher, D.; Scherf, U. *J. Mater. Chem.* **2006**, *16*, 3177–3182.
- [36] Hu, J.-y.; Era, M.; Elsegood, M. R. J.; Yamato, T. *Eur. J. Org. Chem.* **2010**, 72–79.
- [37] Cho, M. J.; Park, S. S.; Yang, Y. S.; Kim, J. H.; Choi, D. H. *Synthetic Met.* **2010**, *160*, 1754–1760.

[38] (a) Grunder, S.; Huber, R.; Wu, S.; Schönenberger, C.; Calame, M.; Mayor, M. *Chimia* **2010**, *64*, 140–144. (d) Błaszczuk, A.; Fischer, M.; von Hänisch, C.; Mayor, M. *Eur. J. Org. Chem.* **2007**, 2630–2642.

[39] (a) Jennum, K.; Vestergaard, M.; Pedersen, A. H.; Fock, J.; Jensen, J.; Santella, M.; Led, J. J.; Kilså, K.; Bjørnholm, T.; Nielsen, M. B. *Synthesis* **2011**, 539–548. (b) Vestergaard, M.; Jennum, K.; Sørensen, J. K.; Kilså, K.; Nielsen, M. B. *J. Org. Chem.* **2008**, *73*, 3175–3183. (c) Sorensen J. K.; Vestergaard, M.; Kadziola, A.; Kilså, K.; Nielsen, M. B. *Org. Lett.* **2006**, *8*, 1173–1176.

[40] In this and subsequent chapters, "benzobisoxazole" will be used in this to denote "benzo[1,2-*d*:4,5-*d'*]bisoxazole"—the systematic name for the central heterocyclic core of the prepared cruciforms **1–9**, their precursors **14–16**, and compound **20–24**.

[41] For structurally related fluorescent benzobisimidazoles (which are not cruciform-shaped), see: (a) Boydston, A. J.; Pecinovsky, C. S.; Chao, S. T.; Bielawski, C. W. *J. Am. Chem. Soc.* **2007**, *129*, 14550–14551. (b) Boydston, A. J.; Vu, P. D.; Dykhno, O. L.; Chang, V.; Wyatt, A. R. II; Stockett, A. S.; Ritschdorff, E. T.; Shear, J. B.; Bielawski, C. W. *J. Am. Chem. Soc.* **2008**, *130*, 3143–3156. (c) Boydston, A. J.; Khramov, D. M.; Bielawski, C. W. *Tetrahedron Lett.* **2006**, *47*, 5123–5125. (d) Khramov, D. M.; Boydston, A. J.; Bielawski, C. W. *Org. Lett.* **2006**, *8*, 1831–1834. (e) Tasior, M.; Hugues, V.; Blanchard-Desce, M.; Gryko, D. T. *Chem. Asian J.* **2012**, *7*, 2656–2661. (f) Lirag, R. C.; Le, H. T. M.; Miljanić, O. Š. *Chem. Commun.* **2013**, ASAP.

[42] (a) Klare, J. E.; Tulevski, G. S.; Nuckolls, C. *Langmuir* **2004**, *20*, 10068–10072. (b) Klare, J. E.; Tulevski, G. S.; Sugo, K.; de Picciotto, A.; White, K. A.; Nuckolls, C. *J.*

*Am. Chem. Soc.* **2003**, *125*, 6030–6031. The latter reference also pioneered the use of the phrase "molecular cruciforms".

[43] (a) Feldman, A. K.; Steigerwald, M. L.; Guo, X.; Nuckolls, C. *Acc. Chem. Res.* **2008**, *41*, 1731–1741. (b) Tang, J.; Wang, Y.; Klare, J. E.; Tulevski, G. S.; Wind, S. J.; Nuckolls, C. *Angew. Chem. Int. Ed.* **2007**, *46*, 3892–3895. (c) Florio, G. M.; Klare, J. E.; Pasamba, M. O.; Werblowsky, T. L.; Hyers, M.; Berne, B. J.; Hybertsen, M. S.; Nuckolls, C.; Flynn, G. W. *Langmuir* **2006**, *22*, 10003–10008. (d) Guo, X.; Small, J. P.; Klare, J. E.; Wang, Y.; Purewal, M. S.; Tam, I. W.; Hong, B. H.; Caldwell, R.; Huang, L.; O'Brien, S.; Yan, J.; Breslow, R.; Wind, S. J.; Hone, J.; Kim, P.; Nuckolls, C. *Science* **2006**, *311*, 356–359. (e) de Picciotto, A.; Klare, J. E.; Nuckolls, C.; Baldwin, K.; Erbe, A.; Willett, R. *Nanotechnology* **2005**, *16*, 3110–3114.

[44] (a) Hegedus, L. S.; Odle, R. R.; Winton, P. M.; Weider, P. R. *J. Org. Chem.* **1982**, *47*, 2607–2613. See also: (b) Weider, P. R.; Hegedus, L. S.; Asada, H.; D'Andreq, S. V. *J. Org. Chem.* **1985**, *50*, 4276–4281. (c) Osman, A.-M.; Bassiouni, I. *J. Org. Chem.* **1962**, *27*, 558–561.

[45] (a) Wolfe, J. F.; Arnold, F. E. *Macromolecules* **1981**, *14*, 909–915. (b) Perry, R. J.; Wilson, B. D.; Miller, R. J. *J. Org. Chem.* **1992**, *57*, 2883–2887. (c) Seha, Z.; Weis, C. *D. Helv. Chim. Acta* **1980**, *63*, 413–419.

[46] (a) Kappe, C. O. *Angew. Chem. Int. Ed.* **2004**, *43*, 6250–6284. (b) Lidström, P.; Tierney, J.; Wathey, B.; Westman, J. *Tetrahedron* **2001**, *57*, 9225–9283.

[47] (a) Sonogashira, K. in *Handbook of Organopalladium Chemistry for Organic Synthesis*, Vol. 1, Negishi, E.-i., Ed.; Wiley: New York, 2002, p. 493 (and cited references). (b) Sonogashira, K.; Tohda, Y. Hagihara, N. *Tetrahedron Lett.* **1975**, *16*, 4467–4470.

[48] Gaussian 09, Revision B.01: Frisch, M. J.; Trucks, G. W.; Schlegel, H. B.; Scuseria, G. E.; Robb, M. A.; Cheeseman, J. R.; Scalmani, G.; Barone, V.; Mennucci, B.; Petersson, G. A.; Nakatsuji, H.; Caricato, M.; Li, X.; Hratchian, H. P.; Izmaylov, A. F.; Bloino, J.; Zheng, G.; Sonnenberg, J. L.; Hada, M.; Ehara, M.; Toyota, K.; Fukuda, R.; Hasegawa, J.; Ishida, M.; Nakajima, T.; Honda, Y.; Kitao, O.; Nakai, H.; Vreven, T.; Montgomery, J. A., Jr.; Peralta, J. E.; Ogliaro, F.; Bearpark, M.; Heyd, J. J.; Brothers, E.; Kudin, K. N.; Staroverov, V. N.; Keith, T.; Kobayashi, R.; Normand, J.; Raghavachari, K.; Rendell, A.; Burant, J. C.; Iyengar, S. S.; Tomasi, J.; Cossi, M.; Rega, N.; Millam, J. M.; Klene, M.; Knox, J. E.; Cross, J. B.; Bakken, V.; Adamo, C.; Jaramillo, J.; Gomperts, R.; Stratmann, R. E.; Yazyev, O.; Austin, A. J.; Cammi, R.; Pomelli, C.; Ochterski, J. W.; Martin, R. L.; Morokuma, K.; Zakrzewski, V. G.; Voth, G. A.; Salvador, P.; Dannenberg, J. J.; Dapprich, S.; Daniels, A. D.; Farkas, O.; Foresman, J. B.; Ortiz, J. V.; Cioslowski, J.; Fox, D. J. Gaussian, Inc., Wallingford, CT, 2010.

[49] (a) Becke, A. D. *J. Chem. Phys.* **1993**, *98*, 5648–5652. (b) Lee, C.; Yang, W.; Parr, G. R. *Phys. Rev. B* **1988**, *37*, 785–789.

[50] This definition is analogous to the definition of e.g. percent enantiomeric excess: Eliel, E. L.; Wilen, S. H.; Mander, L. N., Eds.; *Stereochemistry of Organic Compounds*; Wiley: New York, 1994; p 214. We have also recalculated orbitals of **8** using a 6-31G<sup>+</sup>

basis set. The densities of the HOMO and LUMO were compared to those computed at the 3-21G level. The standard deviation for the differences of the densities for these two basis sets was computed to be only 0.031 electrons with a variance of 0.001. Thus, the 3-21G values were used in this study.

[51] For a collection of  $pK_a$  values, see: [www.zirchrom.com/organic.html](http://www.zirchrom.com/organic.html), and [www.scripps.edu/chem/baran/heterocycles/Essentials1-2009.pdf](http://www.scripps.edu/chem/baran/heterocycles/Essentials1-2009.pdf). Protonation of oxazole ( $pK_a = 0.8$ ) can be ignored, except under highly acidic solutions.

[52] Simple FMO arguments are very useful in predicting the optical response to protonation of pyridyl and 4-(dimethylamino) groups along cruciforms' "arms". However, these arguments are not easily applied to the protonation of the oxazole ring, as both HOMO and LUMO invariably have high orbital densities within that ring. At present, we have no explanation as to why this presumed protonation affects emission but not absorption.

[53] Tentatively,  $^1\text{H}$  NMR spectroscopy supports this assignment of protonation order, although solubility issues precluded us from following protonation-induced NMR changes over the full range of  $-\log[\text{TFA}]$  values used in absorption and fluorescence studies.

[54] (a) Pawlicki, M.; Collins, H. A.; Denning, R. G.; Anderson, H. L. *Angew. Chem. Int. Ed.* **2009**, 48, 3244–3266. (b) Lee, W.-H.; Lee, H.; Kim J.-A.; Choi, J.-H.; Cho, M.; Jeon, S.-J.; Cho, B. R. *J. Am. Chem. Soc.* **2001**, 123, 10658–10667. (c) Zyss, J.; Ledoux, I. *Chem. Rev.* **1994**, 94, 77–105.

- [55] Heck, R. F. *Palladium Reagents in Organic Synthesis*; Academic Press: London/Orlando, 1985; p 18.
- [56] Leonard, K. A.; Nelen, M. I.; Anderson, L. T.; Gibson, S. L.; Hilf, R.; Detty, M. R. *J. Med. Chem.* **1999**, *42*, 3942–3952.
- [57] Ziesel, R.; Suffert, J.; Youinou, M.-T. *J. Org. Chem.* **1996**, *6*, 6535–6546.
- [58] (a) Lim, J.; Nam, D.; Miljanić, O. Š. *Chem. Sci.* **2012**, *3*, 559–563. (b) Lim, J.; Miljanić, O. Š. *Chem. Commun.* **2012**, *48*, 10301–10303.
- [59] (a) Chen, L. D.; Mandal, D.; Pozzi, G.; Gladysz, J. A.; Bühlmann, P. *J. Am. Chem. Soc.* **2011**, *133*, 20869–20877. (b) Bunz, U. H. F.; Rotello, V. M. *Angew. Chem., Int. Ed.* **2010**, *49*, 3268–3279. (c) McRae, R.; Bagchi, P.; Sumalekshmy, S.; Fahrni, C. J. *Chem. Rev.* **2009**, *109*, 4780–4827. (d) Shaughnessy, K. H.; Kim, P.; Hartwig, J. F. *J. Am. Chem. Soc.* **1999**, *121*, 2123–2132. (e) Thomas, S. W.; Joly, G. D.; Swager, T. M. *Chem. Rev.* **2007**, *107*, 1339–1386. (f) Wiskur, S. L.; Ait-Haddou, H.; Lavigne, J. J.; Anslyn, E. V. *Acc. Chem. Res.* **2001**, *34*, 963–972. (g) Yang, J.-S.; Swager, T. M. *J. Am. Chem. Soc.* **1998**, *120*, 5321–5322.
- [60] (a) Rakow, N. A.; Suslick, K. S. *Nature* **2000**, *406*, 710–713. (b) Lin, H. W.; Suslick, K. S. *J. Am. Chem. Soc.* **2010**, *132*, 15519–15521.
- [61] Compiled by Dr. Jón Njarðarson's research group at the University of Arizona. Available at: <http://cbc.arizona.edu/njardarson/group/top-pharmaceuticals-poster>.

- [62] (a) Buglass, A. J. *Handbook of Alcoholic Beverages: Technical, Analytical and Nutritional Aspects*, Wiley, Hoboken, NJ, 2011. (b) Wiskur, S. L.; Anslyn, E. V. *J. Am. Chem. Soc.* **2001**, *123*, 10109–10110.
- [63] (a) Yang, W.; Gao, X.; Wang, B. *Med. Res. Rev.* **2003**, *23*, 346–348. See also: (b) [www.bortezomib.org](http://www.bortezomib.org).
- [64] For reviews, see: (a) James, T. D.; Phillips, M. D.; Shinkai, S. *Boronic Acids in Saccharide Recognition*, RSC Publishing, Cambridge, 2006. (b) James, T. D. in *Boronic Acids: Preparation, Applications in Organic Synthesis and Medicine* (Ed.: D. G. Hall), Wiley-VCH, Weinheim, 2005, pp. 441–480. (c) James, T. D. *Top. Curr. Chem.* **2007**, *277*, 107–152. (d) Fang, H.; Kaur, G.; Wang, B. *J. Fluoresc.* **2004**, *14*, 481–489; (e) Striegler, S. *Curr. Org. Chem.* **2003**, *7*, 81–102. (f) James, T. D.; Shinkai, S. *Top. Curr. Chem.* **2002**, *218*, 159–200.
- [65] For examples and reviews, see: (a) Nishiyabu, R.; Kubo, Y.; James, T. D.; Fossey, J. S. *Chem. Commun.* **2012**, *47*, 1106–1123. (b) Wade, C. R.; Broomsgrove, A. E. J.; Aldridge, S.; Gabbaï, F. P. *Chem. Rev.* **2010**, *110*, 3958–3984. (c) Kubo, Y.; Kobayashi, A.; Ishida, T.; Misawa, Y.; James, T. D. *Chem. Commun.* **2005**, 2846–2848. (d) Badugu, R.; Lakowicz, J. R.; Geddes, C. D. *Curr. Anal. Chem.* **2005**, *1*, 157–170. (e) DiCesare, N.; Lakowicz, J. R. *Anal. Biochem.* **2002**, *301*, 111–116.
- [66] For examples, see: (a) Guo, Z.; Shin, I.; Yoon, J. *Chem. Commun.* **2012**, *48*, 5956–5967, and the references therein. (b) Gallagher, L. T.; Heo, J. S.; Lopez, M. A.; Ray, B. M.; Xiao, J.; Umali, A. P.; Zhang, A.; Dharmarajan, S.; Heymann, H.; Anslyn, E.

V. *Supramol. Chem.* **2012**, *24*, 143–148. (c) Hargrove, A. E.; Reyes, R. N.; Riddington, I.; Anslyn, E. V.; Sessler, J. L. *Org. Lett.* **2010**, *12*, 4804–4807.

[67] Fiegel, H.; Voges, H.-W.; Hamamoto, T.; Umemura, S.; Iwata, T.; Miki, H.; Fujita, Y.; Buysch, H.-J.; Garbe, D.; Paulus, W. Phenol Derivatives, in Ullmann's Encyclopedia of Industrial Chemistry, Wiley-VCH, Weinheim, 2002.

[68] *Quaternary Ammonium Salts: Their Use in Phase-Transfer Catalysis*; Jones, R. A., Eds.; Academic Press, New York, 2001.

[69] Ying, G. G. *Environ. Int.* **2006**, *32*, 417–431.

[70] (a) Zhu, L.; Zhong, Z. L.; Anslyn, E. V. *J. Am. Chem. Soc.* **2005**, *127*, 4260–4269.

(b) Cabell, L. A.; Monahan, M.-K.; Anslyn, E. V. *Tetrahedron Lett.* **1999**, *40*, 7753–7756.

(c) Arimori, S.; Murakami, H.; Takeuchi, M.; Shinkai, S. *J. Chem. Soc., Chem. Commun.* **1995**, 961–962.

[71] Bazzi, M. D. *Biochem. Bioph. Res. Co.* **2002**, *293*, 440–445.

[72] Colour Contrast Analyzer can be freely downloaded from:  
<http://www.visionaustralia.org.au/info.aspx?page=628>.

[73] J. R. Taylor, *An Introduction to Error Analysis: The Study of Uncertainties in Physical Measurements*, University Science Books, Sausalito, CA, 1997. Maximum possible value of  $\sigma$  is 255, corresponding to an unlikely situation in which the first analyte shows pure white emission in all five solvents, and the second analyte shows no emission at all in any solvent.



- [74] See <http://www.zirchrom.com/organic.htm> for a selection of  $pK_a$  values.
- [75] (a) Collins, B. E.; Sorey, S.; Hargrove, A. E.; Shabbir, S. H.; Lynch, V. M.; Anslyn, E. V. *J. Org. Chem.* **2009**, *74*, 4055–4060. (b) Zhu, L.; Shabbir, S. H.; Gray, M.; Lynch, V. M.; Sorey, S.; Anslyn, E. V. *J. Am. Chem. Soc.* **2006**, *128*, 1222–1232. (c) Wiskur, S. L.; Lavigne, J. J.; Ait-Haddou, H.; Lynch, V.; Chiu, Y. H.; Canary, J. W.; Anslyn, E. V. *Org. Lett.* **2001**, *3*, 1311–1314.
- [76] Emission colors of blank solutions of **6** + **B1/B5** (Figure 2.8) differ from those shown for **B1** and **B5** in Figure 2.4. The photos in Figure 2.8 have been taken with ~5 times lower amounts of boronic acids, and have been taken ~7 h after **6** and boronic acids were mixed—unlike the photos in Figure 2.4 which were taken immediately after mixing **6** with **B1/B5**.
- [77] Pyridine is a weaker base ( $pK_a=5.25$  for the conjugated acid) than triethylamine, piperidine, and piperazine, whose conjugated acids have  $pK_a$  values of 10.75, 11.12 and 9.83, successively. See: <http://www.zirchrom.com/organic.htm>.
- [78] Koumoto, K.; Takeuchi, M.; Shinkai, S. *Supramol. Chem.* **1998**, *9*, 203–210.
- [79] (a) Sessler, J. L.; Gale, P.; Cho, W.-S. *Anion Receptor Chemistry*, RSC Publishing, Cambridge, 2006. (b) Gale, P. A. *Chem. Commun.* **2011**, *47*, 82–86. (c) Bayly, S. R.; Beer, P. D. *Top. Curr. Chem.* **2008**, *129*, 45–94. (d) Martinez-Máñez, R.; Sancenón, F. *Chem. Rev.* **2003**, *103*, 4419–4476.
- [80] (a) Abrahán, Y.; Salman, H.; Suwinska, K.; Eichen, Y. *Chem. Commun.* **2011**, *47*, 6087–6089. (b) Carroll, C. N.; Coombs, B. A.; McClintock, S. P.; Johnson II, C. A.;

Berryman, O. B.; Johnson, D. W.; Haley, M. M. *Chem. Commun.* **2011**, 47, 5539–5541.

(c) Kim, D.-S.; Ahn, K. H. *J. Org. Chem.* **2008**, 73, 6831–6834. (d) de Silva, A. P.; Gunaratne, H. Q. N.; McCoy, C. P. *Chem. Commun.* **1996**, 2399–2400.

[81] Wang, T.; Wang, H.-F.; Yan, X.-P. *CrystEngComm* **2010**, 12, 3177–3182.

[82] Lim, J.; Osowska, K.; Armitage, J. A.; Martin, B. R.; Miljanić, O. Š. *CrystEngComm* **2012**, 14, 6152–6162.

[83] (a) Kim, I. T.; Lee, S. W.; Kim, S. Y.; Lee, J. S.; Park, G. B.; Lee, S. H.; Kang, S. K.; Kang, J.-G.; Park, C.; Jin, S.-H. *Synth. Met.* **2006**, 156, 38–41. (b) Kang, J.-G.; Cho, H.-G.; Kang, S. K.; Park, C.; Lee, S. W.; Park, G. B.; Lee, J. S.; Kim, I. T. *J. Photochem. Photobiol. A: Chem.* **2006**, 183, 212–217. (c) Gu, R.; Snick, S. V.; Robeyns, K.; Meervelt, L. V.; Dehaen, W. *Org. Biomol. Chem.* **2009**, 7, 380–385. (d) Gu, R.; Robeyns, K.; Meervelt, L. V.; Toppet, S.; Dehaen, W. *Org. Biomol. Chem.* **2008**, 6, 2484–2487.

[84] For reviews of MOF chemistry, see: (a) MacGillivray, L. R., Ed.; *Metal-Organic Frameworks: Design and Application*; Wiley: New York, 2010. (b) Farrusseng, D. Ed.; *Metal-Organic Frameworks: Applications from Catalysis to Gas Storage*; Wiley-VCH: Weinheim, 2011. (c) MOF-themed issue of *Chem. Soc. Rev.* **2009**, 38, 1201–1504.

[85] For selected examples, see: (a) Spitler, E. L.; Giovino, M. R.; White, S. L.; Dichtel, W. R. *Chem. Sci.* **2011**, 2, 1588–1593. (b) Spitler, E. L.; Dichtel, W. R. *Nature Chem.* **2010**, 2, 672–677. (c) El-Kaderi, H. M.; Hunt, J. R.; Mendoza-Cortés, J. L.; Côté, A. P.; Taylor, R. E.; O’Keeffe, M.; Yaghi, O. M. *Science* **2007**, 316, 268–272. (d) Côté, A. P.; Benin, A. I.; Ockwig, N. W.; Matzger, A. J.; O’Keeffe, M.; Yaghi, O. M. *Science*

**2005**, 310, 1166–1170. (e) Tilford, R. W.; Gemmill, W. R.; zur Loye, H.-C.; Lavigne, J. *J. Chem. Mater.* **2006**, 18, 5296–5301.

[86] (a) Jones, J. T. A.; Hasell, T.; Wu, X.; Bacsá, J.; Jelfs, K. E.; Schmidtman, M.; Chong, S. Y.; Adams, D. J.; Trewin, A.; Schiffman, F.; Cora, F.; Slater, B.; Steiner, A.; Day, G. M.; Cooper, A. I. *Nature* **2011**, 474, 367–371, and the references therein; (b) Tozawa, T.; Jones, J. T. A.; Swamy, S. I.; Jiang, S.; Adams, D. J.; Shakespeare, S.; Clowes, R.; Bradshaw, D.; Hasell, T.; Chong, S. Y.; Tang, C.; Thompson, S.; Parker, J.; Trewin, A.; Bacsá, J.; Slawin, A. M. Z.; Steiner, A.; Cooper, A. I. *Nature Mater.* **2009**, 8, 973–978. (c) Tranchemontagne, D. J.; Ni, Z.; O’Keeffe, M.; Yaghi, O. M. *Angew. Chem. Int. Ed.* **2008**, 47, 5136–5147. (d) Lu, Z.; Knobler, C. B.; Furukawa, H.; Wang, B.; Liu, G.; Yaghi, O. M. *J. Am. Chem. Soc.* **2009**, 131, 12532–12533. (e) Perry IV, J. J.; Perman, J. A.; Zaworotko, M. J. *Chem. Soc. Rev.* **2009**, 38, 1400–1417.

[87] Osowska, K.; Miljanić, O. Š. *Chem. Commun.* **2010**, 46, 4276–4278

[88] Austin, W. B.; Bilow, N.; Kelleghan, W. J.; Lau, K. S. Y. *J. Org. Chem.* **1981**, 46, 2280–2286.

[89] Spek, A. L. *PLATON/SQUEEZE—A multipurpose crystallographic tool*; Utrecht University, 2000.

[90] (a) Nishio, M.; Hirota, M.; Umezawa Y. *The CH/π Interaction: Evidence, Nature, and Consequences*; Wiley-VCH: New York, 1998. (b) Umezawa, Y.; Tsuboyama, S.; Honda, K.; Uzawa, J.; Nishio, M. *Bull. Chem. Soc. Jpn.* **1998**, 71, 1207–1213. (c) Nishio, M.; Umezawa, Y.; Hirota, M.; Takeuchi, Y. *Tetrahedron* **1995**, 51, 8665–5701.

- [91] All C–H bond lengths have been normalized to neutron-diffraction determined internuclear distance of 1.08 Å. See: (a) Steiner, T. *Angew. Chem. Int. Ed.* **2002**, *41*, 48–76. (b) Allen, F. H.; Kennard, O.; Watson, D. G.; Brammer, L.; Orpen, A. G.; Taylor, R. *J. Chem. Soc. Perkin Trans. 2* **1987**, S1–S19.
- [92] Desiraju, G. R.; Steiner, T., Eds.; *The Weak Hydrogen Bond In Structural Chemistry and Biology*; Oxford University Press: Oxford, 1999.
- [93] Alkyne units have been known to deform readily in strained systems. See, *inter alia*: (a) Eisler, S.; McDonald, R.; Loppnow, G. R.; Tykwinski, R. R. *J. Am. Chem. Soc.* **2000**, *122*, 6917–6928. (b) Gleiter, R.; Merger, R. In *Modern Acetylene Chemistry*; Stang, P. J.; Diederich, F., Eds.; VCH: Weinheim, Germany, 1995; p 285. (c) De Graaff, R. A. G.; Gorter, S.; Romers, C.; Wong, H. N. C.; Sondheimer, F. *J. Chem. Soc., Perkin Trans. 2* **1981**, 478–480. (d) Dosa, P. I.; Whitener, G. D.; Vollhardt, K. P. C.; Bond, A. D.; Teat, S. J. *Org. Lett.* **2002**, *4*, 2075–2078.
- [94] (a) Seminario, J. M.; Zacarias, A. G.; Tour, J. M. *J. Am. Chem. Soc.* **1998**, *120*, 3970–3974. (b) Stølevic, R.; Bakken, P. *J. Mol. Struct.* **1990**, *239*, 205–207. (c) Grumadas, A.; Poskus, D. *Zh. Fiz. Khim.* **1987**, *61*, 2838–2841. (d) Okuyama, K.; Hasegawa, T.; Ito, M.; Mikami, N. *J. Phys. Chem.* **1984**, *88*, 1711–1716. See also: (e) Miljanić, O. Š.; Han, S.; Holmes, D.; Schaller, G. R.; Vollhardt, K. P. C. *Chem. Commun.* **2005**, 2606–2608.
- [95] Lim, J.; Miljanić, O. Š. *CrystEngComm* **2011**, *13*, 5309–5312.

- [96] (a) Sessler, J. L.; Lawrence, C. M.; Jayawickramarajah, J. *Chem. Soc. Rev.* **2007**, *36*, 314–325. (b) Sivakova, S.; Rowan, S. J. *Chem. Soc. Rev.* **2005**, *34*, 9–21. (c) Sessler, J. L.; Jayawickramarajah, J. *Chem. Commun.* **2005**, 1939–1949.
- [97] (a) Davis, J. T.; Spada, G. P. *Chem. Soc. Rev.* **2007**, *36*, 296–313. (b) Davis, J. T. *Angew. Chem. Int. Ed.* **2004**, *43*, 668–698.
- [98] First reported in: Gellert, M.; Lipsett, M. N.; Davies, D. R. *Proc. Natl. Acad. Sci. U.S.A.* **1962**, *48*, 2013–2018.
- [99] (a) Ma, L.; Harrell, W. A. Jr.; Davis, J. T. *Org. Lett.* **2009**, *11*, 1599–1602. (b) Ma, L.; Melegari, M.; Colombini, M.; Davis, J. T. *J. Am. Chem. Soc.* **2008**, *130*, 2938–2939. (c) Kaucher, M. S.; Harrell, W. A. Jr.; Davis, J. T. *J. Am. Chem. Soc.* **2006**, *128*, 38–39. (d) Shi, X.; Mullaugh, K. M.; Fettinger, J. C.; Jiang, Y.; Hofstadler, S. A.; Davis, J. T. *J. Am. Chem. Soc.* **2003**, *125*, 10830–10841. (e) Martín-Hidalgo, M.; Camacho-Soto, K.; Gubala, V.; Rivera, J. M. *Supramol. Chem.* **2010**, *22*, 862–869. (f) Gubala, V.; De Jesús, D.; Rivera, J. M. *Tetrahedron Lett.* **2006**, *47*, 1413–1416.
- [100] (a) Das, R. N.; Kumar, Y. P.; Pagoti, S.; Patil, A. J.; Dash, J. *Chem. Eur. J.* **2012**, *18*, 6008–6014. (b) Buerkle, L. E.; von Recum, H. A.; Rowan, S. J. *Chem. Sci.* **2012**, *3*, 564–572. (c) Li, Z.; Buerkle, L. E.; Orseno, M. R.; Streletzky, K. A.; Seifert, S.; Jamieson, A. M.; Rowan, S. J. *Langmuir* **2010**, *26*, 10093–10101. (b) Buerkle, L. E.; Li, Z.; Jamieson, A. M.; Rowan, S. J. *Langmuir* **2009**, *25*, 8833–8840. (c) Betancourt, J. E.; Rivera, J. M. *J. Am. Chem. Soc.* **2009**, *131*, 16666–16668. (d) Sreenivasachary, N.; Lehn, J.-M. *Proc. Natl. Acad. Sci. U.S.A.* **2005**, *102*, 5938–5943.

[101] (a) Pieraccini, S.; Gottarelli, G.; Masiero, S.; Giorgi, T.; Spada, G. P. *Mol. Cryst. Liq. Cryst.* **2003**, *398*, 57–73. (b) Giorgi, T.; Grepioni, F.; Manet, I.; Mariani, P.; Masiero, S.; Mezzina, E.; Pieraccini, S.; Saturni, L.; Spada, G. P.; Gottarelli, G. *Chem. Eur. J.* **2002**, *8*, 2143–2152. (c) Gottarelli, G.; Masiero, S.; Mezzina, E.; Pieraccini, S.; Spada, G. P.; Mariani, P. *Liq. Cryst.* **1999**, *26*, 965–971. (d) Gottarelli, G.; Mariani, P.; Masiero, S.; Mezzina, E.; Recanatini, M.; Spada, G. P. *Helv. Chim. Acta* **1998**, *81*, 2078–2092. (e) Garbesi, A.; Gottarelli, G.; Mariani, P.; Spada, G. P. *Pure Appl. Chem.* **1993**, *65*, 641–646.

[102] (a) Hu, D.; Ren, J.; Qu, X. *Chem. Sci.* **2011**, *2*, 1356–1361. (b) Betancourt, J. E.; Subramani, C.; Serrano-Velez, J. L.; Rosa-Molinar, E.; Rotello, V. M.; Rivera, J. M. *Chem. Commun.* **2010**, *46*, 8537–8539.

[103] (a) Bath, J.; Turberfield, A. J. *Nat. Nanotechnol.* **2007**, *2*, 275–284. (b) Alberti, P.; Mergny, J.-L. *Proc. Natl. Acad. Sci. U.S.A.* **2003**, *100*, 1569–1573. (c) Niemeyer, C. M.; Adler, M. *Angew. Chem. Int. Ed.* **2002**, *41*, 3779–3783. (d) Li, J. J.; Tan, W. *Nano Lett.* **2002**, *2*, 315–318. See also: (e) Ciesielski, A.; Lena, S.; Masiero, S.; Spada, G. P.; Samorì, P. *Angew. Chem. Int. Ed.* **2010**, *49*, 1963–1966.

[104] Sessler, J. L.; Sathiosatham, M.; Doerr, K.; Lynch, V.; Abboud, K. A. *Angew. Chem. Int. Ed.* **2000**, *39*, 1300–1303 (CSD structure code: WISROF).

[105] This angle is defined as the torsional angle between four points: (1) C4 on the guanine nucleus, (2) N9 on the guanine nucleus, (3) C1' of the ribose ring, and (4) the ribose ring centroid.

- [106] (a) Shinohara, Y.; Matsumoto, K.; Kugenuma, K.; Morii, T.; Saito, Y.; Saito, I. *Bioorg. Med. Chem. Lett.* **2010**, *20*, 2817–2820. (b) Saito, Y.; Suzuki, A.; Imai, K.; Nemoto, N.; Saito, I. *Tetrahedron Lett.* **2010**, *51*, 2606–2609. (c) Ogasawara, S.; Saito, I.; Maeda, M. *Tetrahedron Lett.* **2008**, *49*, 2479–2482. (d) Tainaka, K.; Tanaka, K.; Ikeda, S.; Nishiza, K.-i.; Unzai, T.; Fujiwara, Y.; Saito, I.; Okamoto, A. *J. Am. Chem. Soc.* **2007**, *129*, 4776–4784. (e) Okamoto, A.; Ochi, Y.; Saito, I. *Chem. Commun.* **2005**, 1128–1130. (f) Okamoto, A.; Kanatani, K.; Ochi, Y.; Saito, Y.; Saito, I. *Tetrahedron Lett.* **2004**, *45*, 6059–6062. (g) Ochi, Y.; Okamoto, A.; Saito, I. *Nucl. Acid. Symp. Ser.* **2004**, *48*, 73–74.
- [107] Schindler, D.; Eißmann, F.; Weber, E. *Org. Biomol. Chem.* **2009**, *7*, 3549–3560.
- [108] González-Rodríguez, D.; Janssen, P. G. A.; Martin-Rapún, R.; De Cat, I.; De Feyter, S.; Schenning, A. P. H. J.; Meijer, E. W. *J. Am. Chem. Soc.* **2010**, *132*, 4710–4719.
- [109] (a) Sessler, J. L.; Wang, R. *Angew. Chem. Int. Ed.* **1998**, *37*, 1726–1729. (b) Sessler, J. L.; Wang, R. *J. Org. Chem.* **1998**, *63*, 4079–4091.
- [110] Meng, X.; Moriuchi, T.; Tohnai, N.; Miyata, M.; Kawahata, M.; Yamaguchi, K.; Hirao, T. *Org. Biomol. Chem.* **2011**, *9*, 5633–5636.
- [111] Ikehara, M.; Tada, H.; Muneyama, K. *Chem. Pharm. Bull.* **1966**, *14*, 46–49.
- [112] Grünewald, C.; Kwon, T.; Piton, N.; Förster, U.; Wachtveitl, J.; Engels, J. W. *Bioorg. Med. Chem.* **2008**, *16*, 19–26.
- [113] Bond lengths between heavy atoms and hydrogen have not been normalized to neutron-diffraction determined values.

[114] According to this formalism, a perfectly planar guanine ribbon would be characterized by a twisting angle of 0 °, while a guanine quartet would have a 180 ° twisting angle. A twisted ribbon is thus a distortion of a ribbon in the direction of a quartet. For other highly twisted guanine ribbons, see: (a) Sato, T.; Seko, M.; Takasawa, R.; Yoshikawa, I.; Araki, K. *J. Mater. Chem.* **2001**, *11*, 3018–3022 (interplanar angle 36.3 °). (b) Takasawa, R.; Yoshikawa, I.; Araki, K. *Org. Biomol. Chem.* **2004**, *2*, 1125–1132 (interplanar angle 31.6 °).

[115] Hunter, C. A.; Sanders, J. K. M. *J. Am. Chem. Soc.* **1990**, *112*, 5525–5534.

[116] CSD reports ten crystal structures of guanine derivatives with a non-hydrogen substituent in the 8-position (not counting compounds **3** and **4**). Virtually all of these structures feature a *syn*-relationship between the guanine nucleus and the ribose substituent, with torsional angles varying between 2.7 and 53.2°. Despite the structural similarity, this family of crystal structures shows no general pattern of guanine-guanine hydrogen bonding. Nine of the ten reports are structures crystallized from H<sub>2</sub>O as the solvent, which significantly disturbs guanine-guanine hydrogen bonding. Structure codes: BEHLIJ, BGUAOS10, BRGUOS, COXNEI, DEMXEY, FUYKEP, IGUANM, MOXFIO, TONBEE, and WISROF.

[117] Other, even more subtle, effects cannot be fully excluded. These could include: (a) significantly lower guanine–ribose torsional angles in **28** and **29**, relative to **26** (i.e. **28** and **29** are "more *syn*" than **26**); (b) solvent effects (disordered CHCl<sub>3</sub> molecules established short contacts with guanine nuclei), or (c) weak [C–H···X] hydrogen bonds established between α-hydrogens on cyanophenyl and pyridyl rings and carbonyl



oxygen within ribose acetyl groups (see: Desiraju, G. R.; Steiner, T. *The Weak Hydrogen Bond In Structural Chemistry and Biology*; Oxford University Press: Oxford, 1999). We believe that these effects are too small in magnitude to lead to such a pronounced shift in the hydrogen bonding patterns.

[118] Blackburn, B. K.; Lee, A.; Baier, M.; Kohl, B.; Olivero, A. G.; Matamoros, R.; Robarge, K. D.; McDowell, R. S. *J. Med. Chem.* **1997**, *40*, 717–729.

[119] Yashima, E.; Matsushima, T.; Okamoto, Y. *J. Am. Chem. Soc.* **1997**, *119*, 6345–6359.

[120] Soderquist, J. A.; Rane, A. M.; Matos, K.; Ramos, J. *Tetrahedron Lett.* **1995**, *36*, 6847–6850.

[121] Pearson, D. L.; Tour, J. M. *J. Org. Chem.* **1997**, *62*, 1376–1387.

[122] Zhou, Q.; Swager, T. M. *J. Am. Chem. Soc.* **1995**, *117*, 7017–7048.

[123] Takahashi, S.; Kuroyama, Y.; Sonogashira, K.; Hagihara, N. *Synthesis* **1980**, *8*, 627–630.

[124] Pelter, A.; Jones, D. E. *J. Chem. Soc., Perkin Trans. 1* **2000**, *14*, 2289–2294.

[125] Figueira, J.; Rodrigues, J.; Russo, L.; Rissanen, K. *Acta Cryst.* **2008**, *C64*, o33–o36.

[126] Meier, H.; Ickenroth, D.; Stalmach, U.; Koynov, K.; Bahtiar, A. *Eur. J. Org. Chem.* **2001**, 4431–4443.